Fakulteit Ingenieurswese, Bou-omgewing & IT
Faculty of Engineering, Built Environment & IT

Positron Emission Particle Tracking Inside a Laboratory Batch Jig

by

Wynand Roux

Dissertation submitted in partial fulfilment of the
requirements for the degree of

Master in Metallurgical Engineering

Supervisor: Dr N Naudé

School of Engineering
Department of Materials Science and Metallurgical Engineering

UNIVERSITEIT VAN PRETORIA
UNIVERSITY OF PRETORIA
YUNIBESITHI YA PRETORIA
Denkleiers • Leading Minds • Dikgopolo tša Dihlalefi

Abstract

The movement of particles inside a jig ultimately determines the efficiency of the jig. The movement of these particles is a function of the particle properties (size, density and shape) and the jigging parameters (pulse shape, water flow, etc.). The purpose of this study was to investigate how particle properties affect the movement of particles inside a jig.

Positron Emission Particle Tracking (PEPT) is one of the few techniques that can trace the movement of particles inside an enclosed system without interfering with the particle flow and has successfully been used to study mills, hydrocyclones and flotation. In this study, PEPT was evaluated as a possible technique to study the flow of iron ore particles inside a laboratory scale jig. The results showed that very accurate three dimensional trajectories could be obtained, with a temporal resolution high enough to see the movement of a particle during a single pulse.

The vertical component from the trajectories showed the rate at which particles moved through the jig bed (stratification rate). The particle property that affected the stratification rate the most was density, followed by size. Shape didn't have a large influence on the stratification rate. However, it was evident that the flat particles have a slightly higher rate, compared to cubic and elongated particles.

The PEPT testwork showed the existence of a circular flow pattern (secondary flow) that emerged inside the batch jig. Throughout the test results, the effects of the secondary flow pattern on the movement of the tracer particles was observed. It was seen that particles with densities close to that of the jigging bed were affected the most and that some of these particles showed no degree of stratification .A possible origin of this secondary flow can be the uneven water velocity under the jig bed. The uneven velocity profile was confirmed by looking at the difference in pulse height at different position in the jig bed, with the help of PEPT.

None of the existing jigging models in literature take into account this back mixing caused by the secondary flow. An attempt was made to add this effect to King's potential energy model to improve its accuracy with regards to iron ore jigging. From the PEPT observations, the assumption was made that the back mixing experienced by a particle is related to the difference between the mass of the tracer particle and the average particle mass inside the jig. Simulated stratification profiles generated with the modified stratification model were compared to published data of batch iron ore jigging and showed better correlation compared to the standard model.

Plagiarism declaration

Full names	Wynand Roux
Student number	04420845
Topic of work	Master's Thesis – Positron Emission Particle Tracking Inside a Laboratory Batch Jig

Declaration

1. I understand what plagiarism is and am aware of the University's policy in this regard.
2. I declare that this dissertation is my own original work. Where other people's work has been used (either from a printed source, internet or any other source), this has been properly acknowledged and referenced in accordance with the requirements as stated in the University's plagiarism prevention policy.
3. I have not used another student's past written work to hand in as my own.
4. I have not allowed, and will not allow, anyone to copy my work with the intention of passing it off as his or her own work.

Signature

Acknowledgements

I would like to acknowledge the contributions and express my gratitude to the following people and organisations:

- My supervisor, Natasia Naudé, for her esteemed supervision, motivation and guidance.
- Anglo American Kumba Iron Ore for sponsoring the project. Mr Jan van Schoor for instigating the project.
- Mr Danie van Wyk, who was involved in designing of the batch jig.
- The team at PEPT Cape Town for their assistance with the testwork: Andy Buffler, Indresan Govender, Michael van Heerden and Cong Liu.
- My wife and parents for their understanding and support during this project.

Contents

List of Figures

List of Tables

1 INTRODUCTION

1.1 Sishen Iron Ore

Sishen Iron Ore Mine is situated in the northern part of the Northern Cape Province of South Africa (Figure 1-1) near the town Kathu, a 260 km drive north-west of Kimberley. Since mining started in 1953, the mine has expanded to one of the largest open pit mines in the world, employing approximately 8 300 people (Integrated Report, 2014). In 2014 the mine produced 35.5 million tonnes of iron ore, most of which is exported, with a small amount used for local steel production.

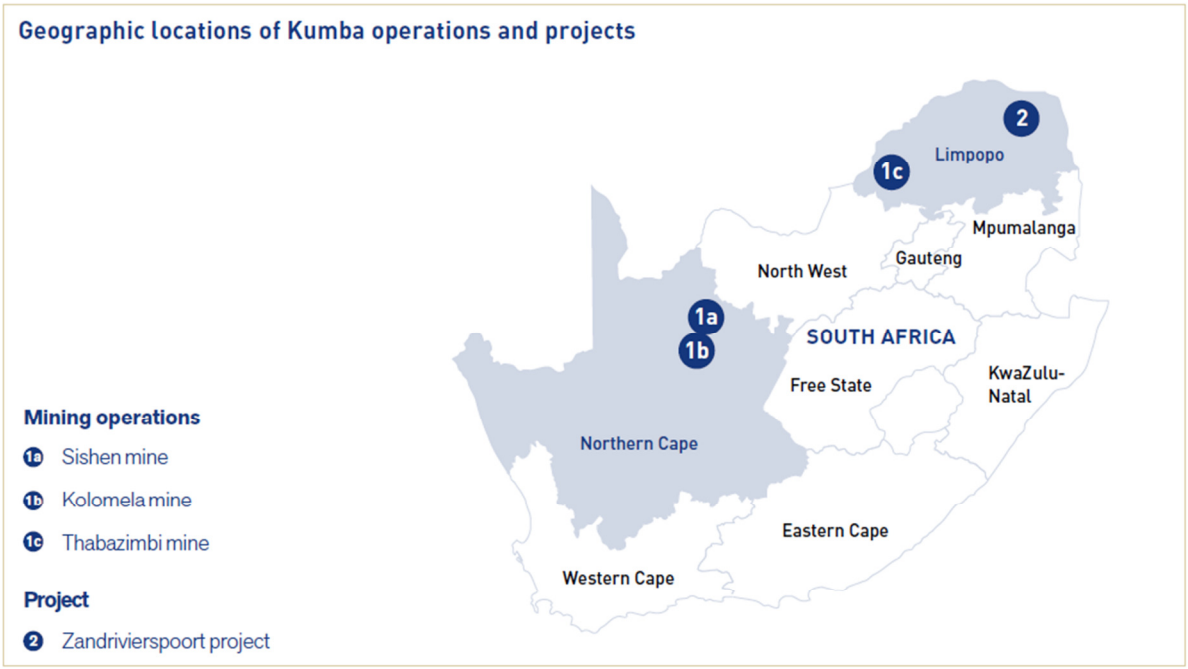

Figure 1-1 Geographic locations of Kumba Iron Ore operations (Integrated Report, 2014)

There is an estimated reserve of 563.8 Mt (2014) exploitable iron ore at Sishen. The bulk of the ore consists of a high-grade laminated massive ores, which is part of the Asbestos Hills Subgroup. The main ore body dips of at about 10° in the westerly direction, as seen in Figure 1-2, and is overlain by calcrete, clay, lava, quartzite, shale, flagstone and conglomerate.

A conventional opencast method is used, which includes the removal of top soil, drilling, blasting and hauling. The run-of-mine (ROM) product is then crushed and beneficiated either by dense medium separation or by jigging. The high grade material (+60% Fe) is fed to the dense medium plant; the process can be seen in Figure 1-3. The material is first sent through three stages of crushing, and

then screened into four size classes. The two larger size classes are beneficiated with dense medium drums and the two smaller size classes with dense medium cyclones.

The lower grade material (45% to 60% Fe) is beneficiated via jigging (Figure 1-4) and the ROM material is sent through a three-stage crushing circuit, after which it is screened into a coarse, medium and fine fraction. These three fractions are sent to three different jigging circuits.
The quality and size specification of the products from Sishen mine is shown in table 1-1 and table 1-2. The products are transported by rail to Saldana Bay, in the Western Cape, where it's exported or transported by rail to local steel producers.

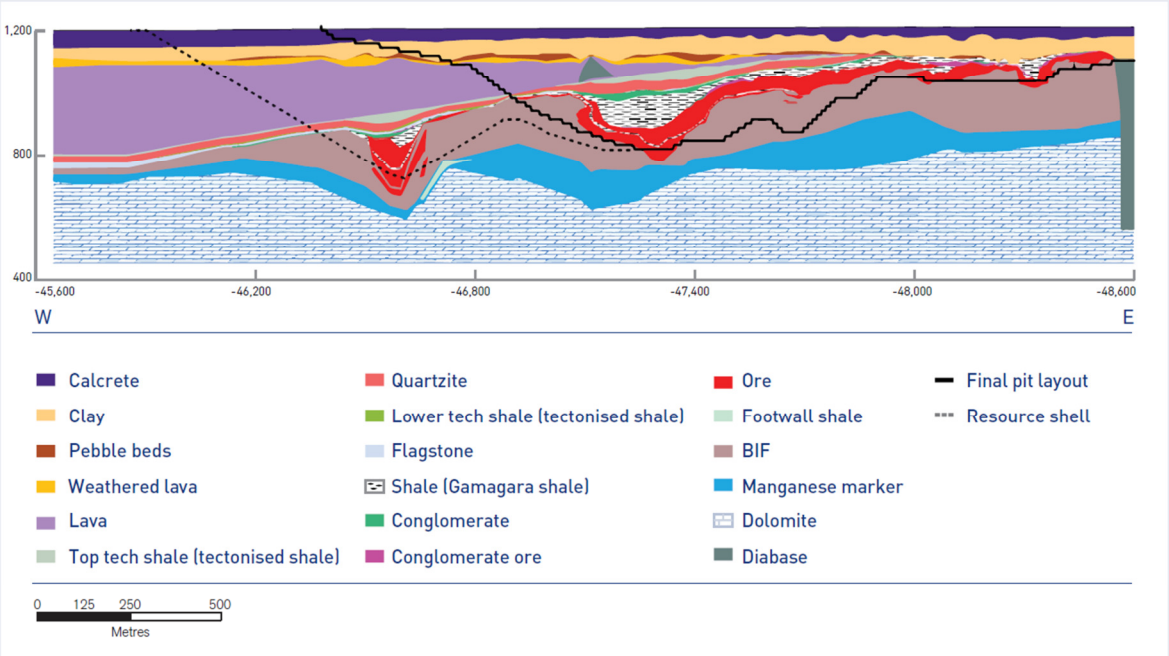

Figure 1-2 West-east profile depicting the local geology through the Sishen North Mine area (Integrated Report, 2014)

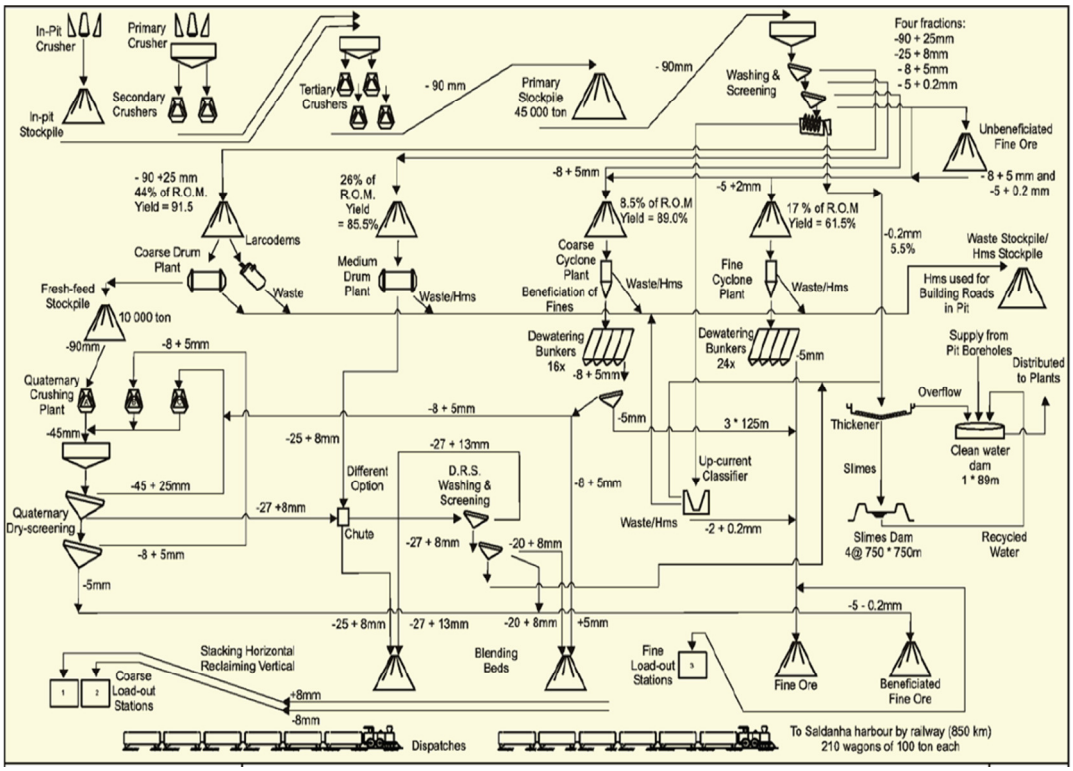

Figure 1-3 Sishen main beneficiation plan (dense medium separation) (SKR Consulting, 2006)

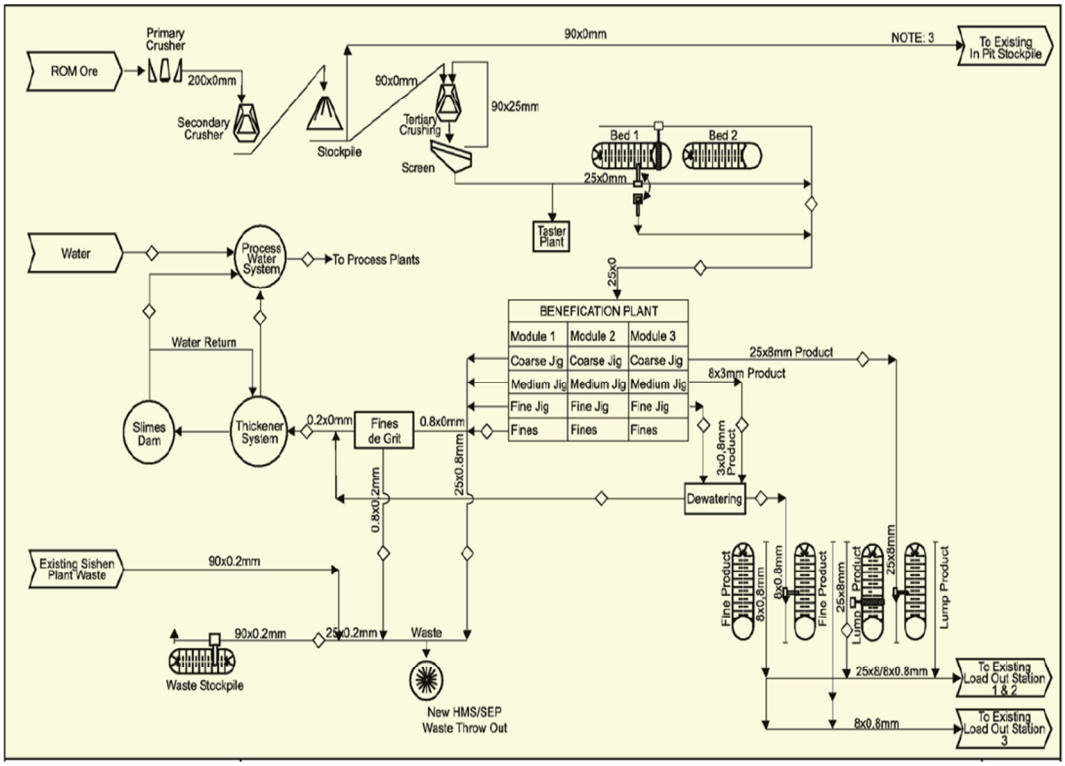

Figure 1-4 Sishen expansion project (jigging beneficiation plant) (SKR Consulting, 2006)

Table 1-1 Sishen Mine: Main plant product qualities (SKR Consulting, 2006)

Description	Units	Fe	SiO_2	Al_2O_3	K_2O	P	Oversize Max	Undersize Max
27mm DR Ore								
2004 – 2005 Average	**(%)**	66.35%	2.92%	1.20%	0.12%	0.054%	10.6%+27mm	4.3%–13mm
Current Specification	**(%)**	66.00%	3.70%	1.50%	0.16%	0.057%	15.0%+27mm	5.0%–13mm
25mm Lump Ore								
2004 – 2005 Average	**(%)**	66.30%	2.90%	1.22%	0.13%	0.055%	6.4%+25mm	4.1%–8mm
Current Specification	**(%)**	66.00%	3.70%	1.50%	0.16%	0.057%	7.5%+25mm	5.3%–8mm
20mm Lump Ore								
2004 – 2005 Average	**(%)**	66.33%	2.88%	1.23%	0.13%	0.055%	8.2%+20mm	6.2%–8mm
Current Specification	**(%)**	66.00%	3.70%			0.057%	20.0%+20mm	9.0%–8mm
8mm CS Ore								
2004 – 2005 Average	**(%)**	65.85%	3.14%	1.40%	0.16%	0.057%	18.6%+8mm	8.5%–5mm
Current Specification	**(%)**	65.00%	4.20%	2.00%	0.24%	0.066%	22.0%+8mm	16.0%–5mm
5mm Fine Ore								
2004 – 2005 Average	**(%)**	65.49%	3.28%	2.08%	0.19%	0.061%	6.5%+5mm	7.0%–0.2mm
Current Specification	**(%)**	65.00%	4.20%	2.00%	0.24%	0.066%	8.4%+5mm	12.0%–0.2mm

Table 1-2 SEP: Plant product qualities (SKR Consulting, 2006)

Description	Units	Fe	SiO_2	Al_2O_3	K_2O	P	Oversize Max	Undersize Max
Lump Ore								
Sishen Specification	**(%)**	66.00%	3.70%	1.50%	0.16%	0.057%	6.5%+25mm	10%–8mm
SEP Specification	**(%)**	64.00%	5.90%	1.50%	0.16%	0.065%	6.5%+25mm	12%–8mm
Sishen Typical	**(%)**	66.27%	2.93%	1.25%	0.15%	0.055%	6.4%+25mm	6.5%–8mm
SEP Expected	**(%)**	64.35%	5.50%	1.22%	0.16%	0.063%		
Fine Ore								
Sishen Specification	**(%)**	65.00%	4.20%	2.00%	0.24%	0.066%	7.5%+5mm	18%–0.2mm
SEP Specification	**(%)**	63.50%	6.30%	2.00%	0.24%	0.074%	10%+8mm	18%–0.2mm
Sishen Typical	**(%)**	65.52%	3.26%	1.59%	0.19%	0.066%	5.1%+5mm	8.5%–0.2mm
SEP Expected	**(%)**	64.37%	5.20%	1.70%	0.24%	0.067%		

1.2 Sishen jig beneficiation plant

To increase output at Sishen's mine and to utilise lower grade ore, a jigging beneficiation plant was built and commissioned at the mine. The first ore from the jig plant was produced in 2007 and, through a steady ramp-up, it reached its full production rate of 12 Mt per annum by the end of 2009 (Myburgh, 2010).

The feed to the plant is screened into three fractions: -25+8 mm, -8+3 mm and -3+1 mm. These fractions were determined by initial testwork on a pilot scale jig, which showed a significant improvement in yield when the feed is split into narrower size fractions (Myburgh & Nortje, 2014), a common issue that affects gravity separation (Wills, 2006; Burt, 1984).

The three fractions are then conveyed to the three jigging modules (coarse, medium and fine), each containing eight jigs in parallel. The product and the waste run over dewatering screens, where the water is recovered and recycled back into the plant (Myburgh, 2010). The full flow sheet for the jig plant can be seen in Figure 1-5.

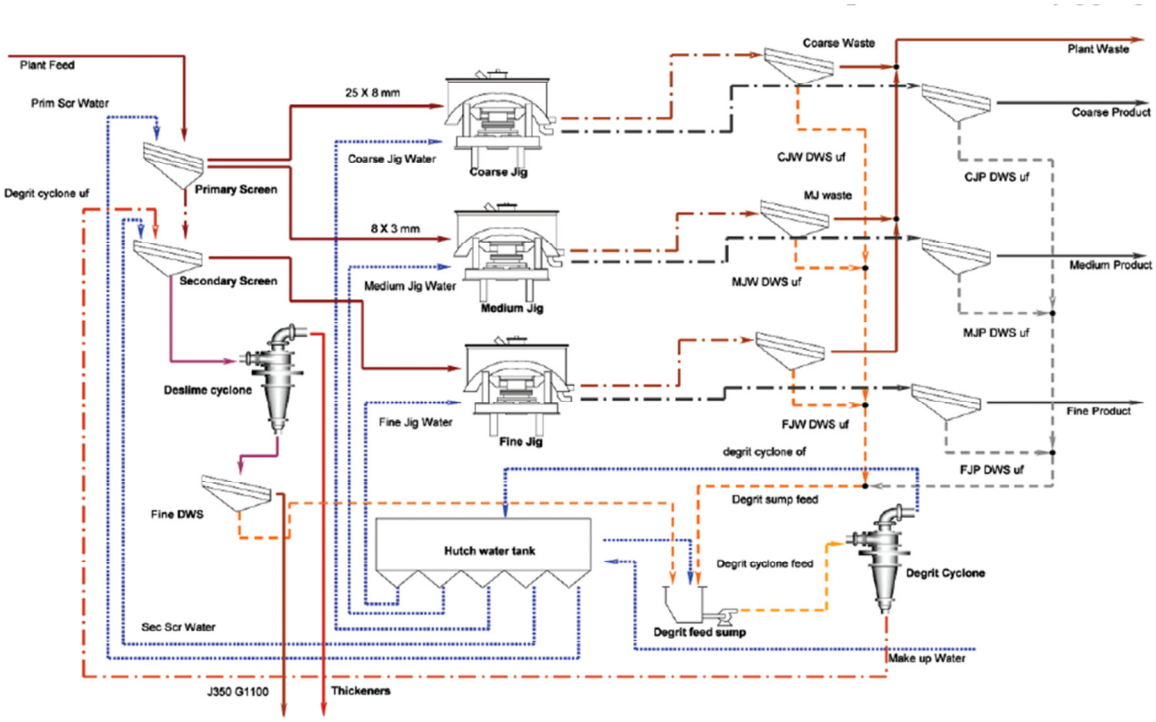

Figure 1-5 Sishen jig plant layout (Myburgh, 2010)

According to Myburgh (2010), one of the biggest issues with the operation of the Sishen jig plant is the possible variation of the feed to the plant. The ROM is trucked from different locations in the 12 km by 2.5 km pit, and this results in a varying chemistry and PSD to the plant. The difficulty is that different feed types require different jig settings (feed rate and jig pulse) to maintain the required efficiency. Large ROM beds are required to ensure that the plant receives a constant feed for a relatively long period of time, to prevent the constant need to change the jigging parameters.

1.3 Hypothesis

The size, density, and shape of a particle affect its movement inside a jig bed and therefore affect the stratification process.

1.4 Project Objectives

The following objectives were identified for the project:

1. To determine whether positron emission particle tracking (PEPT) is a viable technique for investigating iron ore jigging.
2. To determine the effects of the size, density, and shape of a particle on its movement inside a jig, with the aid of PEPT.
3. To use the data obtained with PEPT to develop a stratification model for batch jigging.

2 JIGGING

2.1 Introduction

Jigs belong to a group of minerals processing equipment called gravity concentrators. It is one of the oldest gravity concentration methods used, yet only recently great effort is being made to fully understand the mechanisms and principles.

The first reference to jigging is found in the book *De Re Metallica* by Agricola (1556). Figure 2-1 is a taken from Agricola's book and shows a jigging setup used in the sixteenth century. Jigging screens are manually shaken up and down in a tub of water through a series of sieves with decreasing aperture size. The residue that remains on the screen will form two products, metallic particles that form a bottom layer on the sieve and a layer of lighter material on top.

Jigs are still widely used in industry today, due to its simple operation and low cost compared to that of other processes (e.g. dense medium separation) (Mukherjee, 2006).

Figure 2-1 Jigging process (Agricola, 1556)

2.2 Operating Principles

The basic construction of a jig is shown in Figure 2-2; it consists of a tank, open at the top and filled with water, with a horizontal screen upon which the particle bed is supported and through which water can flow. Feed is added at one side and, while the bed is pulsated by water, the solids move to the discharge end of the jig (Burt, 1984).

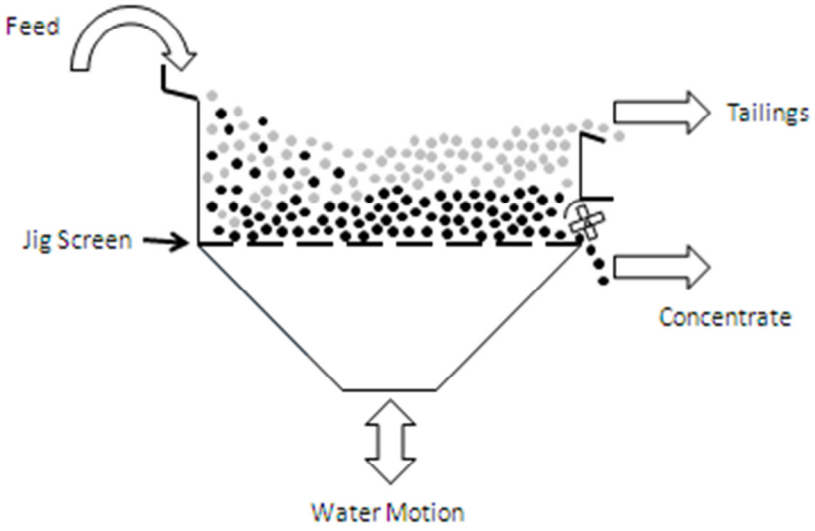

Figure 2-2 Basic construction of a jig (Burt, 1984)

The movement of the water is generated either by a plunger (Denver jig) or by air pressure (Baum jig). A third type of jig exists, where the water remains stationary and the screen is moved up and down. During over screen jigging, a screen with an aperture size smaller than the smallest mineral particle is used (Burt, 1984). A modified method, where the aperture size is larger than the dense mineral, is sometimes used when jigging finer material. The dense mineral then falls through the screen, into the lower part of the jig called the hutch, where it is removed.

The mechanism of jigging is probably the most complex of all the gravity separation processes, due to its continuously varying hydrodynamics (Kelly & Spottiswood, 1989). The mineral bed is subjected to a water pulse, which repeatedly causes the bed to expand and resettle. During settling, particles with different densities and sizes will settle at different rates, resulting in segregation. The jig cycle is represented in Figure 2-3.

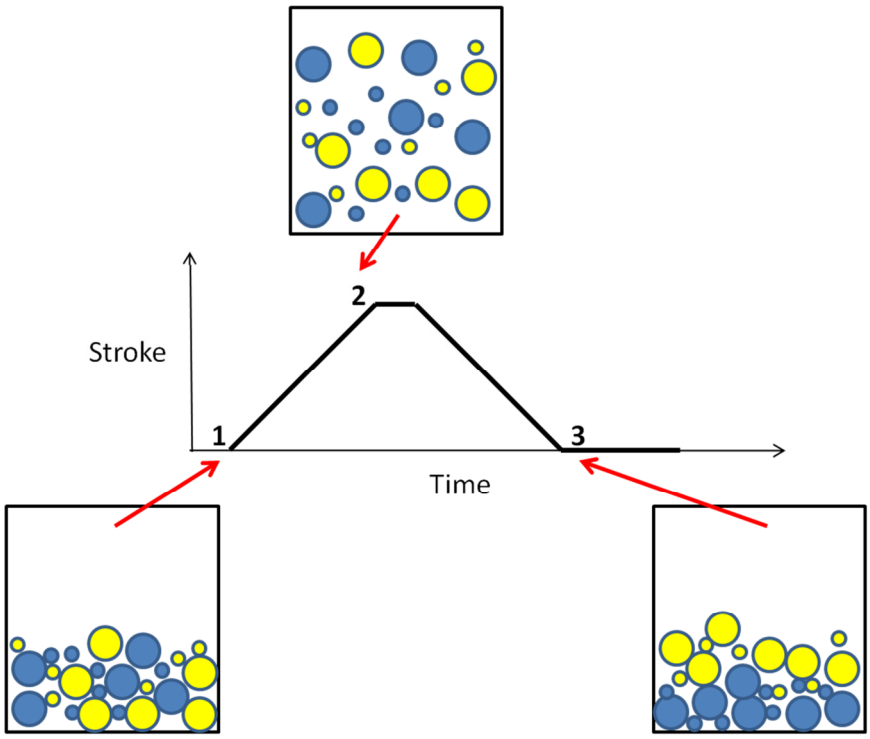

Figure 2-3 Conceptual representation of particle stratification (Mishra, 2006)

The jigging pulse cycle is repeated and segregation increases with each stroke, until a steady state is achieved. Separation occurs due to the relative movement of particles with different densities and sizes, in a particle bed subjected to a water pulse. There are different mechanisms that control particle segregation during the jigging cycle. This is discussed in the next section.

2.3 Types of jigs

As jigs are very widely used, many different types of jigs were developed throughout the years to improve efficiency, to cut down on cost and to fit a specific application. Jigs can be classified into groups based on the mechanism that produces the pulsing action (Fuerstenhau & Han, 2003).

2.3.1 Plunger jigs

Plunger jigs were the first type of jigs that were commercially installed on a large scale early in the 20th century (Cope, 2000). In the design of a plunger jig, the screen is kept stationary and the particles are dilated by a water pulse, generated by a plunger. The Harz jig is an example of such a jig and is shown in Figure 2-4.

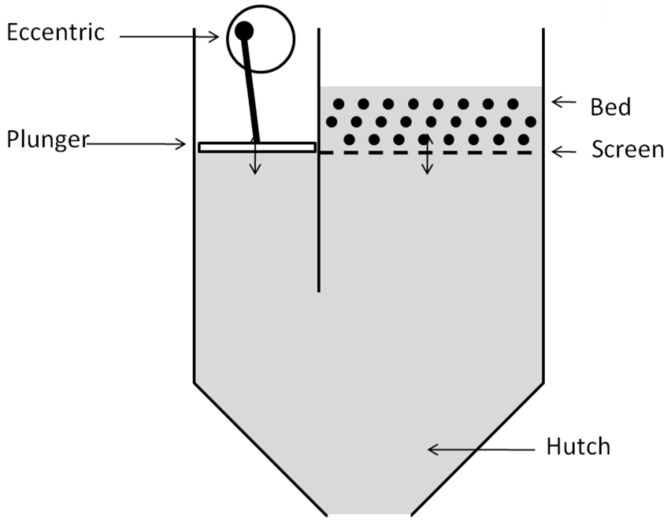

Figure 2-4 Schematic of a Harz jig (Kelly & Spottiswood, 1989)

An eccentric drives a plunger, which is located in a compartment next to where the jigging takes place. The Harz jig has multiple compartments. The number of compartments is dependent on the difficulty of separating the ore and each compartment has its own plunger that can run at different settings (Cope, 2000).

These types of jigs were driven by an eccentric on a drive shaft, which gave a harmonic jig cycle. To improve efficiency, manufacturers developed jigs with different wave forms. One such an example is the Collom jig, where a quick upwards stroke followed by a slow suction stroke is produced (Burt, 1984).

2.3.2 Diaphragm jigs

All plunger jigs had difficulty maintaining a proper seal between the plunger and the compartment walls (Burt, 1984). To overcome this difficulty, diaphragm jigs were developed.

a) The Bendelari jig

In the Bendelari jig, the water pulse is generated by a diaphragm attached directly to the bottom of the hutch box, and the motion is generated by an eccentric drive. Hutch water is added during the suction stroke of the cycle, to loosen the bed and thereby emphasising hindered settling (Burt, 1984).

b) Pan-American placer jig

The Pan-American placer jig has a conical diaphragm, which is pulsed by a balance beam that can pulse two compartments with a single drive motor. Figure 2-5 shows a placer jig schematically. The jig was mainly used for the concentration of placer gold (Burt, 1984).

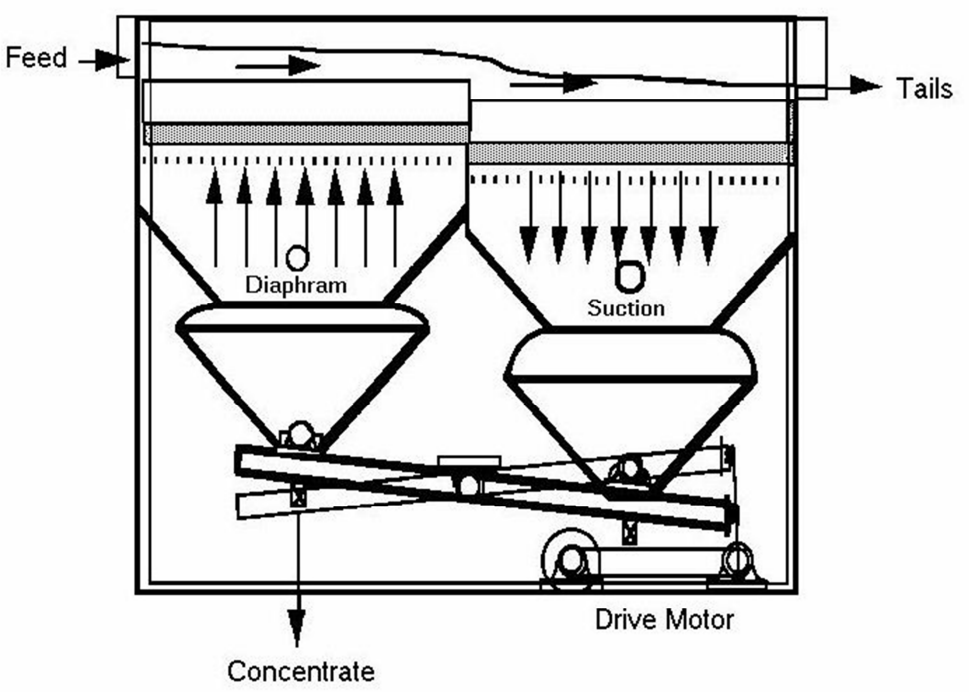

Figure 2-5 a modern placer jig (Coggin, 1995)

c) Remer jig

The Remer jig was originally developed for the cleaning of coal. It had a unique pulsing mechanism, which consisted of two eccentric drives, each with its own motor connected by a short beam. One eccentric has a short stroke at a high frequency and the other a long stroke at a slower frequency. The short stroke keeps the bed lively while jigging (Fuerstenhau & Han, 2003).

2.3.3 Air-pulsed jigs

Today most jigs in operation use air as a means to generate water pulsations (Kelly & Spottiswood, 1989), since a more suitable pulsation cycle can be obtained using air pressure, compared to a mechanical mechanism.

The pulse is generated by the injection of air into a chamber with an open base that forces the water out of the chamber and into the jigging compartment. Two classes of air-pulsed jigs exist, namely side-pulsed jigs and under-bed air-pulsed jigs.

a) Side-pulsed jigs

With the side-pulsed jig, the air chamber is located on the side of the jigging compartment. The air chamber is fitted with an air valve that controls air flow into the chamber from a compressed air source and can also exhaust air on the down stroke. No suction is caused by the air chamber on the down stroke (Burt, 1984). Figure 2-6 shows a cross section of a Baum jig, which is a typical side-pulsed jig.

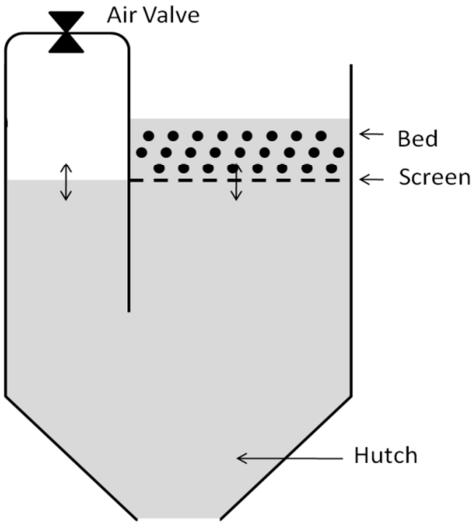

Figure 2-6 Baum jig (Kelly & Spottiswood, 1989)

b) Under-bed air-pulsed jigs

With an increase in bed width, the flow across the bed of the side-pulsed jigs are no longer uniform. To solve this problem, the pulsation chambers are placed underneath the jig bed. This allows for very large jigs with high capacities (Burt, 1984). Figure 2-7 shows a Batac jig, which is an under-bed-pulsed jig, schematically.

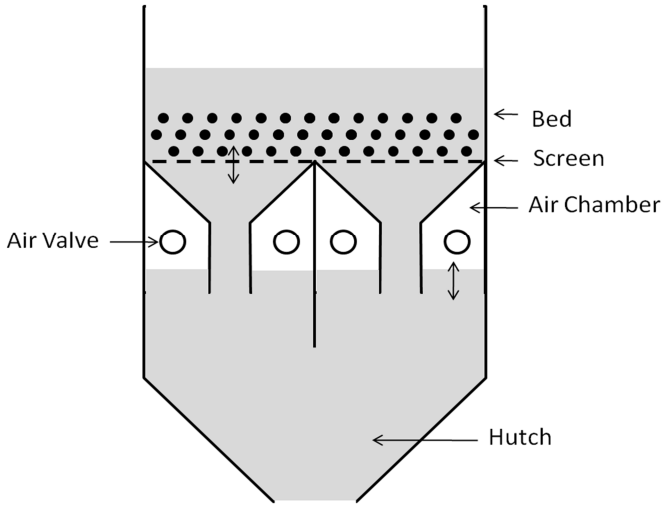

Figure 2-7 Schematic diagram of Batac jig (Kelly & Spottiswood, 1989)

2.3.4 Other types of jigs

a) InLine Pressure jig

The InLine Pressure jig is a circular jig which is fully enclosed to allow the entire unit to be filled with water, eliminating the water-air interface. The particle bed pulsation is achieved by a movable screen, driven by a hydraulic ram. The jig can handle slurries with a high density and has low water consumption (Cope, 2000).

b) Centrifugal jigs

Jigs can generally not efficiently treat very fine particles. To solve this problem, jigs which use forces up to a 100 times larger than that of gravity by using centrifugal forces have been developed. Instead of a flat screen, centrifugal jigs have cylindrical screens that rotate at high speeds. Behind the screen are hutch compartments, from where the pulse is generated by injecting water at a high enough pressure to overcome the centrifugal forces (Kelly & Spottiswood, 1989).

c) Magnetic jigs

Magnetic jigging introduces an upward vertical force that has effect only on magnetic particles that result in lightening of the particles. This upward force will result in increased efficiency in cases where the density of the minerals that need to be separated, are close (Dai, 1999).

2.4 Jigs at Sishen Iron Ore

The jig plant at Sishen Iron Ore features 24 Allmineral under-bed air-pulsed jigs (Figure 2-8) (Myburgh, 2010). These jigs are based on the Batac jig discussed in section 2.3.3. The product (heavy fraction) is discharged through the gates in the jigging screen at the end of the jig (Figure 2-9). The gates are controlled by a float that measures the height of the product bed around a set value (Wills, 2005).

Blowers generate air, which is stored in the working air vessel and is kept at a certain pressure. Poppet valves open up and allow air from the working air vessel to flow into air chambers beneath the jig screen. The expanding air in the chambers pushes water upwards and through the jig bed (Wills, 2005).

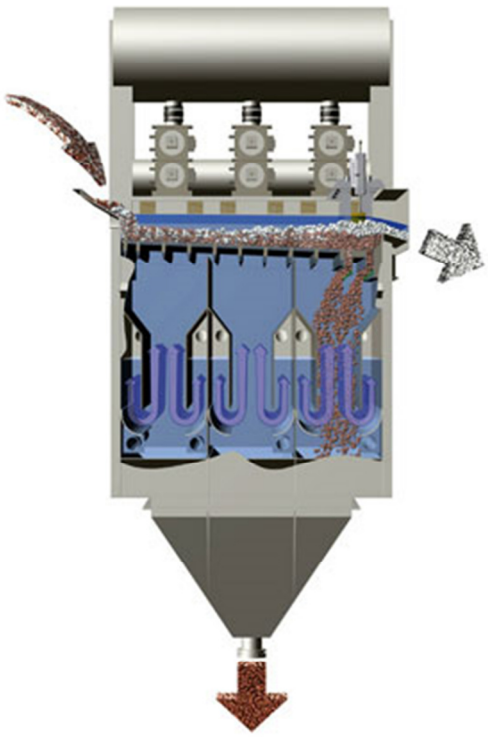

Figure 2-8 Alljig® under-bed air-pulsed jigging machine (Allminerals, 2015)

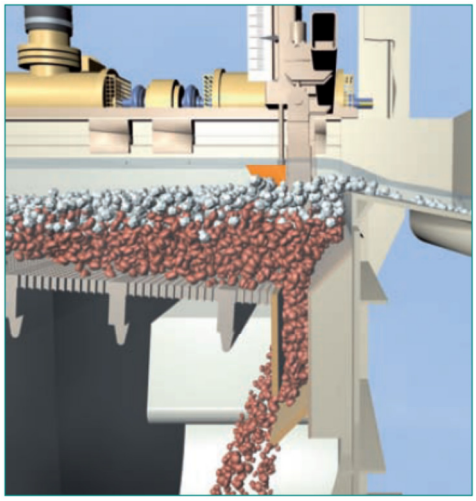

Figure 2-9 Bottom gate discharge (Allminerals, 2015)

2.5 Stratification mechanism of jigging

The mechanisms that bring forth stratification in a jig can be explained by the theory suggested by Gaudin (1939), which is referred to as the classical theory of jigging. The classical theory states that stratification takes place due to three mechanisms: differential acceleration, hindered settling, and interstitial trickling.

2.5.1 Forces on a single particle

Parts of the classical theory of jigging can be derived from first principles, by mathematically looking at a particle falling through a fluid from a resting position. A force balance can be done on such a particle and the forces involved are shown in Figure 2-10.

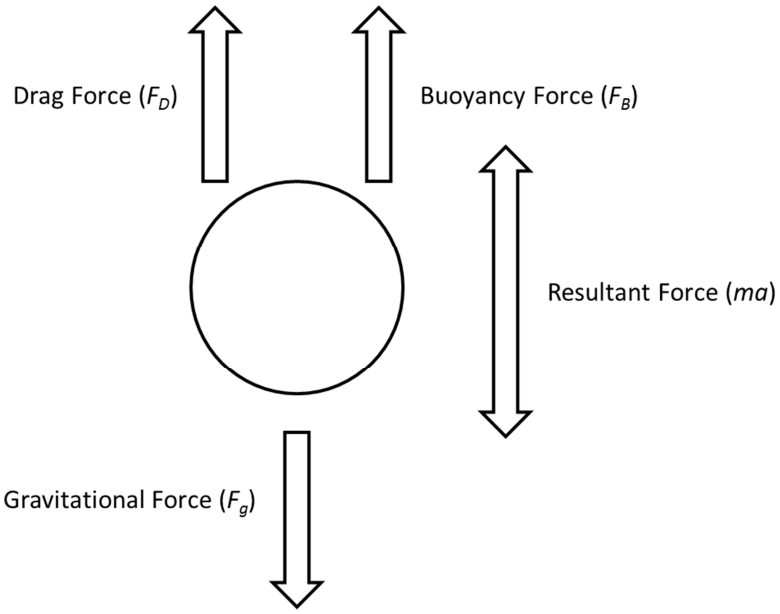

Figure 2-10 Force balance on a particle in fluid (adapted from Wills, 2005)

The equation for the one-dimensional movement of a particle through a fluid under the external force of gravity, is shown in equation 2.1 below (Wills, 2006).

$$m\frac{dv}{dt} = F_g - F_B - F_D \qquad 2.1$$

F_g is the force acting on the particle due to gravity, also known as the *gravity force,* and is expressed as:

$$F_g = \rho V g \qquad 2.2$$

Where:

V = volume of the particle (m^3)

F_g is the *Buoyancy* which is the upward-acting force caused by fluid pressure counteracting the weight of the particle. The force is equal to the mass of water displaced by the particle and is expressed as:

$$F_B = \rho' V g \qquad 2.3$$

Drag force, F_D, for a particle in the absence of other particles is represented by equation 2.4 and 2.5 (Gupta & Yan, 2006):

$$F_D = \frac{C_D v^2 \rho A_p}{2} \qquad 2.4$$

$$C_D = \frac{24\mu}{vd\rho_f} \qquad 2.5$$

The normal drag force equation does not take the surrounding particles into account and, since hindered, settling conditions play a large role. The bed porosity should be taken into account. One of the correlations for drag that takes into account porosity is that of Di Felice (1994) and is given by:

$$F_d = \frac{1}{2} C_D \rho_F \frac{\pi d_P^2}{4} \varepsilon^2 |\Delta v| (\Delta v) \varepsilon^{-(x+1)} \qquad 2.6$$

$$C_D = \left[0.63 + \frac{4.8}{Re^{0.5}}\right]^2 \qquad 2.7$$

$$x = 3.7 - 0.65 exp\left[-\frac{(1.5 - \log(Re))^2}{2}\right] \qquad 2.8$$

Where: C_D = drag coefficient

ε = bed porosity

Δv = relative velocity between particle and fluid

Re = Reynolds number

2.5.2 Differential acceleration

At the end of the upward stroke of the jigging cycle, the particles' velocities are reduced to zero at their maximum displacement. At this point, the particles will start to fall from rest at different accelerations, which – unlike terminal velocity – is not a function of particle size.

Substitute in the equations for gravity (equation 2.2) and buoyancy (equation 2.3) into the equation for a falling particle (equation 2.1), equation 2.9 is obtained (Wills, 2005).

$$m\left(\frac{dv}{dt}\right) = (m - m')g - F_D \qquad 2.9$$

Where:

m = particle mass (kg)
v = particle velocity (ms^{-1})
m'= mass of fluid displaced (kg)
g = gravitational acceleration (ms^{-2})
F_D = drag force (N)

From equations 2.4 and 2.6, it is evident that the drag force is a function of velocity and therefore, when the velocity is close to zero at the point where the particle starts to fall, the drag force (F_D) can be set equal to zero and equation 2.9 can be rewritten as equation 2.10 below.

$$\frac{dv}{dt} = \frac{(m - m')}{m} = \left(1 - \frac{\rho'}{\rho}\right)g \qquad 2.10$$

Where: ρ = particle density (kgl^{-1})
ρ' = fluid density (kgl^{-1})

From equation 2.10 it can be seen that particles with the same density and different sizes will initially have similar accelerations. It then follows that, if the duration of the particles' fall is short and the repetition of the fall is frequent, the relative distance travelled by the particles should represent their initial accelerations.

Solving equation 2.1 will give velocity-time curves similar to the ones seen in Figure 2-11. Particles A and B have different densities, but since the particles have different sizes, they have the same terminal velocities. However, the heavier particle will reach its terminal velocity much quicker than the lighter particle. It is at the beginning of acceleration from rest that the effect of size on the velocity is

small. At this point is seen that the high density particles (A & C) will accelerate much quicker than the low density particle (B).

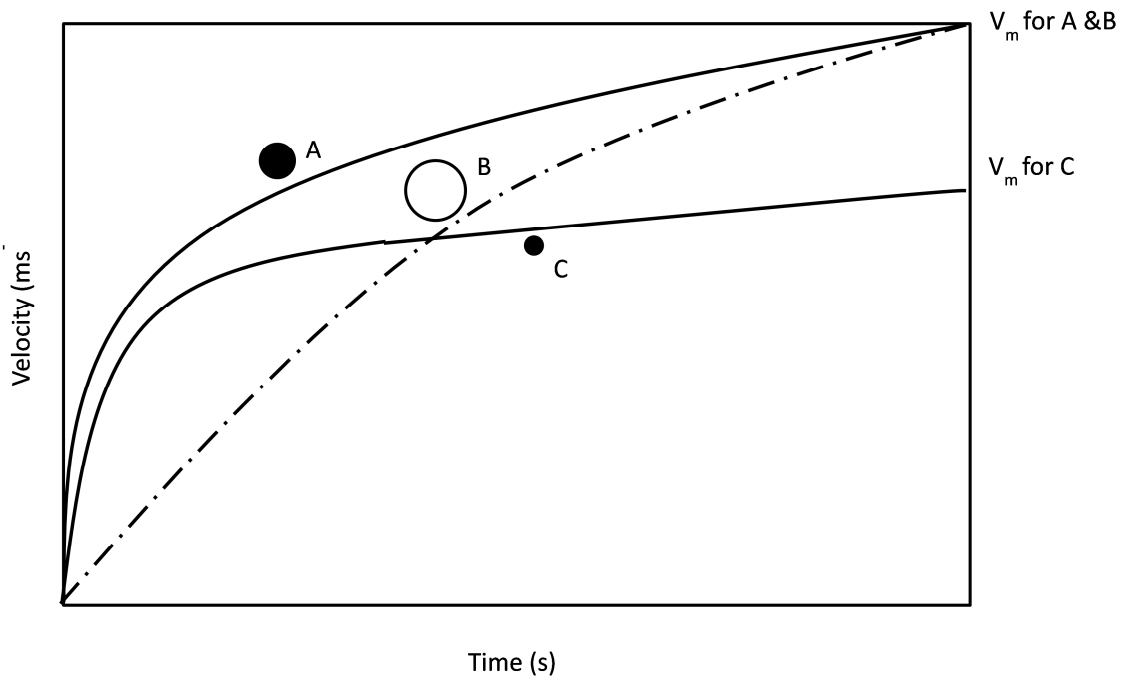

Figure 2-11 Velocity-Time curves for (A) heavy particle, (B) a light particle with the same terminal velocity as particle (A), and (C) a smaller heavy particle (Burt, 1984)

The heavier particles will gain distance over the lighter particles, with the maximum gain taking place at some time t_x, referred to as the critical time (Burt, 1984). For smaller sized particles the critical time, t_x, as well as the distance gained, is smaller. If the feed to the jig is of closely sized particles, the jigging cycle can be varied within a wide range. On the other hand, with a very poorly sized feed, the optimum jigging cycle needs to be carefully selected.

2.5.3 Hindered settling

When particles settle in a stationary fluid, their settling velocities are dependent on their density, shape and size (Taggart, 1954). After initial acceleration, the particles will attain a constant terminal velocity, which will either follow Newton's relationship or Stokes' relationship.

Stokes' relationship holds for fine particles, smaller than 0.1mm in cases where a laminar flow regime is present. For larger particles, larger than about 2 mm, Newton's relationship is followed (Burt,

1984). The equations for Stokes' and Newton's free settling terminal velocity relationships are given in equation 2.11 and 2.12 respectively (Burt, 1984).

$$V_t = \frac{gd^2(\rho - \rho')}{18\mu} \qquad 2.11$$

$$V_t = \sqrt{\frac{4g(\rho - \rho')D_p}{3C_D\rho}} \qquad 2.12$$

Where:

d = Diameter of particle (m)

Vt = terminal velocity (ms^{-1})

μ = Viscosity (Pas)

Whether a particle settles in the Newtonian or Stokesian regime, it is seen from equations 2.11 and 2.12 that the terminal velocity is a function of the relative density and diameter of the particle.

When settling particles are in close proximity to each other, the velocity fields around the particles affect each other and the standard drag relationships do not apply. The effect of hindered settling can be illustrated using the hindered settling ratio (R_h). Two particles with different densities can have the same terminal velocities when the ratio between their diameters is correct. This ratio is called the free settling ratio (R_f) (Gaudin, 1939) and is represented by equation 2.13:

$$R_f = \frac{\rho_a}{\rho_b} = \left[\frac{\rho_b - 1}{\rho_a - 1}\right]^n \qquad 2.13$$

Gaudin (1939) suggested that when the percent solids of a pulp increases, the fluid starts to act as a heavy liquid with a density of the pulp. The hindered settling ratio (R_h) now becomes (equation 2.14):

$$R_h = \frac{\rho_a}{\rho_b} = \left[\frac{\rho_b - \rho_f}{\rho_a - \rho_f}\right]^n \qquad 2.14$$

With ρ_a and ρ_b the densities of the particles and ρ_f the apparent density of the pulp.

2.5.4 Interstitial trickling

As the jig cycle comes to an end and the bed starts to close, the larger particle will interlock, allowing smaller particles to settle through the interstitial spaces between the larger particles before the bed collapses. Burt (1984) showed that the maximum size of a particle that can pass between particles as shown in Figure 2-12 can be calculated by equation 2.15:

$$D' = \sqrt{2D^2} - D = 0.41D \qquad 2.15$$

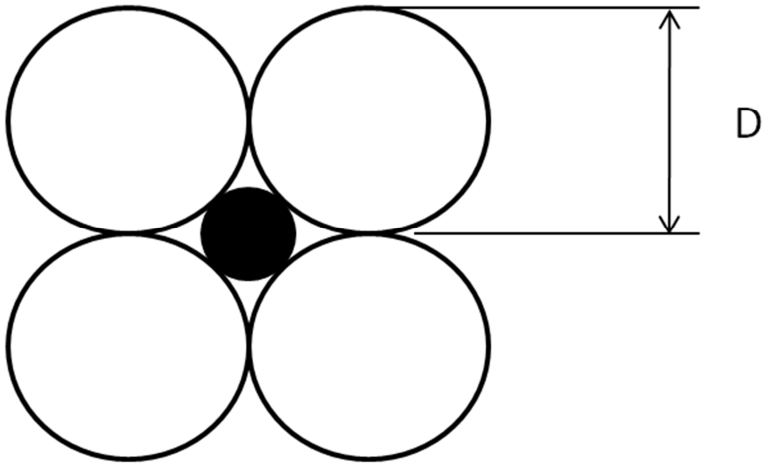

Figure 2-12 Interstitial trickling (Burt, 1984)

If trickling is allowed to continue for too long, it can result in fine low density particles trickling through to the bottom of the jig bed.

2.6 Operating Parameters

2.6.1 Jigging cycle

The jigging cycles used by the various manufacturers will depend on their opinion of which jigging mechanisms are the most important (Burt, 1984). Figure 2-13 shows the displacement and velocity profile of the water movement inside a typical plunger type jig. Due to the reciprocating piston that generates the pulse, a harmonic jig cycle is produced.

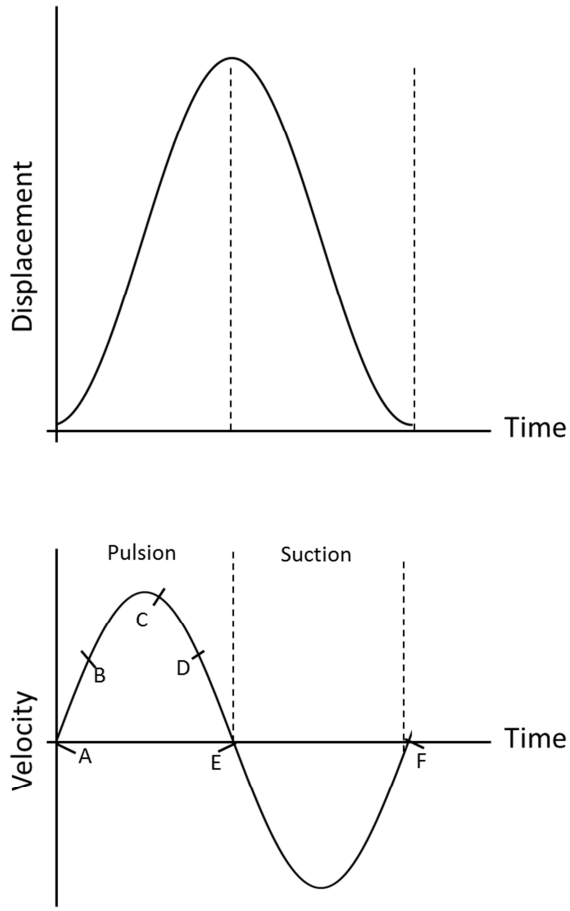

Figure 2-13 Harmonic motion cycle of a plunger type jig. Top: fluid displacement; bottom: fluid velocity (Burt, 1984)

Jig cycles from air-pulsed jigs are different from mechanically actuated plunger jigs. Air valves open and let air into a chamber that pushes the water upwards, whereafter an exhaust valve opens to let the air out. The water then moves downward. A typical jig cycle from an air-pulsed jig is shown in Figure 2-14. The jig cycle has three features: frequency, amplitude, and shape.

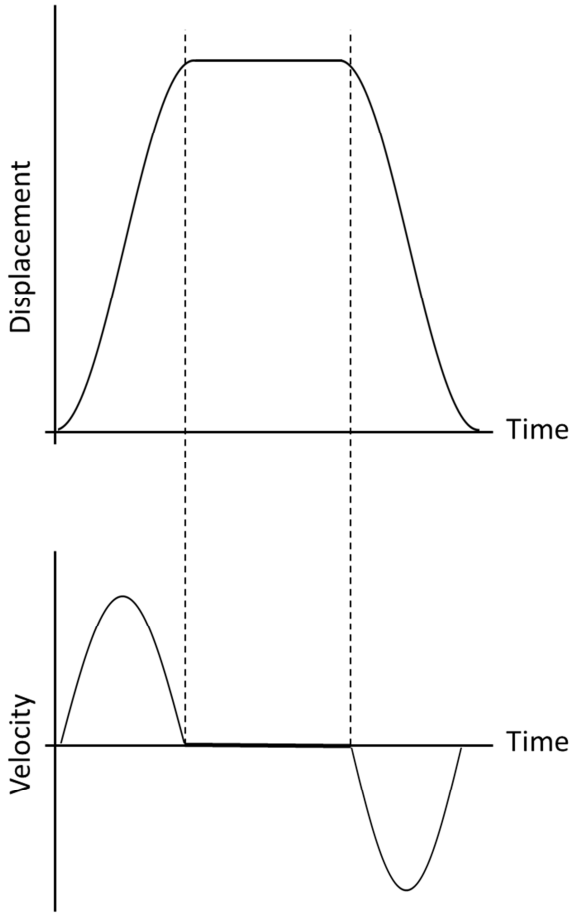

Figure 2-14 Jig cycle of an air-pulsed jig. Top: fluid displacement; bottom: fluid velocity (Burt, 1984)

a) Wave shape

The water motion in a jig is cyclic but rarely uniform. Different jig cycles are used in jigs, depending on the mechanism the manufacturer believes is the most important. Different jig cycles will promote or retard the effect of different mechanisms on the segregation process. (Burt, 1984)

Figure 2-15 shows two different jig cycles: (A) the Bird cycle and (B) the Meyer cycle. The Bird cycle starts with a swift upward velocity, high enough to lift the bed, followed by a pause to open the bed and ending with a swift reversal to suction. The cycle emphasises differential acceleration and interstitial trickling and minimises hindered settling.

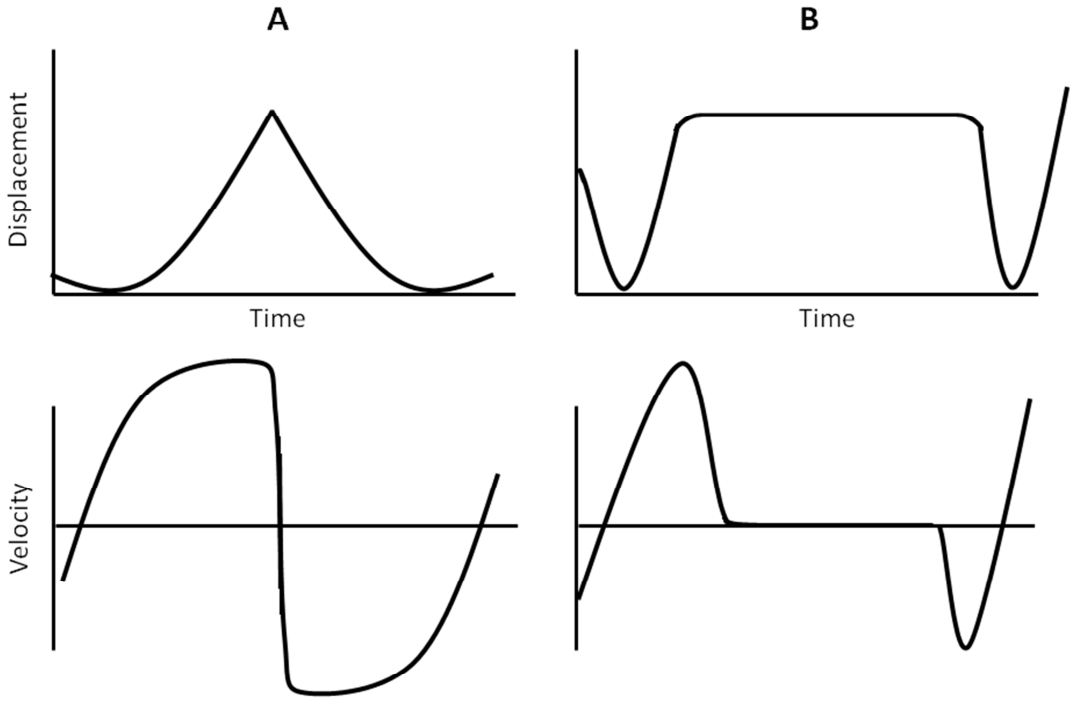

Figure 2-15 Two different types of jig cycles: (A) the Bird Cycle and (B) the Meyer Cycle (Burt, 1984)

The Meyer cycle accentuates the hindered settling mechanism by lifting the entire bed with a swift upstroke, thereafter keeping the water level constant, thus allowing hindered settling to take place.

b) Stroke frequency and amplitude

The required pulse cycle frequency is determined by the feed rate, feed size, feed density, and jig design. The jig cycle should be kept at a minimum time required for efficient segregation. Any cycle time longer than the minimum will negatively affect the capacity of the jig, since no separation takes place in the prolonged compacted state (Gupta & Yan, 2006).

Large jigs have high volumes of water that need to be pulsated. This high mass should be allowed to follow its natural pulsation motion and is given in equation 2.16 (Gupta & Yan, 2006).

$$T = 2t = 2\pi\sqrt{\frac{L}{g}} \qquad 2.16$$

Where: T = period of pulsation (time for the completion of one cycle) (s)

L = distance between the centre of suspension of the compound pendulum and its centre of oscillation (m)

Mishra and Mukherjee (2006) explain the role of frequency on the jig efficiency by comparing the system to a multi-component tuned mass damper system. When the pulse frequency approaches the natural frequency of a particle, the particle will start to resonate, giving it higher mobility. The natural frequency (ω_n) of a particle is given below in equation 2.17

$$\omega_n = \sqrt{k/m} \qquad 2.17$$

Where: k = spring stiffness

m = the particle mass

Figure 2-16 shows the vibration response to the pulse frequency of two different size classes. Operating at a specific frequency will result in the improved density classification of a specific size range, which will improve the overall efficiency.

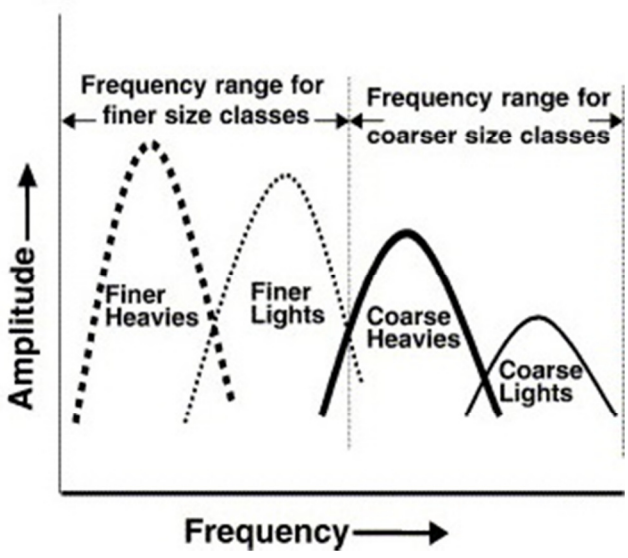

Figure 2-16 Frequency regimes of different groups of particles (Mishra and Mukherjee, 2006)

Amplitude and frequency are interrelated parameters in jigs, where the velocity profile follows a harmonic motion. The dilation of the jig bed is caused by the upward velocity, which is a function of both the amplitude and frequency.

Mishra and Mukherjee (2006) investigated the effect of the maximum water velocity on the jigging efficiency. Since the water velocity determines the fluidisation of the particles in the jig and the water velocity is not constant throughout the jigging cycle, Mishra and Mukherjee suggested that the maximum water velocity is a very important parameter that should be controlled. Through their testwork it was shown that different size particles require different maximum water velocities to achieve maximum separation efficiency. Figure 2-17 shows the results that were obtained with amplitudes of 7.6 cm, 8.9 cm, and 11.4 cm, and frequencies of 50, 65 and 75 cycles/min.

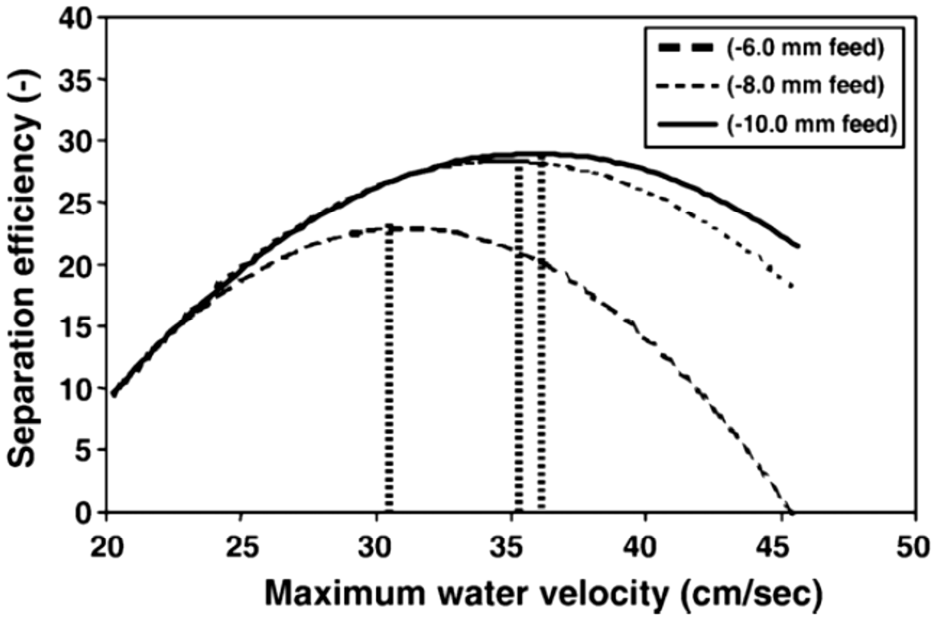

Figure 2-17 Separation efficiency values for three different feeds at different maximum water velocities (Mishra, 2006)

The relationship between the amplitude and the frequency can be simplified by equation 2.18 (Gupta & Yan, 2006).

$$v = \frac{Na\pi}{60} \qquad 2.18$$

Where: v = velocity required to suspend the mineral bed
a = amplitude of the stroke
N = number of strokes per minute

The minimum velocity of water required to lift the bed can be represented by the terminal velocity of the largest particle that needs to be lifted and is calculated by equation 2.12.

The operating parameters of certain industrial jigs are given in table 2-1 and it can be seen that, for larger particles, a large amplitude and low frequency is used.

Table 2-1 Operating Data For various jigs (Gupta and Yan, 2006)

Jig type	Particle size (mm)	Amplitude (mm)	Frequency (Hz)
Baum	5-200	30-40	30-60
Batac	0.5-100	30-60	40-60
Diaphragm	0.25-25	20-30	25-150
Diaphragm	0.2-10	10-15	150-200
Pulsator	0.1-5	3-6	200-400

2.7 Mineral density separator

The mineral density separator (MDS) is used as a design tool to characterise ores into density classes and to evaluate and optimise processing plants. Heavy-liquid separation cannot separate at densities higher than 4 SG and in some mineral applications, characterisation of ores with densities higher than 4 SG is required. The MDS has been successful in characterisation at densities higher than 4 SG (Van Wyk, 2004)

The testwork from a MDS generates information on the following relationships:

- recovery and grade or recovery and density at different residence times
- grade versus density at equilibrium
- recovery versus residence time at the required grade

2.7.1 Construction

The MDS is similar in construction to a diaphragm jig, with a cylindrical jigging chamber attached to the hutch with a rubber diaphragm. An air cylinder connected to the hutch provides the pulsating movement. Figure 2-18 shows a schematic representation of the MDS and its control.

Flow valves are used to control the up and down speeds of the air cylinder, while a directional control valve together with a PLC is used to switch the direction of the air cylinder and to introduce a hold time at the top and bottom position. Water can be added to the hutch to simulate hutch water additions in processing plants.

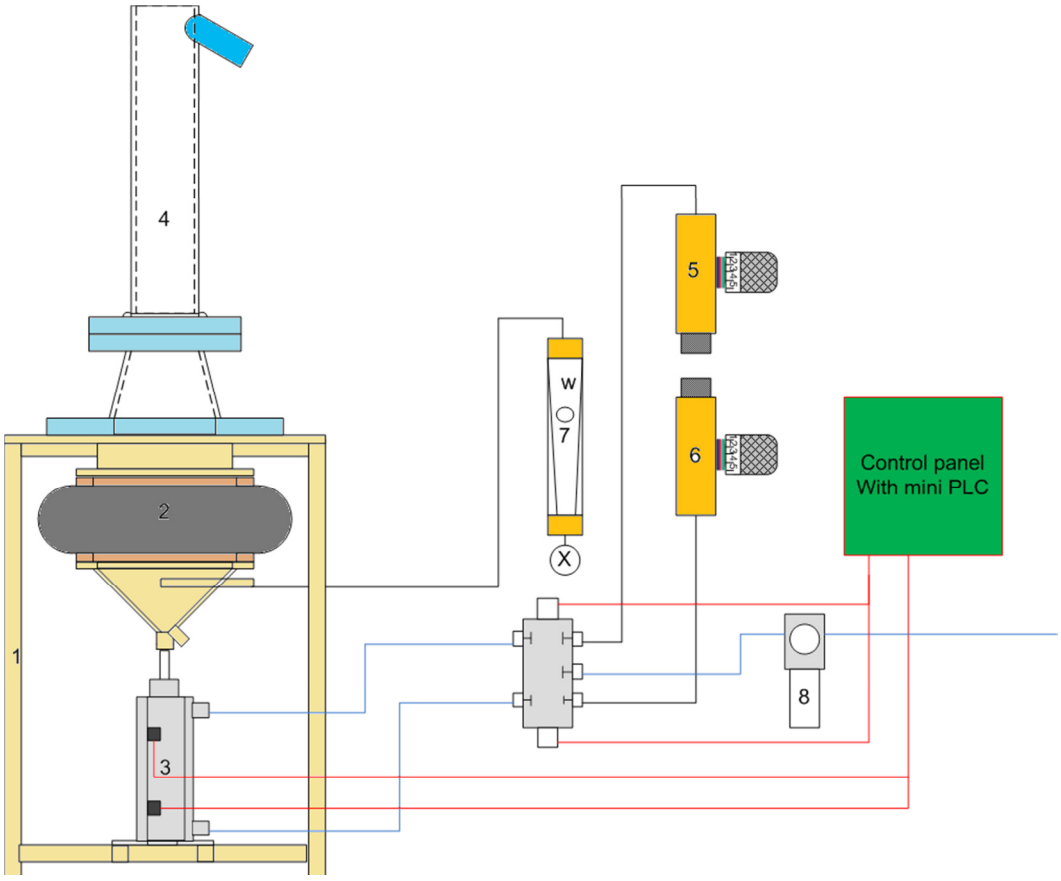

Figure 2-18 A Schematic representation of the MDS (Van Wyk, 2010)

Component list:

1. mini batch jig
2. bellows
3. air cylinder
4. product pulse chamber
5. upstroke flow-valve

6. down-stroke flow-valve
7. water flow-meter
8. pressure regulator
9. start stop control panel with mini PLC

2.7.2 Operating principles

a) Jig cycle

The jig cycle of the MDS is controlled by an air operated ram, which allows for the control of the different features of the wave. The general jig cycle used in the MDS is not harmonic, as seen with diaphragm jigs in Figure 2-12. A hold time can be set at the top and bottom of the stroke. Figure 2-19 shows the typical jig cycle of the MDS.

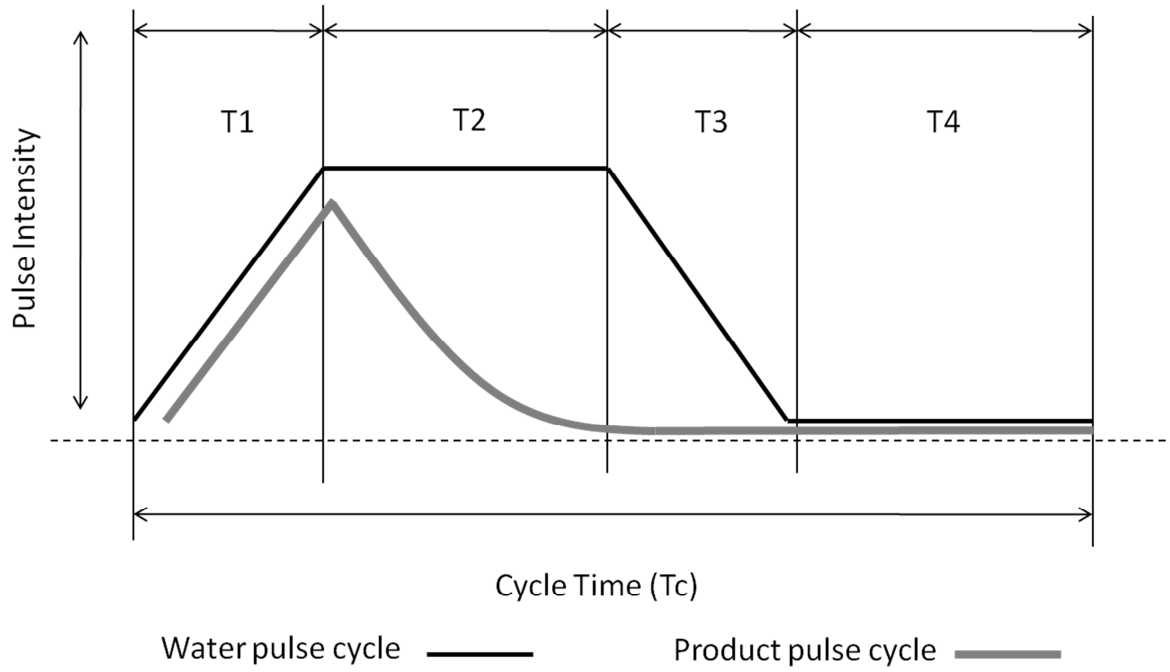

Figure 2-19 Water and product pulse cycle of MDS (Van Wyk, 2010)

Time 1 (T1):

Time 1 (T1) is the time during which the pneumatic ram moves upward, resulting in the upward displacement of water that lifts the particle bed. The upward velocity needs to be high enough to produce enough expansion of the bed. Lighter particles will wash past the heavy particles, loosening the bed. If the cylinder speed is too high, the separation during the upward stroke is reduced and turbulence can occur. The velocity of the ram is determined by the incoming pressure and the control valve that exhausts the air.

Time 2 (T2):

Time 2 (T2) is also referred to as the hold time and is a period of time that the pneumatic ram is kept at the top position, after the bed is fluidised to allow time for the particles to settle before the down stroke starts.

Time 3 (T3):

Time 3 (T3) is also known as the exhaust period and is the time it takes the air cylinder to return to its start position. The speed at which the cylinder moves is controlled by a flow control valve.

Time 4 (T4):

Time 4 (T4) is the run-out time; it is time the air cylinder remains stationary at the bottom position. The run-out time can be adjusted to ensure the same frequency of pulsation at different setting of T1 to T3.

The pulse height is the distance between the position of the material at the start of the pulse and the position of the material at the top of the pulse. A general rule of thumb is that the lift height should be approximately three times the average particle size of the sample. The lift should be high enough to cause sufficient expansion to allow for particle movement, but not so high as to cause turbulence. The lift height is controlled by both the upward speed of the air cylinder and the stroke length setting on the cylinder.

2.7.3 Particle size distribution in the MDS

Particle size and density play a role in the settling velocity of the particles. To increase the contribution of density on the separation, it is important to keep a narrow size distribution. As a general rule of thumb, the top to bottom size ratio should not be larger than 4:1 and in most cases a 3:1 ratio is used (Van Wyk, 2004).

2.8 Modelling of jigs

It is widely accepted that the modelling of jigging is very complex in nature (Mishra & Mehrotra, 1997; Rong & Lyman,1991; Steiner, 1996). That is why, although there have been plenty of attempts to model jigs, none of these models have reached maturity to such an extent that they are widely accepted and used. Figure 2-20 shows a summary of the variables of the jigging process.

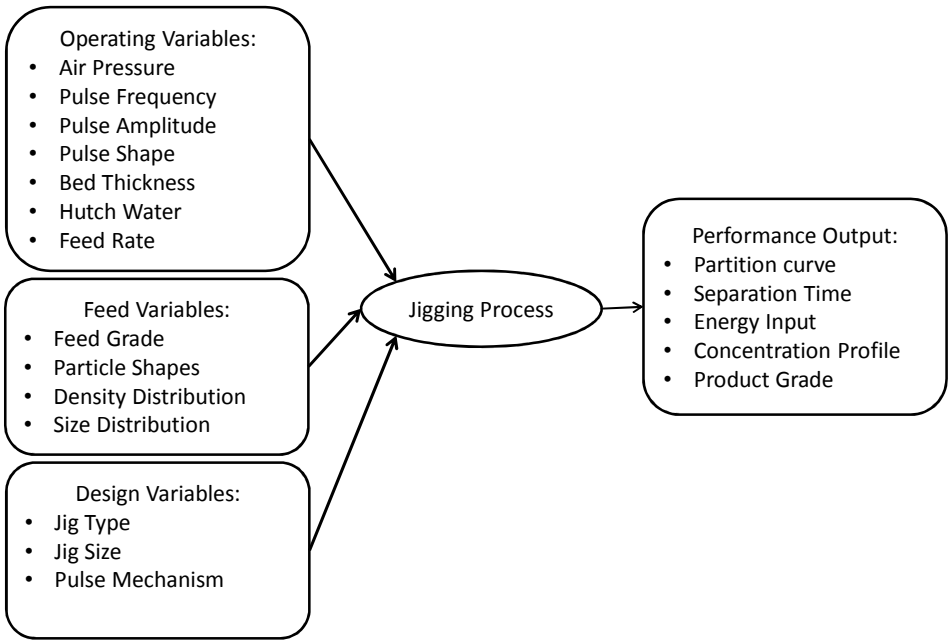

Figure 2-20 Variables of the jigging process (adapted from Mishra & Mehrotra,1997)

The approaches to the modelling can be classified into the following categories:

- classical theory (Gaudin, 1939)
- potential energy theory (Mayer, 1964; King 1987; Rao, 2007; Tavares, 1999)
- energy dissipation theory (Jinnouchi & Kawashima, 1978; Jinnouchi *et al.*, 1984; Rong & Lyman, 1993a,b)
- dispersion theory (Vetter *et al.*,1987)
- statistical analysis (Vinogradav *et al.*, 1968)
- empirical analysis (Karantzavelos & Frangicos, 1984; Rong & Lyman, 1991a,b)
- numerical modelling (Beck & Holtham,1993; Mishra & Mehrotra,1997; Viduka *et al.*, 2013)

The classical theory of jigging is based on the force balance done on a particle and the equations of motion. It is the basis for the popular mechanisms of jigging as explained by Gaudin (1939), and which is discussed in section 2.5.

Numerical models are closely tied in with the classical theory since they involve the solving of the forces on all of the individual particles in a jig. The contact forces between particles are also taken into account (Beck & Holtham, 1993). The major drawback of numerical modelling is the fact that it

requires lots of computing power and even with today's super computers, only simplified models of industrial scaled processes are solved. Since computer processing power is increasing and more complex algorithms are written, numerical modelling is becoming more popular in minerals processing. New approaches such as multiphase-modelling (Naude, 2010) has also emerged which can be used to simulate more complex systems.

With the energy dissipation theory, an energy balance is done across the jigging system, from the air inlet to the jigging bed. The system is reduced to a mechanical system (Jinnouchi & Kawashima, 1978; Jinnouchi *et al.*, 1984) with an energy storage element (the air chamber), frictional element (jigging screen), and inertial elements (water and jig bed). With this approach, the pressure in the air chamber can be related to the movement of the water and the particle bed.

The potential energy theory shows a lot of promise and is elaborated upon in the subsequent section.

2.8.1 Potential energy theory

The potential energy theory was first proposed by Mayer (1964), who suggested that the jigging process minimises the potential energy of the material bed in the jig. This results in the movement of heavier particles to the bottom, displacing lighter particles to the top of the bed.

King (1987, 2012) created a stratification model based on the Mayer's theory, and added a dispersive force that counteracts the stratification driven by the minimisation of potential energy, knowing that perfect stratification doesn't occur.

The change in potential energy of a particle moving over a discrete distance (Figure 2-21) can be calculated and is represented by equation 2.19 (King, 2012).

$$\Delta E = v_p g(\rho - \bar{\rho})\Delta H \qquad 2.19$$

Where the density of the particle is ρ, the average density of the bed is $\bar{\rho}$, the volume of the particle is v_p and the distance that the particle moves is ΔH.

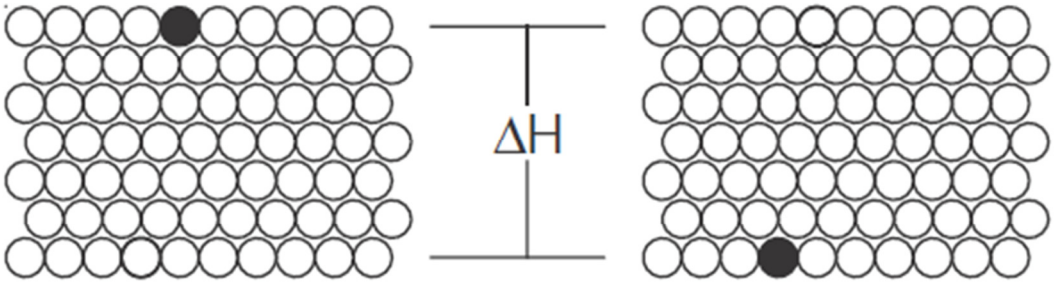

Figure 2-21 Change of potential energy when a heavy particle changes position in a bed of particles (King, 2012)

From equation 2.19, rate of change of the potential energy can be written as equation 2.20 (King, 2012).

$$\frac{dE}{dH} = v_p g(\rho - \bar{\rho}) \qquad 2.20$$

Particles move through the jig bed at a rate that is proportional to the energy gradient. This velocity is given by $u(dE/dH)$, where u is the specific mobility of the particle. Equation 2.21 (King, 2012) therefore represents the flux of a particle, with density ρ, through the jig bed and is dependent on the particles size, shape and bed expansion mechanism, but independent of particle density. C_p is the volumetric fraction of the particles with a density of ρ. The negative sign in the equation is there to correct for the fact that high density particles will move down the bed.

$$n_s = -C_p u \frac{dE}{dH} \qquad 2.21$$

Substituting equation 2.20 into equation 2.21, equation 2.22 (King, 2012) is obtained for the stratification flux.

$$n_s = -C_p u v_p g(\rho - \bar{\rho}) \qquad 2.22$$

According to King (2012), there is an opposing flux to the stratification flux and a Fickian type of equation (equation 2.23) is assumed.

$$n_D = -D\frac{dC_p}{dH} \qquad 2.23$$

The diffusion coefficient *D* is said to be a function of the particle shape, size and expansion mechanism. When the jig reaches steady state, it can be assumed that the diffusive flux (n_D) is equal to the stratification flux (n_s), resulting in equation 2.24 (King, 2012).

$$\frac{dC_p}{dH} = -\frac{uv_p g C_p}{D}(\rho - \bar{\rho}) \qquad 2.24$$

This equation can be re-written in terms of relative height ($h = H/H_b$) and a specific stratification constant (α).

$$\frac{dc_p}{dh} = -\propto C_p(\rho - \bar{\rho}(h)) \qquad 2.25$$

Solving equation 2.25 will provide the vertical concentration profile of the particles with a density of p. However, the equation should satisfy a set of conditions. The discrete form of the equation and its conditions in shown in equation 2.26 to 2.29 (King, 2012).

$$\frac{dC_i(h)}{dh} = -\propto C_i(\rho_i - \bar{\rho}(h)) \quad \text{for } i = 1,2,\ldots\ldots n \qquad 2.26$$

With

$$\bar{\rho}(h) = \sum_{i=1}^{n} C_i(h)\rho_i \qquad 2.27$$

$$\sum_{i=1}^{n} C_i(h) = 1 \qquad 2.28$$

for all *h*

$$C_i^f = \int_0^1 C_i(h)dh \qquad 2.29$$

for all *i*

The equations above can be solved for any number of particle classes. The solution of a hypothetical mixture is shown in Figure 2-22 and compared to the ideal stratification profile from Mayer's original theory.

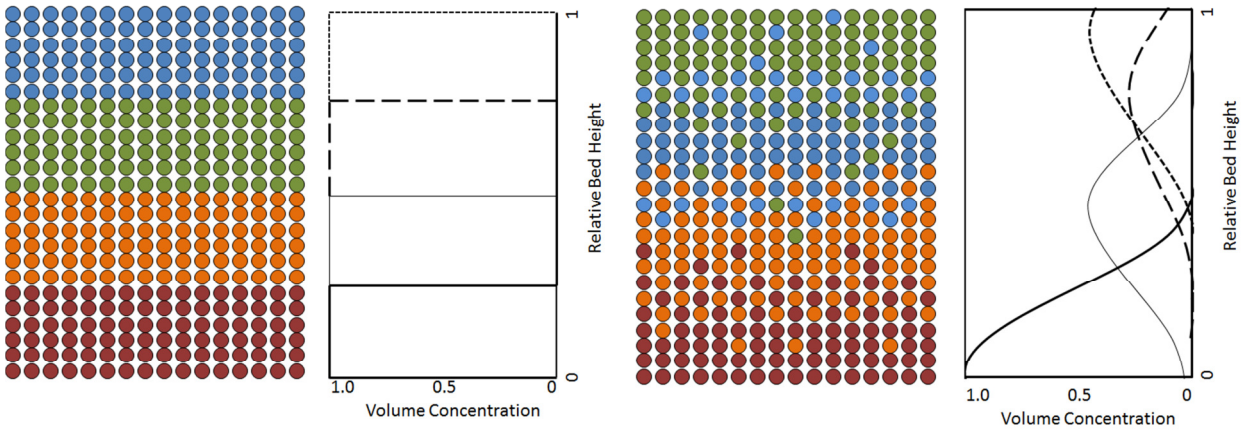

Figure 2-22 Stratification profiles (King, 2012). On the left hand side is the ideal Mayer stratification profile and on the right a simulation from the King model (particle densities = 1.35, 1.5, 1.7, 2.1 and α = 0.03)

The main drawback of King's model is the fact that it was developed for monosized particles. Rao (2007) developed the model further to include the effect of particle size. Equations 2.26 to 2.29 can be rewritten for bivariate species and is shown in equations 2.30 to 2.33 (Rao, 2007).

$$\frac{dC_{ij}(h)}{dh} = -\alpha_i C_{ij}(h)\left(\rho_j - \bar{\rho}(h)\right) \qquad 2.30$$

for $i = 1,2,\dots,n; j = 1,2,\dots,m.$

With

$$\bar{\rho}(h) = \sum_{i=1}^{n}\sum_{j=1}^{m} C_{ij}(h)\rho_j \qquad 2.31$$

$$\sum_{i=1}^{n}\sum_{j=1}^{m} C_{ij}(h) = 1 \qquad \text{for all } h \qquad 2.32$$

$$C_{ij}^{f} = \int_{0}^{1} C_{ij}(h)\, dh \qquad 2.33$$

for all ijth bivariate species

The stratification constant (α) is now assumed to have a power law relationship with size and is shown in equation 2.34 (Rao, 2007).

$$\alpha_i = A(d_i)^b \qquad 2.34$$

Where *A* and *b* are stratification parameters.

3 POSITRON EMISSION PARTICLE TRACKING

Positron emission particle tracking (PEPT) is a relatively new experimental technique that can be used to track a solid particle in a closed system without interfering with the particle's flow. It has been widely used to study granular flow inside engineering equipment. PEPT was adapted from positron emission tomography (PET), a technique mainly used in the medical industry for imaging the physiological processes.

3.1 Positron emission tomography

Positron emission tomography is a medical nuclear imaging technique that makes use of a radioactive tracer injected into the human body to study blood flow and organ function. The radioactive tracer can be detected by a PET camera and an image can be reconstructed.

PET is based on particles called positrons, which are generated by certain radioactive isotopes when they decay. These positrons were first discovered by Anderson (1932) when he observed that cosmic rays contain particles with the same mass as electrons. However, their behaviour in a strong magnetic field showed that these particles had a positive charge.

During positron decay of an isotope, a proton is converted to a neutron. The positive charge is then carried away as a positron. Equation 3.1 is the general equation for positron decay (Valk, 2005).

$$ {}^{A}_{Z}X \rightarrow {}_{Z+1}{}^{A}Y + {}^{0}_{1}\beta^{+} + v + Q(+e^{-}) \qquad 3.1 $$

Where *X* is the proton rich atom which undergoes decay and transforms to atom Y. This decay releases a positron (β^{+}), a neutrino (v), and energy (Q). The positron has high energy and moves away from the nucleus. As it moves, it loses kinetic energy by interaction with matter and will combine with an electron when it comes to rest.

When a positron combines with an electron outside the nucleus, they are annihilated, generating energy in the form of two photons (511 keV, γ-rays). The process can be seen in Figure 3-1 .To conserve momentum, these photons move in opposite directions (180° of each other) and it is this back-to-back photons that make it possible to pinpoint the location of a radioisotope.

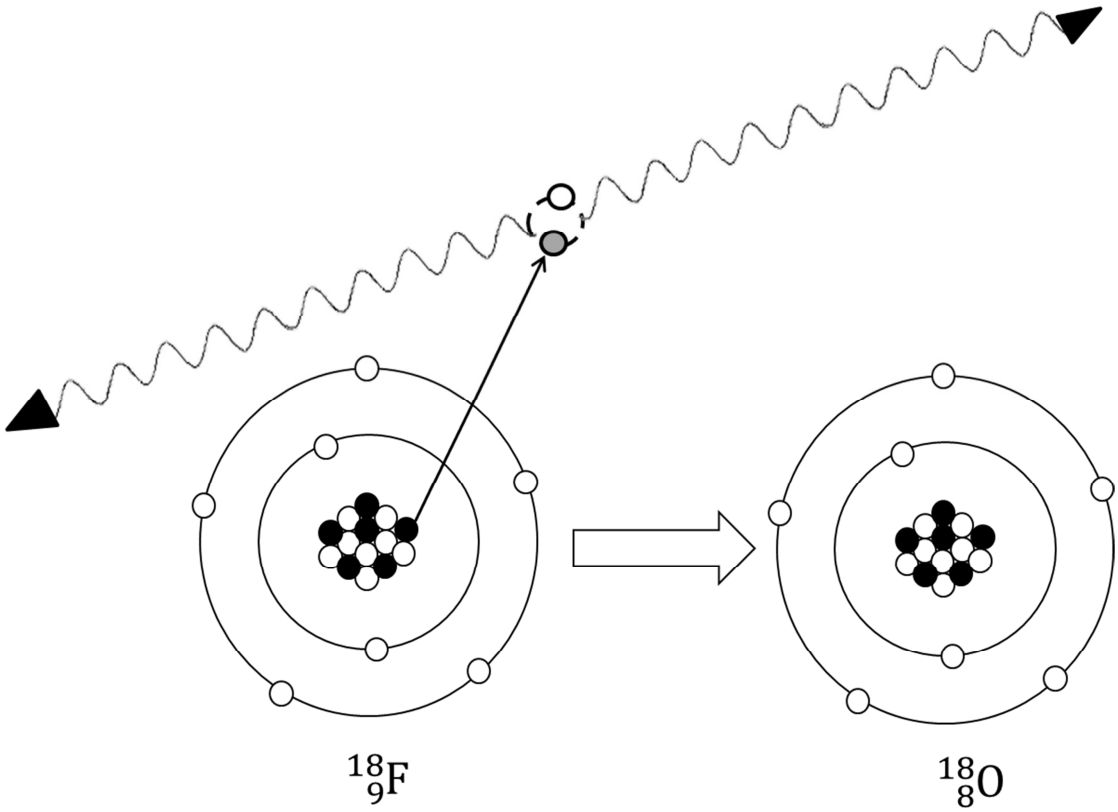

Figure 3-1 Positron annihilation process (Valk, 2005: 22)

High energy radiation will transfer energy to matter it comes into contact with. This interaction or energy transfer forms the basis of radiation detection. The objective of a detector is to convert the deposited energy to an electrical signal that can be measured. In the case of PET, scintillation detectors are used. Scintillation detectors make use of a crystal (scintillator) that, when hit by a high energy photon, will produce light. This light is amplified and converted to an electrical signal (Figure 3-2).

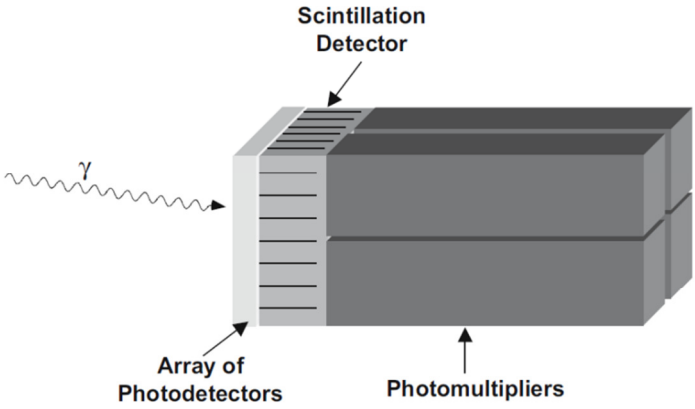

Figure 3-2 Scintillation detector used in PET (Valk, 2005: 38)

To detect the position of a PET tracer, an array of detectors can be used in different configurations. Figure 3-3 shows four popular configuration styles used in PET. The two back-to-back photons will be detected by two different detectors and is assumed to be from the same annihilation, if both are detected within a short time of each other (coincidence window), as shown in Figure 3-4. The position of the annihilation is then assumed to be on a straight line between the two detectors. This line is referred to as the line of response (LOR). A tracer's position can then be obtained by finding the spot where these LOR's cross, as shown in figure 3-5.

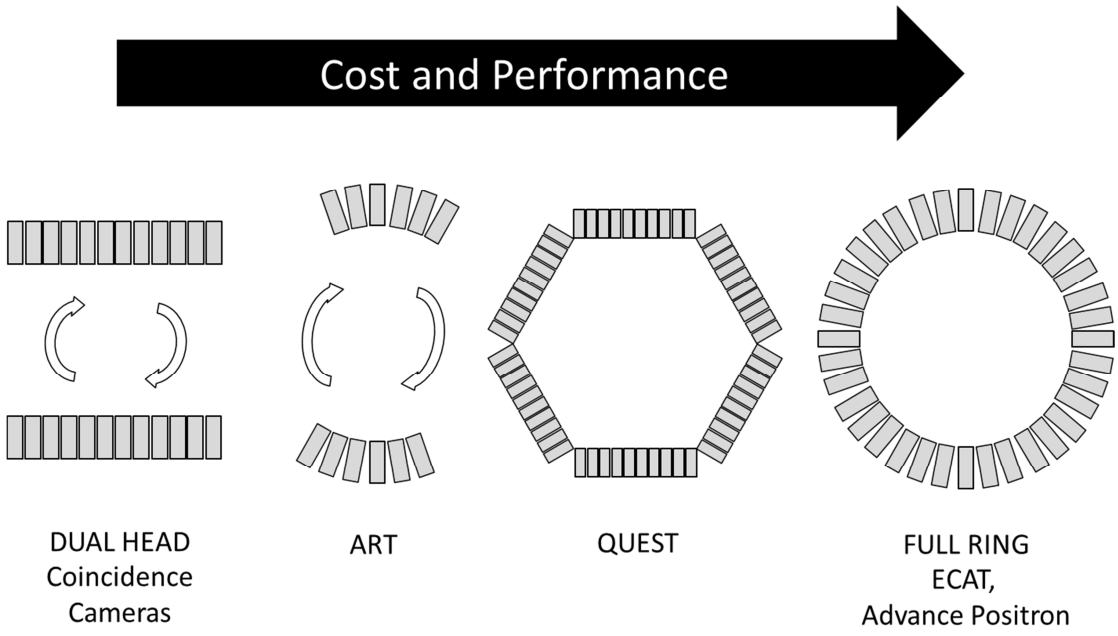

Figure 3-3 Configurations of detectors (Phelps & Cherry, 1998)

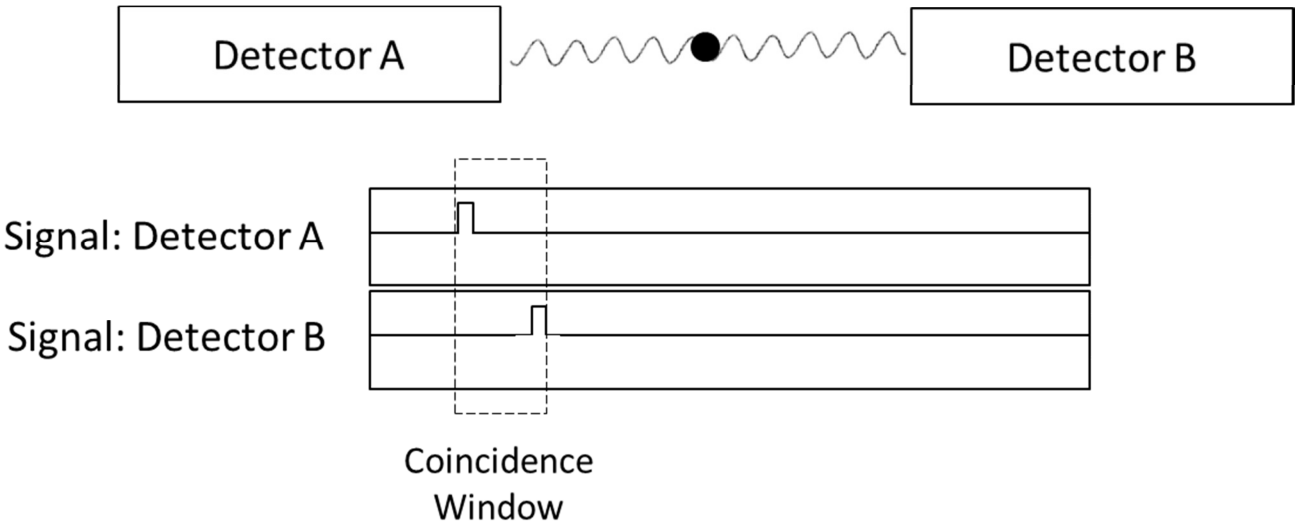

Figure 3-4 Coincedence window (Valk, 2005: 35). A small coincedence window is set to ensure that the detection of a single event is possible

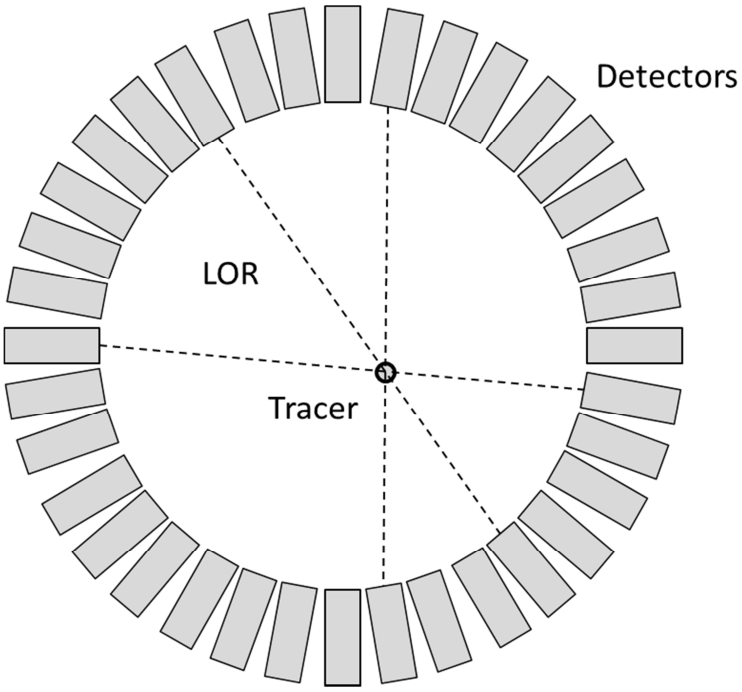

Figure 3-5 Ring configuration of detector. The position of a tracer can be determined by determining where the LOR's cross (Valk, 2005)

The radioactive tracers used for PET are artificially generated in a cyclotron, by exposing a stable element to a beam of accelerated particles (protons). A list of radioactive isotopes that are relevant to PET is given in table 3-1. A lot of the radionuclides used in PET studies are short lived and a cyclotron needs to be in close proximity to the PET (Muehllehner & Karp, 2006).

Table 3-1 List of radionuclides relevant to PET (Phelps, 2006: 4)

Radionuclide	*Half-life*
^{11}C	20.4 min
^{13}N	9.97 min
^{15}O	122 s
^{18}F	109.8 min
^{22}Na	2.6 y
^{62}Cu	9.74 min
^{64}Cu	12.7 h
^{68}Ga	67.6 min
^{76}Br	16.2 h
^{82}Rb	1.27 min
^{124}I	4.17 d

3.2 Positron emission particle tracking

In the mid-eighties PET was considered for industrial applications, due to the penetrating power of the 511 keV photons (Hawkesworth *et al.*, 1986). One such technique was to label a single particle with a radioisotope to study particulate flow (Bemrose *et al.*, 1988), and was subsequently named positron emission particle tracking (PEPT). Tracking the position of a single point requires a lot less LOR's compared to what is needed in PET to track a volume. PEPT allows for the measurement of particles moving up to 10 m/s at a sampling rate of 1KHz in three dimensions, with an accuracy of approximately 0.5 mm (Leadbeater *et al.*, 2012).

Thousands of LOR's are produces each second, and some of these can be corrupt due to scattering and simultaneous events. These are filtered out with the PEPT algorithm and particle trajectories are smoothed during post processing. The activity of the tracer should be high enough to produce enough LOR's to accurately measure its position (Volkwyn *et al.* ,2011). Figure 3-6 shows the effect of tracer activity on the accuracy of tracer position.

Different methods have been developed to label a particle with a radioactive tracer. The main objective with labelling is to make sure that the activation of the particle is high enough for accurate measurement (Fan *et al.*, 2006). Techniques for labelling include direct activation, ion exchange and surface modification.

Direct activation is used to produce tracers larger than 1 mm. A glass or ceramic bead is placed in the path of a proton beam to convert some of the oxygen atoms to ^{18}F radioisotope atoms. Radioisotope ^{18}F can also be produced from purified water and can then be adsorbed into materials either through ion-exchange or surface adsorption (Fan *et al.*, 2006).

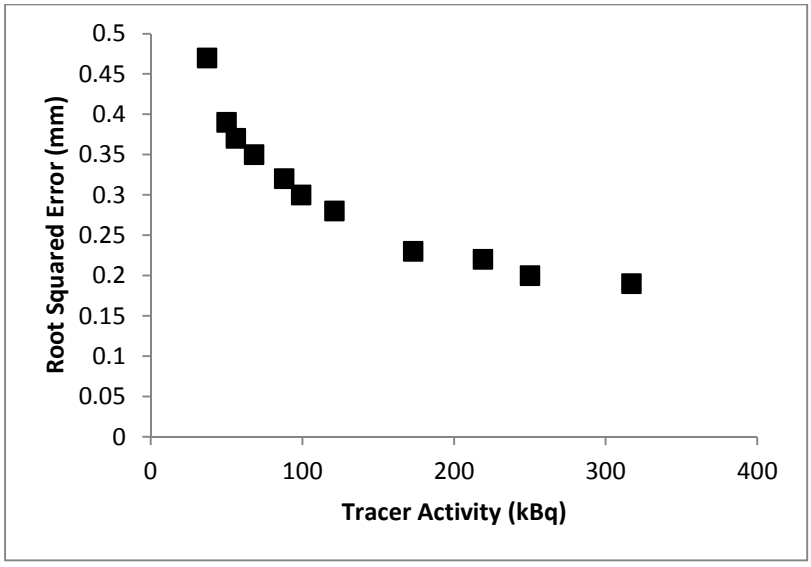

Figure 3-6 Root squared error as a function of tracer activity (Volkwyn *et al.*, 2011)

3.3 Positron emission particle tracking applications

Positron emission particle tracking has been used to study a number of industrial processes related to minerals processing. Comminution processes have received a lot of attention, including tumbling mills (Bbosa *et al.*, 2011; Volkwyn *et al.*, 2011), vertical stirred mills (Conway-Baker *et al.*, 2002), and an IsaMill (Van der Westhuizen *et al.*, 2011). Other processes include mixing vessels (Barigou, 2004; Marigo *et al.*, 2013; Mihailova *et al.*, 2015), and fluidised beds (Van de Velden *et al.*, 2008; Laverman *et al.*, 2012). Beneficiation equipment includes flotation cells (Waters *et al.*, 2008; Fan *et al.*, 2009; Cole *et al.*, 2010) , spiral concentrators (Waters *et al.*, 2012), and jigs (Williams *et al.*, 1997,1998).

Doing a search on Scopus.com for the exact phrase “positron emission particle tracking” in an article’s title or abstract, shows that there is an increase in the number of articles relating to PEPT. The numbers can be seen in Figure 3-7.

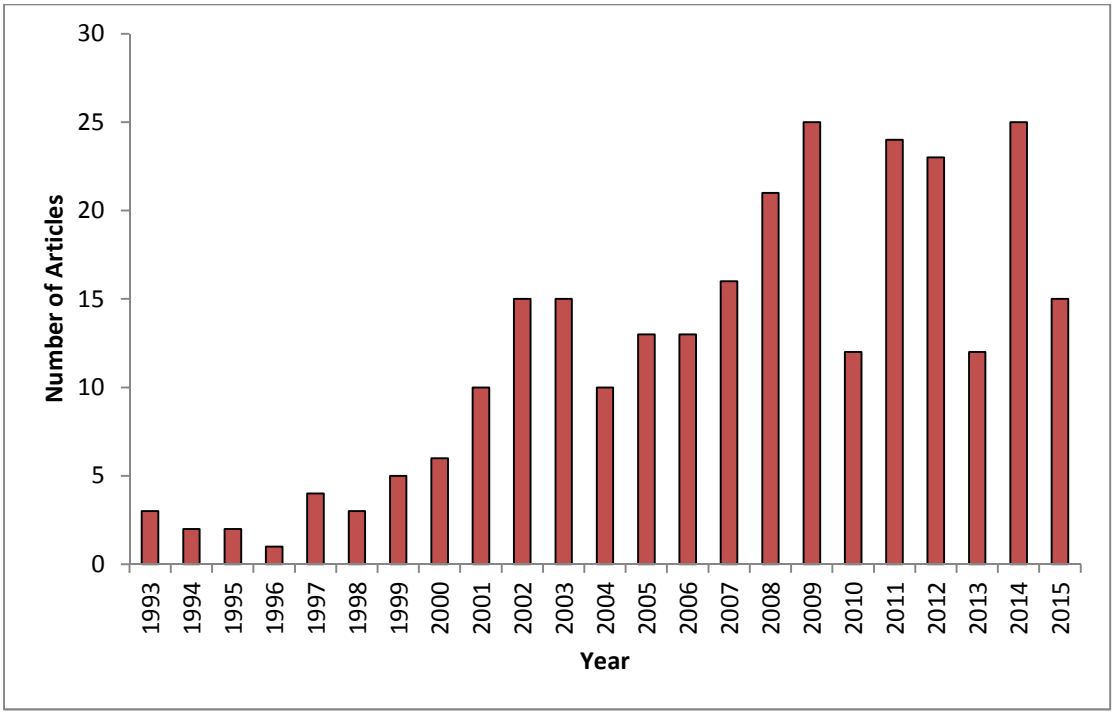

Figure 3-7 Number of articles with the exact string "positron emission particle tracking" in their title or abstract searched on Scopus.com, last checked 31/08/2015

3.4 Positron emission particle tracking jigging applications

In the early years of PEPT, Williams *et al*. (1997, 1998) studied the particle trajectory in a lab scale jig using PEPT. Due to the cost and nature of the experiments, only a small number of tests were conducted (34). The jig bed material was made up of 2 mm glass beads and the particles that were tracked, were glass (2 and 4mm) and copper (4 mm) beads. William *et al*. showed that new patterns that were previously unobtainable, could be revealed with the use of PEPT, such as circular flow patterns that were observed in the jig shown in Figure 3-8.

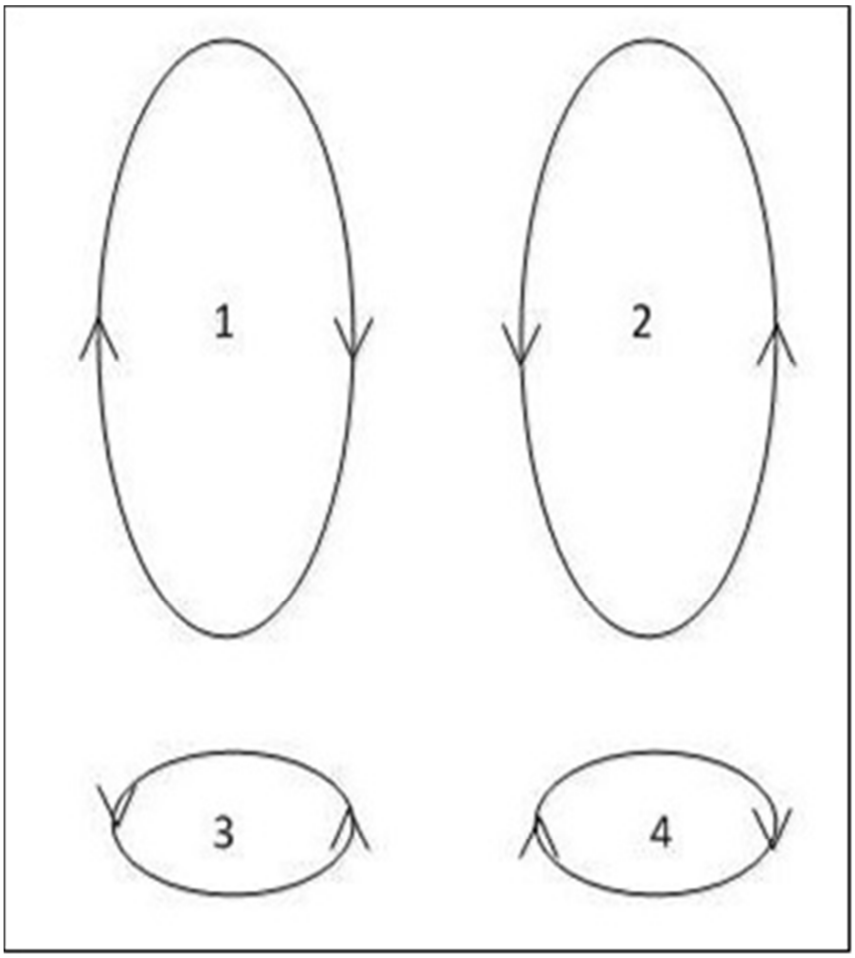

Figure 3-8 Circular flow pattern observed in the XY plane (Williams *et al.*, 1997)

4 METHODOLOGY

4.1 Introduction

The experimental plan was developed to study the effect that a particle's size, density and shape have on its movement through a jig. Since PEPT was the analysis technique, a special lab scale jig was constructed that could fit into the scanning area of the PEPT scanner. The testwork was split into two sections, the initial testwork, conducted with real iron ore tracer particles, and the main body of the testwork, conducted with artificial tracers.

Operating parameters such as the jig pulse and the bed depth were not changed during this study, due to the large number of tests this would require and the limited time that was available on the PEPT setup. Instead, optimum predetermined settings were chosen to ensure sufficient stratification.

4.2 Sample preparation

4.2.1 Bed material

For the initial testwork with the real iron ore tracers, only one jig bed was tested. The bed that was selected was sampled from the medium (-8+3 mm) jig feed stockpile at the Anglo Kumba Iron Ore Sishen plant and used as is. Enough material was used to fill the jig bed to a level of 15 cm.

For the testwork conducted with the artificial tracers, more control was needed over the properties of the jig beds that were used. The Anglo Kumba Iron Ore Sishen plant, medium jig feed, was used as the starting material from which the beds were prepared. The material was first screened into a -8+5 mm size fraction, after which it was separated into density fractions with the use of a dense medium cone and ferrosilicon as a medium (a method discussed in the appendix, section 10.1.1). Three beds were prepared by using medium densities of 3.6, 3.8 and 4 g/cm^3 and collecting the floats in each case.

To get an idea of the density uniformity of the different beds that were prepared, they were subjected to a batch jig analysis. During the batch jig analysis the sample were jigged in a lab scale batch jig for 10 minutes. The stratified bed was then removed in eight layers and the density of each layer was measured with the Archimedes method, which is discussed in the appendix, section 10.1.2. The batch jig is not the ideal method to determine a density distribution, but due to the fact that

conventional heavy liquid separation could not be used for these high densities, jigging was used to estimate the density distribution.

For the artificial tracer testwork, an additional three artificial jig beds were created to obtain beds with homogenous densities. Initial testwork showed that a mixture of silica and ferrosilicon could be used in conjunction with a polyester resin to produce material within the density range of interest and of high strength. Mixtures with different ratios of ferrosilicon, silica and polyester resin were mixed and cast into slabs. The slabs, once dried, were then crushed and screened to produce particles with a size range between 5 mm and 8 mm. A spherical particle bed was made by taking the polyester mixture and rolling the particles into 8 mm spheres. A summary of the artificial particle beds is given in table 4-1.

Table 4-1 The three artificial bed materials that were prepared for the PEPT tests

	Bed Density (g/cm^3)
1 (ASA)	2.1
2 (ASB)	4.1
Spherical	3.6

4.2.2 Tracer particles

The real iron ore tracers were selected from a group of particles that were carefully characterised for a previous study conducted by Anglo Kumba Iron Ore. The four tracers that were selected for the study are shown in table 4-2. The idea behind the selection was to test a high density, a low density, and “near density” particles.

Table 4-2 Properties of the real iron ore tracers

Tracer	1	2	3	4
Density (SG)	5.01	2.92	4.11	3.99
Weight (g)	1.20	0.63	1.24	1.51
Size (mm)	6.53	5.39	4.15	6.65
Shape	Equant	Tabular	Bladed	Equant

As size, density and shape of the tracer particles were the main variables for this study, it was decided to manufacture the tracer particles instead of selecting natural iron ore particles for the bulk of the testwork.

Mixtures with different ratios of ferrosilicon, silica and polyester resin were mixed and cast into slabs approximately 20 mm thick. The ratio of ferrosilicon, silica and resin was initially calculated to produce specific densities. However, the calculations could not account for the formation of micro bubbles in the mixture. The approach was then changed, whereby a whole range of tracer mixtures were produced and the densities of these mixtures measured after they hardened. Tracers were then cut from the slabs with a diamond blade tile cutter and finishing was done using a mini grinder with a diamond blade.

Shapes selected for the tracers were cubic, elongated, and flat. Figure 4-1 shows the three different shapes schematically and indicates the ratios that were associated with each shape. Tracers ranging in size from 6 mm to 12 mm and densities ranging from 2.5 g/cm^3 to 4.2 g/cm^3 were made. A few round tracers were made by grinding cubes into spheres with the mini grinder.

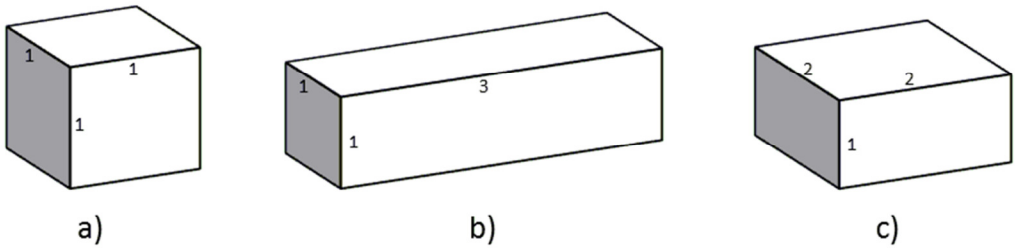

Figure 4-1 Tracer particle shapes

Table 4-3 Properties of the planned tracers

	Size (mm)			Shape	Density
	L	W	H		
1	8			Sphere	Low
2	8			Sphere	Medium
3	12	12	12	Cubic	Medium
4	10	10	10	Cubic	Medium
5	8	8	8	Cubic	Medium
6	10	10	10	Cubic	High
7	10	10	10	Cubic	Low
8	6	6	6	Cubic	Medium
9	12.5	4.2	4.2	Elongated	Medium
10	7.6	7.6	3.8	Flat	Medium
11	6	6	6	Cubic	High
12	12.5	4.2	4.2	Elongated	High
13	7.6	7.6	3.8	Flat	High
14	6	6	6	Cubic	Low
15	12.5	4.2	4.2	Elongated	Low
16	7.6	7.6	3.8	Flat	Low

4.3 Lab scale jig

The jig used for the experiments was designed around the available space inside the PEPT scanner, which has a working cylindrical area with a diameter of 82 cm and a depth of 23.4 cm. The design of the jig was based on the mineral density separator (section 2.7). The jig design is shown schematically in Figure 4-2. A magnetic actuator was used to compress and expand a rubber bellow below the jigging chamber and generated a water pulse. The magnetic actuator allowed for careful control of the jig's pulse and was driven by a controller specifically designed for this application.

The actuator's controller was set up to generate a trapezium-shaped pulse, as shown in figure 4-3. There were six settings that could be changes on the pulse shape, which included the speed of the up stroke, the wait time at the top of the stroke, the speed of the down stroke, the wait time at the bottom of the stroke, the height of the pulse, and the run time. In this study, the evaluation of the jig setting was not part of the scope and an optimal pulse was selected with preliminary test runs to ensure sufficient stratification. These settings are shown in table 4-4.

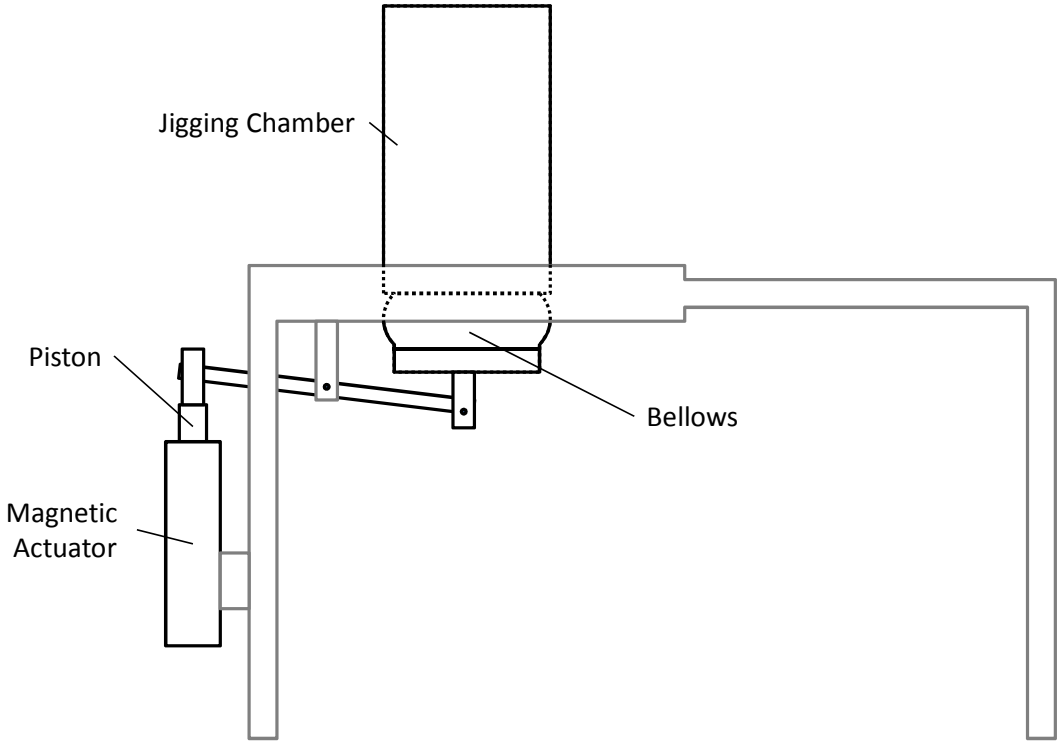

Figure 4-2 The lab scale batch jig shown schematically

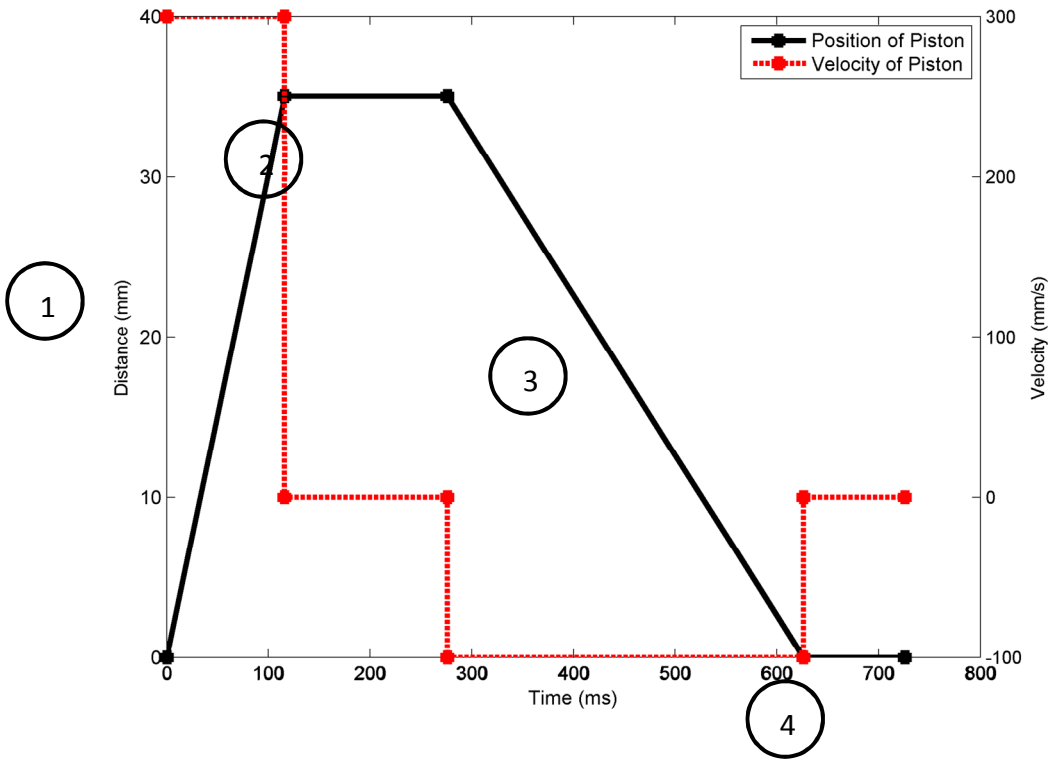

Figure 4-3 The pulse shape of the lab scale jig

Table 4-4 Batch jig pulse settings

Setting	Value
Up stroke (1)	300 mm/s
Upper hold time (2)	160 ms
Down stroke (3)	100 mm/s
Lower hold time (4)	100 ms
Pulse height	35 mm
Run time	10 min

4.4 Positron emission particle tracking

The facilities used for the PEPT studies were iThemba Laboratory for Accelerator Based Sciences (UCT) in Faure, Cape Town, South Africa. The PET scanner the facility uses for PEPT is the EXACT3D (CTI/Siemens 966) PET scanner. At the time of its original installation at the Hammersmith Hospital in 1995, it was the most sensitive PET scanner ever built (Spinks *et al.*, 1996). The scanner consists of 48 rings of detector elements and there are 576 detectors per ring (27 648 detectors in total). The ring array of detectors can be seen in figure 4-4. The detectors are of the BGO (Bismuth germinate) block type, which is used in the majority of commercial PET Scanners (Cherry *et al.*, 1995). The detector arrangement of the scanner allows for a cylindrical viewing area with an 82 cm diameter and a 23.4 cm depth.

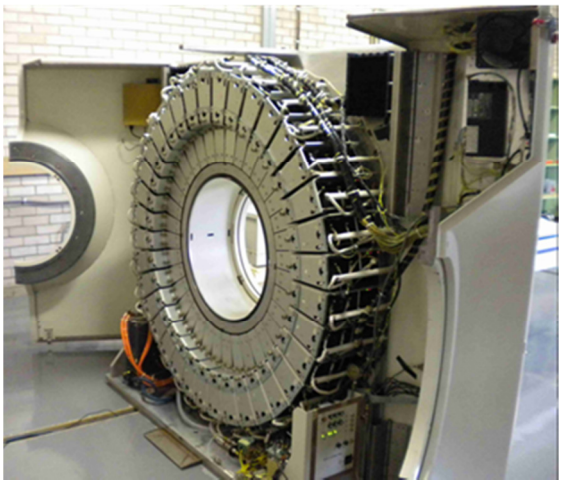

Figure 4-4, EXACT3D (CTI/Siemens 966) PET scanner, showing the ring array of detectors (http://www.pept.uct.ac.za, 2014)

4.5 Labelling of tracers

From the possible tracer materials that were discussed in section 3.1, PEPT at the University of Cape Town generally makes use of a ^{68}Ga positron emitting radio isotope, which was used for this project. The ions exchange method is used to produce a small ^{68}Ga loaded resin particle, which is then sealed inside a small hole that is drilled into the tracer particles. A ^{68}Ga generator, similar to the one seen in Figure 4-5, is used to produce the ^{68}Ga isotopes. The generator contains ^{68}Ge ($t_{1/2}$ = 270.9 d) ions, which decays to ^{68}Ga ($t_{1/2}$ = 67.7 min), which in turn decays to ^{68}Zn (Stable). The ^{68}Ga is eluted selectively from the ^{68}Ge with hydrochloric acid and is then absorbed into an ion exchange resin (Cole *et al.*, 2012).

Figure 4-5 Gallium 68 generator (http://s15.a2zinc.net, 2014)

4.6 PEPT algorithm

As discussed in section 3.1, the traced particle emits two back-to-back gamma rays, which are detected by the ring array of detectors. If the two rays are detected within a very small time window, it is assumed that they originated from the same event. A line of response (LOR) can be drawn between the two points where the impacts of the gamma rays were detected. Thousands of these LORs are generated every second. Figure 4-6 shows the LORs generated during a fraction of a millisecond. An algorithm is used to discard the 'false' LORs and to best estimate the position of the

traces at a specific time by minimising the sum of the distances of the tracer to the LORs (Cole *et al.*, 2012).

The current algorithm requires the specification of *N* and *f*. *N* is the number of LORs that are grouped together to determine the location at a specific time, and *f* the percentage of LORs used in the triangulation of the location. The higher the activity of a tracer, the larger *N* can be, resulting in higher accuracy. If there is a large amount of corrupted LORs, a lower *f* should be chosen to reject the corrupted LORs, as these LORs will decrease the accuracy.

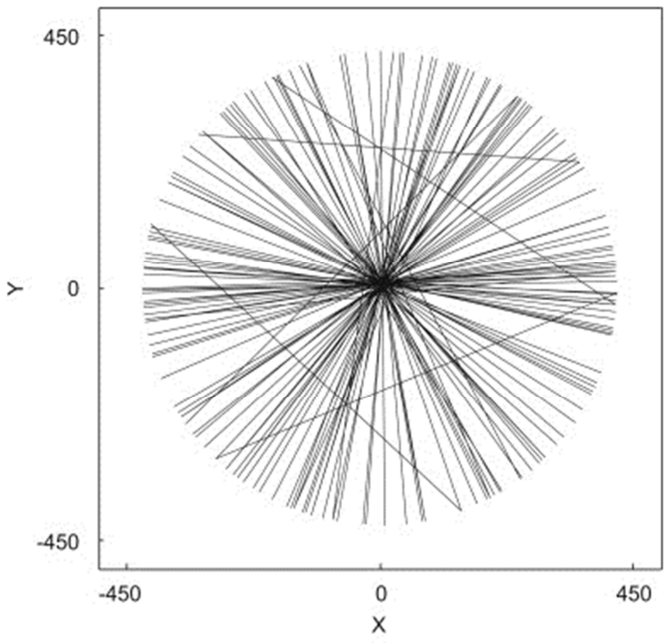

Figure 4-6 Lines of response generated during PEPT (Chang *et al.*, 2011)

The activity of the tracer and the choice of *N* will also determine the time interval at which locations are determined. For example, if the detection rate is high (high activity of the tracer) at 20 000 (s-1) and an *N* of 400 is chosen, the number of locations per second will be 50.

4.7 Experimental setup

The PEPT scanner has a cylindrical working area in which the jigging chamber should be during test runs. To have access to the jigging chamber for exchanging the jig bed and recovering the tracer, the jigging chamber cannot be inside of the scanner's working area. The jig is therefore designed to slide in and out of the working area. The batch jig and the PEPT scanner can be seen in experimental

setup in Figure 4-7. To remove the bed material from the jig, a vacuum cleaner was adapted to allow for the removal of the particles with suction.

The amount of testwork that was done was limited by the time it takes for a single test run, the time a tracer lasts and the fact that only two tracers can be labelled in a day. Each test was run for 10 minutes and the resetting of the bed and the tracer took a minimum of 10 minutes. Therefore, the total time for a test run was approximately 20 minutes. At that rate, it was possible to run eight tests with each tracer before the activity of the tracers dropped too low.

Figure 4-7 The PEPT-jig experimental setup

The PEPT experimental procedure consisted of the following steps:

- The bed material was thoroughly mixed and added to the jigging chamber.
- The tracer, which was stored in in a lead container, was added to the jig bed, its position depending on the specific experimental conditions.
- Water was added to the jig to a fixed level above the jig bed.
- The jig was moved into position, ensuring the jigging chamber was within the field of view of the scanner.
- The scanner was turned on, after which the jig was started.
- The timer for the scanner was set to the same length as the timer on the jig.
- After the run was complete, the jig was moved out of the scanner to gain access.
- The water was drained and the bed material removed with a vacuum system.
- Whilst the bed material was removed, the tracer was recovered and placed into the lead container to limit radioactive exposure.
- The bed material and the water were checked for radioactive contamination.

4.8 Experimental design

4.8.1 Initial testwork with real iron ore tracers

The main purpose of the initial testwork with the real iron ore particles was to determine if PEPT was a legitimate technique to use with iron ore. It was unknown if the gamma rays would penetrate a bed of iron ore without being distorted.

Four tracer particles were selected, as discussed in section 4.2.2 These tracers were placed at different positions in the particle bed for each experiment, and for each test the tracers were tracked for 10 minutes. These tests were also repeated four times. A total of 33 tests were conducted and lists of these tests with the conditions are shown in the appendix, section 10.2.

4.8.2 Artificial tracer particle testwork

The nature of the PEPT testwork was such that all the testwork on a specific tracer needed to be completed before the activity of the tracer drops below a value that might compromise the results. Therefore it was not possible to fully randomise the test variables to possibly eliminate systematic errors. Eight test runs were performed with one tracer and a typical set of tests involved testing four different bed materials per tracer. The full list of experiments is shown in table 4-5.

Table 4-5 Eight test runs performed with tracer 1

Tracer 1	
Test run	**Bed material**
1	ASA
2	3.6
3	3.8
4	ASB
5	ASA
6	3.6
7	3.8
8	ASB

The limit on the number of tracers that could be tested (18) didn't allow for a full factorial design. Table 4-3 shows the properties of the tracers that were selected. To capture the effect of size, cubic tracers with the same density and sizes of 6, 8, 10, 12 mm were tested. To test the effect of density three 10 mm and three 6 mm tracers with varying densities were used. Three sets of tracers, each

containing a flat, elongated and cubic tracer, were used to evaluate the effect of shape on the movement of the tracers.

4.8.3 Secondary flow inside the jig

Williams *et al*. (1998) showed that there is a secondary flow inside a batch jig that might affect its performance. These secondary flow patterns were determined and are discussed in section 3.4. Initial testwork done for this project also showed some anomalies that might be linked to the secondary flow, which required further investigation.

Table 4-6 Test runs to investigate secondary flow

Tracer	Bed material	Run time
8 mm, 2.5 SG, spherical (glass beads)	8 mm, 2.5 SG, spherical (glass beads)	2 hours
8 mm, 3.6 SG, spherical	8 mm, 3.6 SG, spherical	2 hours

4.9 Coding of the stratification model

Visual basic for applications (VBA) is a programming language that can control objects in a specific application, such as Microsoft Excel or Word. VBA was chosen as the programming language due to the easy integration with Excel. Another big advantage is that the model can be compiled as an add-in and can then be installed and run on any computer that has Microsoft Excel installed.

Two functions were written as part of the model. The first function sets up a form that allows the user to enter all of the inputs. When the code is run, it asks for the number of density and size fractions and uses the information to set up a table. An example of the table can be seen in Figure 4-8. The blue and green blocks must be completed by the user.

	2	Size			
3		0.001	0.005	A	b
Density	1300	0.25	0.25	290	1.5
	1500	0.15	0.15	Relative T	1
	2650	0.1	0.1		

Figure 4-8 The data-input table for the model

After the table is filled with data, the main function is run and the model is solved, generating stratification profiles similar to what is seen in Figure 2-22 for all of the size and density fractions. From this data recovery curves can be generated by selecting a specific cut height. The code for the two functions can be seen in the appendix, section 10.4 and 10.5.

The model is based on the work done by Rao *et al*. (2007): solving equation 2.30 by adjusting the density profile whilst subjected to the constraints in equation 2.31 to 2.33, a method similar to what was used by King (2012).

4.10 Safety

The PEPT division at the iThemba Laboratory, where the testwork was done, complies strictly to the nuclear safety regulations to ensure that its guests and employees are protected against radiation. Each person that works in the laboratory has to wear a monitor that detects and records the amount of radiation that a person receives. These numbers are recorded to ensure that the dose limits are not exceeded. The dose limits are determined by a regulatory organisation. The typical dose limit for a radiation worker is 20 mSv per year and for a member of the public 2.5 mSv per year (IWQS, 2002). According to the National Nuclear Regulatory Act (1999), all radiation facilities should adopt the ALARA (As Low as Reasonably Achievable) principle to ensure that its employees are not unnecessarily exposed to any radiation.

During the duration of the testwork, the following steps were taken to ensure the lowest possible exposure to radioactivity:

- Lab coats and gloves were worn at all times and a new set of gloves were worn every time the lab was entered.
- The radioactive tracer was kept in a lead container when not in use and only added to the jig at the last possible moment before the test commenced.
- No unnecessary time was spent in the lab while the test was run.
- A radiation scan was done every time before exiting the lab to ensure no contamination.

5 RESULTS AND DISCUSSIONS

5.1 Bed material

As discussed in section 4.2.1, the bed material for the artificial testwork was prepared by splitting the sample into density fractions, using a dense medium cone. Table 5-1 shows the average densities measured (Archimedes method) for the three samples. It can be seen that the densities are higher than that of the medium densities, when in fact the densities should be lower. It is suspected that the upwards flow in the dense medium cone applies a drag force to the particles, resulting in higher density particles in the floats.

Table 5-1 The three bed material samples that were prepared for the PEPT tests

	Medium density (g/cm^3)	Average bed density (g/cm^3)
1	3.6	3.7
2	3.8	4.3
3	4	4.6

Figure 5-1 shows the density distribution for the beds, as determined with the batch jig test discussed in section 4.2.1. It is seen that the density separation that was done with the dense medium cone is far from ideal, with the density fractions wider than the 0.2 g/cm^3 and overlapping.

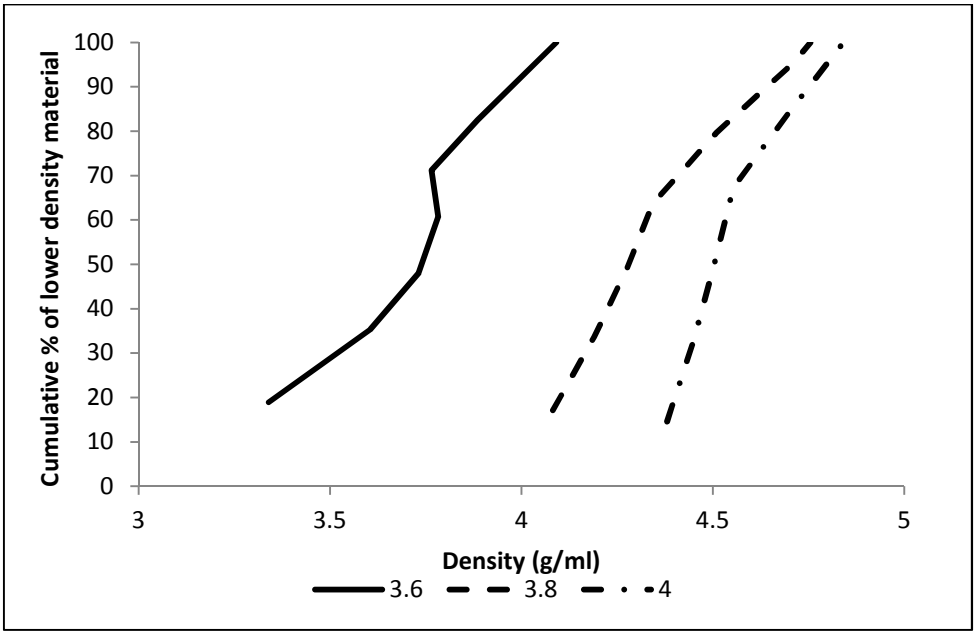

Figure 5-1 Density distribution of bed material, determined by a batch jig

The particle size distribution (PSD) of each of the beds was also determined with a sieve shaker and is shown in figure 5-2. The PSD's for all three of the beds were almost exactly the same with approximately 80% of the material between 3 mm and 8 mm in size.

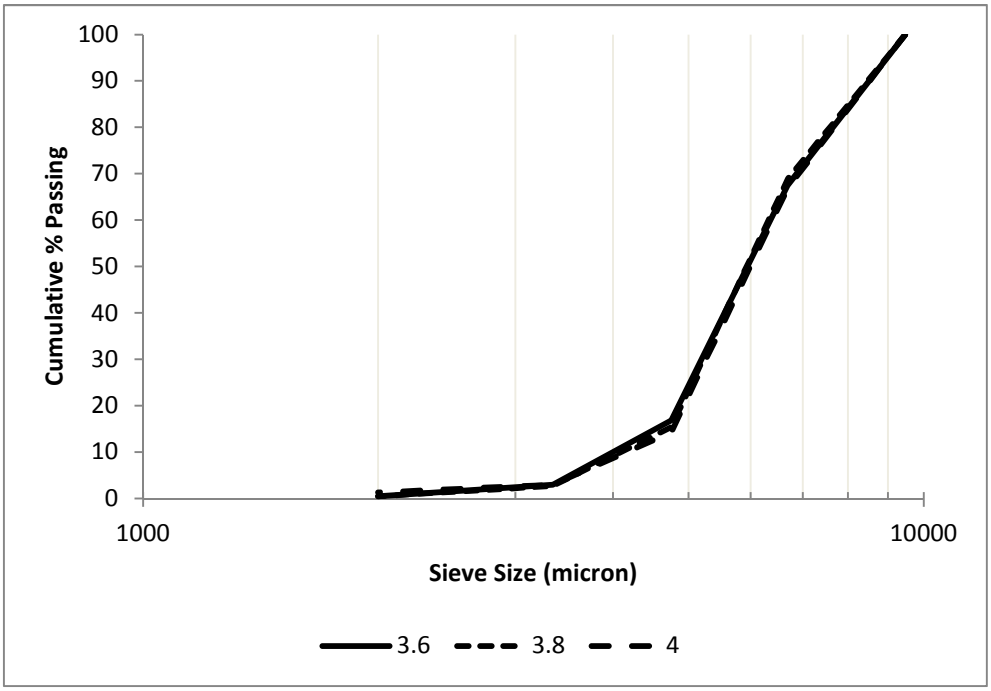

Figure 5-2 Particle size distributions of bed material

5.2 Tracer particles

The manufacturing of the tracer particles proved to be more challenging than expected. A specific batch prepared to obtain a specific density almost never attained that density. This was most likely due to the formation of micro bubbles, resulting from the release of gas during the curing process of the resin. To overcome this problem, it was decided to make numerous different mixes and to measure the density of each of the mixes after they have hardened. From these different mixes, several were chosen from which the tracers were cut. The densities of each of the tracers were individually determined, not merely assuming that the density is the same as the material from which the tracer was cut. Table 5-2 shows the properties of the tracers that were produced, and Figure 5-3 shows a photo of these tracers.

.

Table 5-2 Properties of prepared tracers

	Size (mm)			Shape	Density (g/cm^3)
	L	W	H		
1	8			Sphere	2.5
2	8			Sphere	3.6
3	12.6	11.7	12.1	Cubic	3.96
4	10.6	11	9.7	Cubic	3.97
5	7.6	7.6	7.7	Cubic	3.93
6	10.2	9.7	9.2	Cubic	4.2
7	9.3	10.1	10.3	Cubic	3.76
8	14.9	4	4.8	Elongated	3.93
9	8.1	8.5	4	Flat	3.91
10	6.5	6.5	6.6	Cubic	3.89
11	15.7	4	3.7	Elongated	3.94
12	7.8	7.8	4	Flat	3.91
13	6.2	6.2	6.3	Cubic	3.99
14	16.3	3.9	3.9	Elongated	3.73
15	8	8.2	3.8	Flat	3.73
16	6.3	6.3	6.3	Cubic	3.72
17	8			Sphere	3.72
18	8.2			Sphere	3.48

Figure 5-3 Photo of the artificial tracers used for the PEPT jigging experiments

5.3 Analysis of data

As discussed in sections 4.6, the algorithm used for the triangulation of the tracer affects the accuracy and resolution of interpretation. For the entire set of tests conducted, it was found that an *N* (number of events per slice) of 250 and an *f* (fraction of events used) of 0.3 delivered a good result with high accuracy and high resolution. On average, these settings gave a sample rate of 50 locations per second, depending on the position and the activity of the tracer.

The triangulated data represents the three dimensional position versus time for the tracer particle. Figure 5-4 shows the X, Y and Z coordinates versus time for a single PEPT test (tracer density of 5.01 g/cm^3). The X and Z are the horizontal coordinates and the Y the vertical coordinate. The data can be compiled in such a way to show the trajectory a particle followed over a specific time in three dimensions. Figure 5-5 shows such an example, showing the tracer particle (density of 5.01 g/cm^3) moving down the jig bed. Once it reaches the bottom, there is some movement around the centre as time progresses.

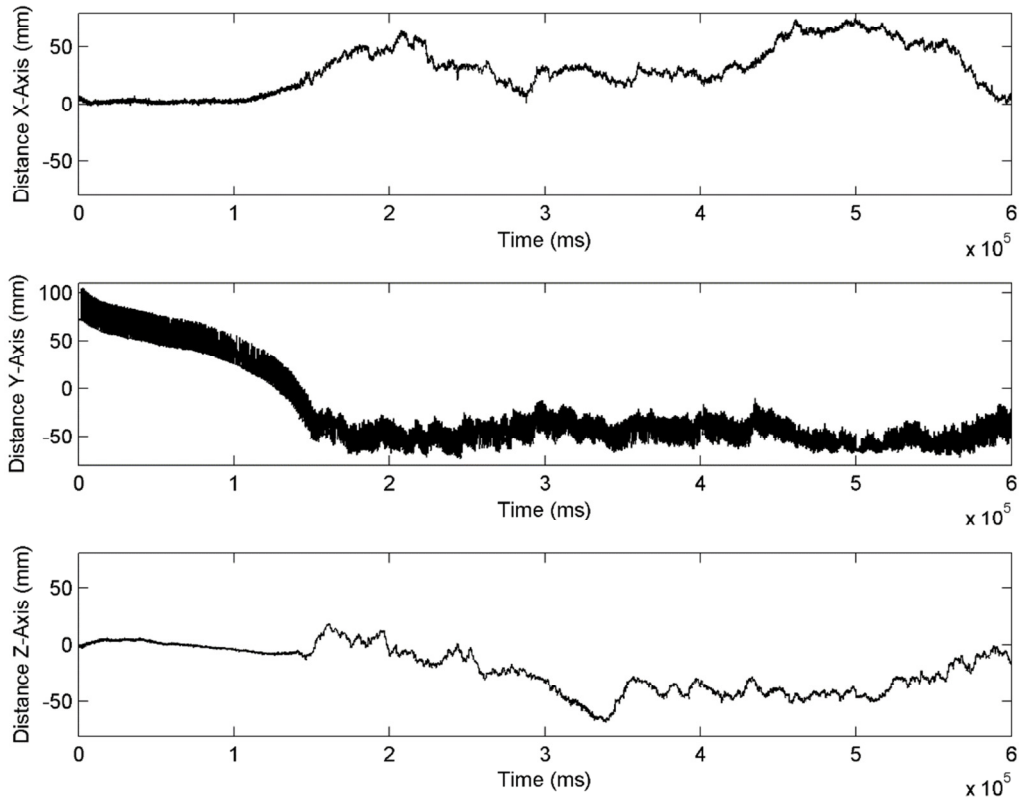

Figure 5-4, The X, Y and Z position as a function of time, for a particle with a density of 5.01 g/cm^3

For most of the discussion, the focus will be on the vertical movement of the tracer, since it is the differential movement of particles in the vertical direction that brings about separation. Furthermore, the vertical trajectory can give vital information regarding the pulse shape, rate of movement and the final position of the particle being traced.

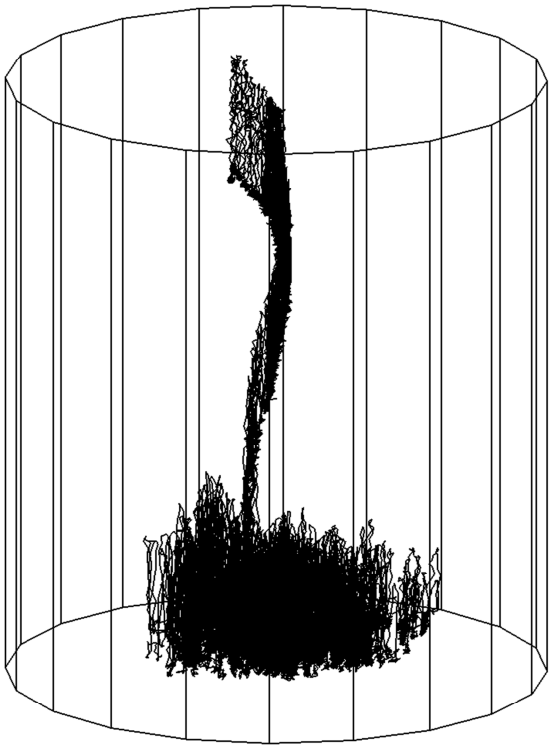

Figure 5-5 3D representation of the particles trajectory during a test, for a particle with a density of 5.01 g/cm^3

From fgure 5-4 it is clear that the movement along the Y-axis (vertical) is significantly different compared to the X- and Z-axis. It appears that the Y-axis has a wide 'band' in which the particle moves. This band is in fact the individual pulses of the tracer which is very close to one another and appears as a solid band on this time scale. The movement of the tracers through the bed is also clearly visible from its start at the top of the bed to its resting position at the bottom. The bottom of the band is the position of the tracer at the bottom of the pulse and would be the position of the tracer when the jig is stopped at any specific time. A routine to extract this baseline was therefore written in Matlab and this baseline was used to represent the position of the tracer in the Y-axis when the

movement of the tracer through the jig bed was studied. This baseline can be seen in figure 5-6. Using the baseline makes it easier to compare the vertical movement of the tracer particles for the different tests.

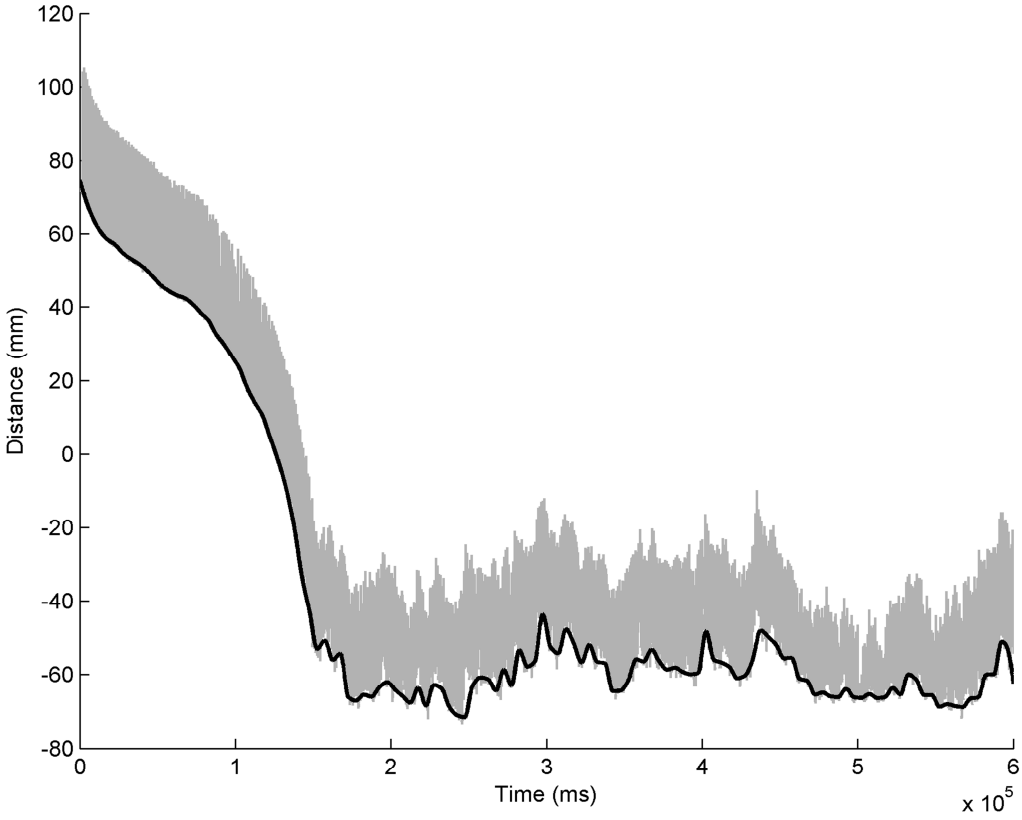

Figure 5-6 The vertical coordinate, with the baseline highlighted

5.4 Accuracy and repeatability

There is an inherent uncertainty in the PEPT measurements that exists due to the randomness of positron annihilation, detection of gamma rays and the nature of the triangulation algorithm (Cole *et al.*, 2012). It is therefore important to investigate whether PEPT will have sufficient accuracy for a specific application. A test was conducted to determine the spatial resolution for a particle at rest in the jig bed. A tracer particle was placed in the centre of the jig bed and a measurement was taken without pulsation of the jig. The result of this test is shown in figure 5-7 and it can be seen that the measurement does contain noise.

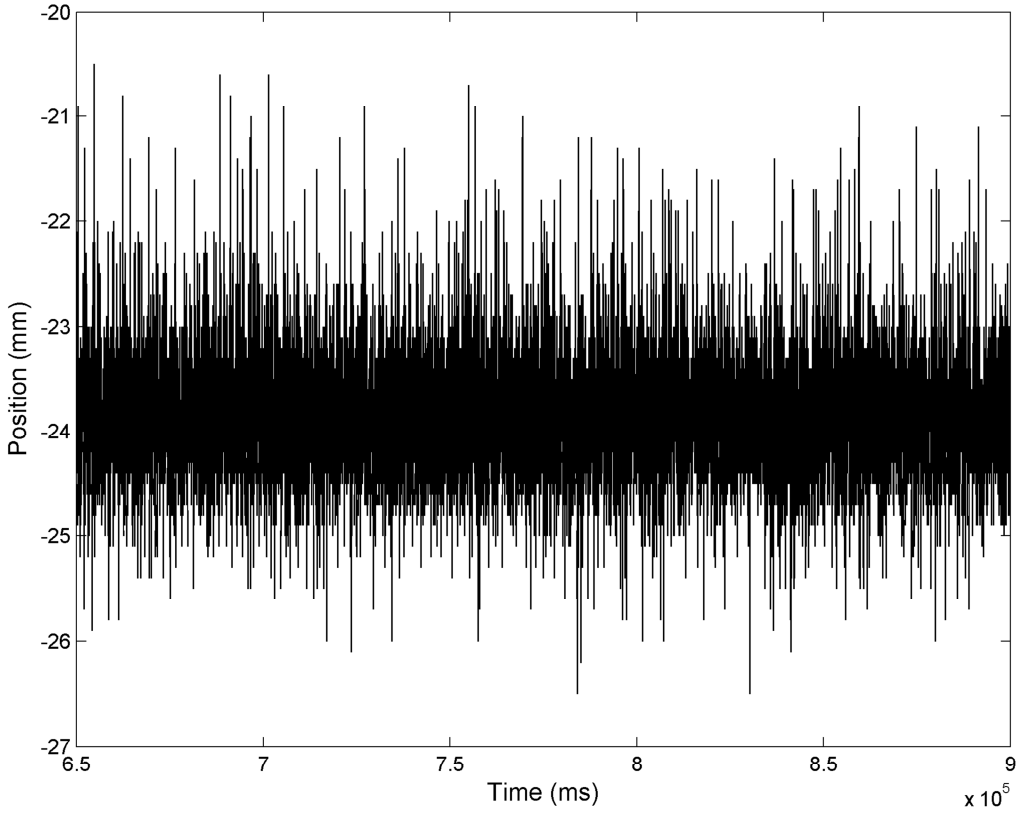

Figure 5-7 Vertical position vs. time for a stationary particle

Figure 5-8 shows the cumulative probability curves for each of the three axis of the tracer's position from this test. The slope of the curve represents the distribution of the data – the steeper the slope the narrower the distribution of data. The curve shows that there is a wider distribution of the data points along the X-axis, compared to that of the Y- and Z-axis. This lower accuracy is due to the arrangement of the detectors (Parker *et al.*, 1997).

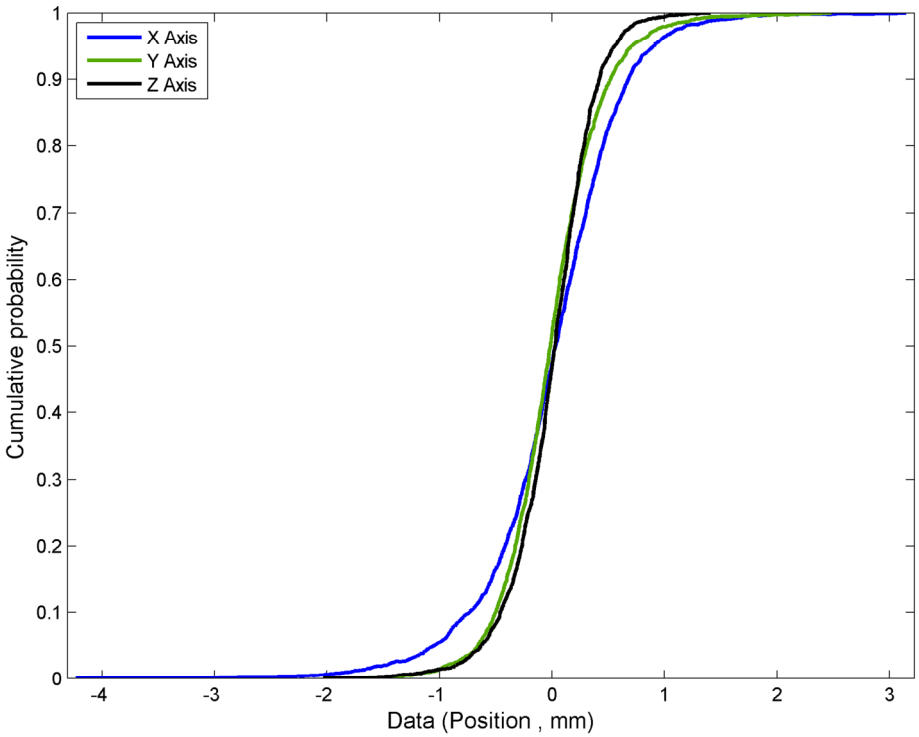

Figure 5-8 Normalised cumulative probability curve of an accuracy test for the three axis directions

Although there is a wide range of up to 7.4 mm on the X-axis, the standard deviation is fairly low (0.6 mm). With such a low standard deviation, the average position calculated will be a good representation of the actual position of the tracer. Table 5-3 shows the mean, standard deviation and the range for the three different axes. The accuracy will depend on the amount of points used to calculate the average position at a specific position.

Table 5-3 Standard deviations for the accuracy test

	Mean	Standard deviation	Range
X-axis	15.59	0.62	7.37
Y-axis	-23.9	0.44	3.83
Z-axis	7.36	0.37	3.44

All of the tests that were conducted in the initial testwork set with the real iron ore tracers were repeated four times to get an idea of what the repeatability would be. One such set of test repeats is shown in Figure 5-9 and 5-10. These two Figures are baseline plots (baseline discussed in section 5-3). Figure 5-9 shows the position of the tracer along the vertical axis for the entire time of the test run

(600 seconds), and Figure 5-10 shows the position of the tracers along the vertical axis for the first 60 seconds of the test run.

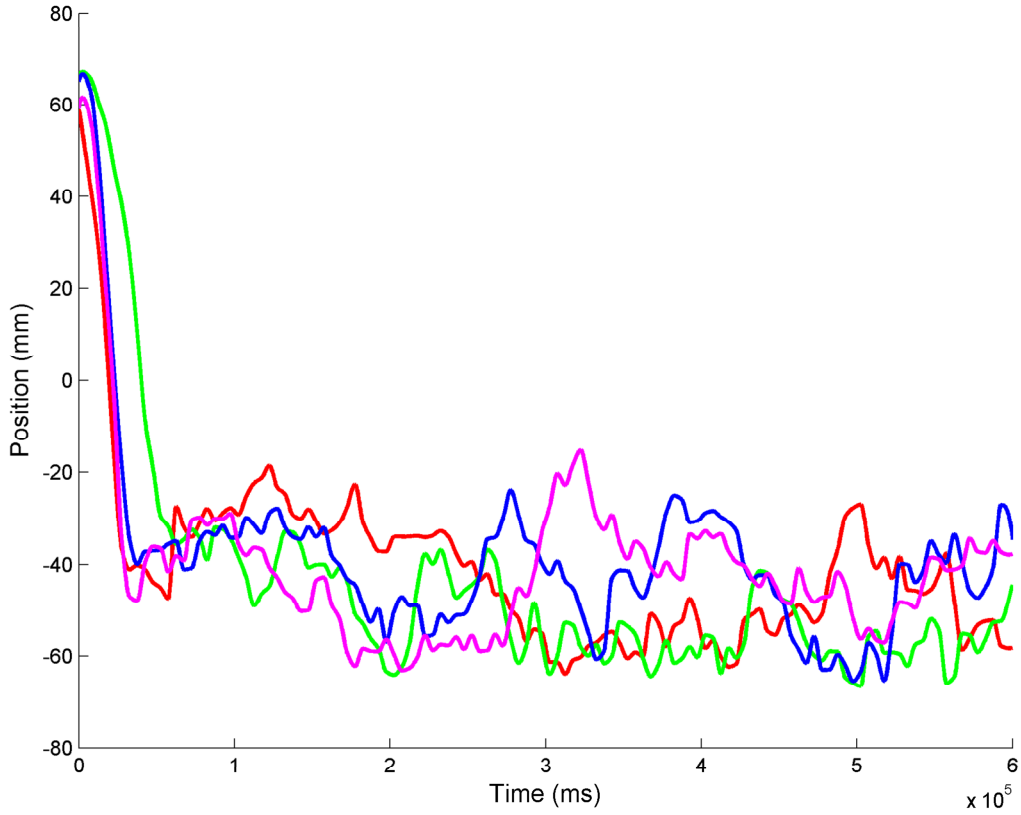

Figure 5-9 Initial testwork repeats (particle density 4.11 g/cm^3)

Perfect repeatability of the trajectories of the particles is not expected, since each trajectory is driven by hundreds of pulses of the jig, each with complex hydrodynamics. Therefore, from the resulting trajectory curves (figure 5-9 and 5-10), repeatability is not great, but the trends observed are similar. Three of the trajectories for the initial movement of the tracer (Figure 5-10) are very close to each other. The position range in which the tracers end up (-20 to -60 in Figure 5.9) is the same for all four of the test runs.

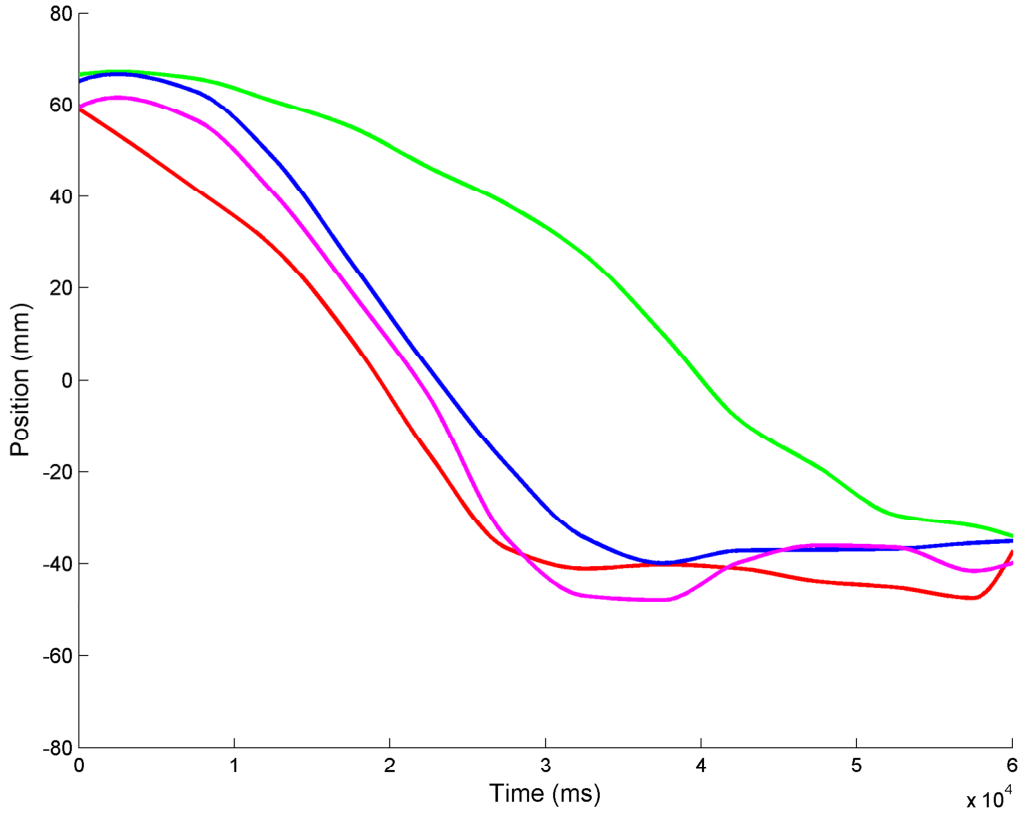

Figure 5-10 Initial testwork repeats (particle density 4.11 g/cm^3)

5.5 Tracer trajectory during a single pulse

Zooming in on the horizontal coordinate (Figure 5-11), it can be seen that the resolution from the measurement is high enough to see the tracer's movement through an individual pulse of the jig. The movement of a tracer particle during a single pulse is shown in Figure 5-12. Superimposed over the graph is the actual movement of the piston that generates the water pulse. The particle moves up during the upward pulse and immediately starts to move down when the piston is halted at the top of the pulse. At a certain point during the downward movement of the particle, the particle seems to slow down and stop. Only when the piston starts to move down, the particle moves down further. If we think in terms of the classical theory of jigging (as discusses in section 2.5), it would suggest that the bed starts to interlock at a certain point during the downward movement of the particle, which slows its movement and brings it to a stop. When the downward pulse is applied, the bed collapses and compacts, resulting in the further downward movement of the particle.

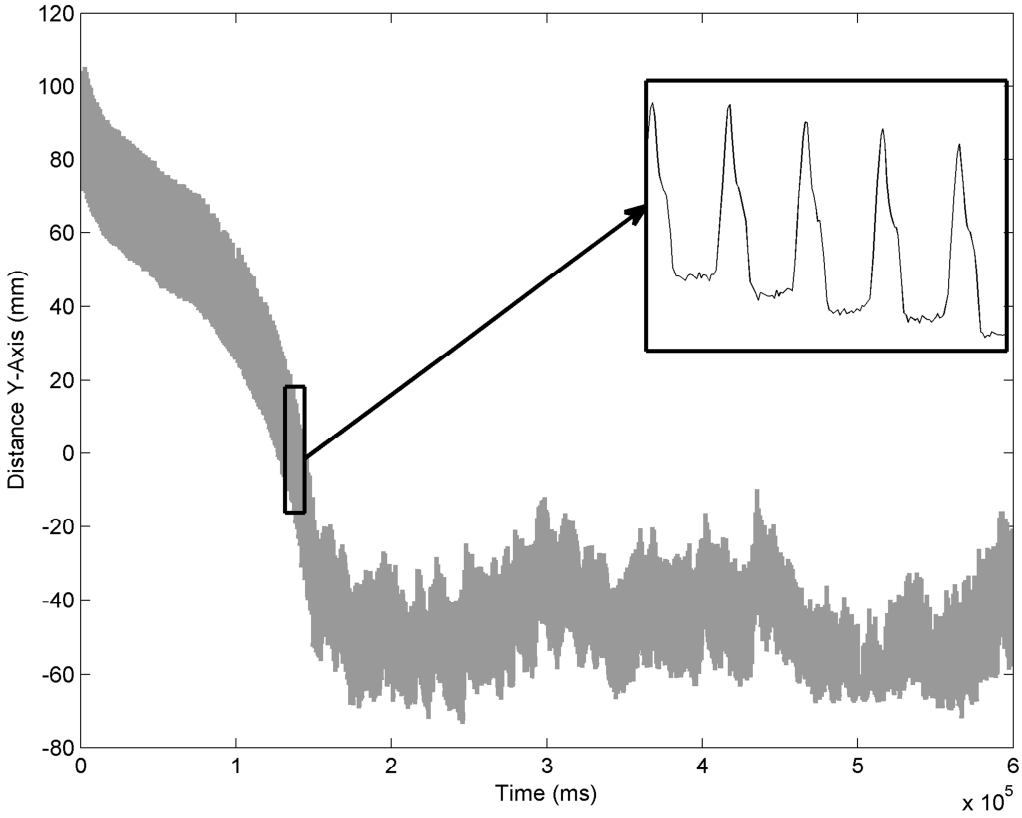

Figure 5-11 The horizontal coordinate versus time, in the top left corner showing the individual pulses once zoomed in

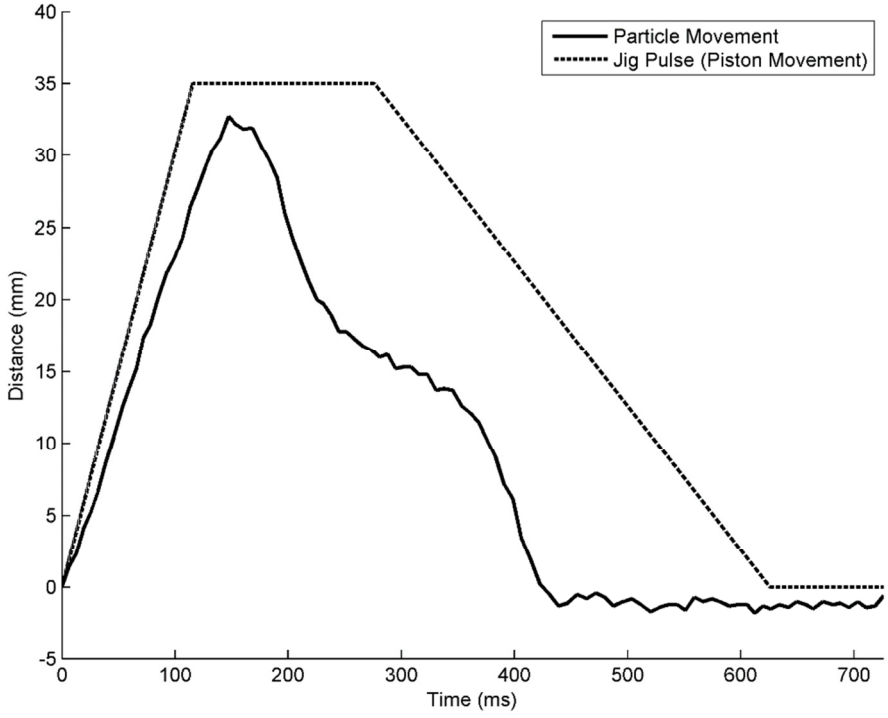

Figure 5-12 Particle trajectory during a single pulse

This theory is further supported when the movement of a particle is observed at different heights in the jig bed. In Figure 5-13, the movement of a particle during a single pulse when it is at the top and bottom of the jig bed is shown. When the particle is at the bottom of the bed, it is seen that it doesn't slow down during its downward movement, as in the case of the particle at the top of the bed. When the particle is at the bottom of the bed, there are fewer particles to form an interlocking bed and slow down the tracer particle's movement.

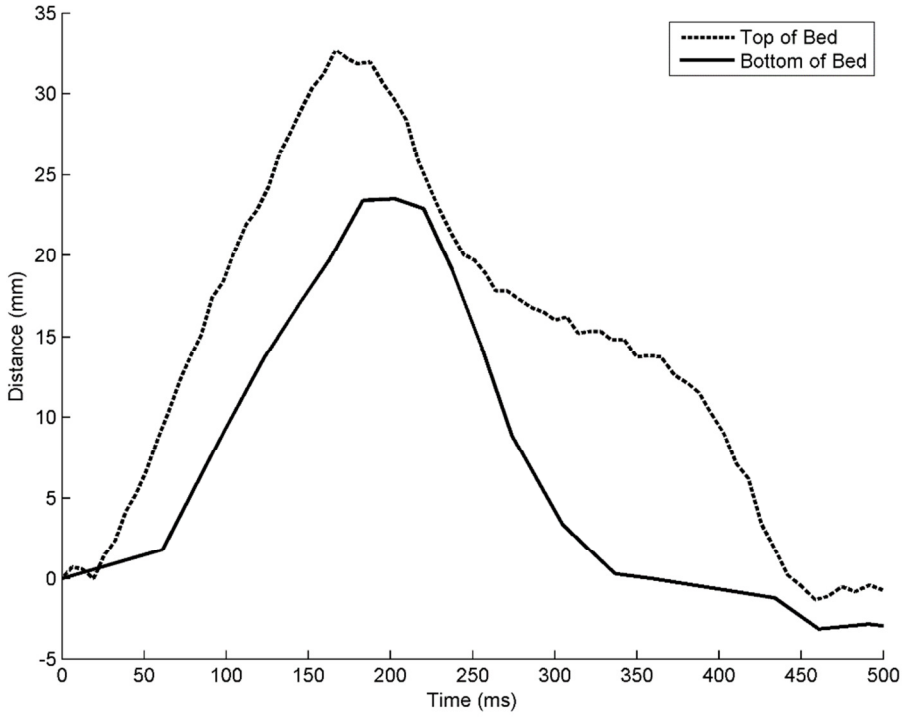

Figure 5-13 The particle trajectory during a single pulse at the top of the bed and the bottom of the bed

5.6 Particle trajectory – vertical direction (a visual inspection)

The vertical movement of the tracer particle in the batch jig gives us important information regarding the rate at which a particle moves, where a tracer will end up and its behaviour once it's reached its final position. Figure 5-14 shows the two features of the tracer's vertical movement that will be examined. Part A is the movement of a tracer through the jig bed, from which a rate of movement can be calculated. Part B on the curve shows what a tracer will do once it has reached its final position. It can be seen that in some circumstances the tracer will move up and down in a "layer". The effect of a tracer particle's size, density and shape on its movement through the vertical direction will be discusses in the subsequent sections.

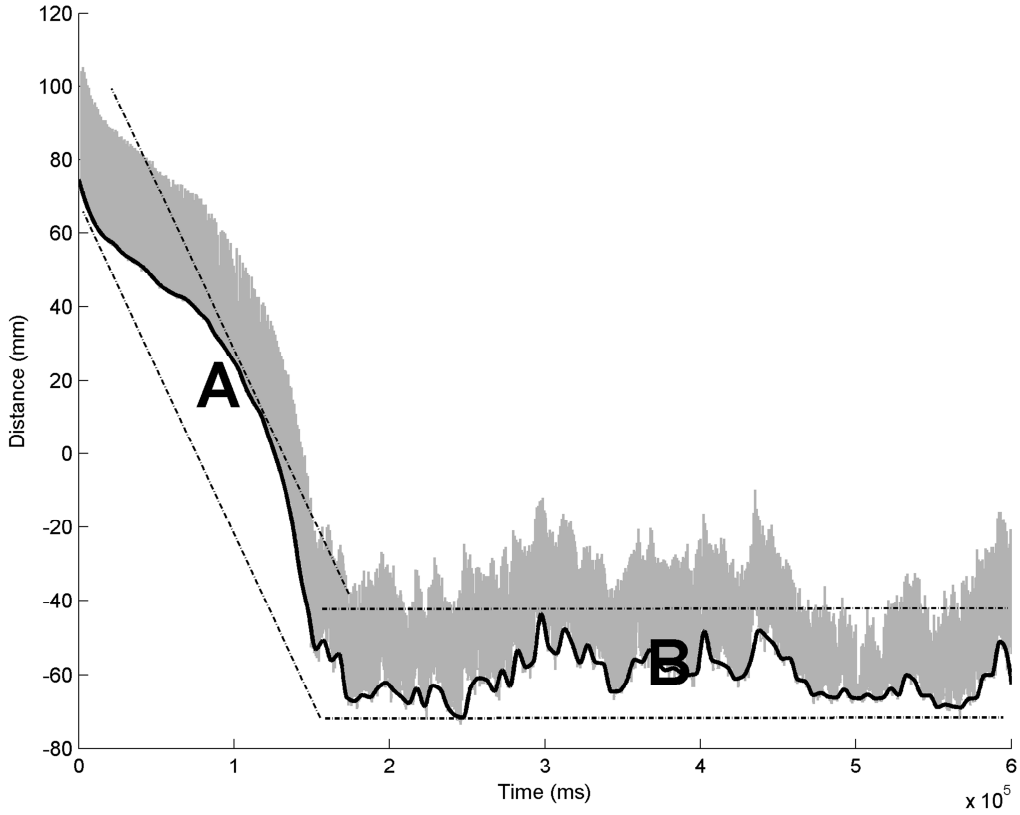

Figure 5-14 The vertical coordinate, with the baseline highlighted

5.6.1 Effect of tracer size

To evaluate the effect of a tracer's particle size on its movement, different sized cubic tracers with the same densities were made. The manufacturing of these tracers are discussed in section 4.2.2 and section 5.2. The properties of these cubic tracers are summarised in table 5-4.

Table 5-4 Properties of tracers used to investigate the effect of size on the movement of a particle

	Size (mm)	Shape	Density (g/m^3)
3	12.6x11.7x12.1	Cubic	3.96
4	10.6x11x9.7	Cubic	3.97
5	7.6x7.6x7.7	Cubic	3.93
10	6.5x6.5x6.6	Cubic	3.89
13	6.2x6.2x6.3	Cubic	3.99

The PEPT test procedure, as described in section 4.7, was followed for each of the tracers and each tracer was tested in four different bed materials. Figures 5-15 to 5-18 show some of the baseline plots to compare the movement of different sized tracers. Each of these Figures shows the trajectories 12 mm, 10 mm, and 8 mm and their duplicates.

Size has a significant effect on where a particle ends up in the jig bed. In Figure 5-15, all the tracers move to the bottom of the jig and don't move much once they get there. This is expected, due to the high density difference between the tracer particles (3.95 SG) and the bed (2.91 SG). In Figure 5-16, the bed has a higher density (3.74 SG) and it is seen that the tracers have much more movement at the bottom of the jig. Looking carefully at this Figure, it can be noted that the 8 mm particle moves more at the bottom of the jig, compared to the 10 mm and 12 mm particles.

When the bed has a very high density, such as that in Figure 5-17 (4.1 SG) and 5-18 (4.3 SG), the 12 mm tracer moves to the bottom of the jig and remains fairly motionless on the screen. The 10 mm particle shows more movement once it reaches the bottom, and the 8 mm particle moves back up the jig bed once it has reached the bottom and can end up in any position once the jigging stops. It is possible that this particle follows the secondary flow inside the jig, a concept observed by Williams *et al*. (1996), which will be discussed further in section 5.8. Even though these particles have lower densities than that of the bed material, they still moved to the bottom. This is possibly due to the smaller particle size of the bed material (3 mm to 8 mm) compared to the size of the tracers.

In all of the Figures (5-15 to 5-18), it is difficult to see a clear relationship between the size of a particle and the stratification rate or the time it takes a particle to reach its final position. When looking at a specific position in the jig bed, as an example -20 mm position in Figure 5-15, the sequence at which the particles reach this position is as follows: the 10, 8, 12, 10, 8 and then the 12 mm particle. Visual inspection of the curves will clearly not give an indication of the effect of size on stratification and a more rigorous method is required and is discussed in chapter 5.7.

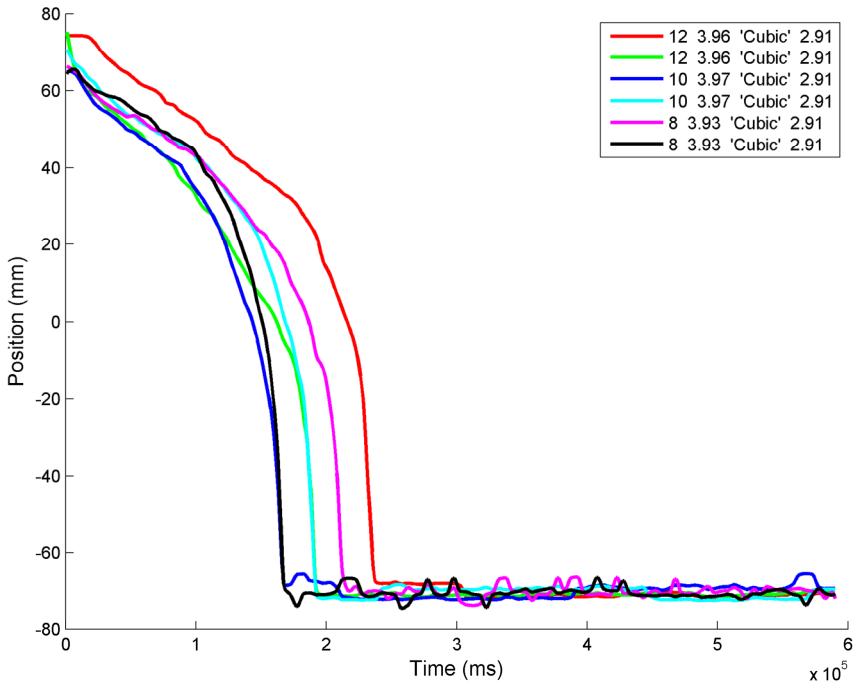

Figure 5-15 Baseline plots of different sized cubic particles of similar density (+-3.95) and a particle bed with density 2.91 SG

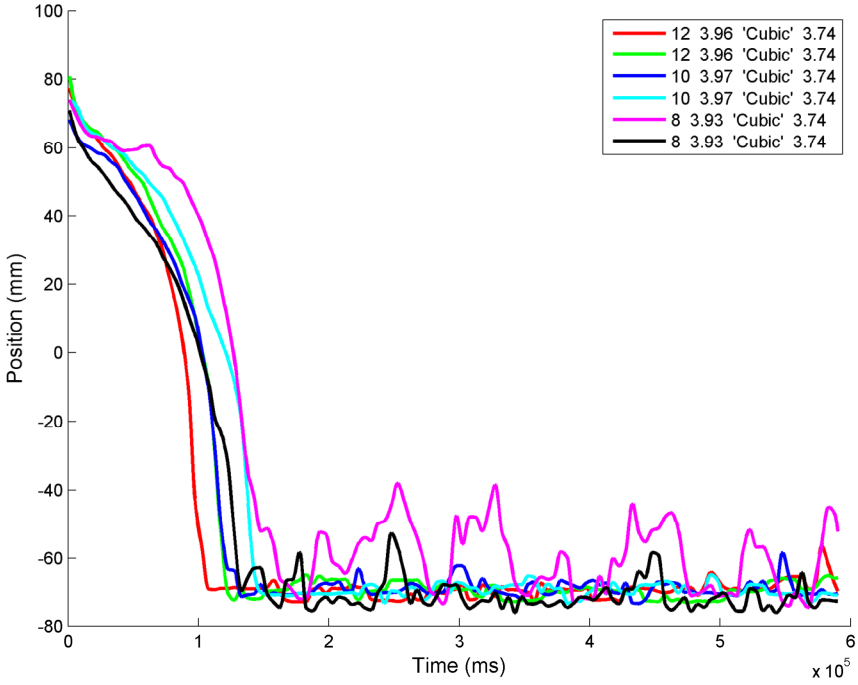

Figure 5-16 Baseline plots of different sized cubic particles of similar density (+-3.95) and a particle bed with density 3.74 SG

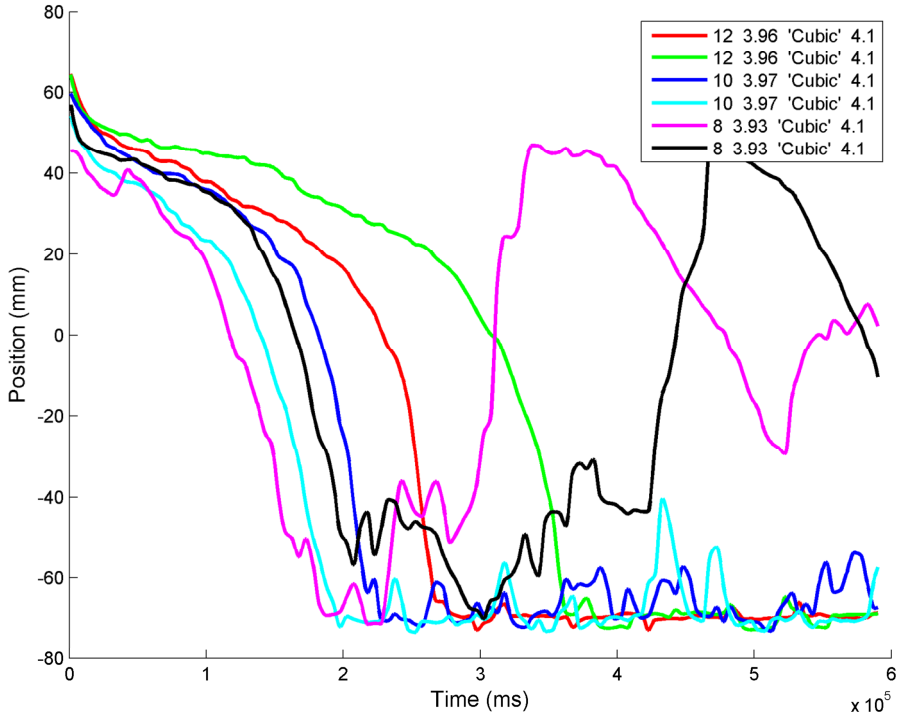

Figure 5-17 Baseline plots of different sized cubic particles of similar density (+-3.95 SG) and a particle bed with density 4.1 SG

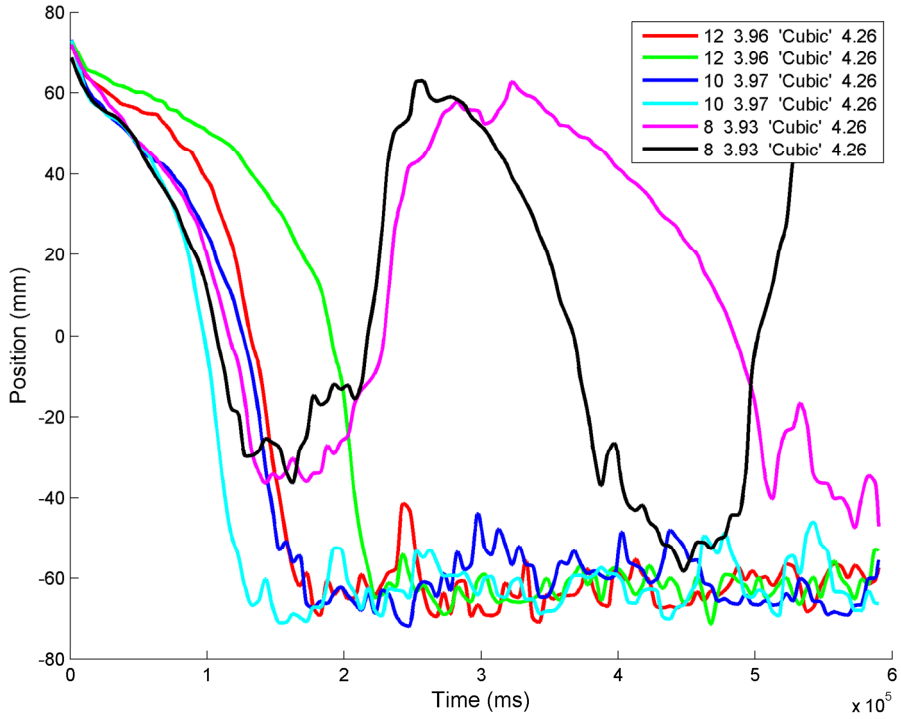

Figure 5-18 Baseline plots of different sized cubic particles of similar density (+-3.95 SG) and a particle bed with density 4.26 SG

5.6.2 Effect of tracer density

To investigate the effect of a tracer's density on its movement through the jig bed, tracers with the same shape and size with different densities were evaluated. The properties of the tracers looked at in this section are summarised in table 5-5. It can be seen from the table that the densities used do not vary by much and they are all in the "near density" range for iron ore jigging.

Table 5-5 Properties of tracers used to investigate the effect of density on the movement of a tracer

	Size (mm)	Shape	Density (g/m^3)
4	10.6x11x9.7	Cubic	3.97
6	10.2x9.7x9.2	Cubic	4.20
7	9.3x10.1x10.3	Cubic	3.76
10	6.5x6.5x6.6	Cubic	3.89
13	6.2x6.2x6.3	Cubic	3.99
16	6.3x6.3x6.3	Cubic	3.72

Figures 5-19 to 5-21 show some of the baseline plots to compare the movement of particles with different densities through the different jig beds. Similar observations can be made to that in section 5.6.1, and again there is no clear indication through visual inspection of the graphs that different density tracers move at different speeds through the bed, especially in the low density bed (Figure 5-19).

In the low density bed (figure 5-19), where the bed has a density of 2.91 SG and the particle densities range from 3.76 to 4.20 SG, it is seen that the particle do not move much when the bottom of the bed is reached. In the higher density beds (Figures 5-20 and 5-21), it is seen that the lower density tracers move more when they reach their stratification positions, and the lowest density tracers tend to move back up to the top of the bed – similar behaviour to that of the 8 mm tracer in the high density bed, discussed in section 5.6.1. In Figure 5-20, the 3.76 SG tracer initially doesn't

move downward. When it does move down the bed, the rate is similar to that of the other particles.

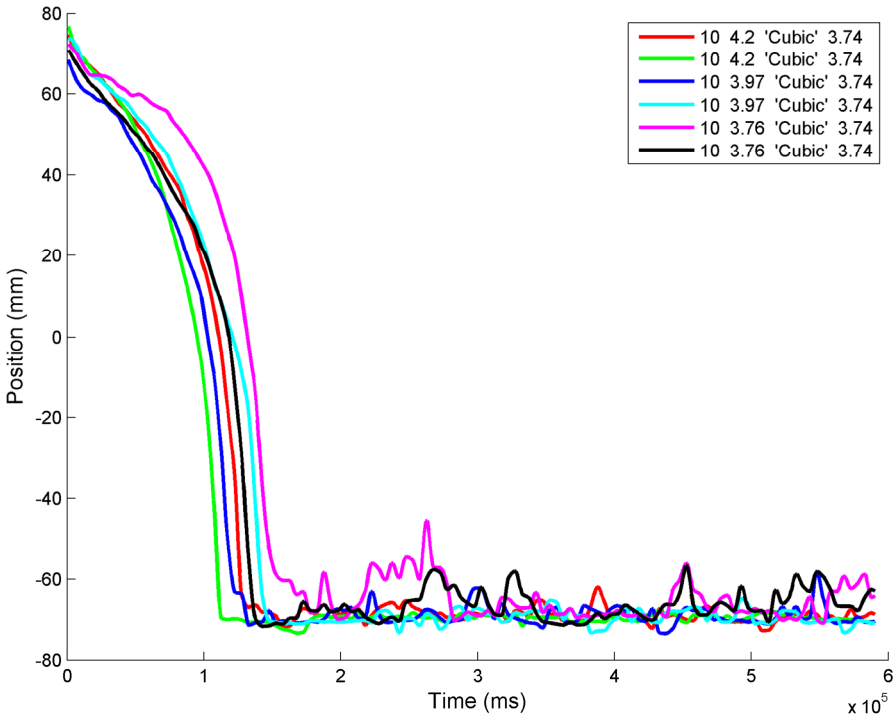

Figure 5-19 Baseline plots of different density, 10 mm, cubic particles and a particle bed with density 3.74 SG

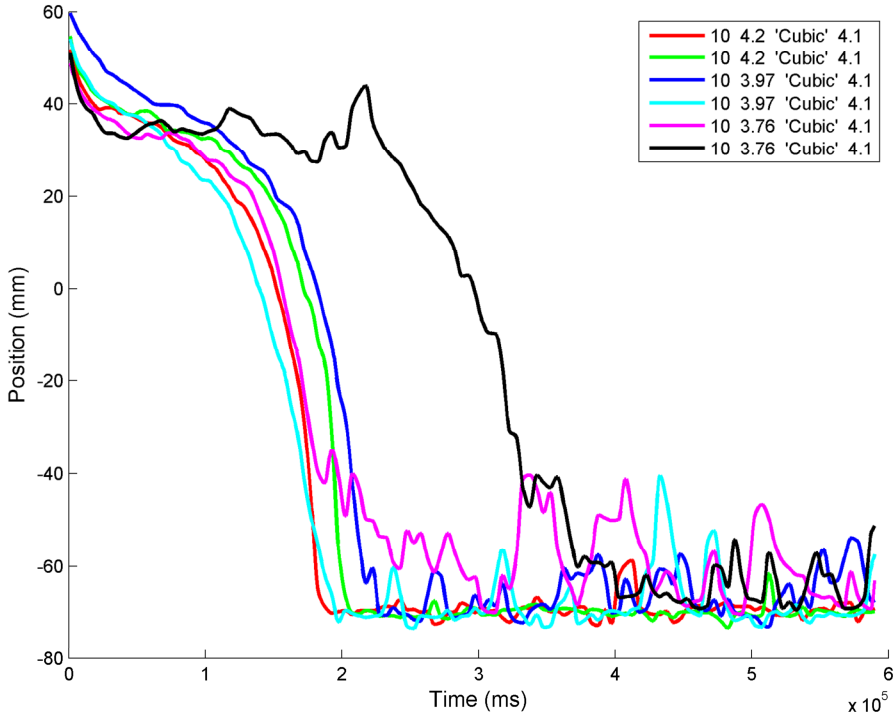

Figure 5-20 Baseline plots of different density, 10 mm, cubic particles and a particle bed with density 4.1 SG

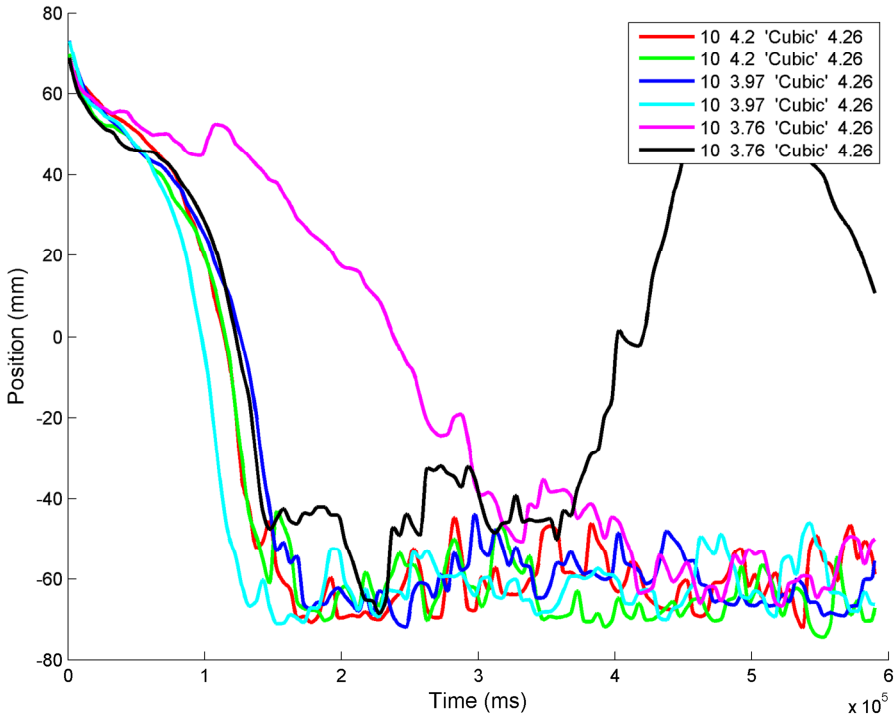

Figure 5-21 Baseline plots of different density, 10 mm, cubic particles and a particle bed with density 4.26 SG

5.6.3 Effect of tracer shape

To investigate the effect of a tracer's shape on its movement through the jig bed, tracers with the same density and volume (size) with different shapes were evaluated. The properties of the tracers looked at in this section are summarised in table 5-6. Three groups of tracers were made, each group from a different tracer material with a different density.

Table 5-6 Properties of tracers used to investigate the effect of shape on the movement of a tracer

	Size (mm)	Shape	Density (g/m^3)
8	14.9x4x4.8	Elongated	3.93
9	8.1x8.5x4	Flat	3.91
10	6.5x6.5x6.6	Cubic	3.89
11	15.7x4x3.7	Elongated	3.94
12	7.8x7.8x4	Flat	3.91
13	6.2x6.2x6.3	Cubic	3.99
14	16.3x3.9x3.9	Elongated	3.73
15	8x8.2x3.8	Flat	3.73
16	6.3x6.3x6.3	Cubic	3.72

The baseline plots done on the first group of tracers from table 5-6 is shown in Figures 5-22 to 5-25. The same effect that was observed in section 5.6.1 and 5.6.2 is seen, where the tracers will move back up the jig bed at higher bed densities. Again there is no clear indication through visual inspection of the graphs that different shapes move at different speeds through the bed. In Figure 5-22, it can be seen that there is a wide range of stratification times from 100 to 200 seconds. However, this is no real indication that the different shapes have an effect on this time.

The differently shaped particles behave similar to each other. In Figure 5-23 it is seen that the amount of movement that the particles have after they have reached

their stratification positions are almost identical. The same can be said for Figure 5-24 and 5-25, where all of the particles move back up the bed.

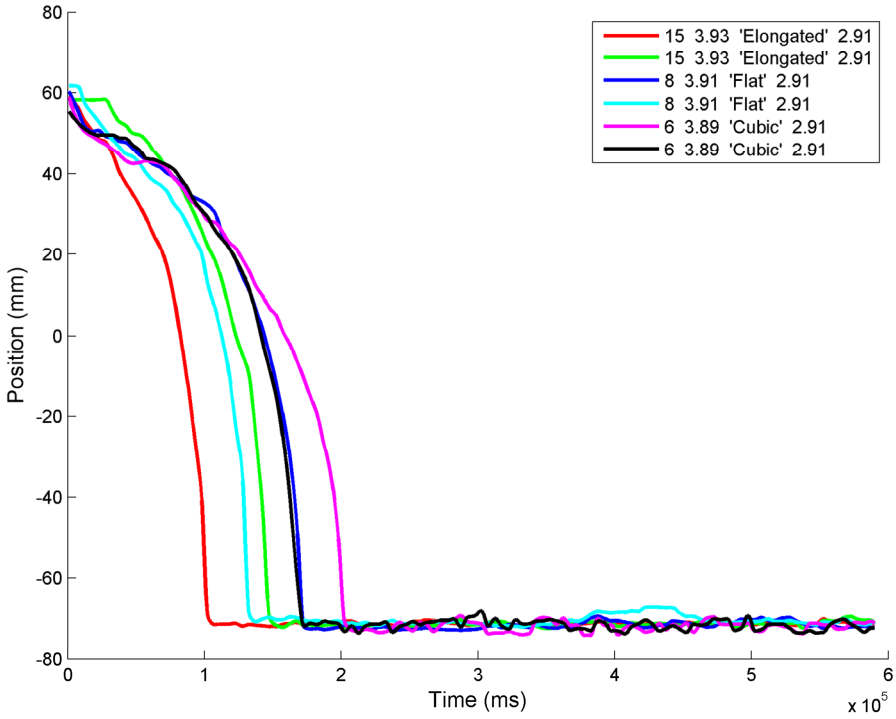

Figure 5-22 Baseline plots of differently shaped particles and a particle bed with density 2.91 SG

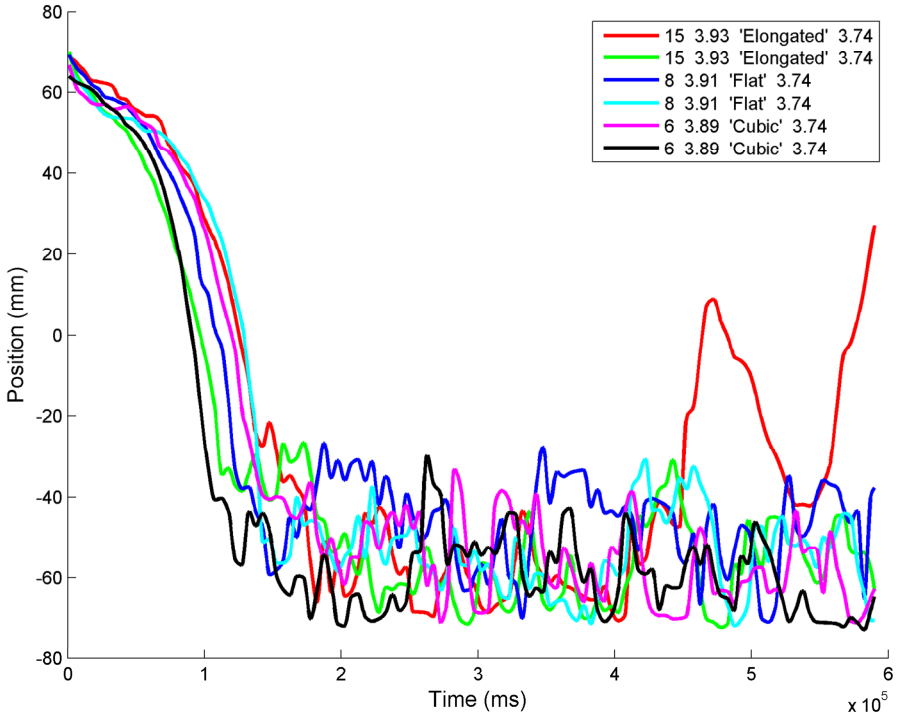

Figure 5-23 Baseline plots of differently shaped particles and a particle bed with density 3.74 SG

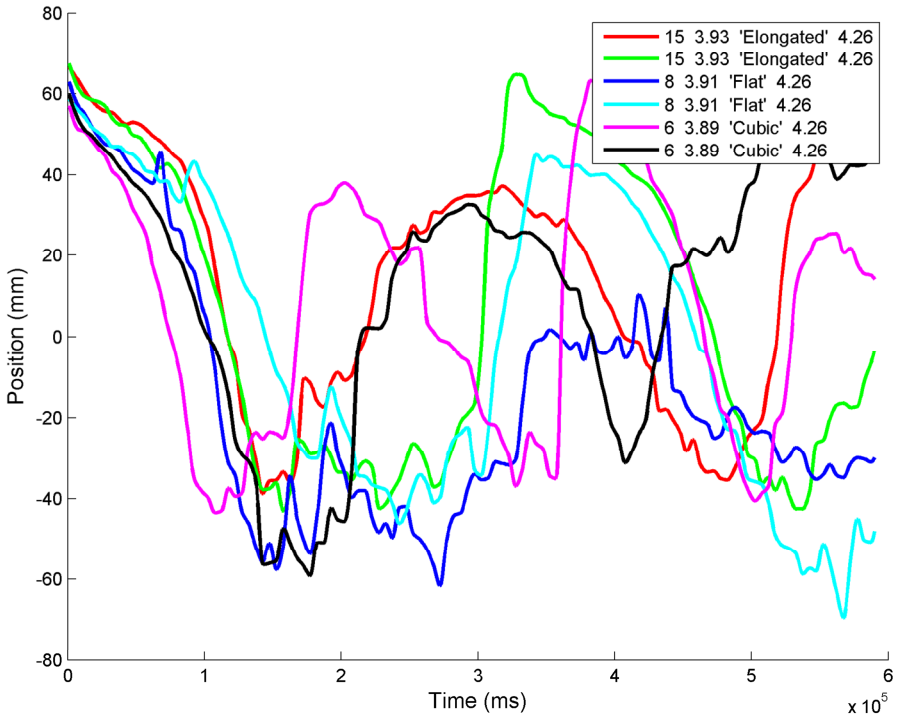

Figure 5-24 Baseline plots of differently shaped particles and a particle bed with density 4.26 SG

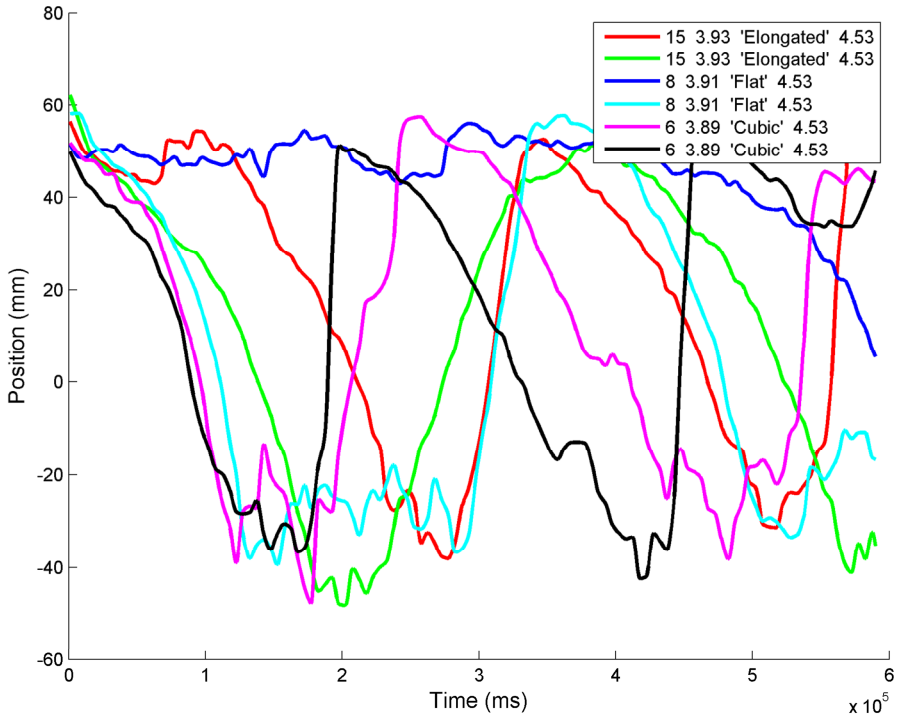

Figure 5-25 Baseline plots of differently shaped particles and a particle bed with density 4.53 SG

5.6.4 Effect of tracer size, density and shape on tracer position inside the batch jig

The baseline plots seen in sections 5.6.1 to 5.6.3 show that, in some conditions, particles will move back up the jig bed. This behaviour can have a significant effect on the performance of a jig, since these particles don't settle at a specific position in the jig bed. In work done by Naude *et al*. (2013), it was found that some of the lighter particles can be found in a very large section along the depth of the jig bed after jigging, which is something that will happen if the particles move back up the bed. This behaviour can be attributed to secondary flow, as observed by Williams *et al*. (1996).

To summarise this effect of the particles moving back up the jig bed, all of the applicable test runs were divided into three categories:

1) The tracer particle stays at the bottom of the bed.
2) The tracer moves up slightly.
3) The tracer moves back to the top of the bed.

A percentage size difference versus percentage density difference is then plotted for each of the three groups and is shown in Figure 5-26. The percentage size difference is the difference between the tracer size and the average size of the particles in the bed, and the percentage density difference is the difference between the density of the tracer and the average density of the bed material. From Figure 5-26 it is seen that both the size and the density of the particle play a role on this type of behaviour and that it is the particles that are close to the density and size of the bed that will be affected the most. The consequence of this behaviour is that the lighter particles report to the lower parts of the jig, instead of just the top layers where they belong.

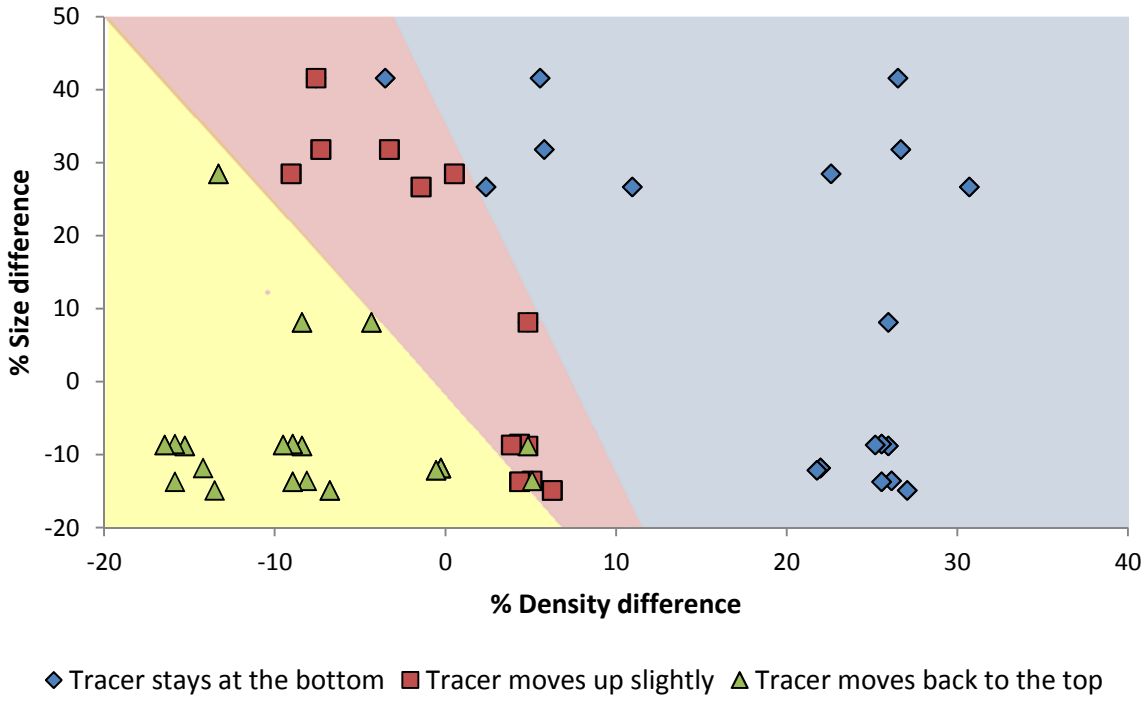

Figure 5-26 The effect of size and density on particles moving back up the jig bed

A similar analysis was done to determine if shape has an influence on the tracer moving up the jig bed and the results is shown in Figure 5-27. The shape of the tracer is expressed in terms of sphericity, which is the ratio between the surface area of a sphere with the same volume as the tracer and the surface area of the tracer itself. In this case, the cubic tracers will have the highest sphericity, the flat particles the second highest and the elongated the lowest values. From Figure 5-27 it is seen that the shapes used for this study had no to little influence on the movement of the tracers back up the jig bed, compared to the effect of density. This conclusion can be drawn from the fact that at no point does the change in shape cause a particle to jump from one category to the other.

It is a very real possibility that the secondary flow is directly responsible for this behaviour and that particles with properties close to that of the bed will follow this secondary flow. Figures 5-26 and 5-27 show that a particle starts to follow the secondary flow when its density is around the average density of the bed (% density difference = 0) and lower.

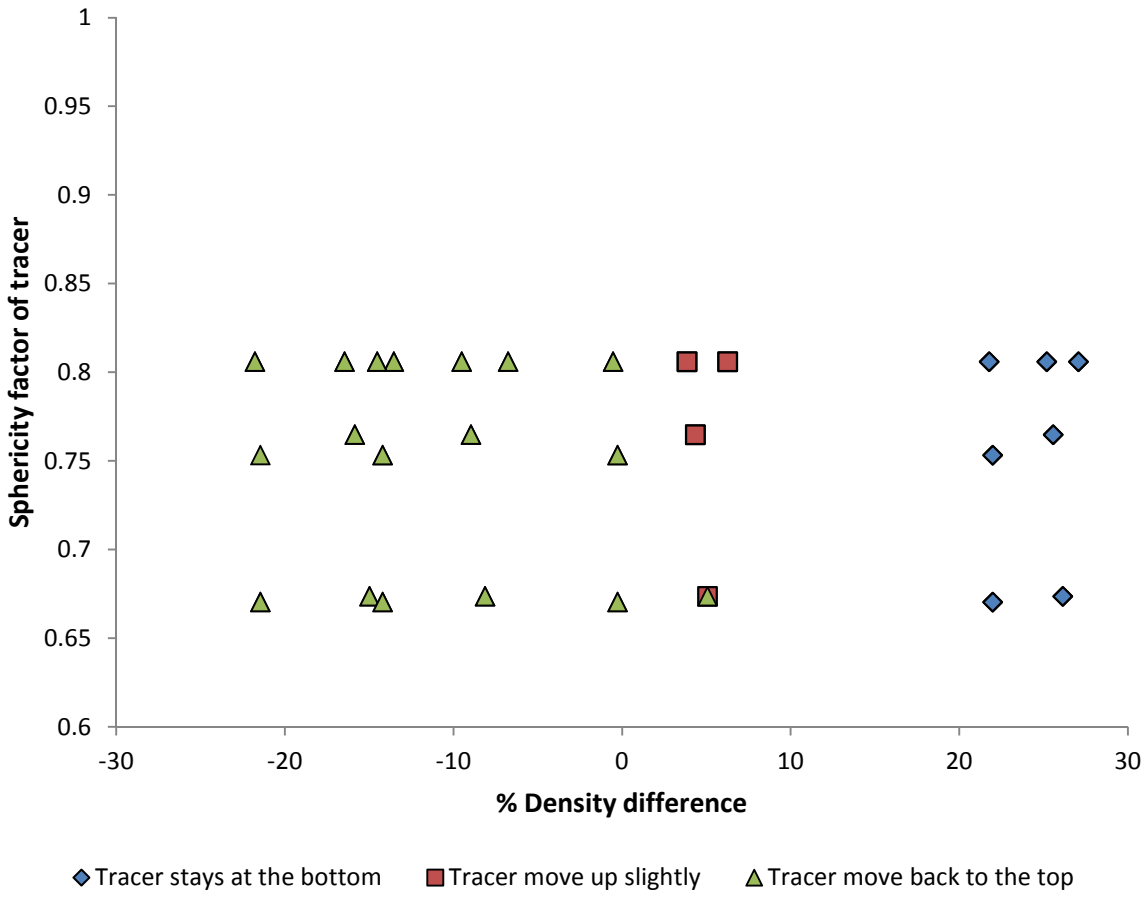

Figure 5-27 The effect of shape and density on particles moving back up the jig bed

5.7 Effect of tracer size, density and shape on stratification rate

In section 5.6, visual inspection of the baseline plots (Figures 5-15 to 5-25) could not indicate the effect that a tracer's properties (size, density and shape) have on the rate (stratification rate) at which it moves through the jig bed. A multivariate regression approach was then taken to determine what effect the variables have on the stratification rate.

It was observed that the movement of a tracer through the jig bed has a general shape (figure 5-28). The tracer moves at a constant initial rate and at a certain height in the jig bed, the rate at which the tracer moves increases dramatically. To simplify the analysis, two straight lines were fitted to each curve – the first straight line to fit the initial slope of the line, and the second straight line to fit the final slope of the line. The slopes of these two lines are hereafter referred to as the initial stratification rate and the final stratification rate.

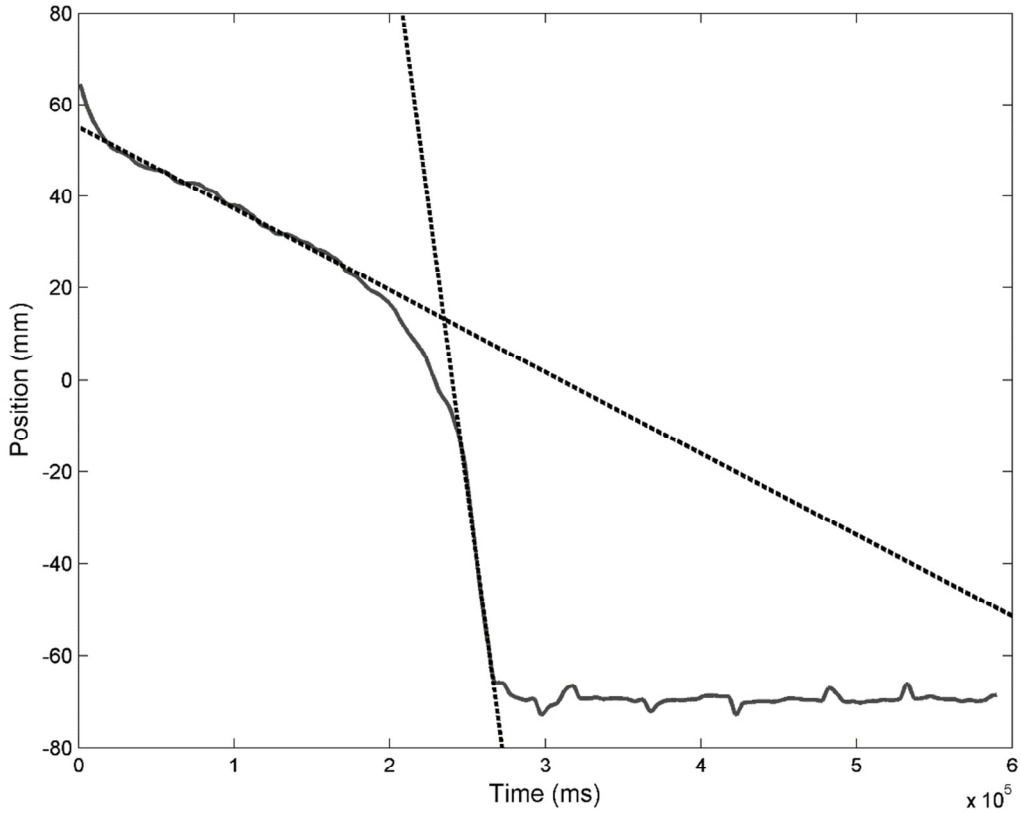

Figure 5-28 Lines fitted to the initial and the final slopes of the baseline plot.

The data analysis plugin for Excel was used to perform the multivariate regression to determine the effect of the different variable on the stratification rate. The following variables were considered: tracer shape, tracer density, tracer volume (which represents its size), and bed density. The results from the multivariate regression on the final stratification rate are shown in table 5-7. From the table, the adjusted R squared indicates how well the multivariate model fits, with a value of 1 meaning a perfect fit. To determine if a variable has a significant influence on the stratification rate, a t-stat is calculated. A t-stat of more than 2 or less than -2 suggests that the variable has a significant effect on the stratification rate. The coefficients determine how much a specific variable affects the stratification rate.

The particle volume and bed density have a definite effect on the slope, with t-stat values of 2.54 and -12.96. The particle density and the flat shape have values less than, but close to two and might have to be considered.

Table 5-7 Multivariate regression results for the final slope

Regression statistics	
Multiple R	0.814
R Square	0.663
Adjusted R Square	0.644
Standard Error	0.833
Observations	96

	Coefficients	*Standard Error*	*t Stat*	*P-value*	*Lower 95%*	*Upper 95%*
Intercept	3.791	2.911	1.302	0.196	-1.993	9.574
Elongated'	-0.017	0.253	-0.065	0.948	-0.519	0.486
Flat'	0.476	0.249	1.910	0.059	-0.019	0.972
Particle density	1.462	0.747	1.957	0.053	-0.022	2.947
Particle volume	0.566	0.223	2.536	0.013	0.123	1.010
Bed density	-1.940	0.150	-12.958	0.000	-2.238	-1.643

Since the elongated variable shows no significance, it is removed as a variable and the regression is redone and shown in table 5-8. It can be seen that the t-stat for the remaining four variables have improved. Different combinations and representations of variables were used to try and improve the regression, but none showed any improvement on the analysis in table 5-8.

The information in table 5-8 can now be written as equation 5-1, where FSR is the final stratification rate, ρ_p is the particle density, v_p is the particle volume, and ρ_p is the bed density. For a flat particle, a value of 0.483 should be added to the final stratification rate.

Table 5-8 Optimised multivariate regression results for the final slope

Regression statistics	
Multiple R	0.814
R Square	0.663
Adjusted R Square	0.648
Standard Error	0.829
Observations	96

	Coefficients	*Standard Error*	*t Stat*	*P-value*	*Lower 95%*	*Upper 95%*
Intercept	3.7612	2.8602	1.3150	0.1918	-1.9202	9.4426
Flat'	0.4829	0.2269	2.1283	0.0360	0.0322	0.9336
Particle density	1.4677	0.7387	1.9867	0.0500	0.0002	2.9351
Particle volume	0.5725	0.2013	2.8437	0.0055	0.1726	0.9725
Bed density	-1.9399	0.1489	-13.0308	0.0000	-2.2356	-1.6442

$$FSR = 1.468\rho_p + 0.573v_p - 1.940\rho_b$$
$$if\ particle\ is\ flat\ add\ 0.483 \qquad \text{5-1}$$

Plotting the actual values of the stratification rate against the values predicted by equation 5-1, gives the Figure 5-29 and is an indication of how well the model predicts the stratification rate. It is clear that the model doesn't give perfect prediction, and it should also be noted that there might be variables that can affect this stratification rate that were not considered.

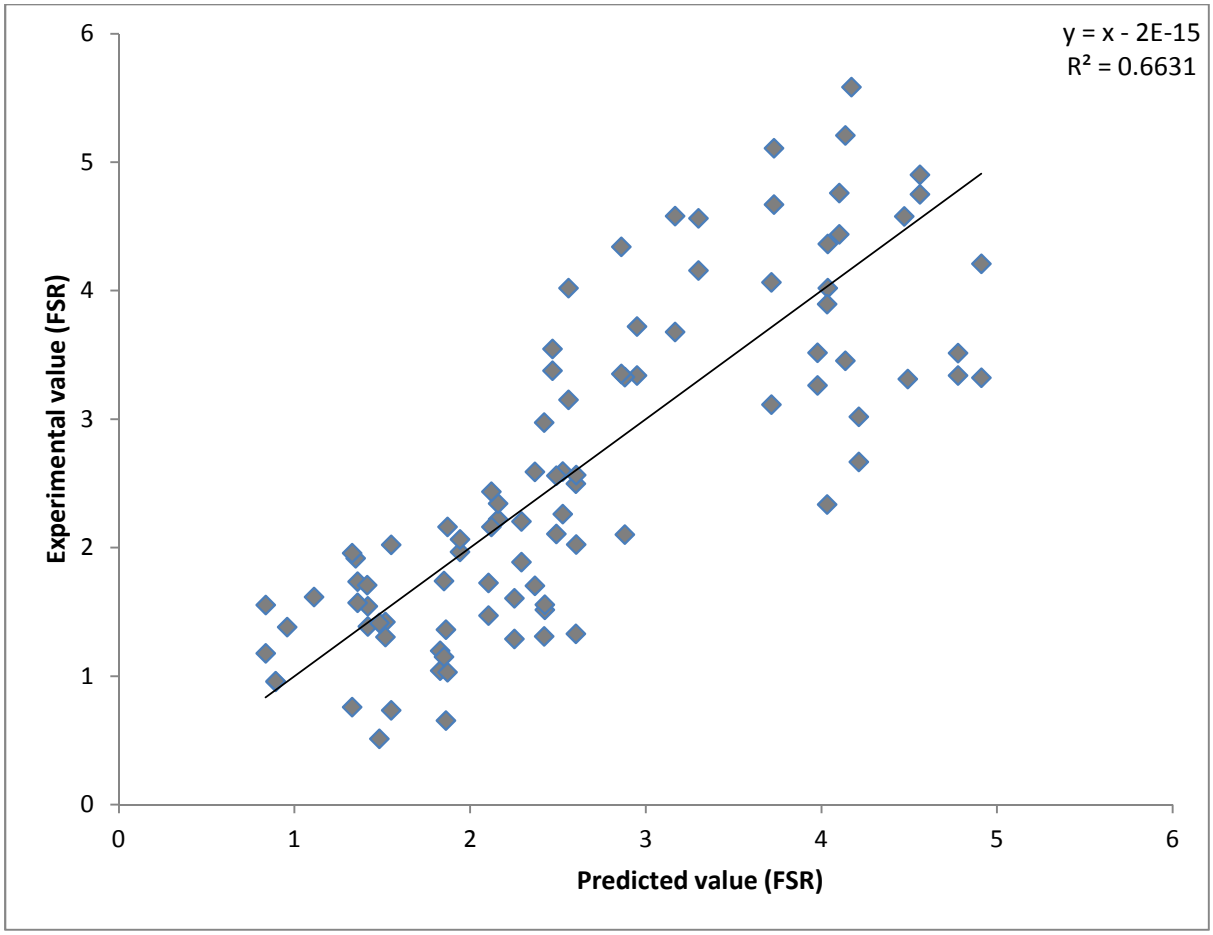

Figure 5-29 Experimental value of final stratification rate plotted against the predicted value from equation 5-1

A similar multivariate analysis was attempted on the initial stratification rate (initial slope) and the results are shown in table 5-9. From the table, it can be seen that none of the variables showed to have any significant influence on the initial stratification. Multiple attempts were made with different variable combinations, but none showed any significant improvement over the results in table 5-9. It can be concluded that none of the feed variables (size, density and shape) affect the initial stratification, and since none of the machine variables were changed, it can be assumed that the different initial stratification values are due to random interactions.

Plotting a histogram of the initial stratification values (Figure 5-30) shows the distribution of these values – 75% of the values are between 0.1 and 0.4 mm/s and the average initial stratification rate is 0.315 mm/s.

Table 5-9 Multivariate regression results for the initial slope

Regression statistics	
Multiple R	0.24588
R Square	0.06046
Adjusted R Square	0.00767
Standard Error	0.00016
Observations	95

	Coefficients	*Standard Error*	*t Stat*	*P-value*	*Lower 95%*	*Upper 95%*
Intercept	-0.000686	0.000545	-1.259	0.211	-0.001768	0.000396
Elongated'	-0.000052	0.000047	-1.093	0.277	-0.000146	0.000042
Flat'	0.000039	0.000047	0.821	0.414	-0.000055	0.000133
Particle density	0.000069	0.000140	0.490	0.625	-0.000209	0.000346
Particle volume	0.000034	0.000042	0.826	0.411	-0.000048	0.000117
Bed density	0.000023	0.000028	0.808	0.421	-0.000033	0.000079

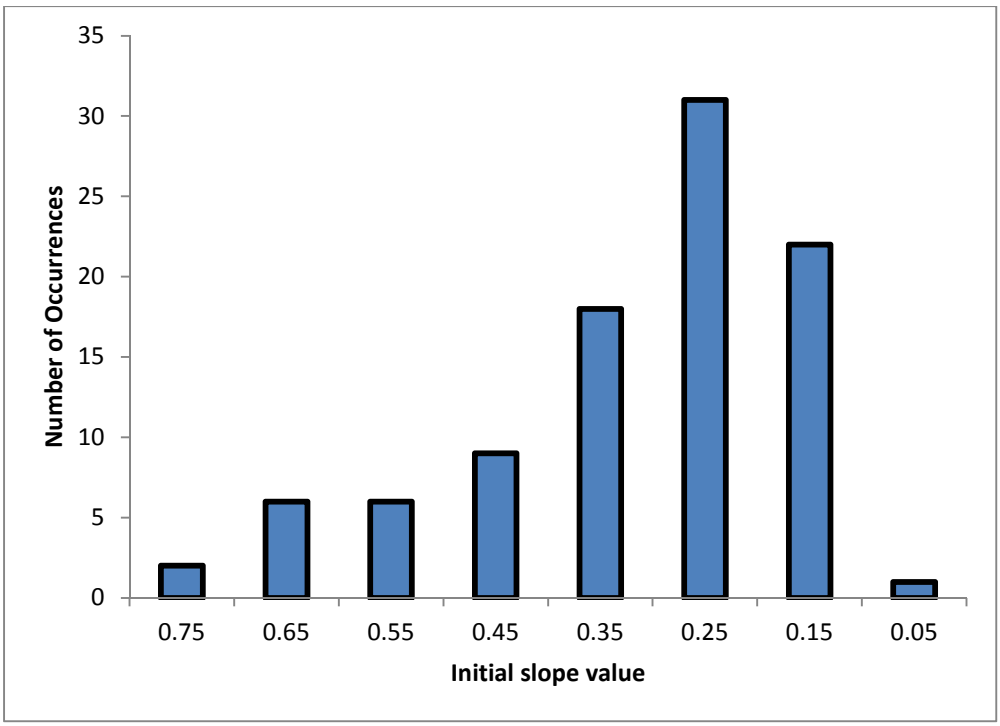

Figure 5-30 Histogram of the initial slope values

5.8 Secondary flow inside the batch jig

The testwork showed interesting behaviour in the batch jig, which is shown in Figure 5-31. A heavy particle that started at the top centre of the jig bed, moved straight down. However, if it was started near the wall of the jigging chamber on top of the bed, it first moved to the centre of the jig before it moved down the bed. A light particle was observed to preferentially move up the jig bed next to the jigging chamber wall. This behaviour suggests that a secondary flow is generated during jigging. Similar observations were made by Williams *et al*. (1996).

Further testwork was done to observe this secondary flow in the batch jig. Table 5-10 shows the properties of the tracers used specifically for investigating the secondary flow. Homogenous spherical particle beds were used for these test runs and the tracer particle had exactly the same properties as the particles in the bed.

Table 5-10 Properties of tracers used to investigate the secondary flow effect

	Size (mm)	Shape	Density (g/m^3)
1	8	Sphere	2.50
2	8	Sphere	3.60

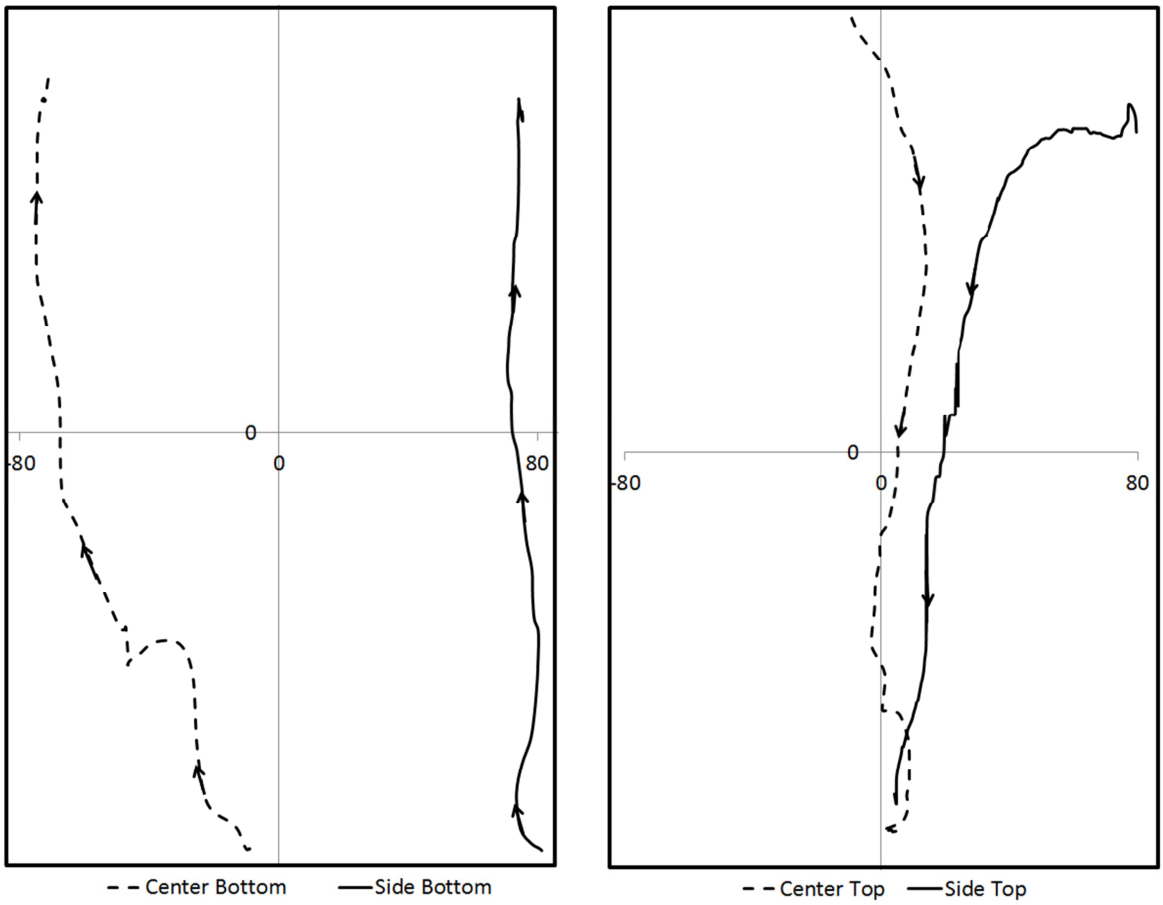

Figure 5-31 Low density 2.91 SG heavy particle 5.01 SG

The flow field can clearly be observed when looking at animations of the particle movement created from the PEPT data. To display the flow fields in a picture form, the data has to be displayed as a vector field. When plotting the baseline of particles affected by the secondary flow (Figure 5-32) on a 3D axis, it can be observed that there is circular motion in the jig. However, it is not possible to observe the direction of the circular movement.

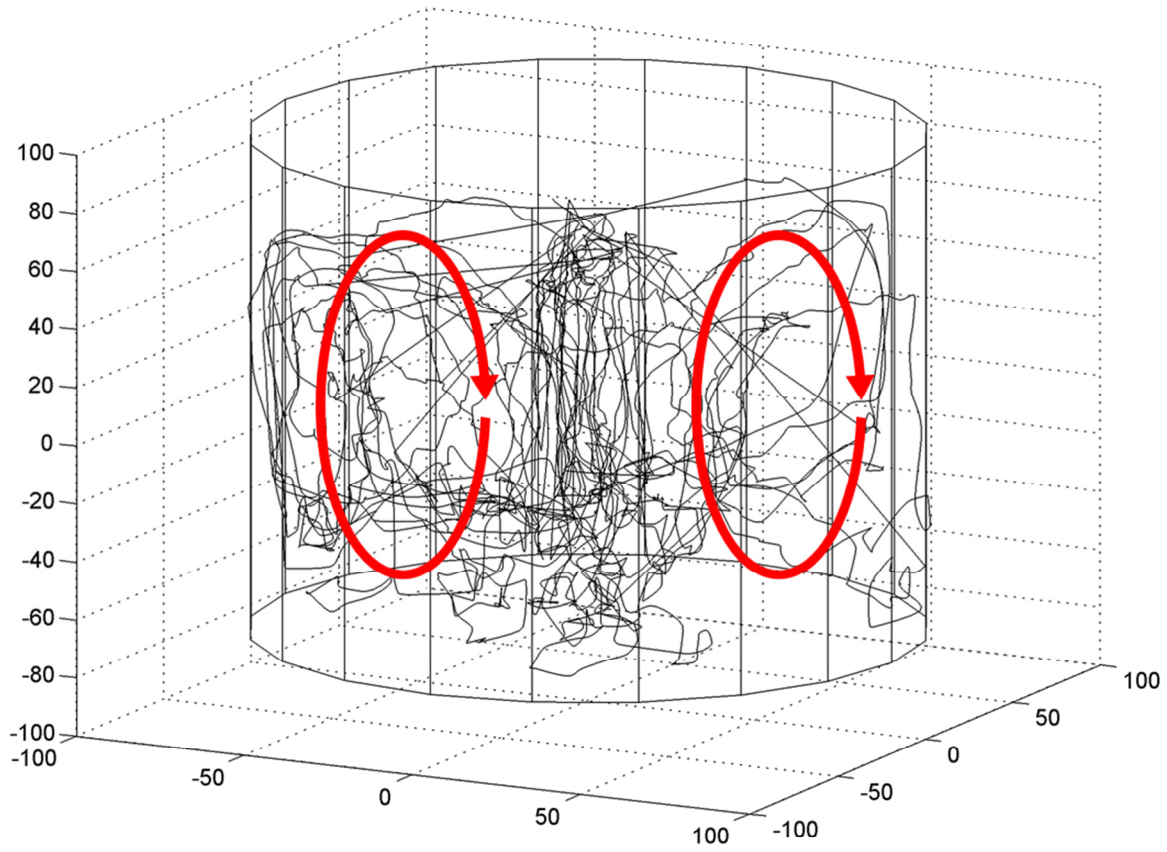

Figure 5-32 3D baseline plot of particles affected by secondary flow

To get more information on the secondary flow, velocity vector fields were created by calculating the average velocity at different position in the jig, using the baseline data. Since it was observed that the circular motion from the secondary flow can occur in any direction in the X-Z plane, the X- and Z-coordinates were combined into an R-coordinate, which is simply the distance that the particle is from the centre of the jig. Figures 5-33 to 5-35 show these velocity vector fields, the X-axis is the R-coordinate and therefore the 0 on the axis is the centre of the jig and the maximum value the wall of the jig.

In Figures 5-33 to 5-35, the secondary flow can clearly be observed. A very detailed pattern was observed with the test that used the 3.6 SG spherical particles (figure 5-33). These particles were observed to move around a lot more, therefore providing more data to construct the velocity vector field. It should be noted that the bed height

in this case was only 80 mm, compared to the 150 mm in the other cases, due to a lack of sample.

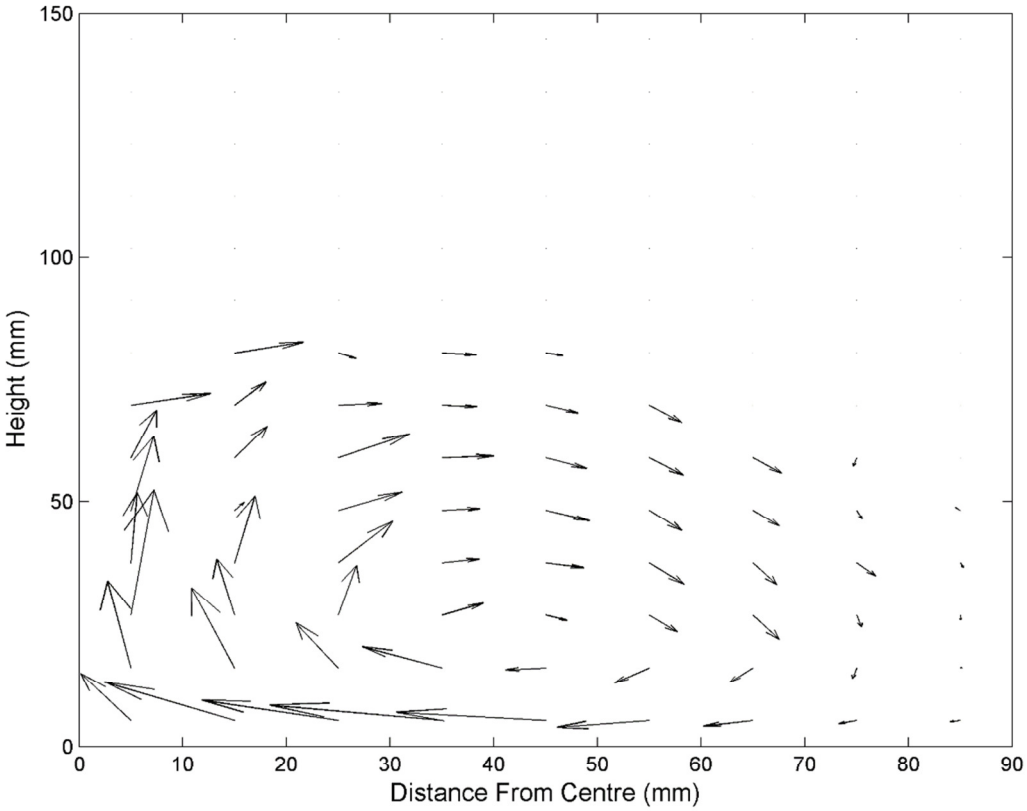

Figure 5-33 Velocity vector field of the 3.6 SG tracer in a homogenous bed that was run for two hours

For figure 5-34, a bed made from glass beads was used to provide a very homogenous jig bed. In this case the tracer particle moved around a lot less, resulting in a Figure that seems a little more chaotic. The two Figures show many similarities, both showing a clockwise rotational velocity vector field, which corresponds to an upward flow in the centre and a downward flow at the sides of the jig. This is contradictory to the information gathered in the preliminary tests and the work that was done by Williams *et al*. (1996).

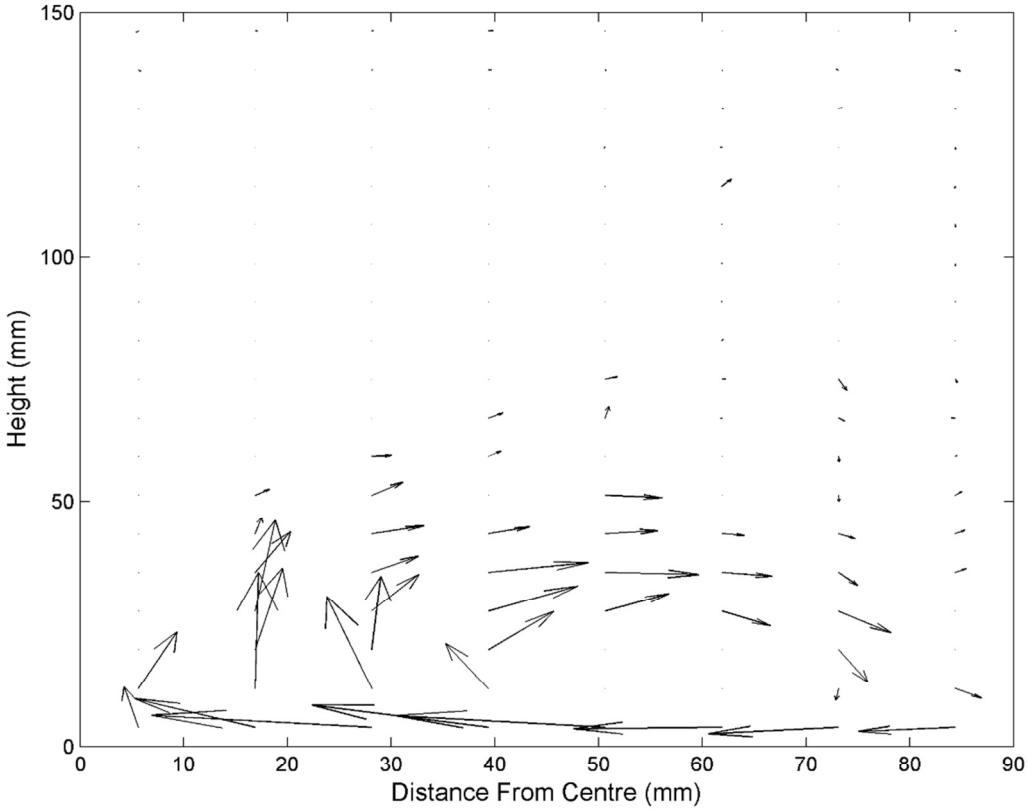

Figure 5-34 Velocity vector field of a glass spherical tracer in a homogenous bed that was run for two hours

A velocity vector field was compiled from the tests that were conducted with the different size, density and shape tracers and is shown in Figure 5-35. A total of 17 tests were combined. In this Figure, it is seen that the flow is downward in the centre and upwards at the side of the jig, which corresponds to what was seen in the testwork (Figure 5-31) and is similar to what Williams *et al*. (1996) found. It is clear that the movement of particles in a batch jig is much more complex than anticipated, and that the secondary flow is not just a function of the batch jig design, but also the bed material in the jig.

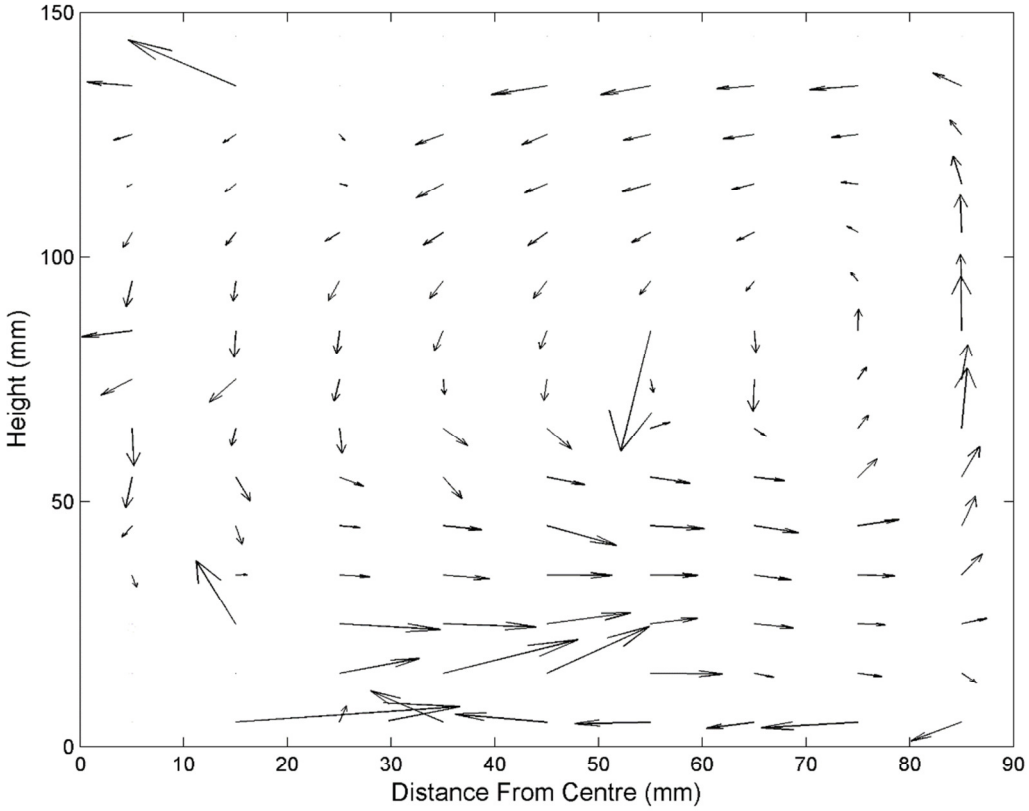

Figure 5-35 Combined velocity vector field of multiple tests where the tracers were affected by the secondary flow

It is suspected that the secondary flow pattern is a result of uneven water flow entering the batch jig, resulting in uneven expansion or pulsing throughout the bed. To visualise the uneven pulse height in the bed, the datasets that were used to plot the vector fields (Figures 5-33 to 5-35) were used to plot the pulse height as a function of position in the jig. Figures 5-36 to 5-38 show colour maps plotted to illustrate the difference in the pulse height at different positions in the bed, with the same coordinate system as used with the vector field plots. In all three of the plots it is seen that, in the centre of the batch jig, the pulse height is a lot higher compared to the side of the jig, especially in the bottom layers of the jig. This difference in the pulse height from the centre to the side decreases in the higher layers. This big difference in pulse height, from 30 mm in the centre to 15 mm at the side, can be a possible reason why the secondary flow is so apparent.

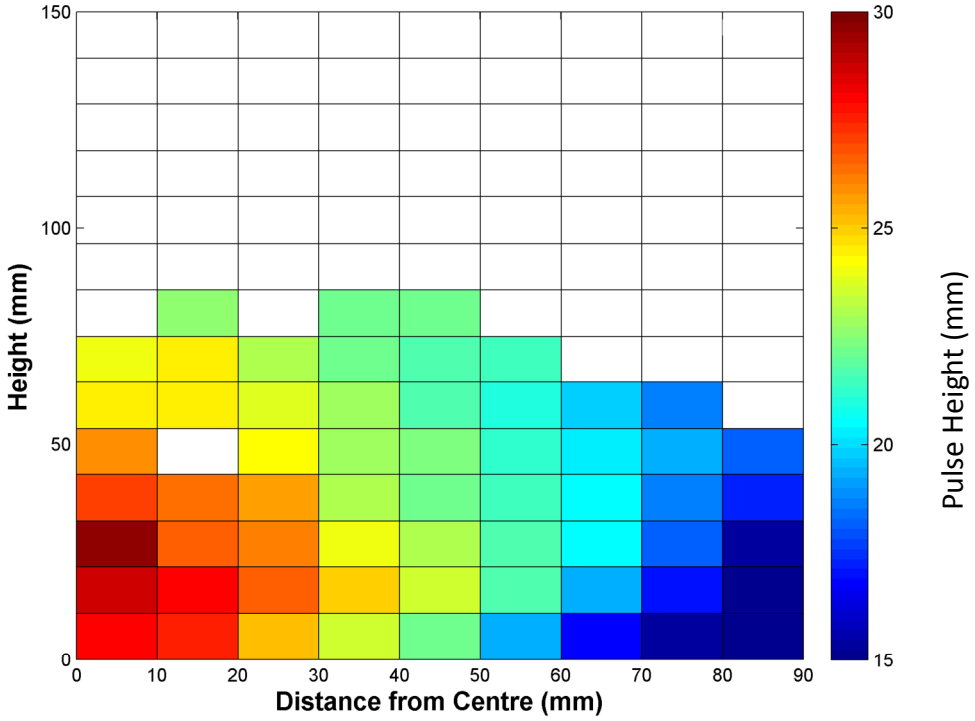

Figure 5-36 A pseudocolour plot indicating the difference in pulse height vs. the position in the bed. Data in the figure is from the 3.6 SG tracer in a homogenous bed run for two hours.

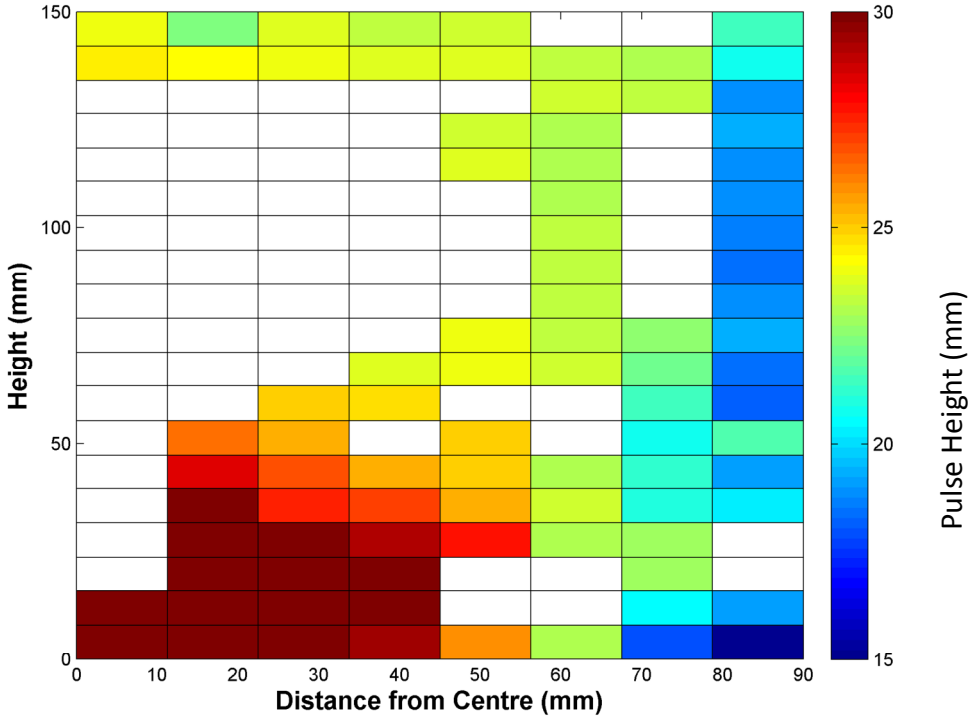

Figure 5-37 A pseudocolour plot indicating the difference in pulse height vs. the position in the bed. Data in the Figure is from the spherical glass tracer in a homogenous bed run for two hours.

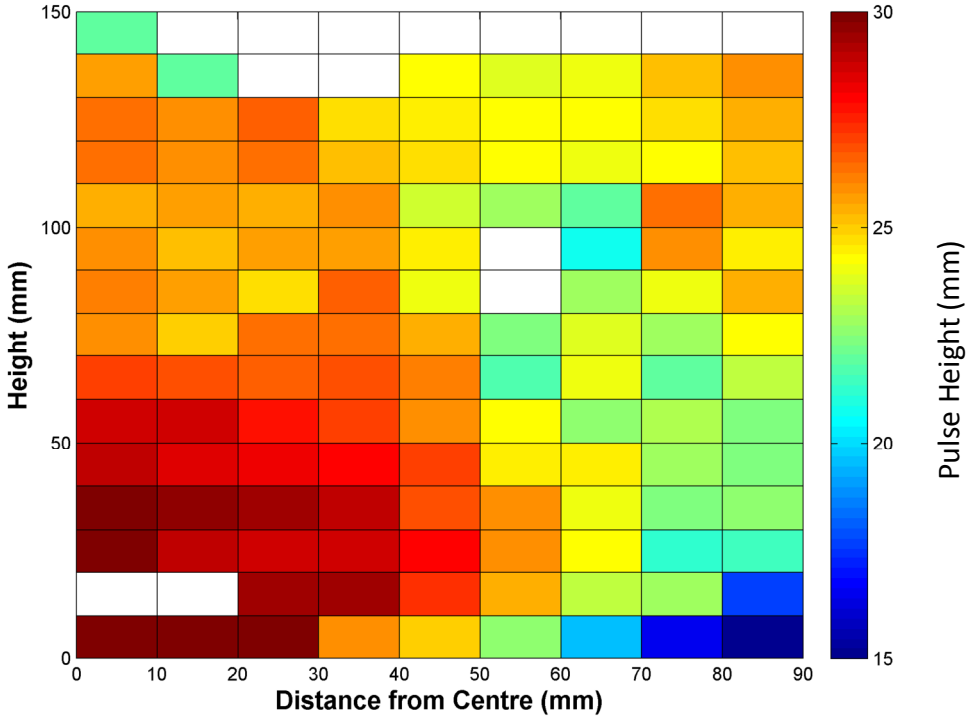

Figure 5-38 A pseudocolour plot indicating the difference in pulse height vs. the position in the bed. Data in the figure is from multiple tests where the tracers were affected by the secondary flow.

It is clear that the secondary flow can have a significant effect on the efficiency of batch jigging. Whether it is observed in industrial jigs is not known.

5.9 Conclusions

Positron emission particle tracking was shown to be a very good technique to track the individual trajectories of particles inside a laboratory scale batch jig. The accuracy and resolution obtained were more than sufficient for the study.

Through observation of the particle trajectories, important parameters such as stratification rate and the final position of a tracer can be determined. In this study, an attempt was made to correlate a particle's properties (size, density and shape) to its stratification rate. Through visual inspection of the particle trajectories, it was very difficult to see what effect the tracer properties have on the stratification rate. Fitting lines to the curves and doing a multivariate analysis provided much more information on the stratification rate. A particle experiences two separate stratification rates in the process: the initial rate at the top part of the jig and the final rate at the bottom part of the jig, which is significantly larger. A straight line can be fitted to both of these. It was found that the initial rate is not a function of any of the particle properties (size, density and shape). However, the final stratification rate is a strong function of the particle size and density, as well as the bed density, and to a lesser extent a function of shape.

Throughout the study, it was observed that there was a circular flow pattern (secondary flow) that resulted in certain particles moving around in the jig bed and preventing them from coming to rest at a specific height in the jig bed. It was found that particles with densities close to and lower than that of the jig bed were affected the most by this secondary flow. By calculating and plotting velocity vector fields, the secondary flow can be clearly visualised. A possible reason for the secondary flow patterns is the uneven flow of water into the jig. It was observed that the pulse height is lower at the sides of the jig compared to the centre, confirming the uneven flow.

6 MODELLING

6.1 Stratification model (potential energy theory)

The model that was developed in Excel-VBA, as described in section 4.9, was first tested against the work done by King (2012) and other authors (Rao, 2007; Tavares, 1999) to determine whether the algorithm worked. The first set of data used for validation is that of King (2012), which is data generated by his model. The comparison is shown in Figure 6-1. It can be seen from the Figure that there is a very good fit between King's (2012) data and the stratification model.

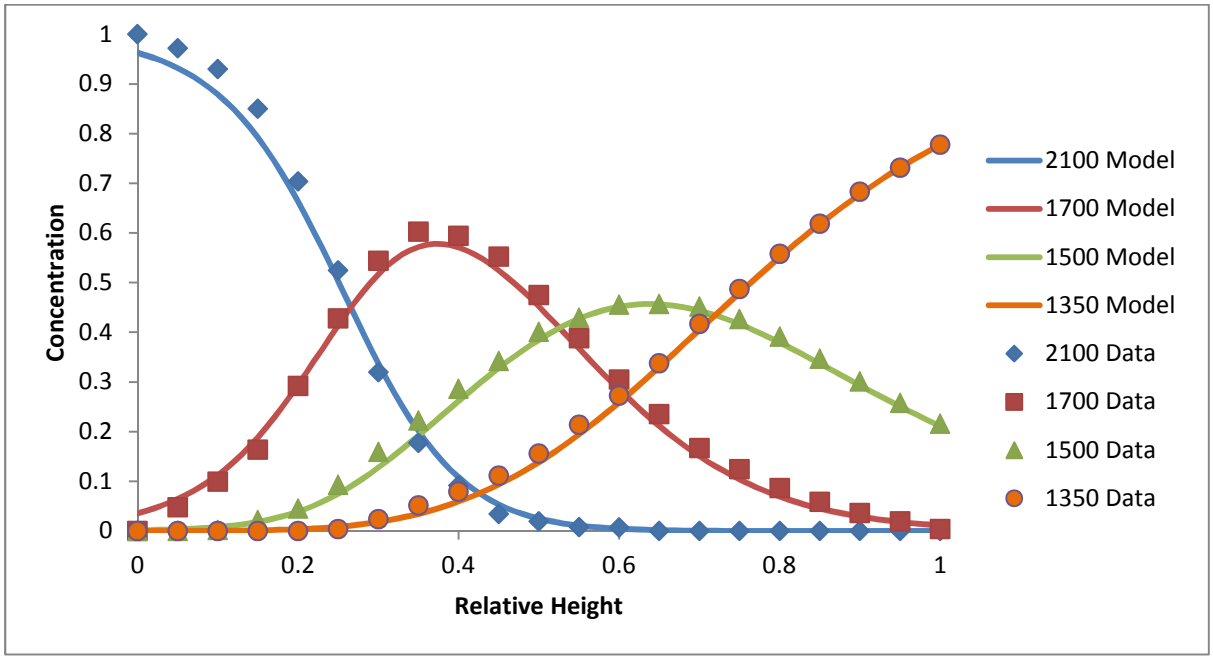

Figure 6-1 Comparison of stratification profiles from the model in King (2012) and the stratification model. The points represent King's data and the lines the model.

The next set of data used for verification was that of Tavares (1999). He solved the potential energy theory in an entirely different manner by making use of Monte Carlo simulations. The comparison between Tavares's model and the stratification model can be seen in Figure 6-2. The markers represent Tavares's (1999) data and the solid lines the stratification model. It is clear from the Figure that there is a very good fit between the data and the model. It can therefore be concluded that the stratification model developed in Excel-VBA, based on Rao's (2007) model, does behave as expected. However, it does not mean that the model will give a good representation of real life applications.

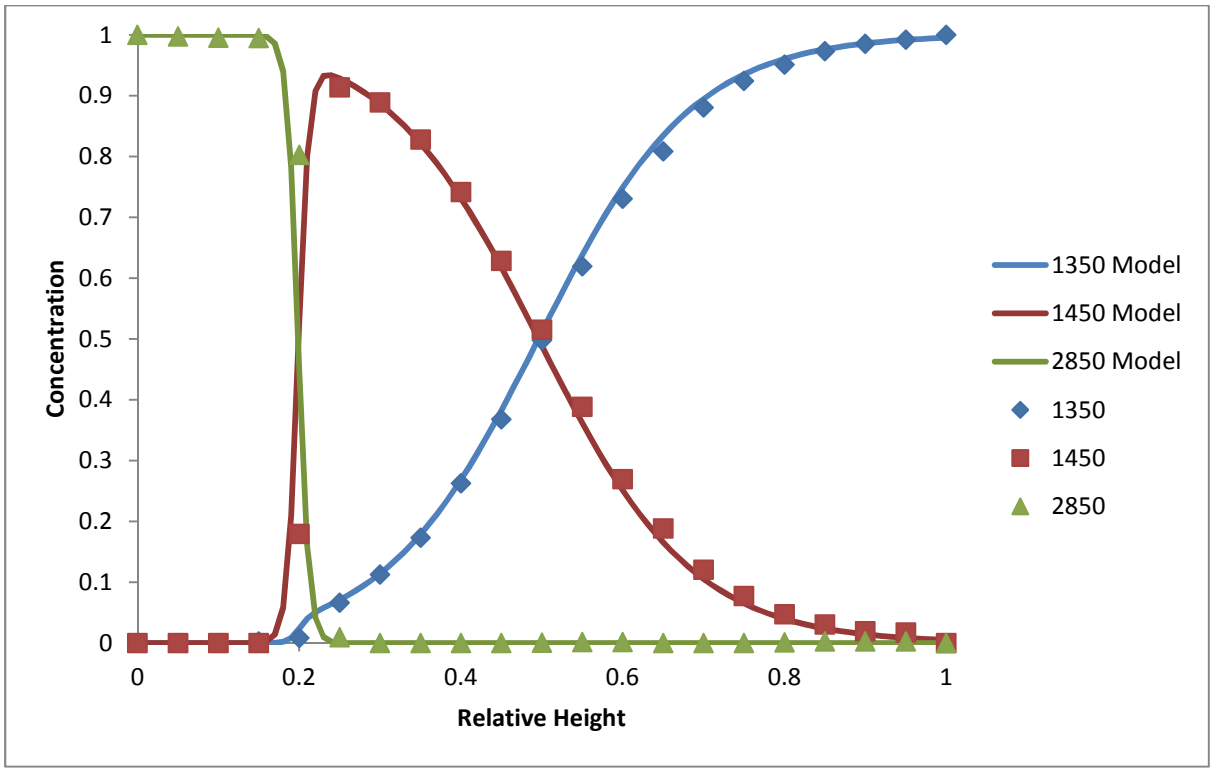

Figure 6-2 Comparison of stratification profiles from the model in Tavares (1999) and the stratification model. The points represent Tavares's data and the lines the model.

Data from Naude (2010) was used to test the relevance of the stratification model for iron ore batch jigging. Naude's (2010) work is ideal for testing the stratification model, since the iron ore was removed from the jigging chamber in layers and each layer was characterised into six density fractions and six size fractions. From Naude's data, stratification profiles for each of the 36 fractions can be calculated. In Figure 6-3, the stratification profiles for the six different density fractions for the 4.5 mm particles are shown. It can be noted from Figure 6-3 that the high density (4500 kg/m^3) and the low density (2700 kg/m^3) material show good separation. However, the intermediate density particles (e.g. 3500 kg/m^3) do not separate very well. This is probably due to the near density effect caused by a secondary flow, as discussed in section 5.6.4.

Naude's (2010) data was then used as input into the model (size, density and volume fractions). The input table can be seen below (Table 6-1). An initial guess is made for the stratification parameters (A and b) and the stratification profiles are

generated by the model. The stratification parameters can then be optimised to obtain a good fit with the data. The results from the stratification model can be seen in Figure 6-4. The same six stratification profiles that were shown in Figure 6-3 were chosen, so that a direct comparison of the data and the model can be made. When comparing the data (Figure 6-3) and the model (Figure 6-4), it can be seen that there is some correlation between the two. However, the model shows more idealistic separation and does not account for the inefficiencies generated by the near density effect, or rather the secondary flow inside the jig. It is clear that the stratification model, based only Rao's (2007) assumptions, is insufficient to predict more realistic jigging situations and further adjustments to the model are needed.

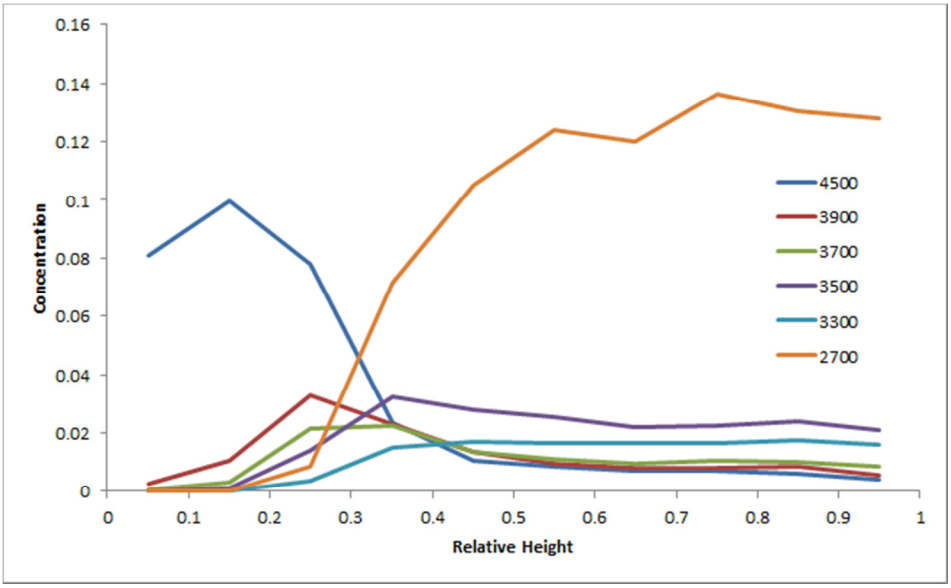

Figure 6-3 Stratification profiles adapted from testwork done by Naude (2010)

Table 6-1 Stratification model input table with the data from Naude (2010)

	6	Size							
	6	0.00966	0.00735	0.0065	0.00565	0.0045	0.0035	A	b
Density	4500	0.00066	0.06013	0.03706	0.08904	0.03135	0.00712	80	1.6
	3900	0.00062	0.01287	0.01083	0.02480	0.01200	0.00181		
	3700	0.00049	0.00966	0.00831	0.01997	0.01105	0.00227		
	3500	0.00059	0.01507	0.01421	0.03345	0.01910	0.00423		
	3300	0.00086	0.01425	0.01112	0.02463	0.01216	0.00201		
	2700	0.01446	0.09303	0.09132	0.19766	0.08447	0.02735		

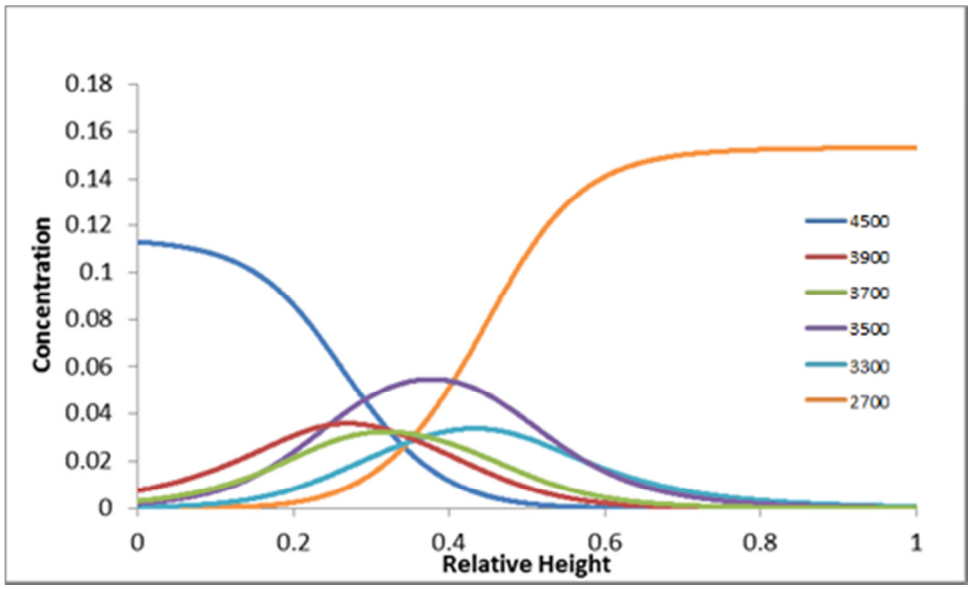

Figure 6-4 Stratification profiles generated by the stratification model, with input data from Naude (2010). *A*=80 and *b*=1.6

6.2 Addition of the near density effect to the stratification model

It is clear from the stratification model that its predictions are for very ideal cases, where there aren't any additional factors that can influence efficiency, such as the secondary flow affecting the near density material.

Rao (2007) improved on King's stratification model by just making a simple modification – assuming that the stratification constant (α) has a power law relationship with size, as shown in equation 2.34 and discussed in section 2.9.2.

$$\alpha_i = A(d_i)^b \qquad 2.34$$

A similar approach was taken to add the effect of the secondary flow by adding a function to modify the stratification constant. In section 5.6.4 it was shown that the secondary flow starts to affect stratification efficiency of a particle when the particle is around and slightly lower than the average density of the bed. It can also be assumed that the very high and very low density material will have good stratification efficiencies.

This effect was assumed to be Gaussian in nature, meaning that the closer to the average bed density a particle is, the lower its efficiency will be, and the further away from the average bed density the particle is, the higher its efficiency will be.

The following equations (equations 6.1 and 6.2) were added to the model to account for the lower efficiencies of the near density material.

$$F = 1 - EXP\left(\frac{-1 * (\rho_i - \bar{\rho})^2}{2 * c^2}\right) \qquad 6.1$$

$$\alpha_i = FA(d_i)^b \qquad 6.2$$

Where: $\bar{\rho}$ = average density of the bed

ρ_i = particle density

c = variance factor

F = near density correction factor

A and b = stratification parameters

Equation 6.1 is an inverted Gaussian distribution (Weisstein, 2015) and an example of its form can be seen in Figure 6-5. The stratification constant α_i is now calculated with equation 6.2. The only difference from equation 2.34 is the addition of the near density correction factor (F).

Taking the same input data as used in the previous example (table 6-1) and initially guessing initial values for A, b and c, new stratification profiles can be generated. The A, b and c values can then be adjusted to best fit the data. Figures 6-6 (c=400) and 6-7 (c=600) show the stratification profiles generated by the modified model. The same six fractions are shown, that are shown in Figure 6-3.

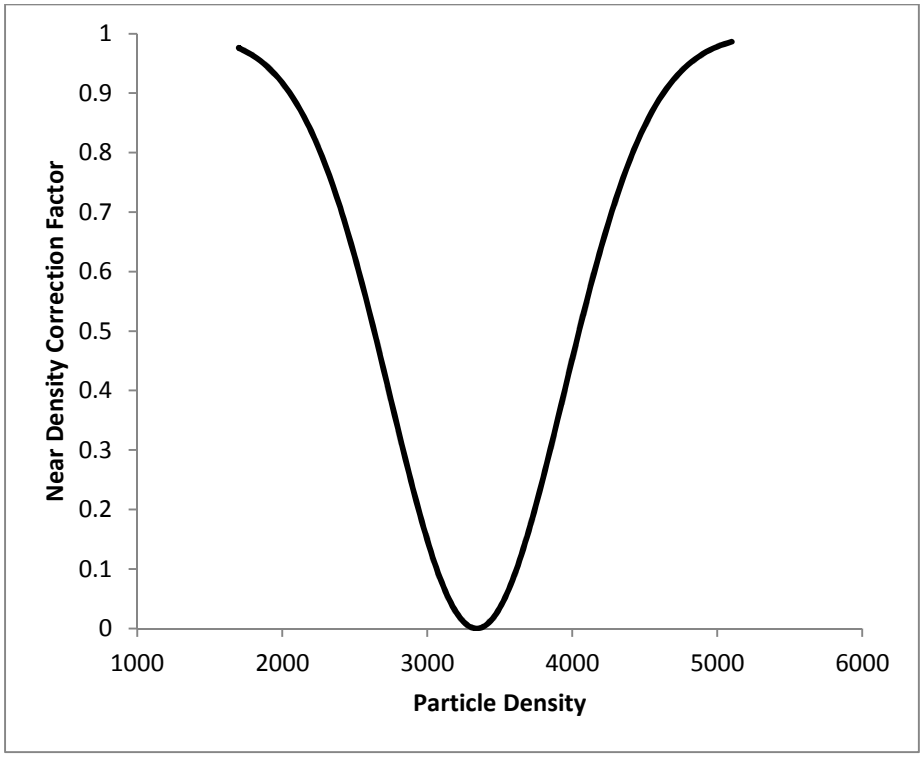

Figure 6-5 Near density factor, average density = 3340 kg/m3 and c = 600

When comparing Figure 6-3 to Figures 6-6 and 6-7, it is clear that the modified model represents the testwork a lot better compared to the standard stratification model (Figure 6-4). The modified model takes into account the lower efficiency of the near density material, the high density (4500 kg/m³) and the low density (2700kg/m^3) material shows good efficiency, and the intermediate density material (3300 to 3500 kg/m³) is more spread out across the bed.

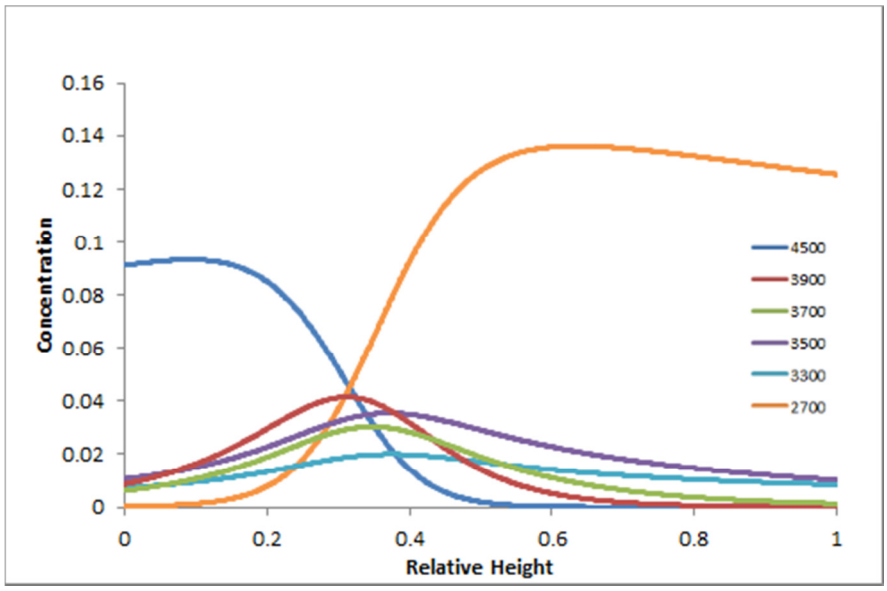

Figure 6-6 Stratification profiles generated by the modified model, with input data from Naude (2010). A=80, b=1.6 and c=400

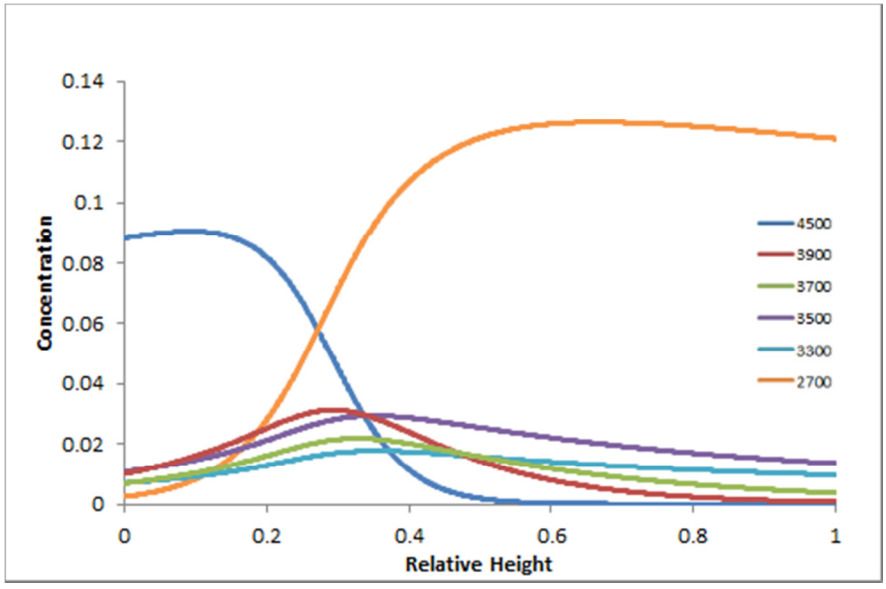

Figure 6-7 Stratification profiles generated by the modified model, with input data from Naude (2010). A=80, b=1.6 and c=600

6.3 Stratification model conclusions

A model based on King's (2001) stratification model with the modifications done by Rao (2007) was set up in Excel VBA. The model was tested against the data used by King and Tavares (1999), to verify that the model gave the appropriate results.

The King's (2001) and Roa's models did not fit iron ore batch jig testwork very well, probably due to the fact that these models does not take into account phenomena that affect the efficiencies of certain particle groups, such as the back mixing that is caused by the secondary flow seen during the PEPT testwork.

The stratification model was then modified to include this effect. Observations from the PEPT work indicated that the closer the density of the particle to that of the bed material, the more it is affected by the secondary flow, and the lower the separation efficiency of that specific particle. After the back mixing effect was added to the model, the model fitted the data much better. From the modelling and the PEPT work, is can be said that a lot of inefficiency in batch jigging is due to the secondary flow.

7 CONCLUSIONS

Positron emission particle tracking was proven to be a viable technique to study particle movement inside an iron ore batch jig. It was a concern that a bed of dense iron ore particles might affect the Gama rays and distort the results. When testing the accuracy for this application, it was shown not to be the case.

The PEPT scanner gave very accurate three dimensional trajectories for the selected tracers as they moved through the jig. The spatial and temporal resolutions were sufficient to view the movement of a tracer particle during a single pulse with very high detail.

Even though the high cost of the PEPT testwork put limitations on the number of test runs that could be conducted, very valuable observations were made and good conclusions were drawn.

The vertical component of the particle trajectories showed very important features of the particles' movement through the jig bed. Looking at the vertical component, the *stratification rate* can be seen during the initial movement of the particle through the jig bed, and the *stratification position* can be seen as the layer in which the particle ends up in, after steady state is reached.

While analysing what effect size, density and shape have on the stratification rate, it was found that no specific trends could be clearly observed through visual inspection of the particle trajectories. Fitting straight lines to the initial part (stratification) of the trajectory and using multivariate analysis on the slopes of the fitted curves, it was shown that an increase in both size and density increase the rate at which a particle moves through the bed. The elongated particle showed to have the same stratification rates as that of the cubic particles. However, the flat particles have a slightly larger stratification rate.

During the analysis of the effect of size, density and shape on the stratification position, it was shown that size and density have clear effect on how a particle will behave when it reaches its stratification position. High density and large particles will

move to the bottom of the jig and remain in that position. Lower density and smaller particle will move down the bed, but they have the tendency of moving back up the bed, following a circular flow pattern in the jig.

The testwork showed the existence of a secondary circular flow pattern inside the batch jig. Particles with densities close to that of the bed material are affected by this secondary flow. The origin of the secondary flow seemed to be the result of an uneven velocity profile in the water that lifts the jig bed. It was showed that the pulse is significantly higher at the centre of the jig compared to the sides of the jig, due to the uneven water front entering the bottom of the jigging chamber.

Following the PEPT testwork, a stratification model was set up based on King's (2001) stratification model with the modifications done by Rao (2007). The model did not fit iron ore batch jig testwork very well, since it did not take into account the back mixing of the particles caused by the secondary flow. The stratification model was then modified to include this effect. Observations from the PEPT work indicated that the closer the density of the particle to that of the bed material, the more it is affected by the secondary flow and the lower the efficiency of that specific particle. After the back mixing affect was added to the model, a very good correlation between the model and the batch jig data was found.

8 RECOMMENDATIONS

It was shown that PEPT is a very good technique for studying the movement of different types of particles inside a batch jig. It is, however, unfortunate that only a limited number of tracers could be tested in this study, which resulted in an incomplete picture of how size, density and shape affect a particle's movement in a batch jig. If the effect of the tracer's properties on its movement is to be further investigated, many more test runs will be required. It might not be a viable option, due to the costs involved in PEPT testwork.

PEPT showed phenomena inside the batch jig that are not attainable with any other methods, and it is entirely possible that there are more phenomena that were not seen in this study that will be revealed in further PEPT work.

It was shown in the study that the movement of a tracer particle during an individual pulse can be observed. This high resolution obtained with PEPT might make it possible to investigate the fundamental mechanisms (differential acceleration, hindered settling, etc) of jigging.

The secondary flow that was observed in the batch jig might serve as explanation for the near density effect observed in jigging. It would be an interesting study to determine if the secondary flow is also present in industrial jigs.

The stratification model that was developed based on King and Rao's work shows significant promise, especially since it was shown that effects such as back mixing can be added. More experimental runs are required to verify its applicability and to determine if normal distributing is the best equation to use for the secondary flow correction. This testwork would require doing batch jigging tests on different feed samples and then removing the stratified bed in layers. Each layer should then be carefully spilt into size and density fractions.

King showed that his model can be fit to continuous jigs with some modifications. It should therefore be possible to fit the stratification model to continuous jigging as

well. It would be interesting to see the stratification model developed for continuous jigging and then to compare it to data from pilot or industrial scale jigs.

9 REFERENCES

Adhikari, B. & Mishra, B. K. 1999. Analysis of Fluid Motion During Jigging. *Minerals Engineering*, vol.12, no.12, pp.1469-1477.

Agricola, G. 1556. *De Re Metallica*. Translated from the first Latin edition by H.C and L.H. Hoover. 1912. New York: Dover Publications.

Barigou, M. 2004. Particle tracking in opaque mixing systems: an overview of the capabilities of PET and PEPT. *Chemical Engineering Research and Design*, vol. 82, no. 9, pp. 1258–1267.

Bbosa, L. S., Govender, I., Mainza, A. N. & Powell, M. S. 2011. Power draw estimations in experimental tumbling mills using PEPT. *Minerals Engineering*, vol. 24, No 3–4 , pp. 319–324

Burt, R. O. 1984. *Gravity concentration technology*. New York: Elsevier.

Chang, Y. Ã., Ilea, C. G., Aasen, Ø. L. & Hoffmann, A. C. 2011. Particle flow in a hydrocyclone investigated by positron emission particle tracking. *Chemical Engineering Science*, vol. 66, no. 18, pp. 4203–4211.

Cherry, S. R., Tornai, H. P., Levin, C. S., Siegel, S. & Hoffman, E. J. 1995. A comparison of PET detector modules employing rectangular and round photomultiplier tubes. *IEEE Transactions on Nuclear Science*, vol. 42, no. 4, pp.1064-1068.

Cole, K. E., Buffler, A., Van der Meulen, N. P., Cilliers, J. J., Franzidis, J. P., Govender, I., Liu, C. & Van Heerden, M. R. 2012. Positron emission particle tracking measurements with 50 micron tracers. *Chemical Engineering Science*, vol. 75, pp. 235–242.

Cole, K. E., Waters, K. E., Fan, X., Neethling, S. J. & Cilliers, J. J. 2010. Combining positron emission particle tracking and image analysis to interpret particle motion in froths. *Minerals Engineering*, vol. 23, no, pp. 1036–1044.

Conway-Baker, J., Barley, R. W., Williams, R. A., Jia, X., Kostuch, J., McLoughlin, B. & Parker, D. J. 2002. Measurement of the motion of grinding media in a vertically stirred mill using positron emission particle tracking (PEPT). *Minerals Engineering*, vol. 15 no. 1/2, pp. 53–59.

De Felice, R. 1994. The Voidage Function for Fluid-Particle Interaction Systems. *International Journal of Multiphase Flow*, vol. 20, no. 1, pp.153-159.

Dieudonne, V., Jonkers, A. & Loveday, G. 2006. An approach to confidently predicting jigging performance. *The Journal of the South African Institute of Mining and Metallurgy*, vol. 106, pp. 191–204.

Fan, X., Parker, D. J. & Smith, M. D. 2006. Labelling a single particle for positron emission particle tracking using direct activation and ion-exchange techniques. *Nuclear Instruments and Methods in Physics Research Section A: Accelerators, Spectrometers, Detectors and Associated Equipment*, vol. 562, pp. 345–350.

Fan, X., Waters, K. E., Rowson, N. A. & Parker, D. J. 2009. Modification of ilmenite surface chemistry for enhancing surfactants adsorption and bubble attachment. *Journal of Colloid and Interface Science*, vol. 329, no. 1, pp. 167–172.

Gaudin, A. M. 1939. *Principles of Mineral Dressing*. New York: McGraw Hill.

Gupta, A. & Yan, D. S. 2006. *Mineral Processing Design and Operation*. Amsterdam: Elsevier.

Habashi, F. 2006. *A Short History of Mineral Processing.* Proceedings of the XXIII International Mineral Processing Congress, Volume 1, Istanbul, Turkey.

Heath, T. L. (ed.). 2009. *The Works of Archimedes*. London: Cambridge University Press.

Independent competent person's report on the principal assets which will be incorporated into Exxaro Limited and Kumba Iron Ore Limited (2006). Available at: http://www.exxaro.com/pdf/icpr/intro/introduction.htm. [Cited August 2015].

IWQS, 2002. *Radioactivity Dose Calculation and Water Quality Evaluation Guideline For Domestic Water Use*. Department of Water Affairs and Forestry, pp. 13-19.

Kelly, E. G. & Spottiswood, D. J. 1989. *Introduction to Mineral Processing*. New York: Wiley & Sons.

King, R. P. 2001. *Modeling and Simulation of Mineral Processing Systems*. Woburn: Butterworth-Heinemann.

Kumba Iron Ore Limited Integrated Report 2014. Available at: http://www.angloamericankumba.com/~/media/Files/A/Anglo-American-Kumba/documents/integrated-report-2014.pdf. [Cited August 2015].

Laverman, J. A., Fan, X., Ingram, A., Van Sint Annaland, M., Parker, D. J., Seville, J. P. K. & Kuipers, J. A. M. 2012. Experimental study on the influence of bed material on the scaling of solids circulation patterns in 3D bubbling gas–solid fluidized beds of glass and polyethylene using positron emission particle tracking. *Powder Technology*, vol. 224, pp. 297-305.

Louis, W. 2000. Jigs:The forgotten machine. *Engineering and Mining Journal,* vol.201, no. 8, pp. 30

Marigo, M., Davies, M., Leadbeater, T., Cairns, D. L., Ingram, A. & Stitt, E. H. 2013. Application of Positron Emission Particle Tracking (PEPT) to validate a Discrete Element Method (DEM) model of granular flow and mixing in the Turbula mixer. *International Journal of Pharmaceutics*, vol. 446, no. 1–2, pp. 46–58

Mihailova, O., Lim, V., McCarthy, M. J., McCarthy, K. L. & Bakalis, S. 2015Laminar mixing in a SMX static mixer evaluated by positron emission particle tracking (PEPT) and magnetic resonance imaging (MRI). Chemical Engineering Science, vol. 137, pp. 1014-1023

Mishra, B. K. & Mukherjee, A. K. 2006. An integral assessment of the role of critical process parameters on jigging. *International Journal of Mineral Processing*, vol. 81, pp.187–200.

Mukherjee, A., Bhattacharjee, D. & Mishra, B. 2006. Role of water velocity for efficient jigging of iron ore. *Minerals Engineering*, vol. 19, no. 9, pp. 952–959.

Myburgh, H. A. 2010. The influence of control and mechanical conditions of certain parameters on jigging. *Journal of the Southern African Institute of Mining and Metallurgy*, vol. 110, no. 11, pp. 655-661.

Myburgh, H. A. & Nortje, A. 2014. Operation and performance of the Sishen jig plant. *Journal of the Southern African Institute of Mining and Metallurgy*, vol. 114, no. 7, pp. 569-574.

Naudé, N. 2010. Evaluation and Modelling of a Mineral Density Separator. Stellenbosch University.

Naudé, N., Lorenzen, L., Kolesnikov, A. V., Aldrich, C. & Auret, L. 2013. Observations on the separation of iron ore in a prototype batch jig. *International Journal of Mineral Processing*, vol. 120, pp. 43-47.

Parker, D. J., Allen, D. A., Benton, D. M., Fowles, P., McNeil, P. A., Min Tan & Beynon, T. D. 1997. Developments in particle tracking using the Birmingham Positron Camera. *Nuclear Instruments and Methods in Physics Research Section A: Accelerators, Spectrometers, Detectors and Associated Equipment*, vol. 392, no. 1–3, pp. 421-426.

Parker, D. J., Broadbent, C. J., Fowles, P., Hawkesworth, M. R. & McNeil, P. 1993. Positron emission particle tracking - a technique for studying flow within engineering equipment. *Nuclear Instruments and Methods in Physics Research Section A: Accelerators, Spectrometers, Detectors and Associated Equipment*, vol. 326, no. 3, pp. 592–607.

Pasha, M., Hassanpour, A., Ahmadian, H., Tan, H. S., Bayly, A. & Ghadiri, M. 2015. A comparative analysis of particle tracking in a mixer by discrete element method and positron emission particle tracking. *Powder Technology*, vol. 270, part B, pp. 569-574.

Radman, J. R., Langlois, R., Leadbeater, T., Finch, J., Rowson, N. & Waters, K. 2014. Particle flow visualization in quartz slurry inside a hydrocyclone using the positron emission particle tracking technique. *Minerals Engineering*, vol. 62, pp. 142-145.

Rao, B. 2007. Extension of particle stratification model to incorporate particle size effects. *International Journal of Mineral Processing*, vol. 85, no. 1-3, pp 50–58.

Spink, T. J., Bailey, D. L., Bloomfield, P. M., Miller, M., Murayama, H., Jones, T., Jones, W., Reed, J., Newport, D., Casey, M. E. & Nutt, R. 1996. Performance of a new 3D-only PET scanner-the EXACT3D. *Nuclear Science Symposium,* vol. 2, pp.1275-1279.

Spink, T. J., Bailey, D, L,, Bloomfield, P. M., Miller, M., Young, J., Moyers, C., Hogg, D., Vaigneur, K., Jones, T., Jones, W., Reed, J., Newport, D., Casey, M. E. & Nutt, R. 2000. Physical characteristics of the ECAT EXACT3D positron tomograph. *Physics in Medicine and Biology*, vol. 45, pp. 2601-2618.

The National Nuclear Regulatory Act, 1999 (Act no. 47 of 1999), on safety standards and regulatory practices. Available at: http://www.nnr.co.za/wp-content/uploads/2015/02/No-388-NNR-Regulation-on-Safety-Standards-and-Regulatory-Practices.pdf. [Cited August 2015].

Van de Velden, M., Baeyens, J., Seville, J. P. K., Fan, X. 2008. The solids flow in the riser of a Circulating Fluidised Bed (CFB) viewed by Positron Emission Particle Tracking (PEPT). *Powder Technology*, vol. 183, no. 2, pp. 290–296.

Van der Westhuizen, A. P., Govender, I., Mainza, A. N. & Rubenstein, J. 2011, Tracking the motion of media particles inside an IsaMill™ using PEPT. *Minerals Engineering*, vol. 24, no. 3–4, pp. 195-204.

Volkwyn, T. S., Buffler, A., Govender, I., Franzidis, J. P., Morrison, A. J., Odo, A., Van der Meulen, N. P. & Vermeulen, C. 2011. Studies of the effect of tracer activity on time-averaged positron emission particle tracking measurements on tumbling mills at PEPT Cape Town. *Minerals Engineering*, vol. 24, no. 3–4, pp. 261–266.

Waters, K., Langlois, R. & Leadbeater, T. 2012. Using positron emission particle tracking to understand spiral concentrators. 9th International Mineral Processing Conference – Procemin 2012.

Waters, K., Rowson, N. A., Fan, X., Parker, D. J. & Cilliers, J. J. 2008. Positron emission particle tracking as a method to map the movement of particles in the pulp and froth phases. *Minerals Engineeting*., vol. 21 , pp. 877–882.

Weisstein, E. W. *Gaussian Function* [Online]. Available at MathWorld--A Wolfram Web Resource: http://mathworld.wolfram.com/GaussianFunction.html [Cited Jul 2015].

Williams, R. A., Jia, X. & Clarke, A. 1997. Verification of distinct element jigging models using positron emission tomography. *Proceedings of 20th International Minerals Processing Congress*, pp. 579-588.

Williams, R. A., Jia, X., Clarke, A. J. & Parker, D. J. 1998. Tomographic visualisation of particle motion during jigging. *Innovation in Physical Separation Technologies: Richard Mozley Symposium Volume.* Institution of Mining & Metallurgy, London, pp. 139-154.

Wills, B. A. & Napier-Munn, T. 2006. *Gravity concentration technology*. New York: Elsevier.

10 Appendix

10.1 Sample characterization and preparation

10.1.1 FeSi Cone Test Work

The Dense medium cone uses an upward current to keep the medium, in this case a mixture of ferrosilicon and water, in suspension. The material with a density higher than that of the medium will then sink and the material with a density lower than that of the medium will float. Figure 10-1 shows a schematic of the dense medium cone and its operation. Due to the upward flow the particle may experience a drag force which will add a significant size effect to the separation in the cone and it is therefore important to keep this upward velocity as small as possible. The drag force will also increase with an increase in the mediums density due to the increase in the medium's viscosity.

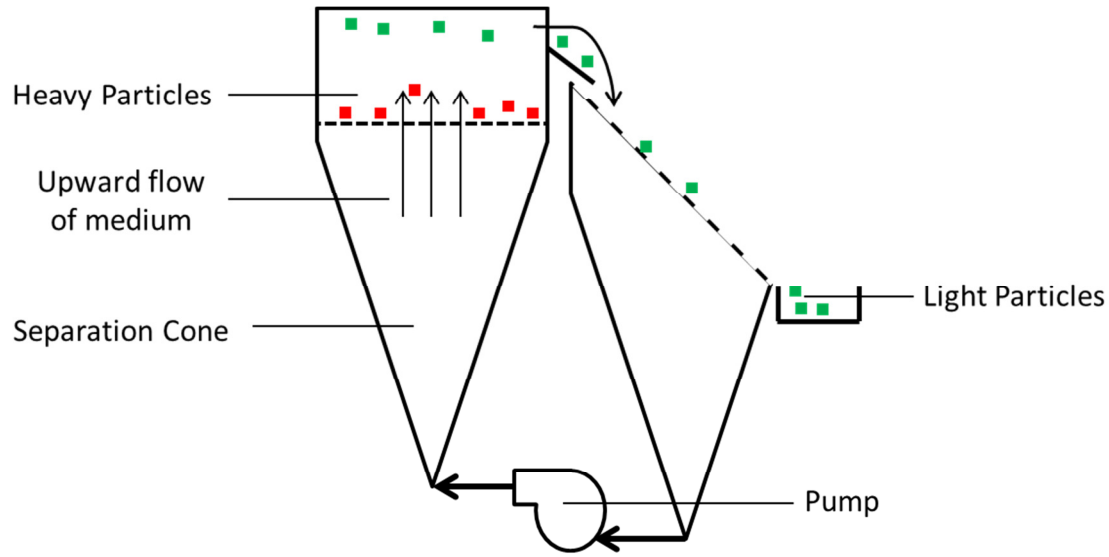

Figure 10-1 Schematic of a dense medium cone separator

The procedure for using the dense medium cone to generate density fractions:

- Calculate the FeSi to water ratio required to make up the required medium density.
- Add the amount of water calculated to the dense medium cone and start the pump.

- Slowly add the FeSi making sure to measure the density of the medium often.
- Once the required density is obtained add the ore to the cone basket.
- Stir the ore in the basket to aid in the separation of the floats and the sinks, the floats will overflow and is collected.
- If no more floats overflow, remove the basket with the sinks.
- Measure the medium density and add FeSi to adjust the density to the next cutpoint.
- The basket can now be replaced to collect the floats for the next fraction.

10.1.2 Archimedes Principle

Heath (1897) edited the original work of Archimedes and in the book written as proposition 8 it was:

'A solid heavier than a fluid will, if places in it, descend to the bottom of the fluid, and the solid will, when weighed in the fluid, be lighter than its true weight by the weight of the fluid displaced'

From the above statement it is clear that if the solid is weighed in water and the weight of the solid in air is subtracted, the result is the mass of the water displaced. If the density of the water is assumed to be 1 g/ml, the volume of the water displaced can be calculated and that volume will be the same as the volume of the solid. Since the mass of the solid and the volume of the solid are now known its density can be calculated. Figure 10-2 shows a typical setup that can be used to measure the density of solid material.

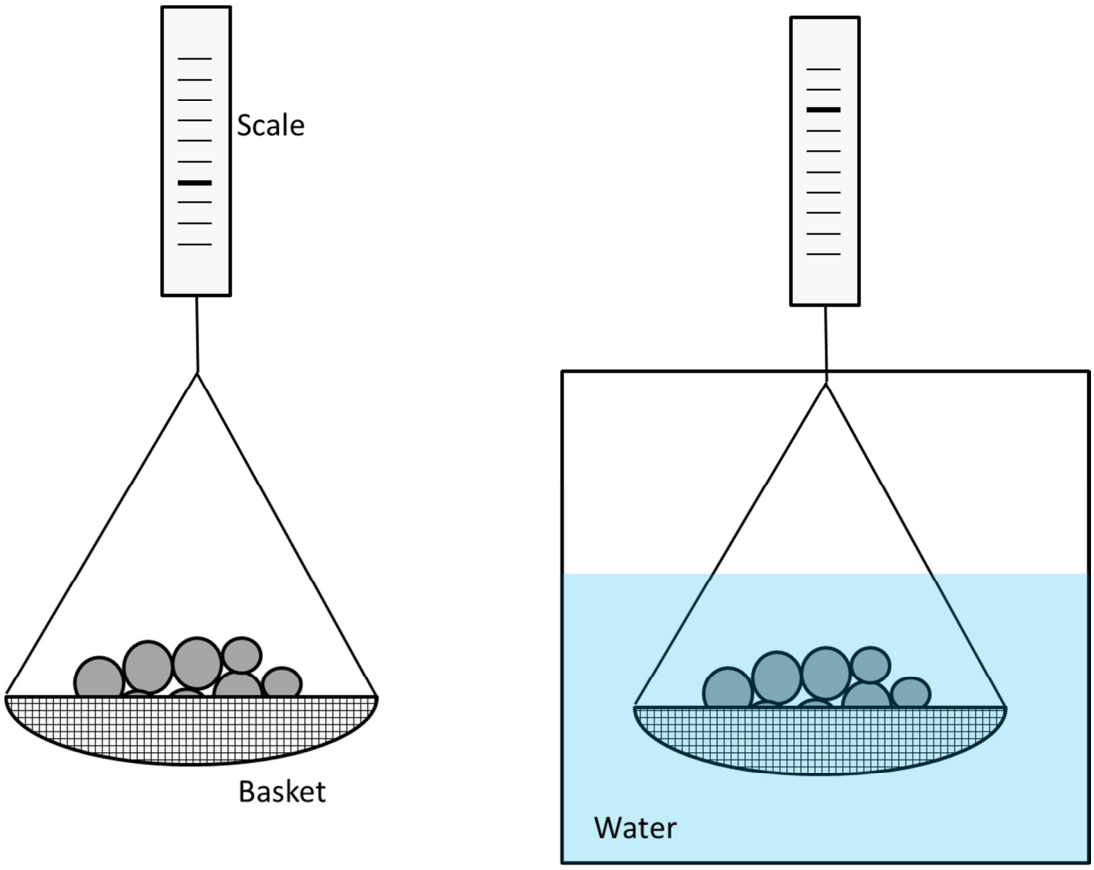

Figure 10-2 Illustration of the Archimedes principle for measuring density

The procedure used for testing the density of a sample is as follow:

- Make sure the sample is completely dry
- Weigh the sample in air and record the measurement (W_D)
- Weigh the sample in water and record the measurement (W_S)
- The density of the sample can now be calculated with:

$$\rho_s = \frac{W_D}{W_D - W_S}$$

10.2 Initial test runs with real iron ore particles

10.2.1 List of Tests Conducted

Test Run	Tracer		
	Density (g/ml)	Shape	Size (mm)
1	5.01	Equant	6.53
2	5.01	Equant	6.53
3	5.01	Equant	6.53
4	5.01	Equant	6.53
5	5.01	Equant	6.53
6	5.01	Equant	6.53
7	2.92	Tabular	5.39
8	2.92	Tabular	5.39
9	2.92	Tabular	5.39
10	2.92	Tabular	5.39
11	2.92	Tabular	5.39
12	5.01	Equant	6.53
13	5.01	Equant	6.53
14	5.01	Equant	6.53
15	5.01	Equant	6.53
16	4.11	Bladed	4.15
17	4.11	Bladed	4.15
18	4.11	Bladed	4.15
19	4.11	Bladed	4.15
20	4.11	Bladed	4.15
21	4.11	Bladed	4.15
22	4.11	Bladed	4.15
23	2.92	Tabular	5.39
24	2.92	Tabular	5.39
25	2.92	Tabular	5.39
26	2.92	Tabular	5.39
27	2.92	Tabular	5.39
28	2.92	Tabular	5.39
29	2.92	Tabular	5.39
30	3.99	Equant	6.65
31	3.99	Equant	6.65
32	3.99	Equant	6.65
33	3.99	Equant	6.65
34	3.99	Equant	6.65
35	3.99	Equant	6.65

10.2.2 Vertical Baseline Plots

The Baseline plots of the vertical component of the entire set of test runs from the initial work with the real ore particles

2

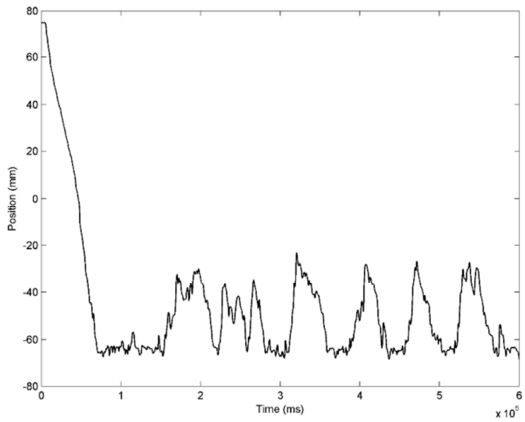

3

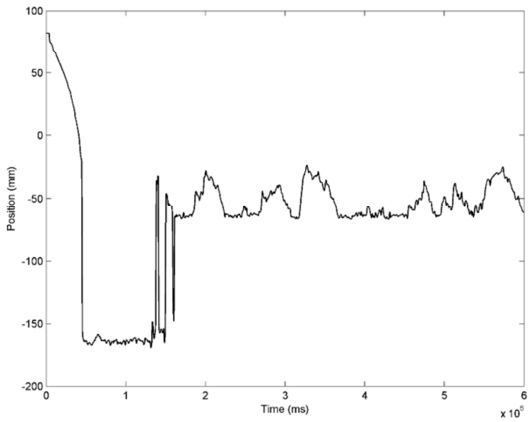

4

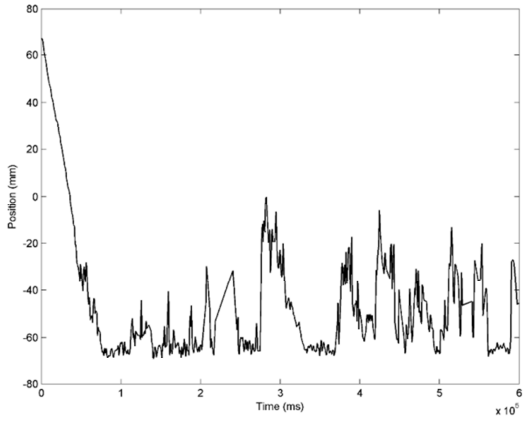

5

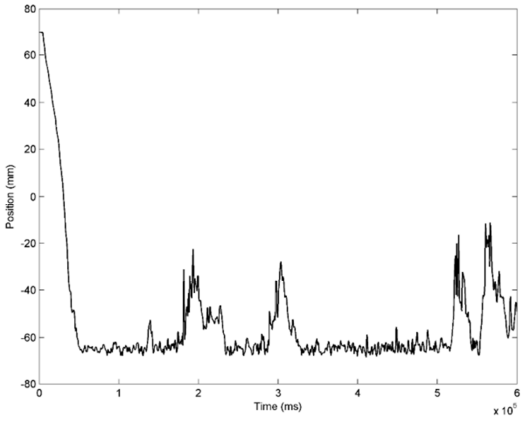

6

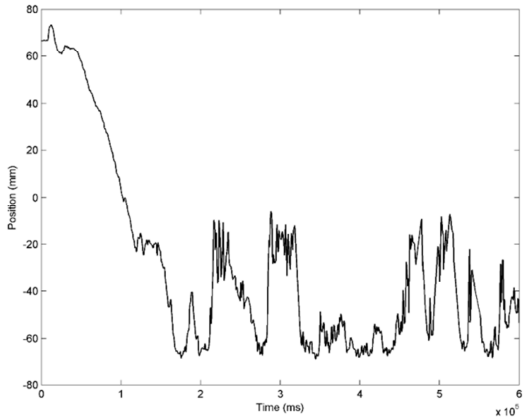

7

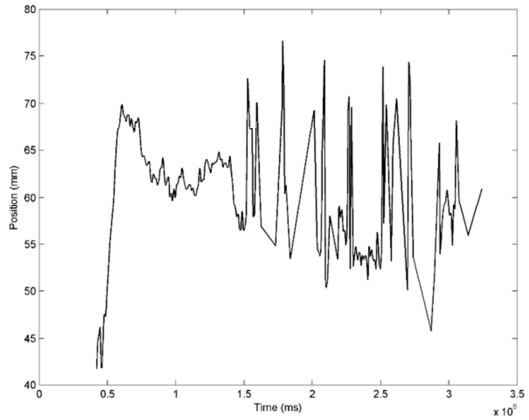

8

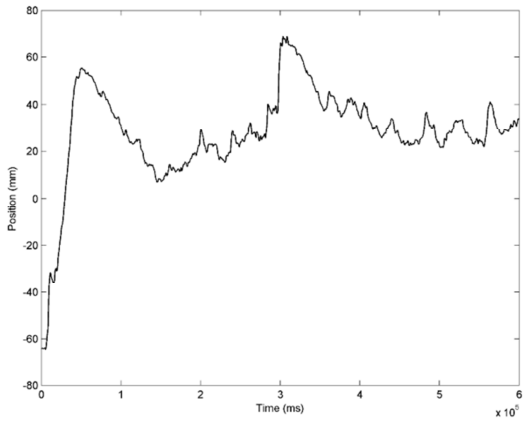

9

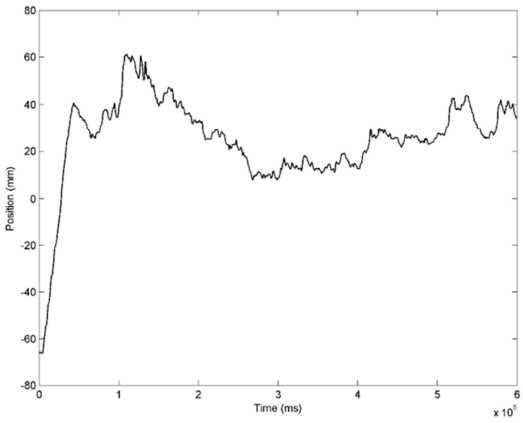

10

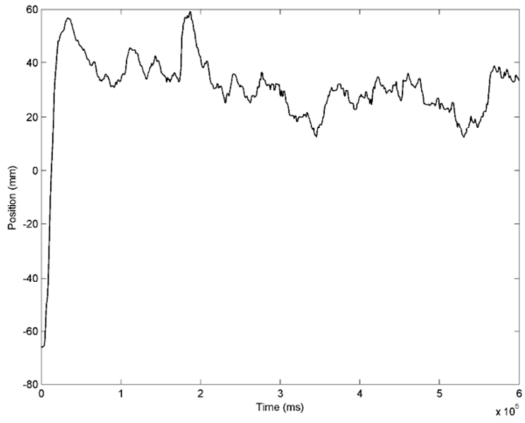

11

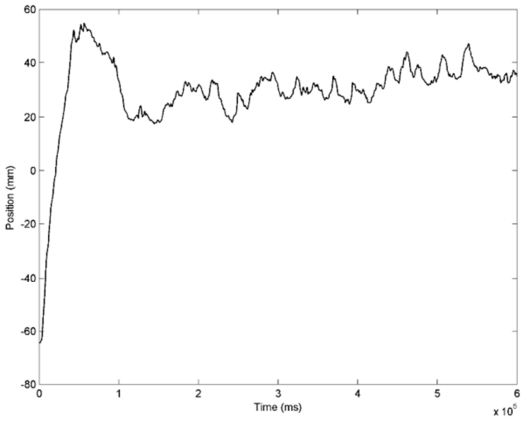

12

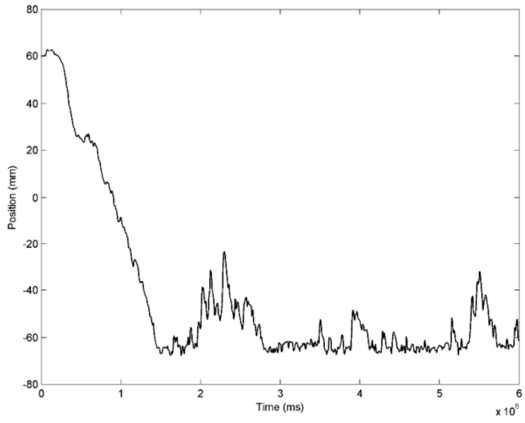

13

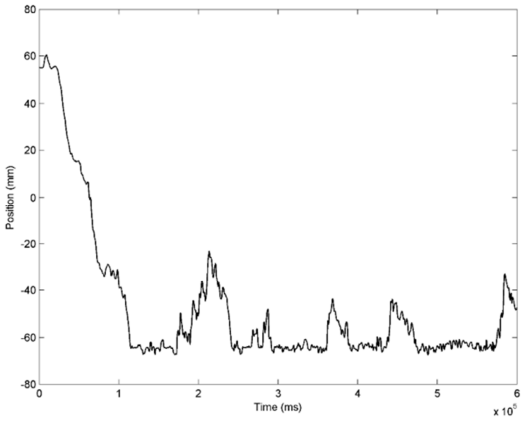

14

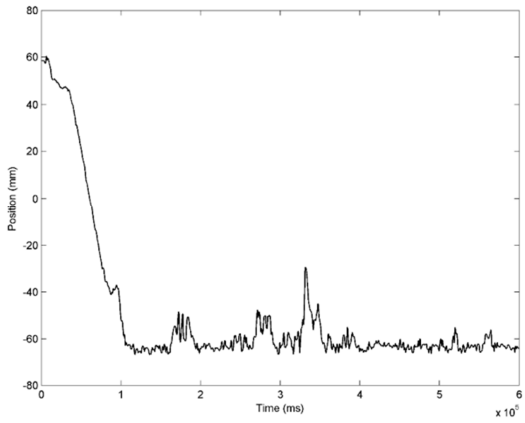

15

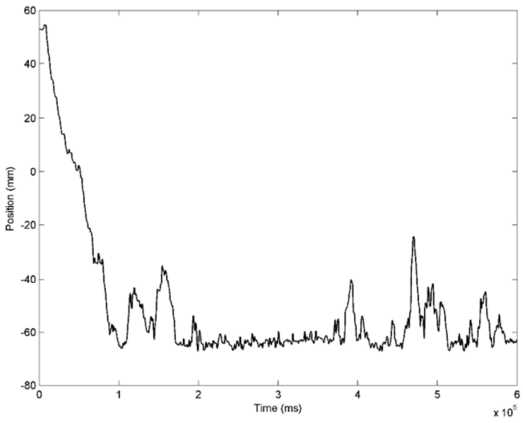

16

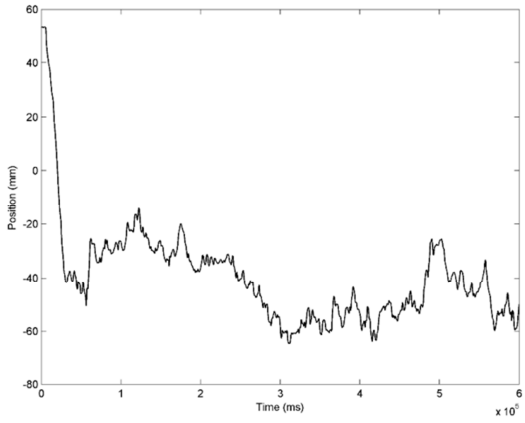

17

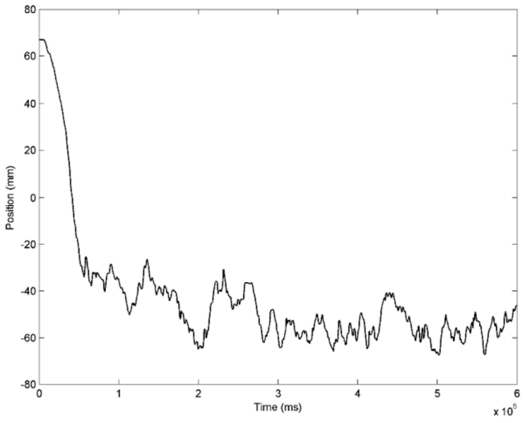

18

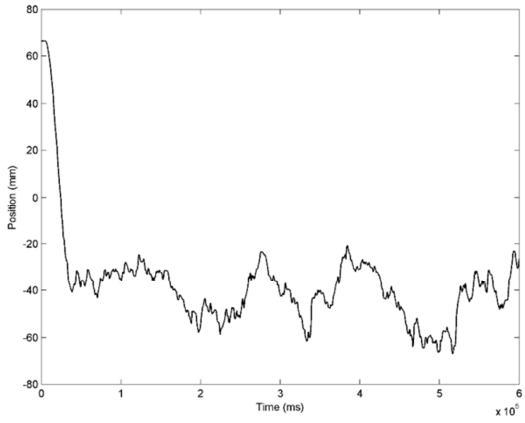

19

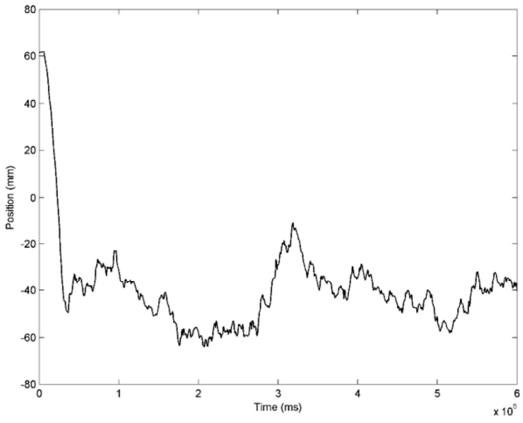

20

21

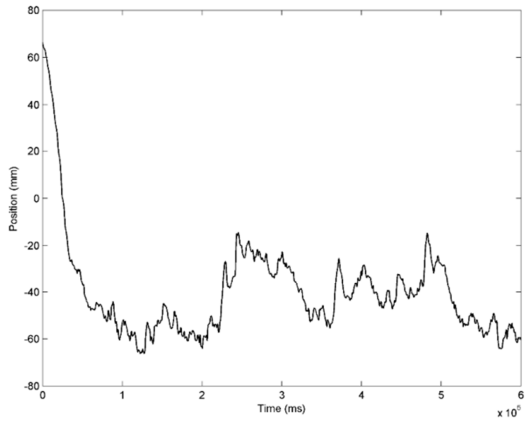

22

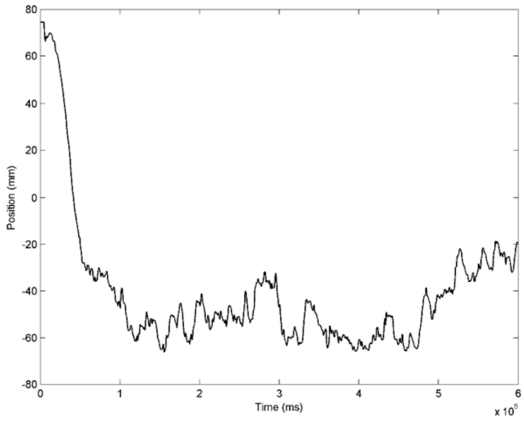

23

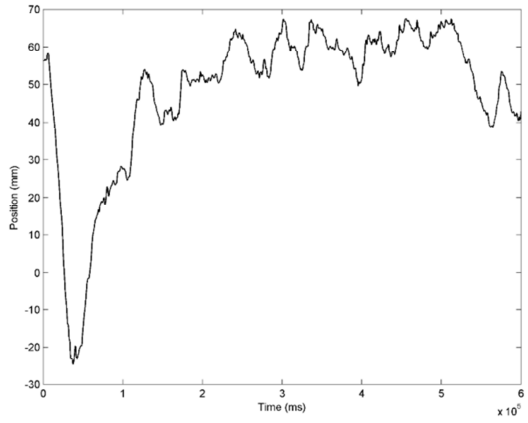

24

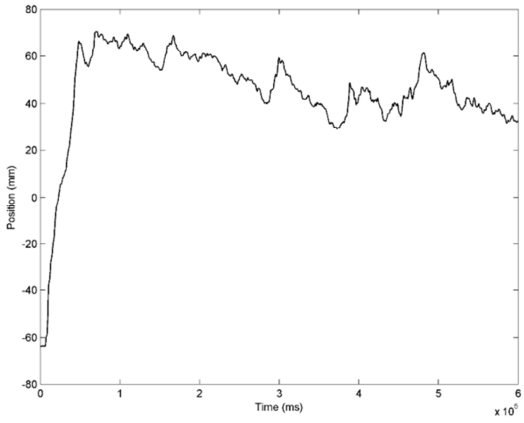

25

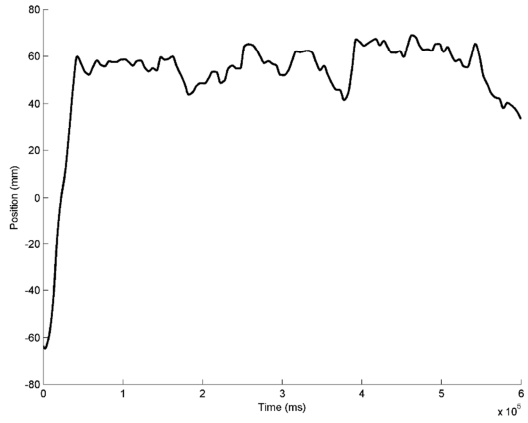

26

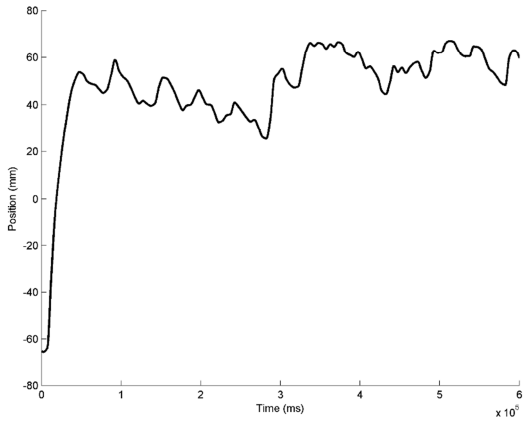

27

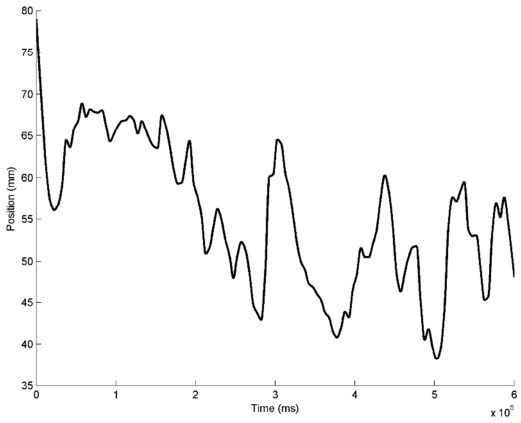

28

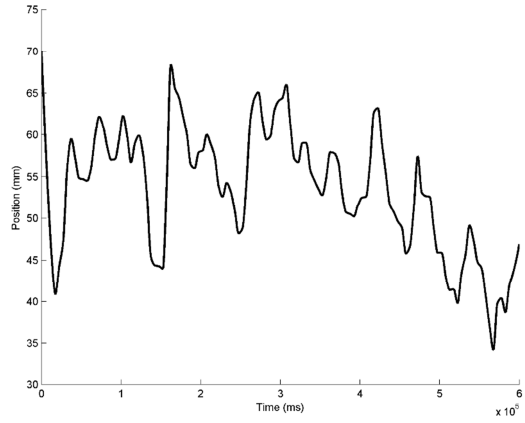

29

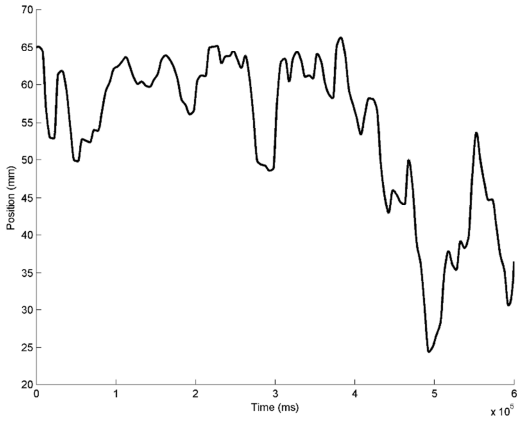

30

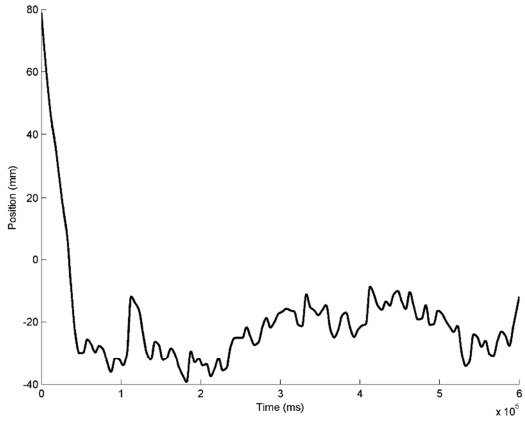

31

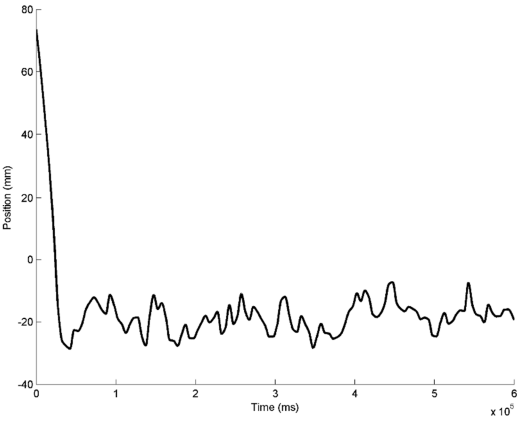

32

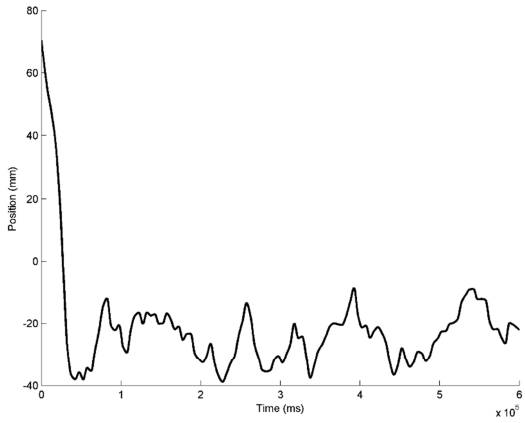

33

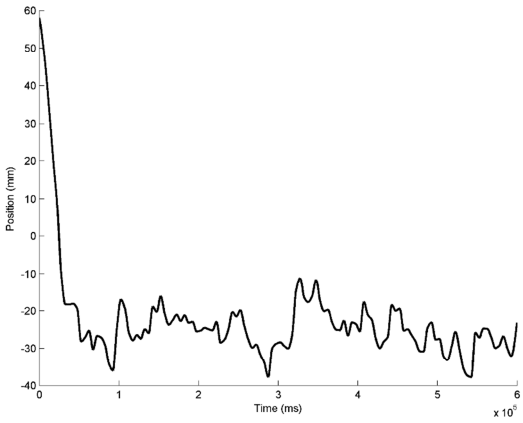

34

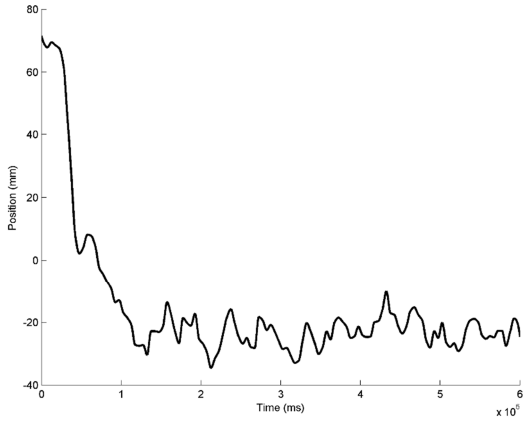

35

10.3 Test runs with artificial particles

10.3.1 List of Tests Conducted

Test	Tracer						Bed Density (g/ml)
	Nr	Density (g/ml)	Shape	Size (mm)			
				L	W	D	
1	2	3.60	Sphere	8			3.6
2	1	2.50	Sphere	8			2.5
3	3	3.96	Cubic	12.6	11.5	11.7	2.91
4	3	3.96	Cubic	12.6	11.5	11.7	3.76
5	3	3.96	Cubic	12.6	11.5	11.7	4.27
6	3	3.96	Cubic	12.6	11.5	11.7	4.1
7	3	3.96	Cubic	12.6	11.5	11.7	2.91
8	3	3.96	Cubic	12.6	11.5	11.7	3.76
9	3	3.96	Cubic	12.6	11.5	11.7	4.27
10	4	3.97	Cubic	12.6	11.5	11.7	4.1
11	4	3.97	Cubic	11.2	9.7	10.5	2.91
12	4	3.97	Cubic	11.2	9.7	10.5	3.76
13	4	3.97	Cubic	11.2	9.7	10.5	4.27
14	4	3.97	Cubic	11.2	9.7	10.5	4.1
15	4	3.97	Cubic	11.2	9.7	10.5	2.91
16	4	3.97	Cubic	11.2	9.7	10.5	3.76
17	4	3.97	Cubic	11.2	9.7	10.5	4.27
18	4	3.97	Cubic	11.2	9.7	10.5	4.1
19	5	3.93	Cubic	7.7	7.6	7.6	2.91
20	5	3.93	Cubic	7.7	7.6	7.6	3.76
21	5	3.93	Cubic	7.7	7.6	7.6	4.27
22	5	3.93	Cubic	7.7	7.6	7.6	4.1
23	5	3.93	Cubic	7.7	7.6	7.6	2.91
24	5	3.93	Cubic	7.7	7.6	7.6	3.76
25	5	3.93	Cubic	7.7	7.6	7.6	4.27
26	5	3.93	Cubic	7.7	7.6	7.6	4.1
27	6	4.20	Cubic	9.6	10.1	8.9	2.91
28	6	4.20	Cubic	9.6	10.1	8.9	3.76

29	6	4.20	Cubic	9.6	10.1	8.9	4.27
30	6	4.20	Cubic	9.6	10.1	8.9	4.1
31	6	4.20	Cubic	9.6	10.1	8.9	2.91
32	6	4.20	Cubic	9.6	10.1	8.9	3.76
33	6	4.20	Cubic	9.6	10.1	8.9	4.27
34	6	4.20	Cubic	9.6	10.1	8.9	4.1
35	7	3.76	Cubic	9.1	10.1	10.2	2.91
36	7	3.76	Cubic	9.1	10.1	10.2	3.76
37	7	3.76	Cubic	9.1	10.1	10.2	4.27
38	7	3.76	Cubic	9.1	10.1	10.2	4.1
39	7	3.76	Cubic	9.1	10.1	10.2	2.91
40	7	3.76	Cubic	9.1	10.1	10.2	3.76
41	7	3.76	Cubic	9.1	10.1	10.2	4.27
42	7	3.76	Cubic	9.1	10.1	10.2	4.1
43	8	3.93	Elongated	4.1	4.1	15	3.76
44	8	3.93	Elongated	4.1	4.1	15	4.27
45	8	3.93	Elongated	4.1	4.1	15	4.49
46	8	3.93	Elongated	4.1	4.1	15	4.71
47	8	3.93	Elongated	4.1	4.1	15	3.76
48	8	3.93	Elongated	4.1	4.1	15	4.27
49	8	3.93	Elongated	4.1	4.1	15	4.49
50	8	3.93	Elongated	4.1	4.1	15	4.71
51	9	3.91	Flat	8	8	3.9	3.76
52	9	3.91	Flat	8	8	3.9	4.27
53	9	3.91	Flat	8	8	3.9	4.49
54	9	3.91	Flat	8	8	3.9	4.71
55	9	3.91	Flat	8	8	3.9	3.76
56	9	3.91	Flat	8	8	3.9	4.27
57	9	3.91	Flat	8	8	3.9	4.49
58	9	3.91	Flat	8	8	3.9	4.71
59	10	3.89	Cubic	6.2	6.4	6.2	3.76
60	10	3.89	Cubic	6.2	6.4	6.2	4.27
61	10	3.89	Cubic	6.2	6.4	6.2	4.49
62	10	3.89	Cubic	6.2	6.4	6.2	4.71
63	10	3.89	Cubic	6.2	6.4	6.2	3.76
64	10	3.89	Cubic	6.2	6.4	6.2	4.27

65	10	3.89	Cubic	6.2	6.4	6.2	4.49
66	10	3.89	Cubic	6.2	6.4	6.2	4.71
67	11	3.94	Elongated	3.9	3.7	15.7	3.76
68	11	3.94	Elongated	3.9	3.7	15.7	4.27
69	11	3.94	Elongated	3.9	3.7	15.7	4.49
70	11	3.94	Elongated	3.9	3.7	15.7	4.71
71	11	3.94	Elongated	3.9	3.7	15.7	3.76
72	11	3.94	Elongated	3.9	3.7	15.7	4.27
73	11	3.94	Elongated	3.9	3.7	15.7	4.49
74	11	3.94	Elongated	3.9	3.7	15.7	4.71
75	12	3.91	Flat	7.6	7.8	3.9	3.76
76	12	3.91	Flat	7.6	7.8	3.9	4.27
77	12	3.91	Flat	7.6	7.8	3.9	4.49
78	12	3.91	Flat	7.6	7.8	3.9	4.71
79	12	3.91	Flat	7.6	7.8	3.9	3.76
80	12	3.91	Flat	7.6	7.8	3.9	4.27
81	12	3.91	Flat	7.6	7.8	3.9	4.49
82	12	3.91	Flat	7.6	7.8	3.9	4.71
83	13	3.99	Cubic	5.9	6	6.2	3.76
84	13	3.99	Cubic	5.9	6	6.2	4.27
85	13	3.99	Cubic	5.9	6	6.2	4.49
86	13	3.99	Cubic	5.9	6	6.2	4.71
87	13	3.99	Cubic	5.9	6	6.2	3.76
88	13	3.99	Cubic	5.9	6	6.2	4.27
89	13	3.99	Cubic	5.9	6	6.2	4.49
90	13	3.99	Cubic	5.9	6	6.2	4.71
91	14	3.73	Elongated	15.3	3.9	3.8	3.76
92	14	3.73	Elongated	15.3	3.9	3.8	4.27
93	14	3.73	Elongated	15.3	3.9	3.8	4.49
94	14	3.73	Elongated	15.3	3.9	3.8	4.71
95	14	3.73	Elongated	15.3	3.9	3.8	3.76
96	14	3.73	Elongated	15.3	3.9	3.8	4.27
97	14	3.73	Elongated	15.3	3.9	3.8	4.49
98	14	3.73	Elongated	15.3	3.9	3.8	4.71
99	15	3.73	Flat	7.9	8	3.7	3.76
100	15	3.73	Flat	7.9	8	3.7	4.27

101	15	3.73	Flat	7.9	8	3.7	4.49
102	15	3.73	Flat	7.9	8	3.7	4.71
103	15	3.73	Flat	7.9	8	3.7	3.76
104	15	3.73	Flat	7.9	8	3.7	4.27
105	15	3.73	Flat	7.9	8	3.7	4.49
106	15	3.73	Flat	7.9	8	3.7	4.71
107	16	3.72	Cubic	6.2	6.2	6.3	3.76
108	16	3.72	Cubic	6.2	6.2	6.3	4.27
109	16	3.72	Cubic	6.2	6.2	6.3	4.49
110	16	3.72	Cubic	6.2	6.2	6.3	4.71
111	16	3.72	Cubic	6.2	6.2	6.3	3.76
112	16	3.72	Cubic	6.2	6.2	6.3	4.27
113	16	3.72	Cubic	6.2	6.2	6.3	4.49
114	16	3.72	Cubic	6.2	6.2	6.3	4.71
115	17	3.72	Sphere	8			2.5
116	17	3.72	Sphere	8			3.6
117	17	3.72	Sphere	8			2.5
118	17	3.72	Sphere	8			3.6
119	18	3.48	Sphere	8.2			2.5
120	18	3.48	Sphere	8.2			3.6
121	18	3.48	Sphere	8.2			2.5
122	18	3.48	Sphere	8.2			3.6

10.3.2 Vertical Baseline Plots

Test runs for tracer 3 to tracer 16. The vertical component baseline plot is shown.

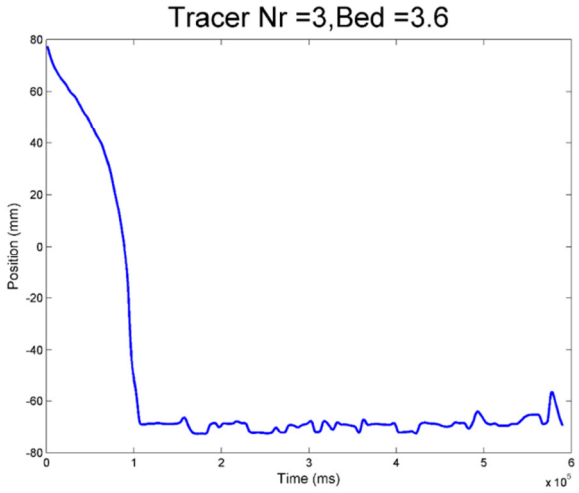

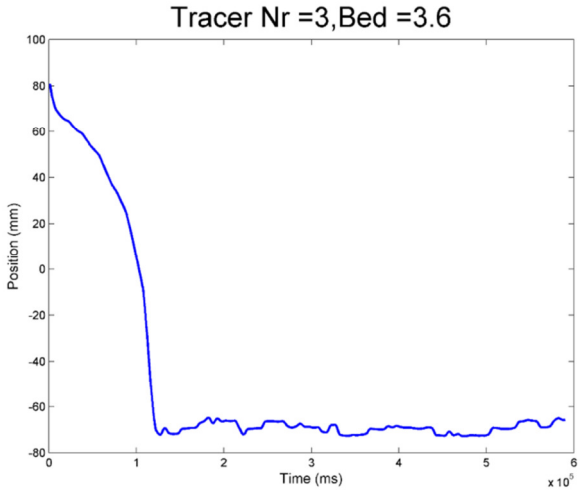

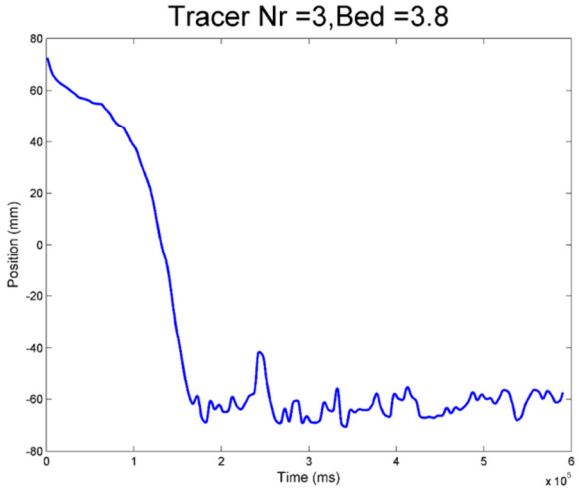

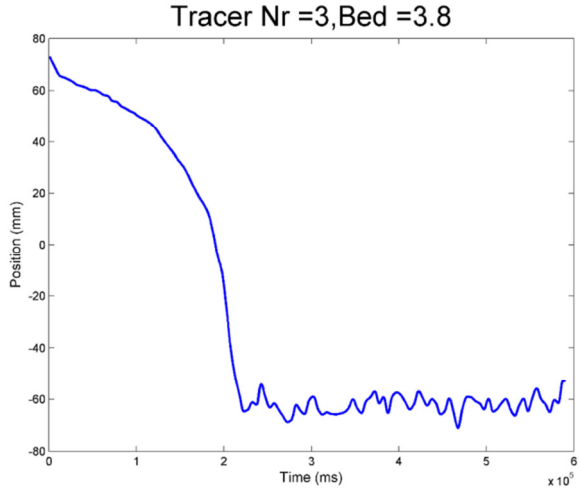

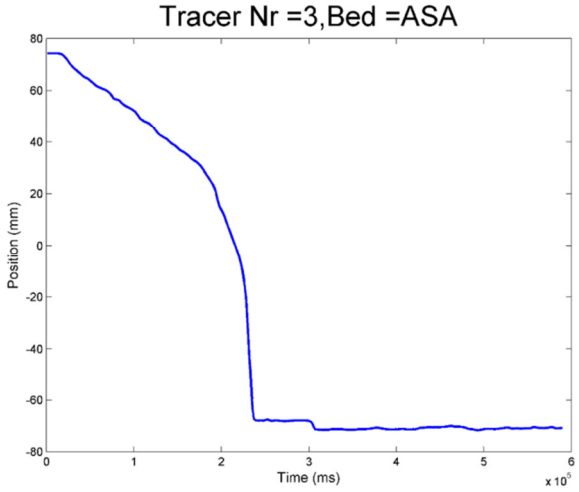

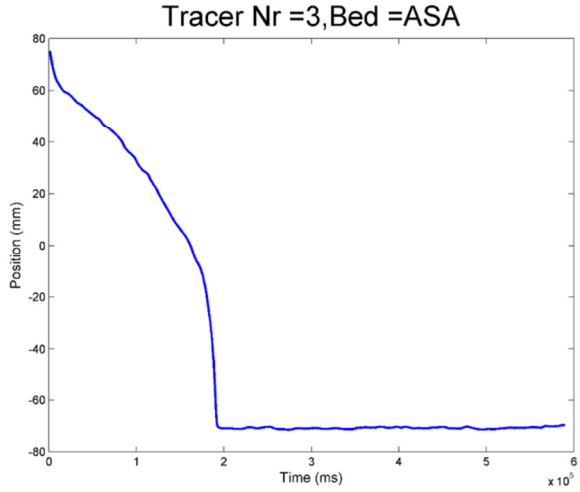

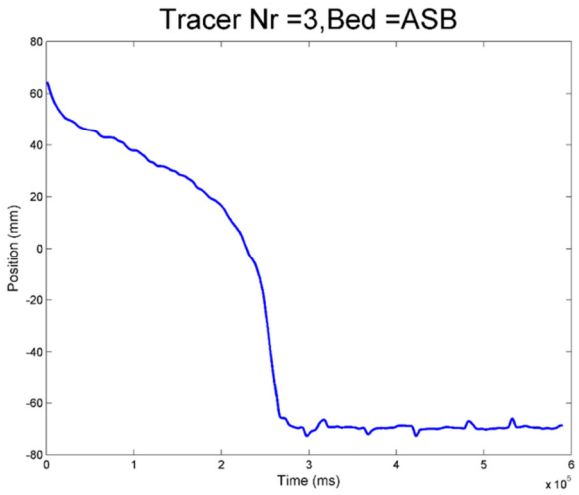

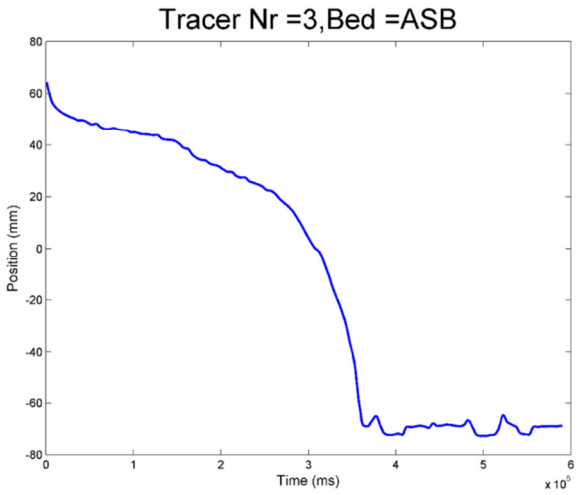

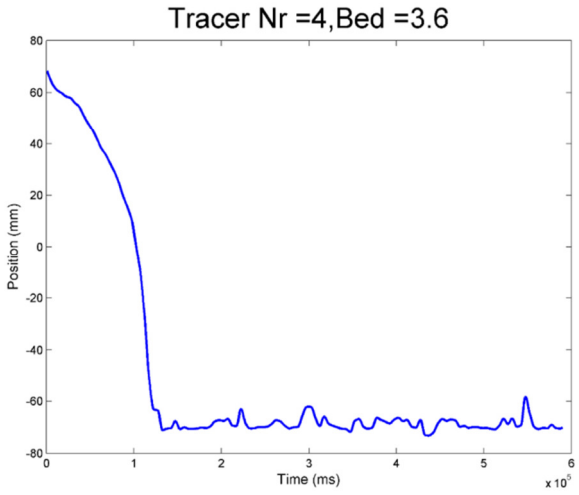

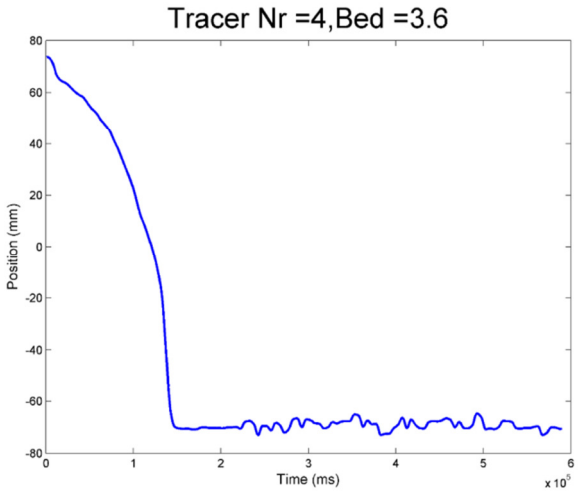

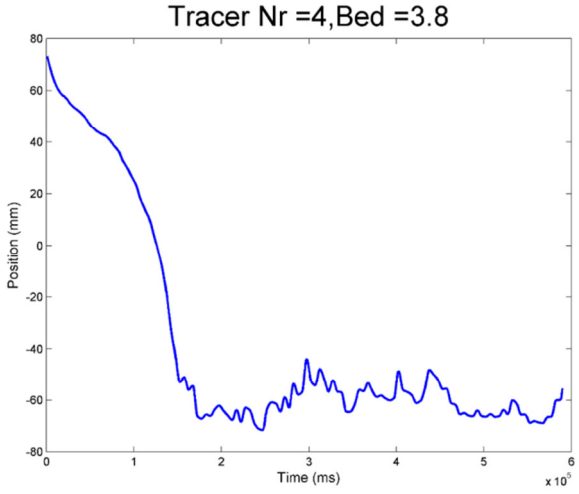

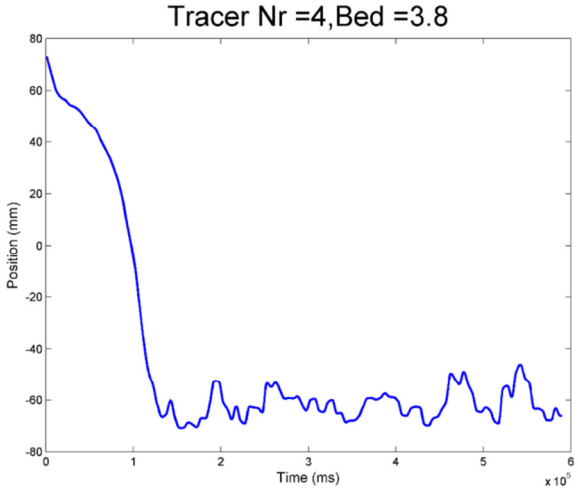

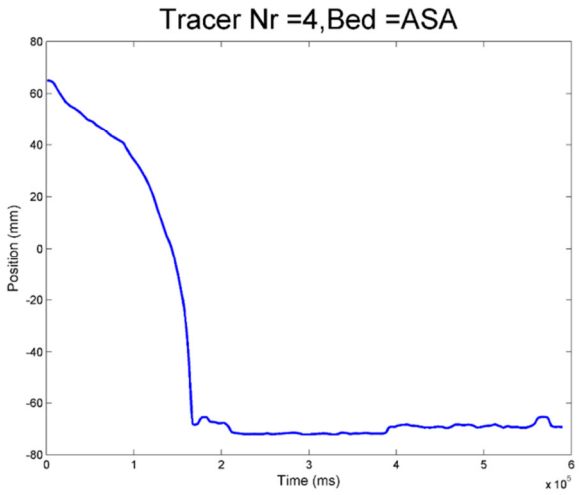

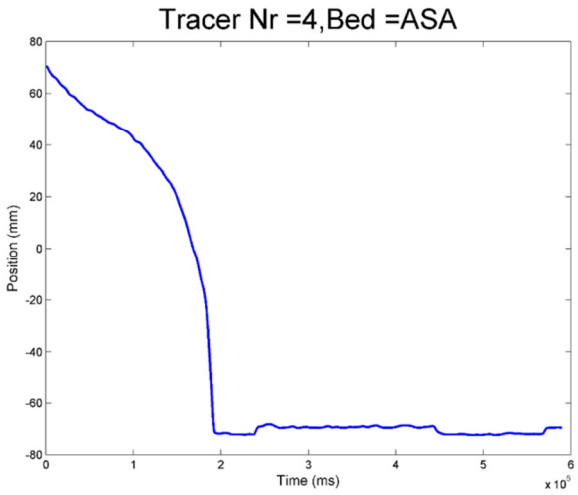

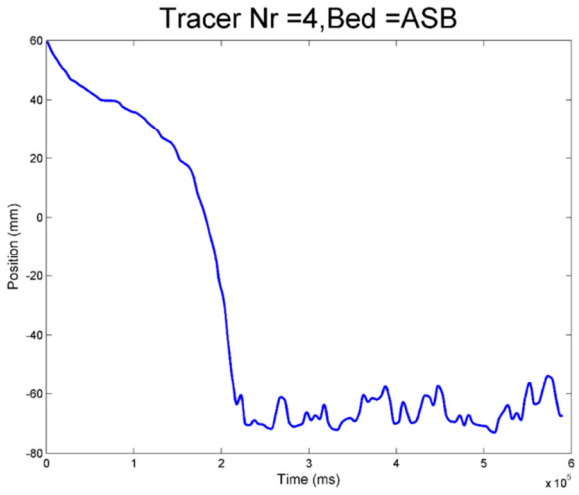

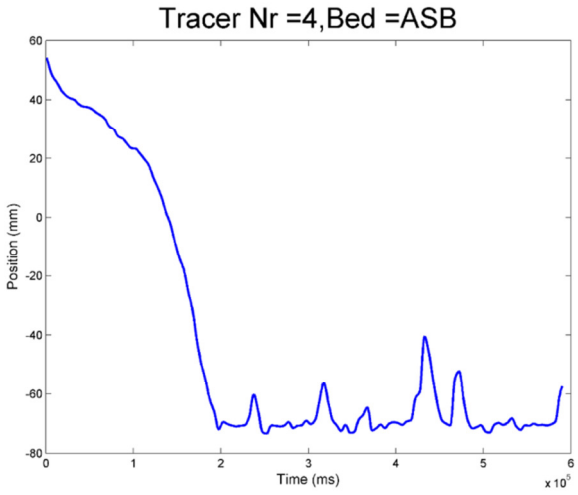

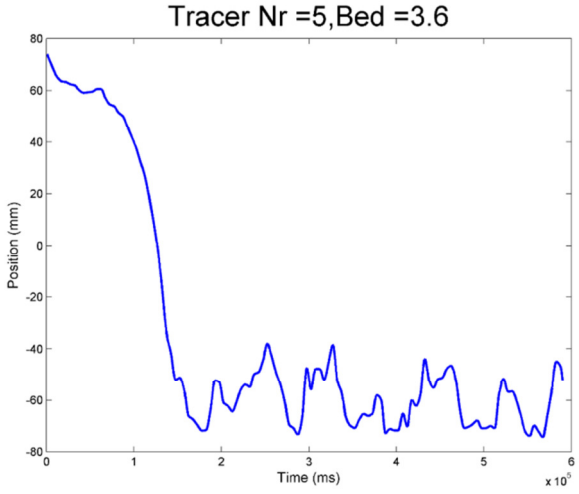

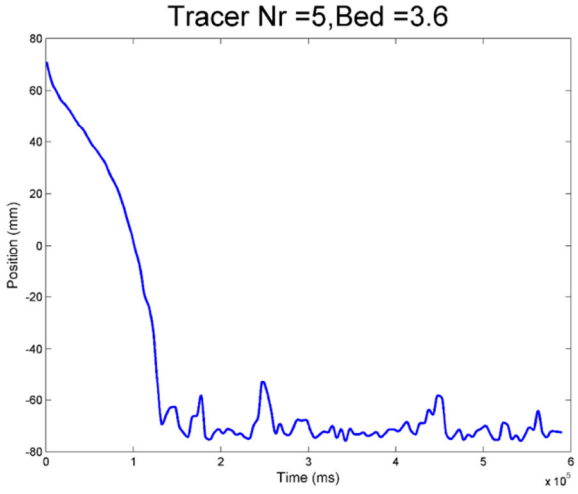

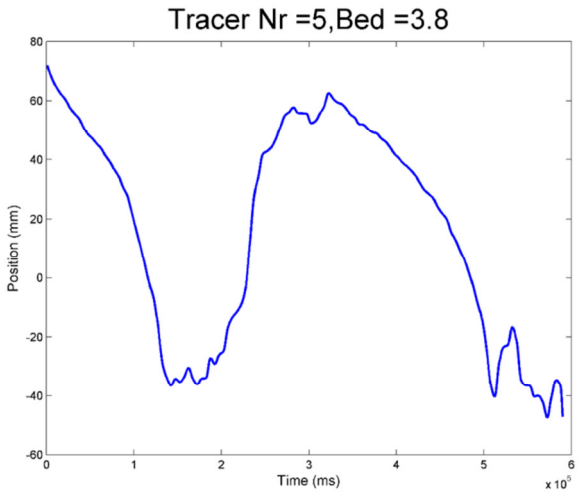

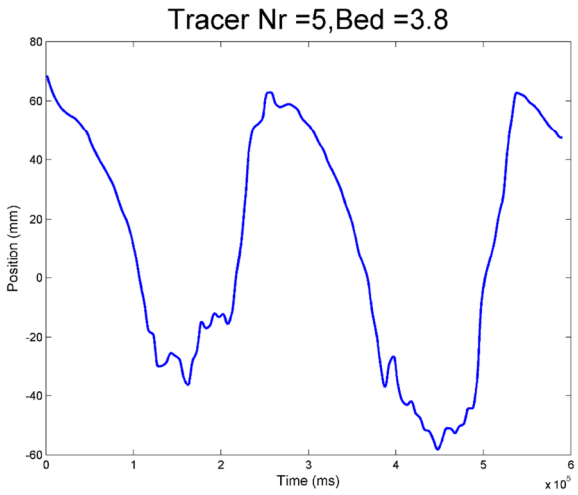

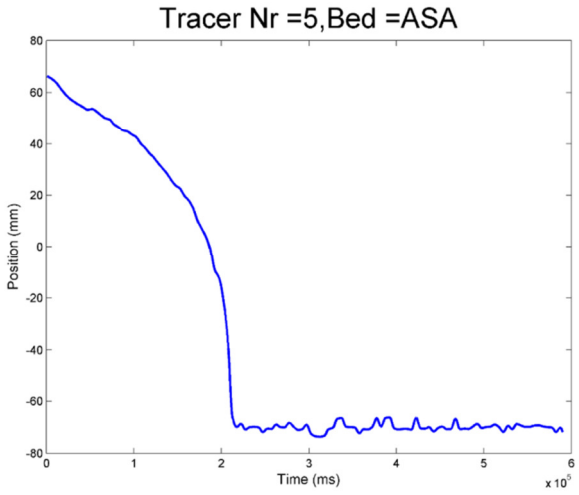

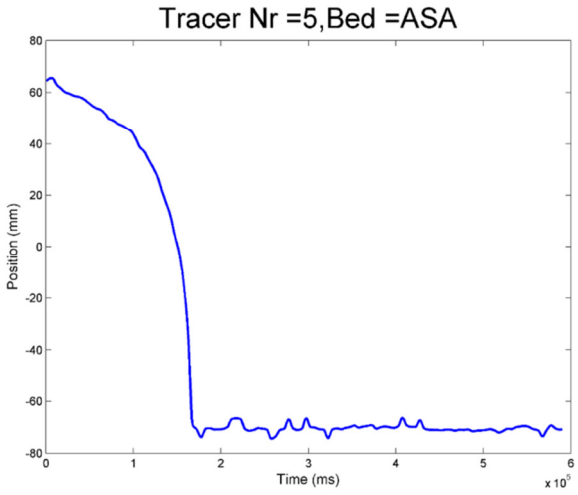

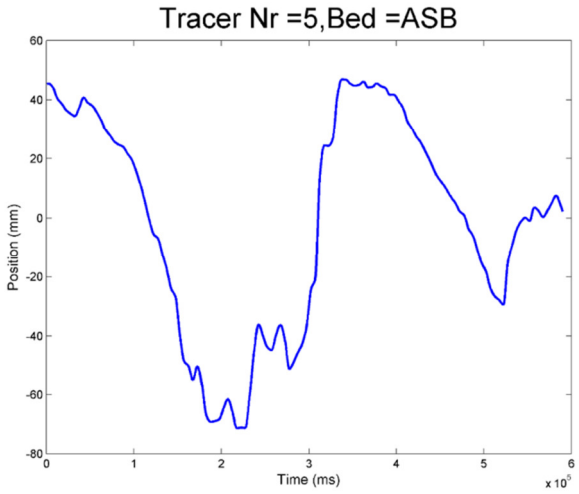

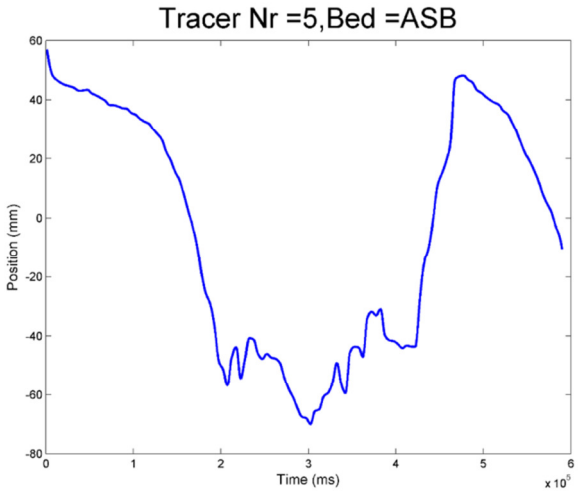

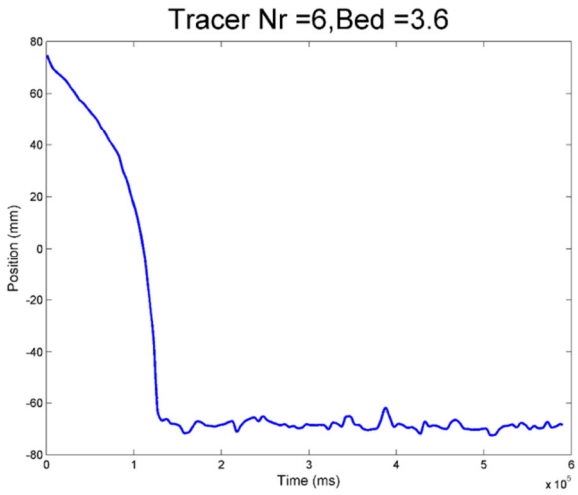

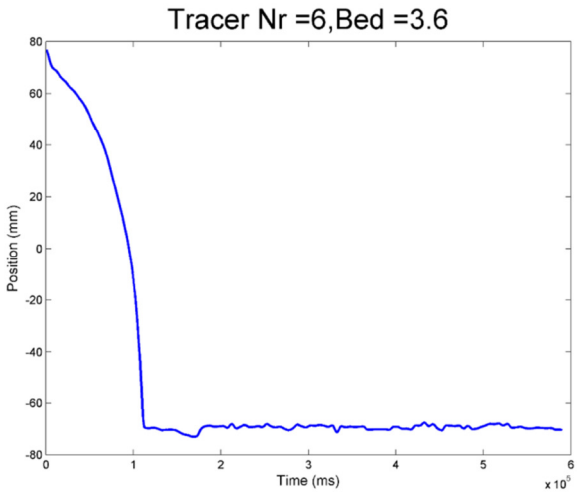

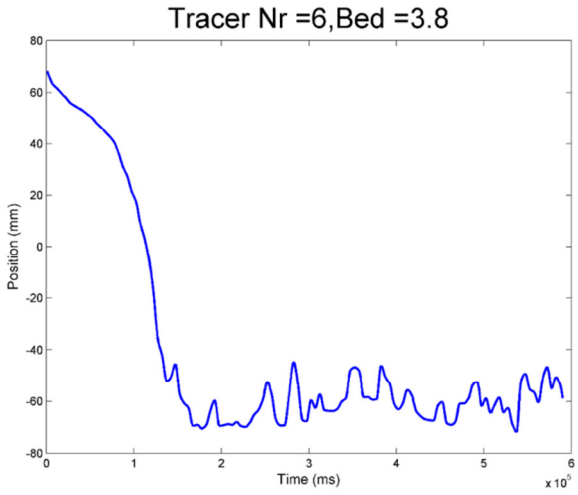

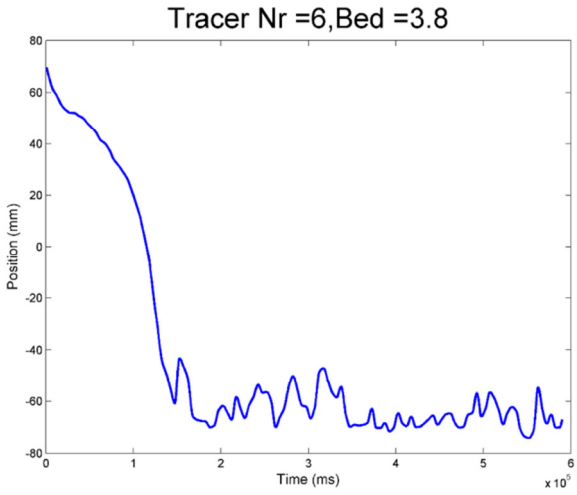

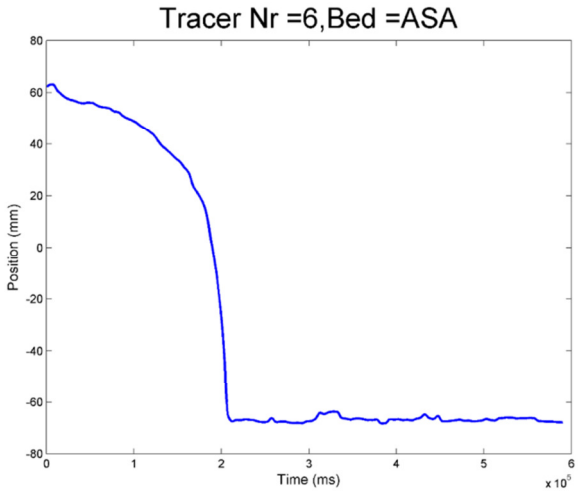

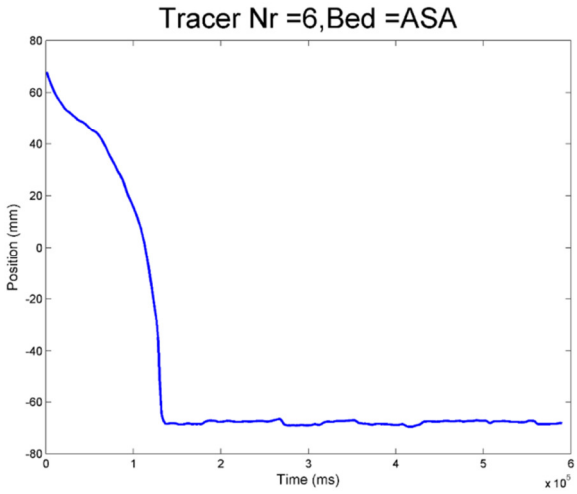

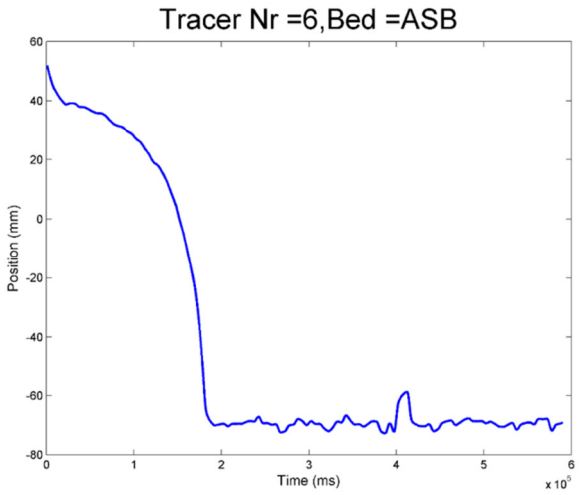

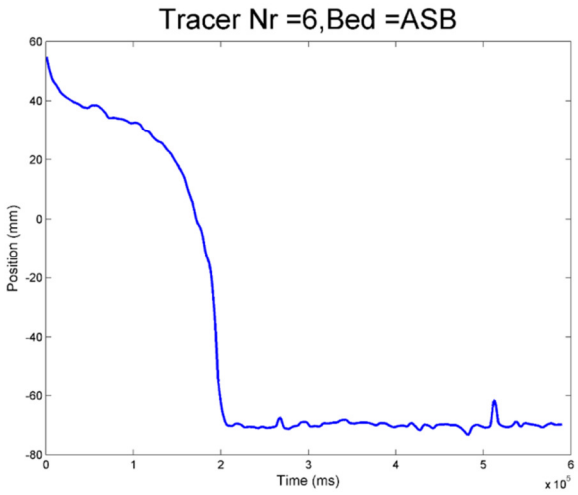

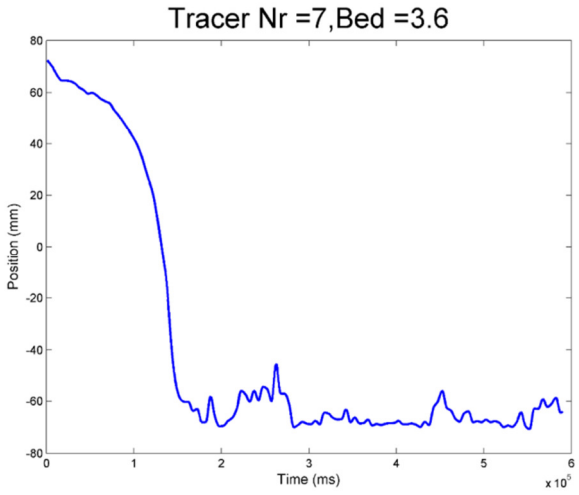

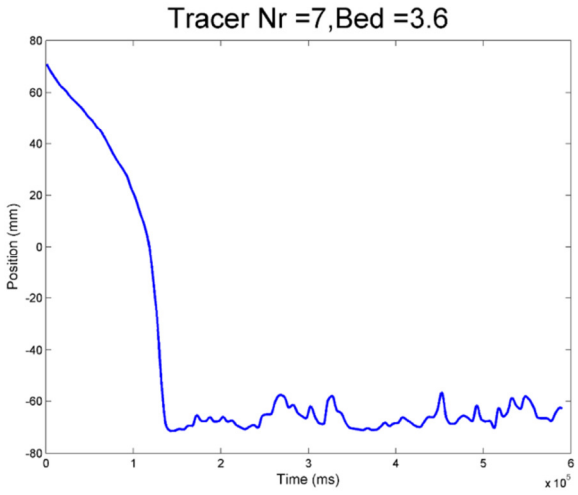

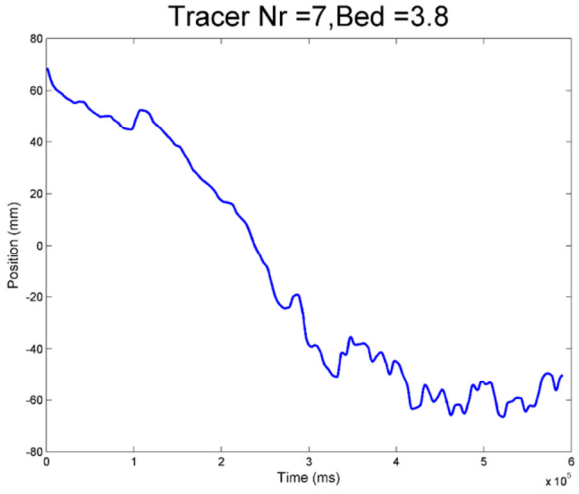

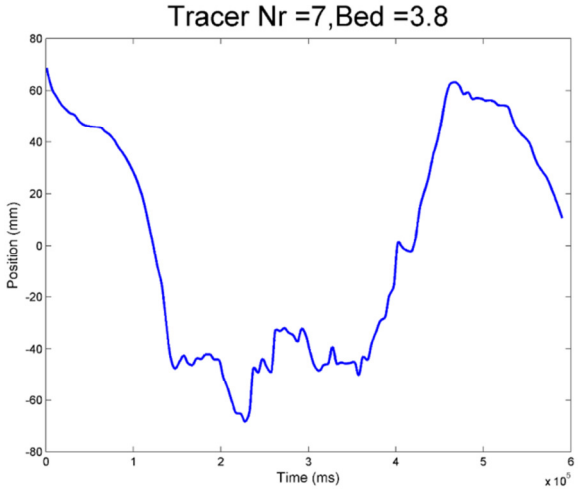

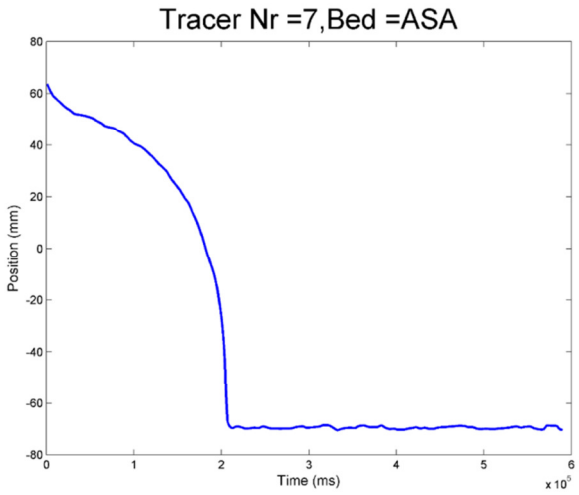

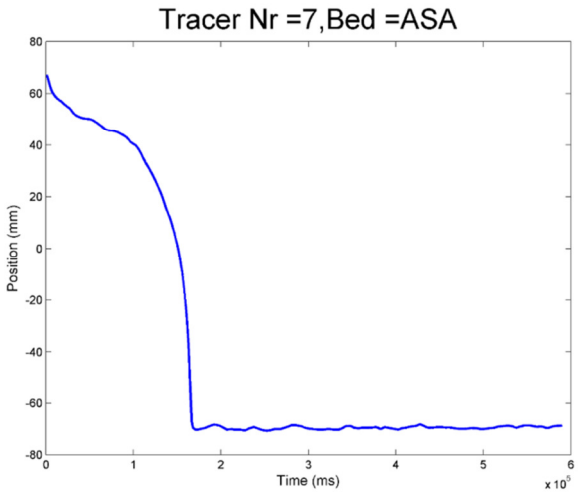

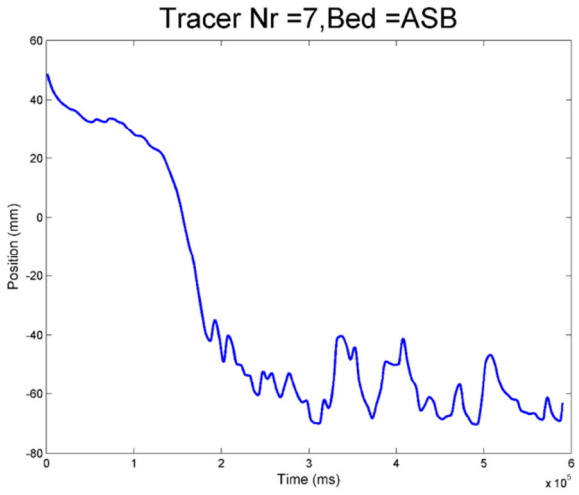

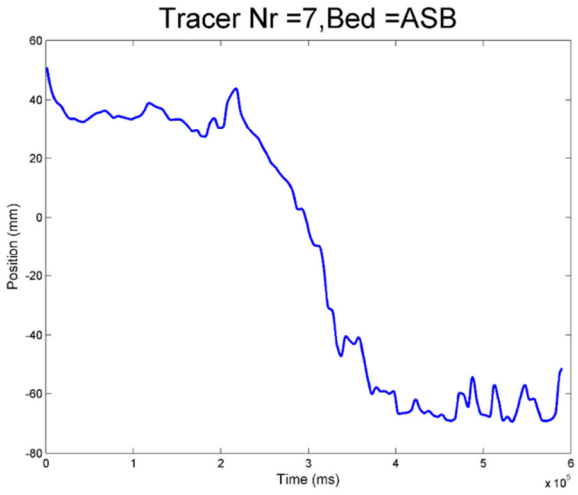

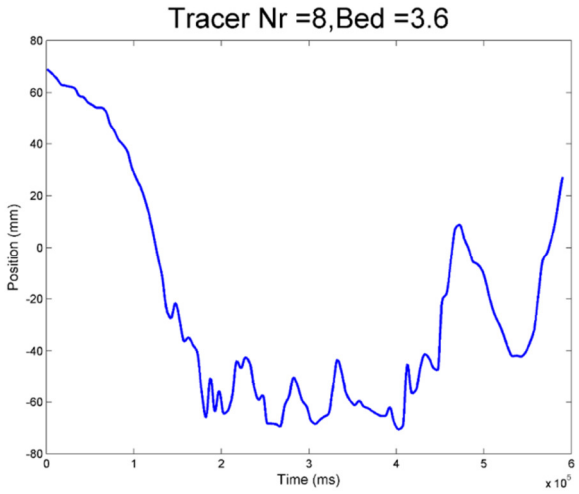

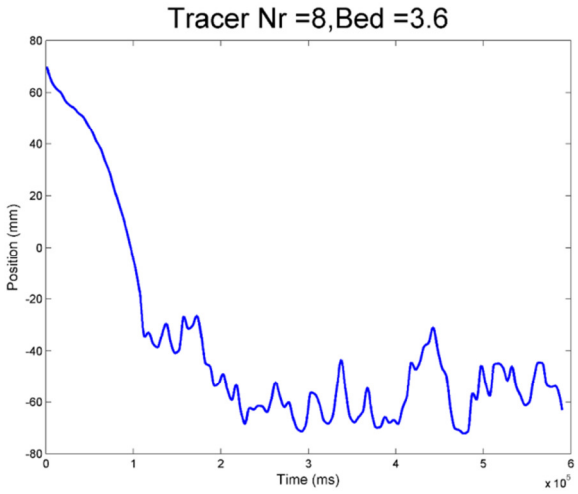

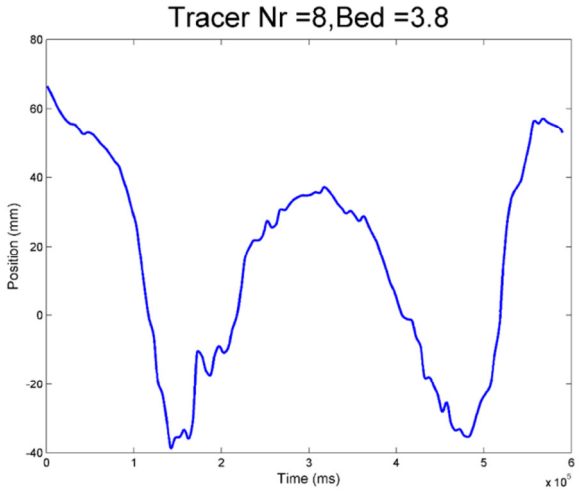

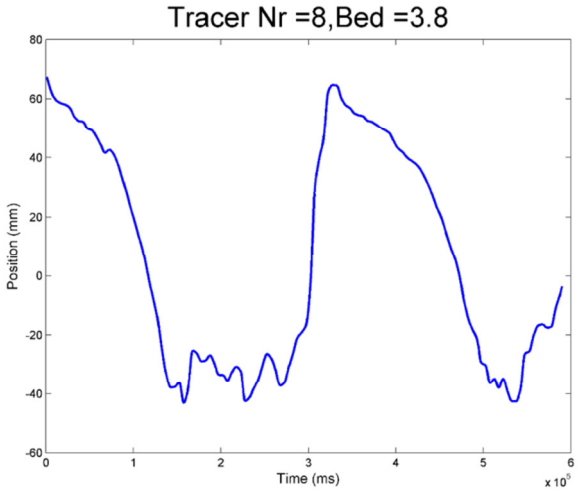

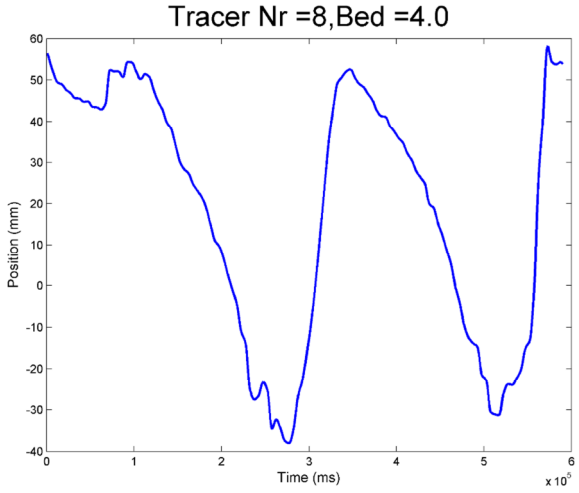

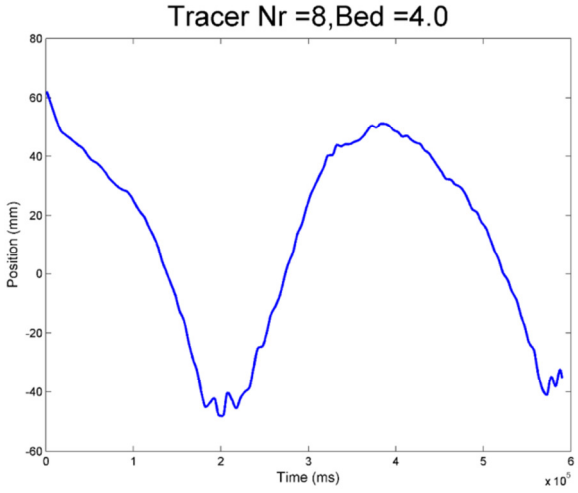

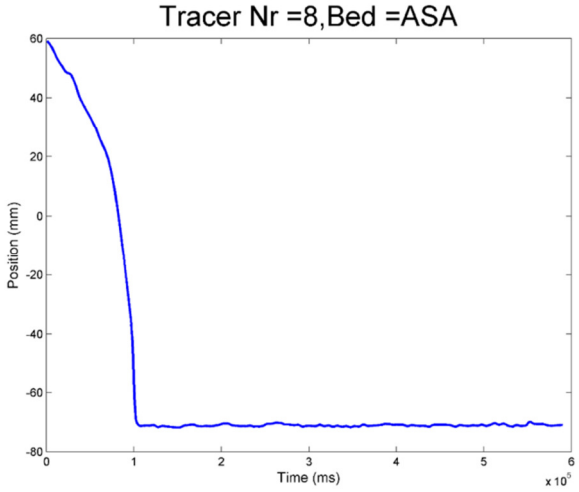

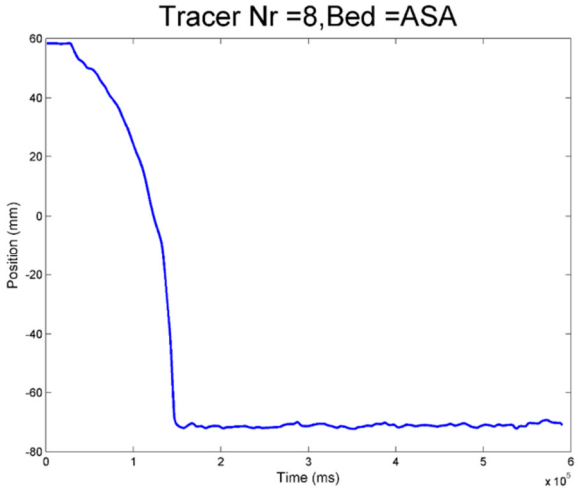

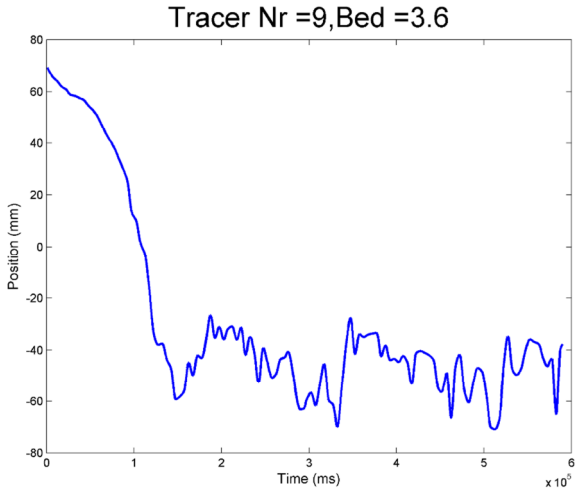

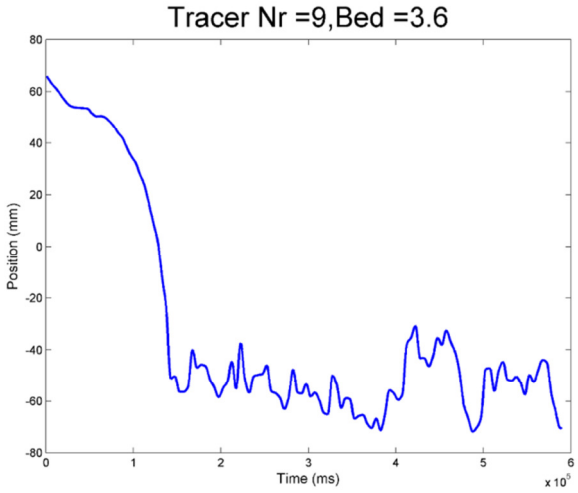

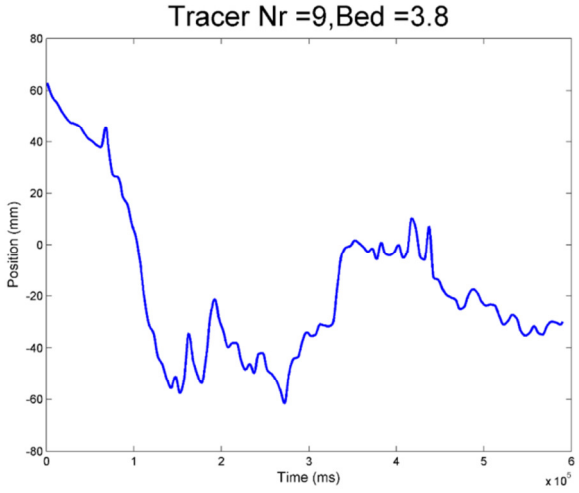

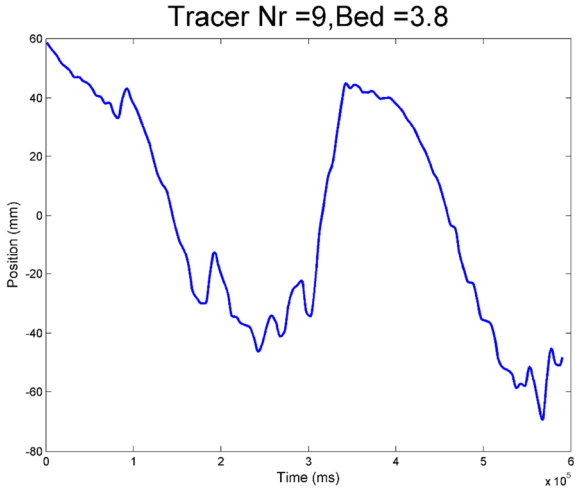

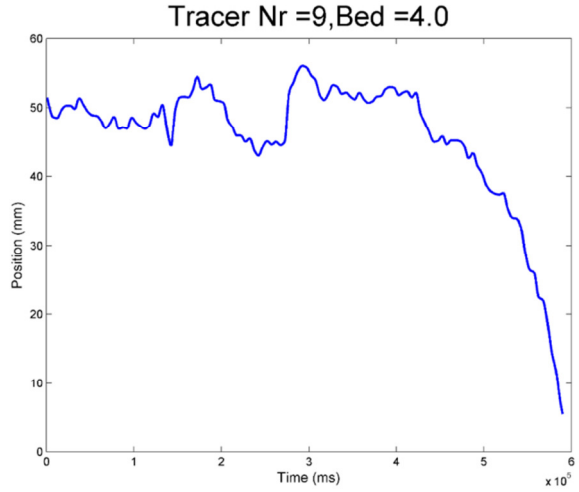

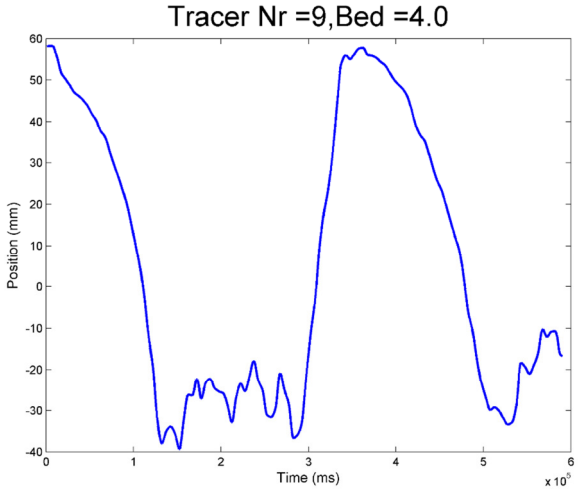

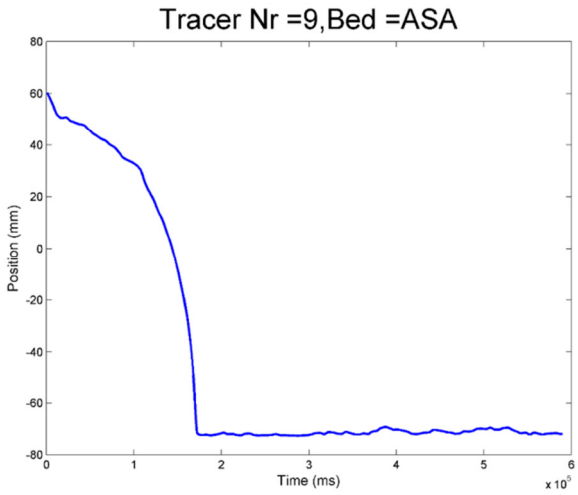

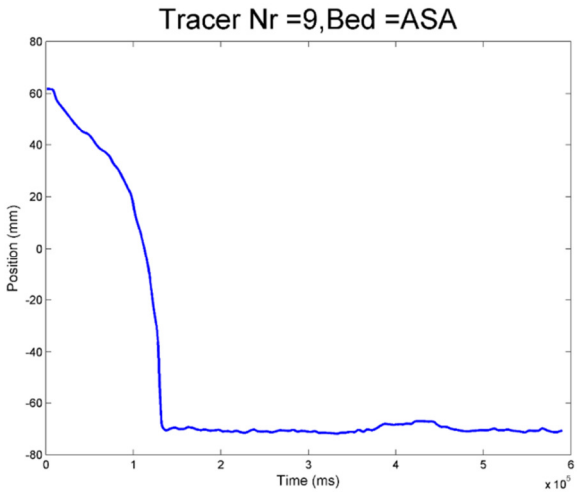

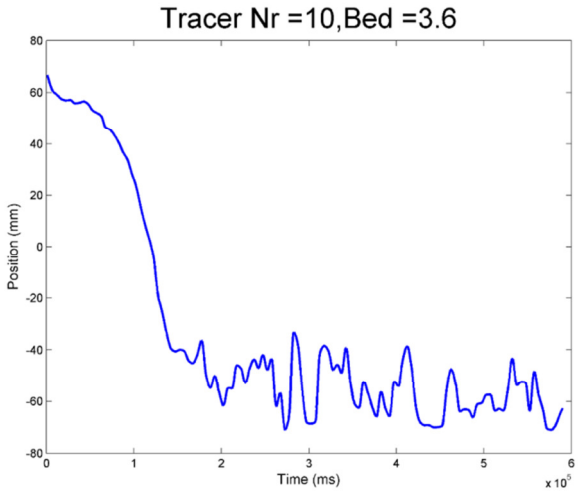

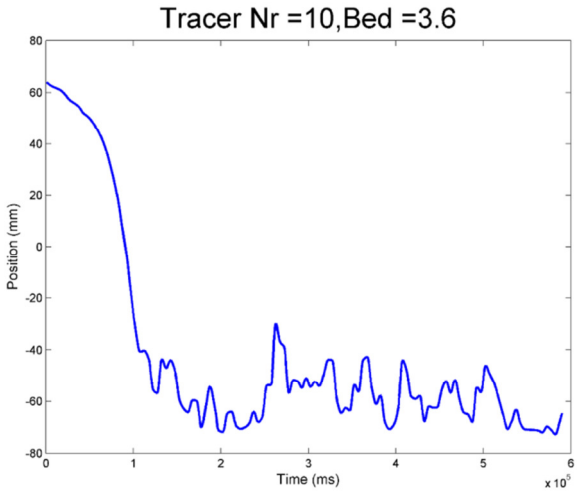

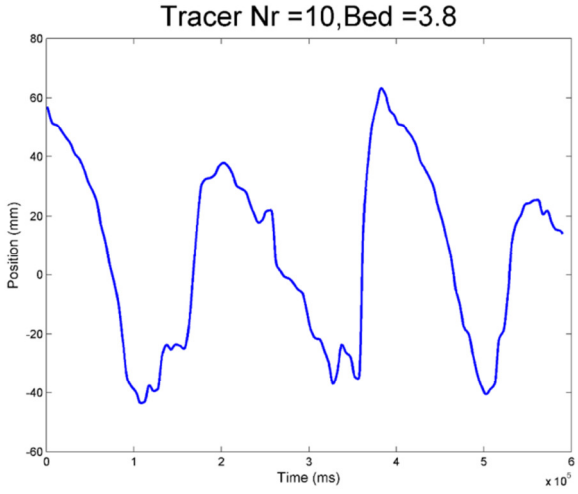

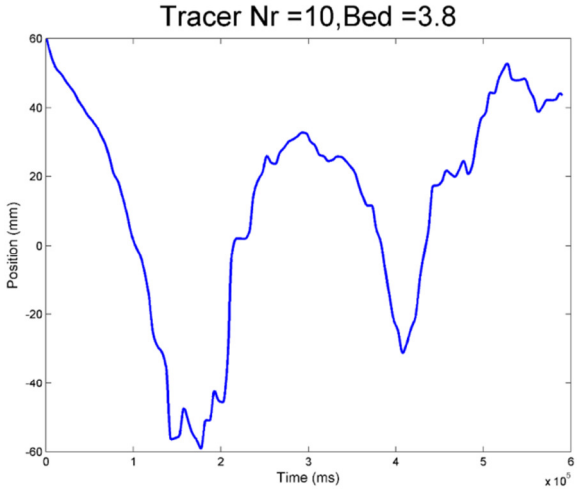

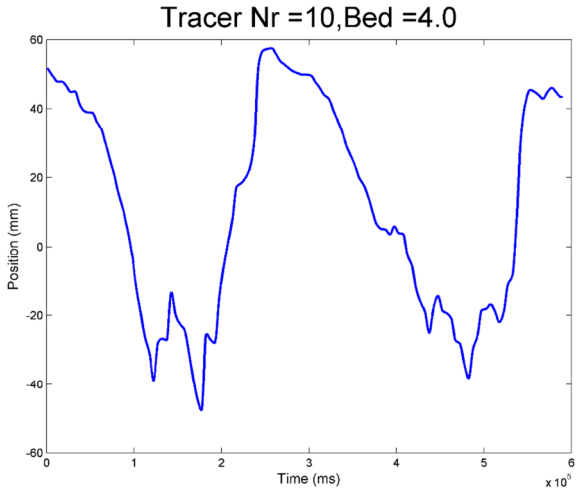

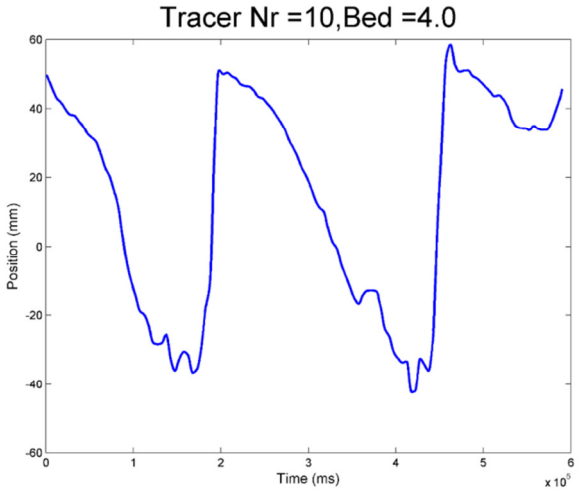

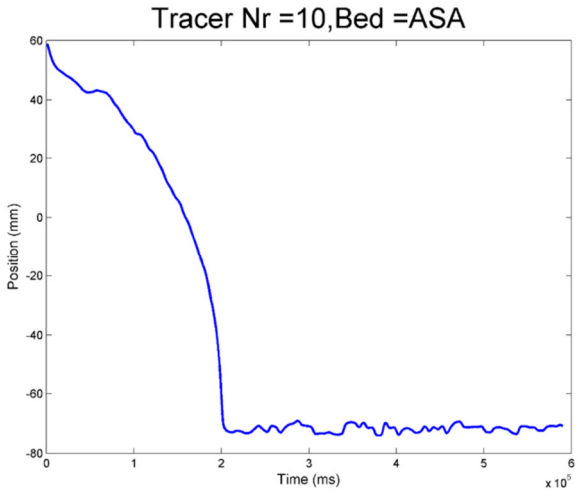

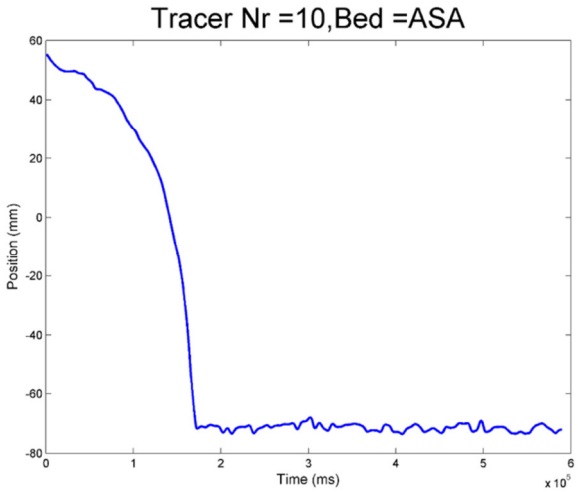

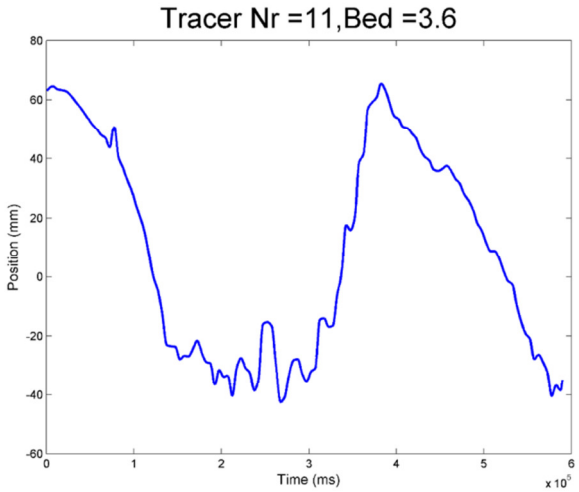

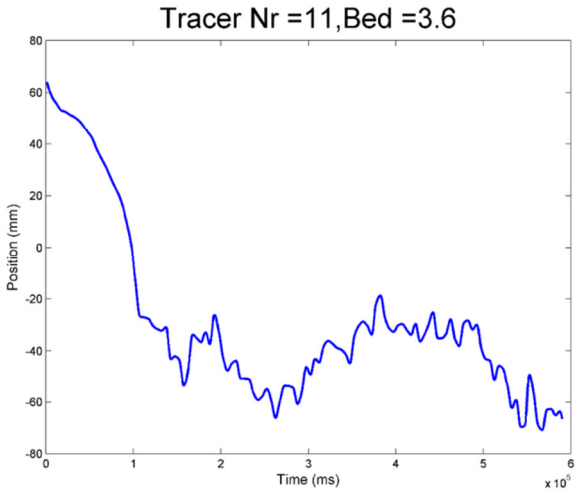

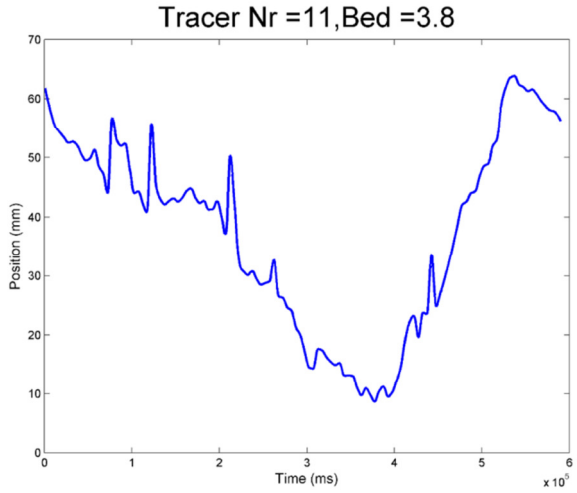

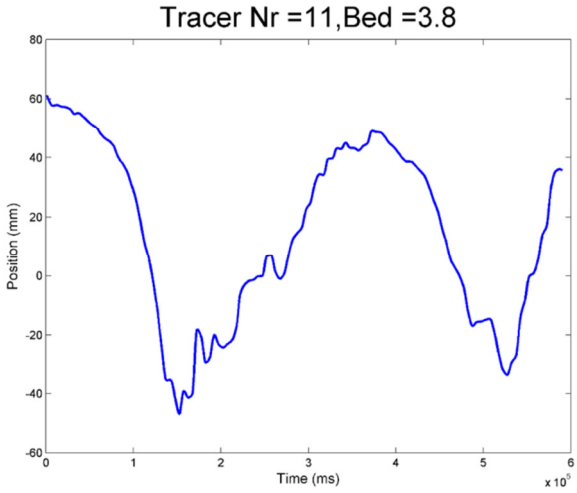

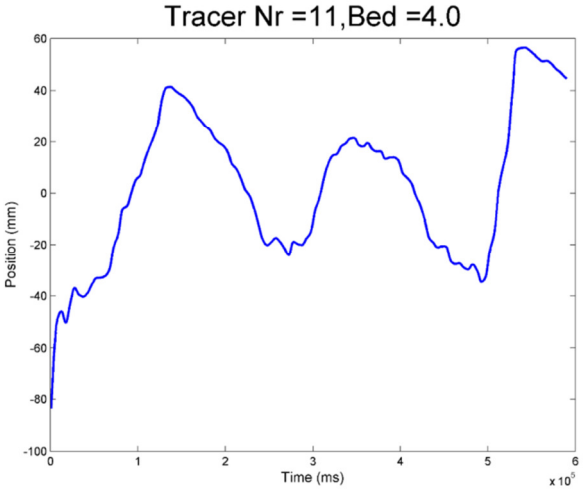

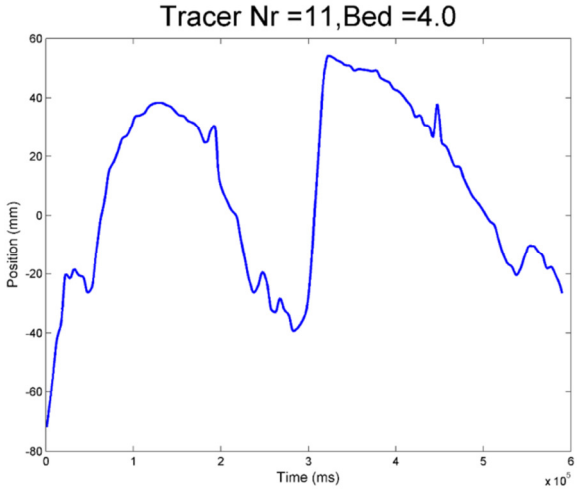

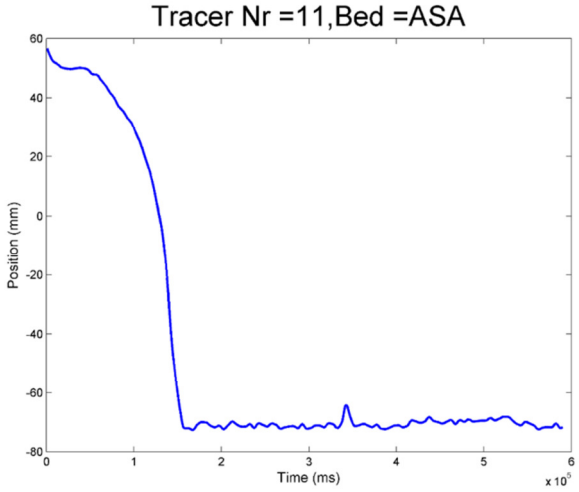

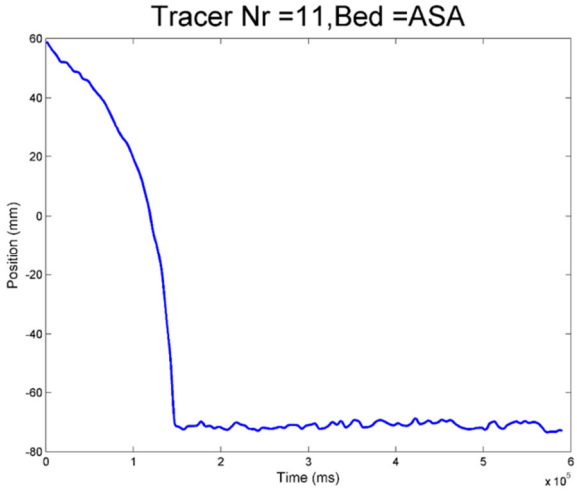

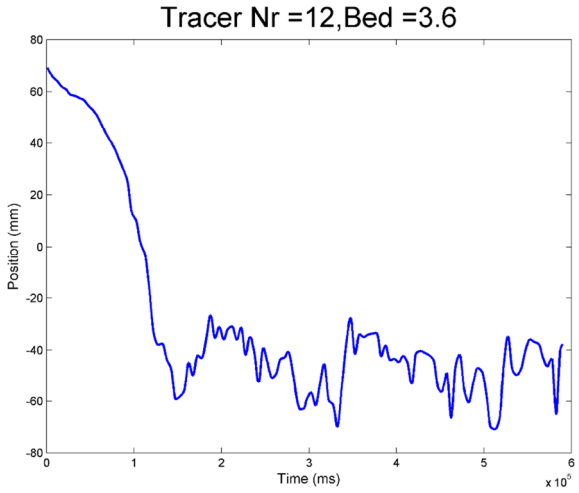

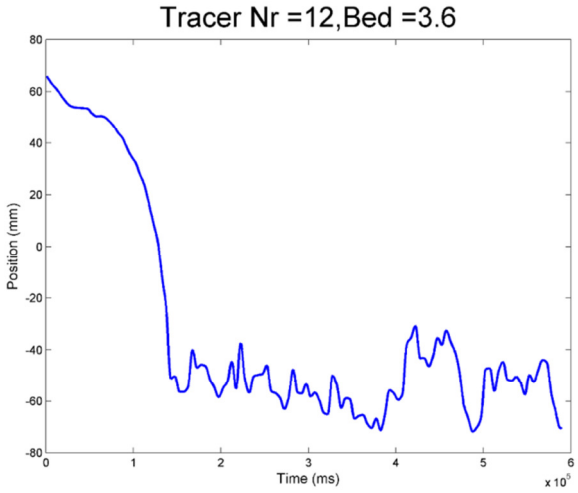

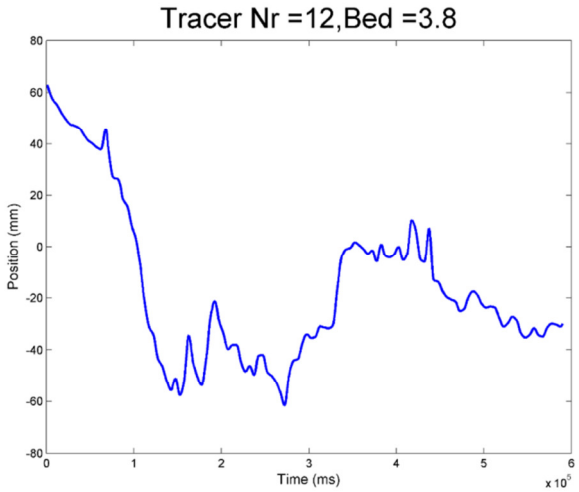

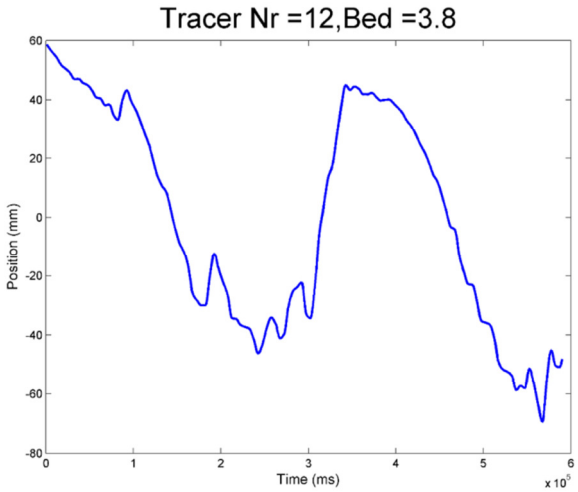

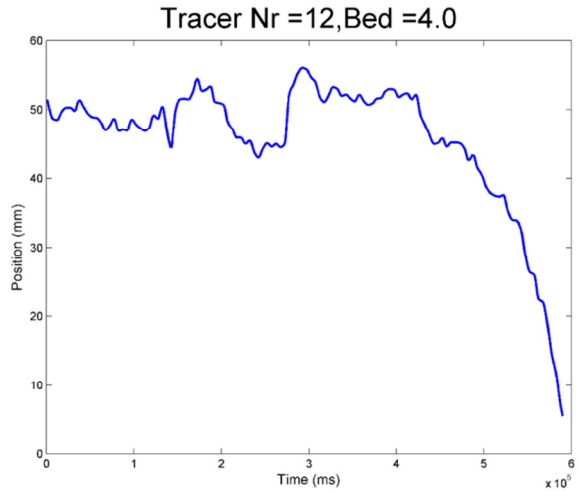

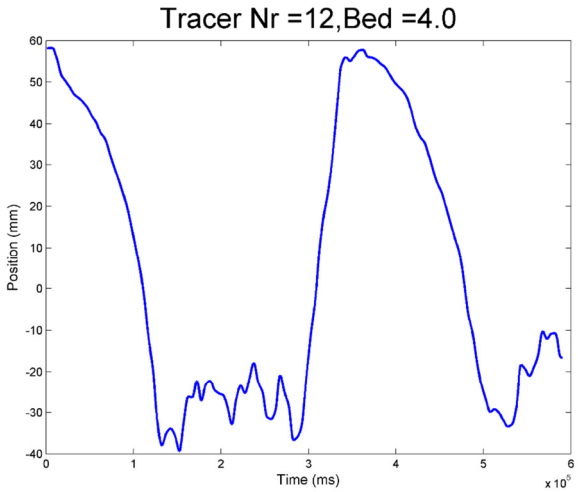

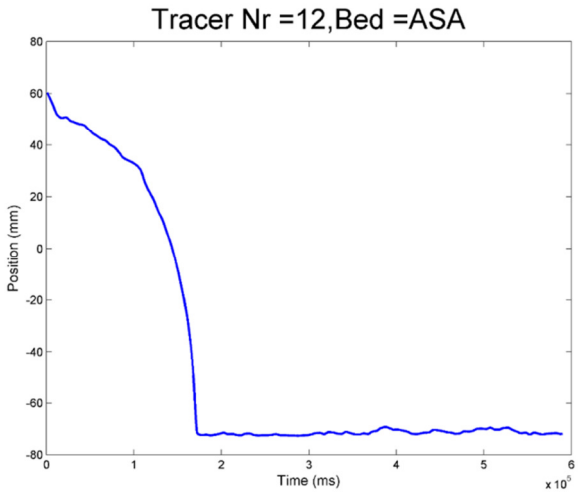

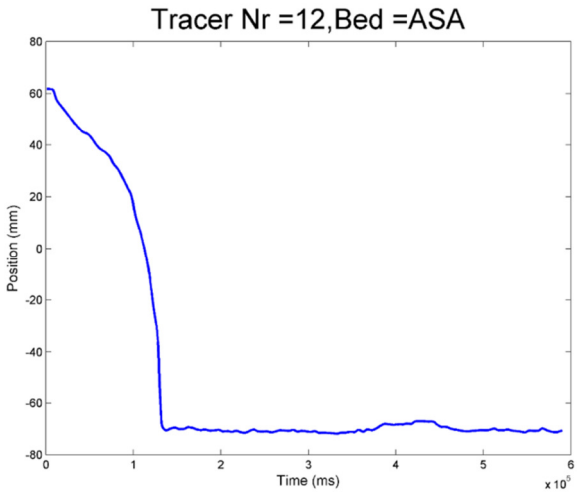

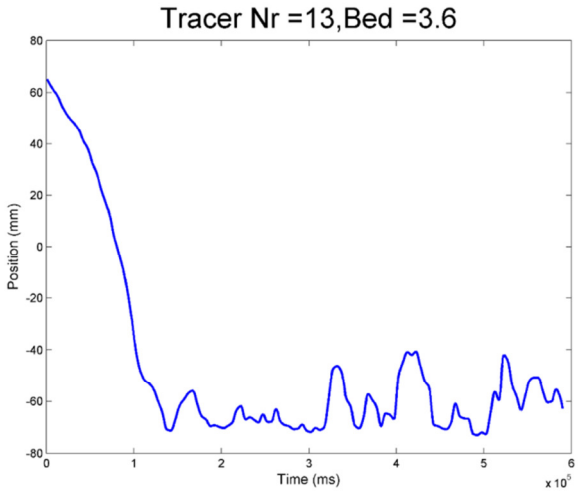

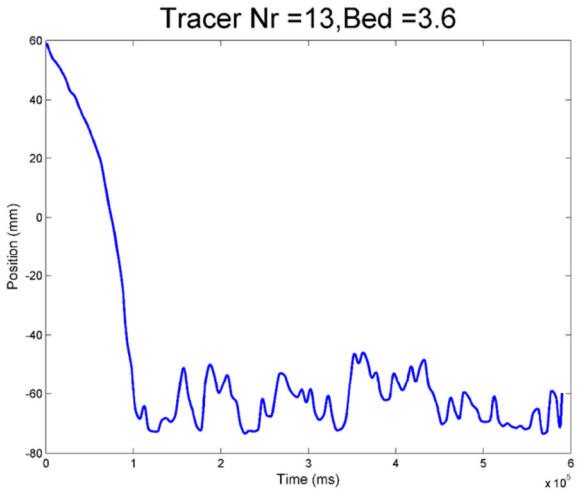

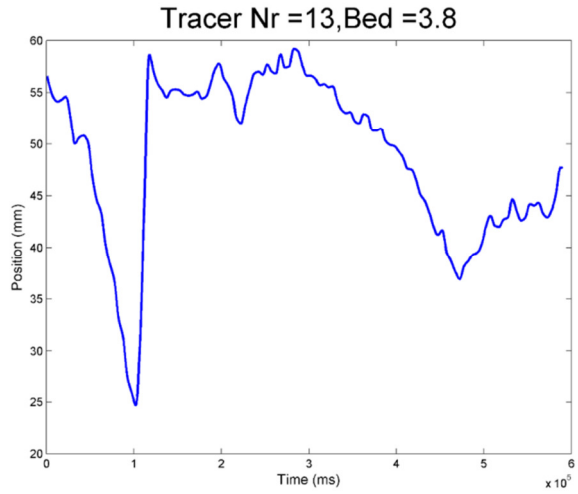

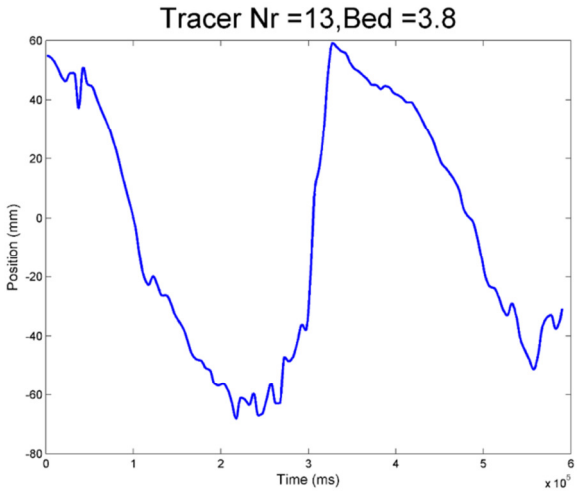

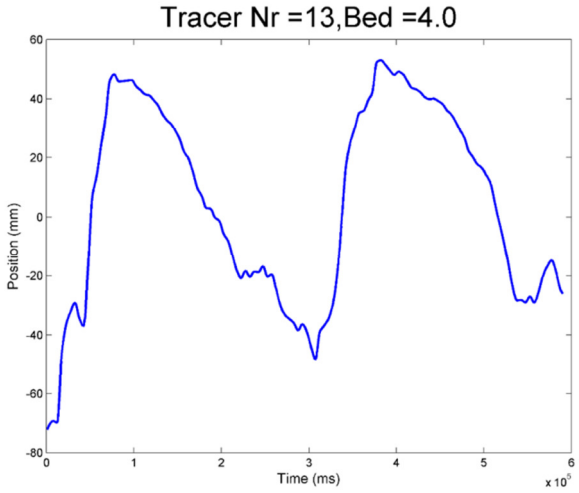

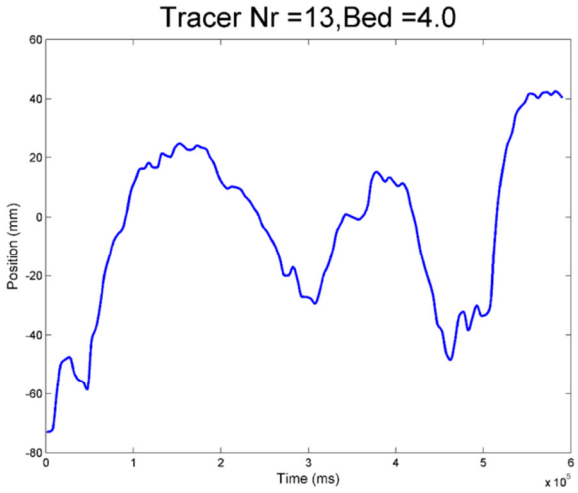

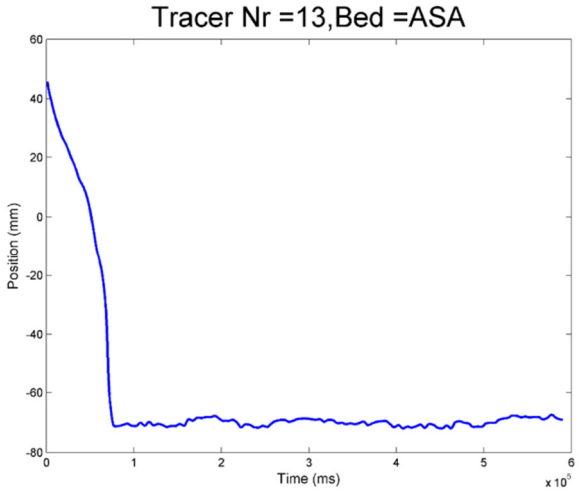

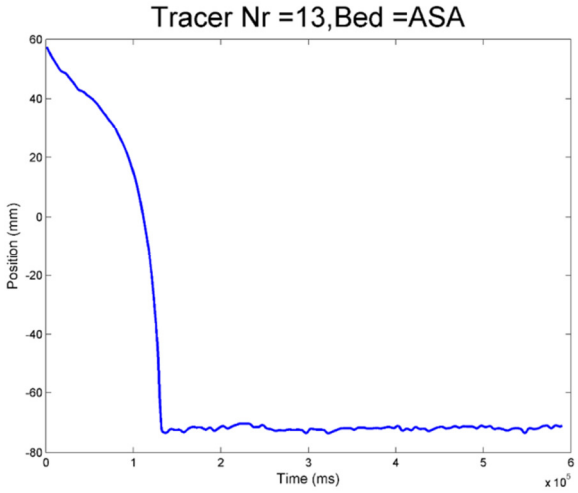

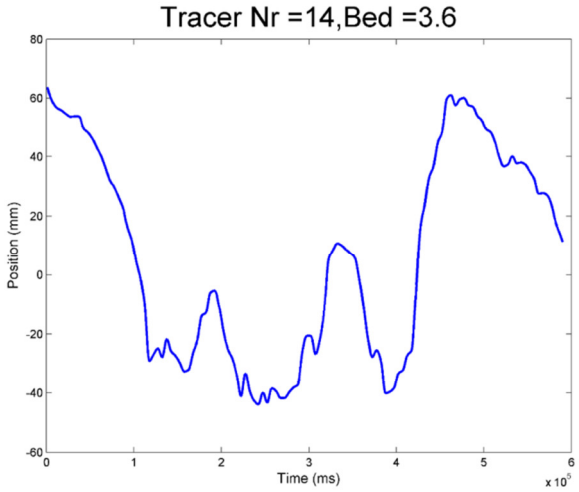

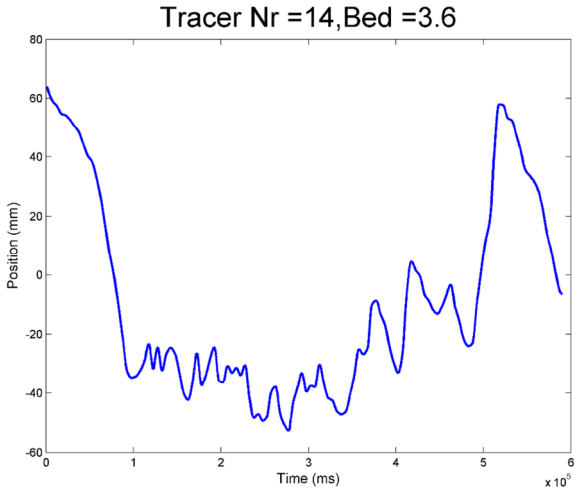

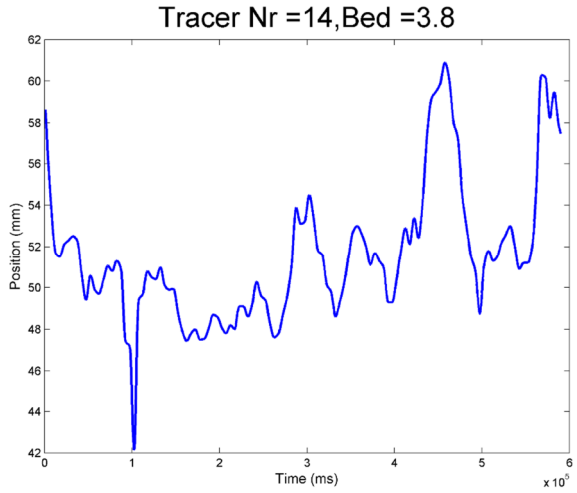

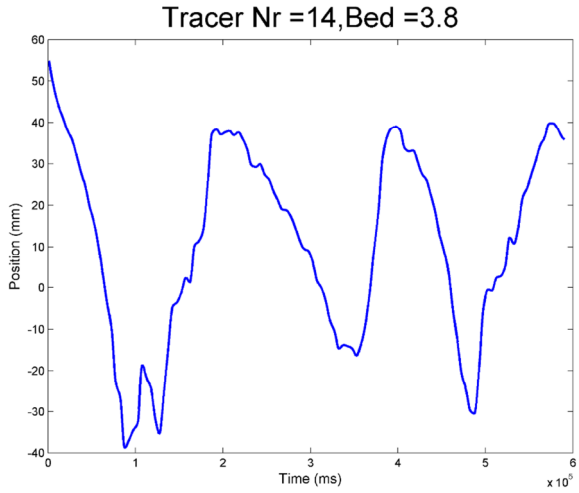

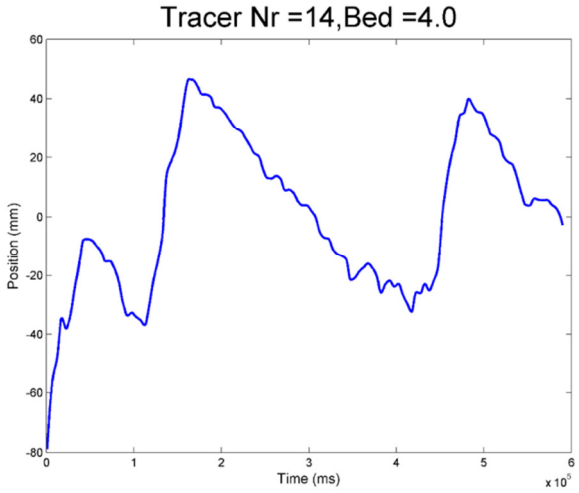

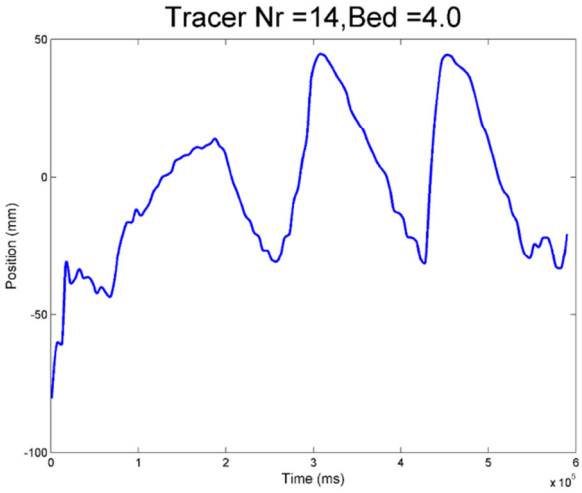

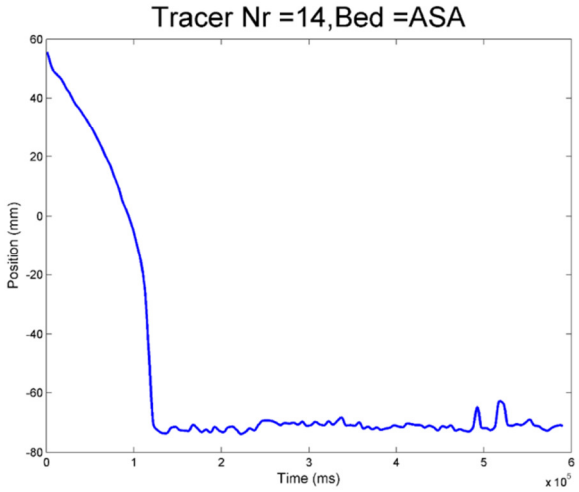

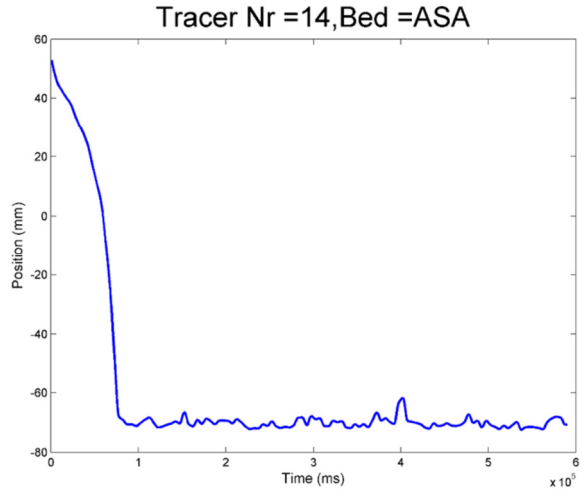

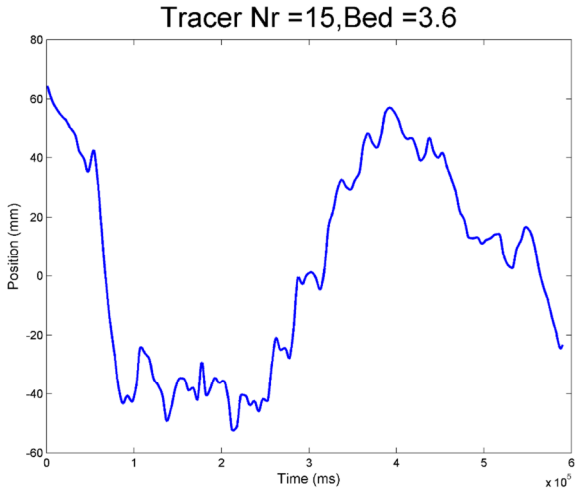

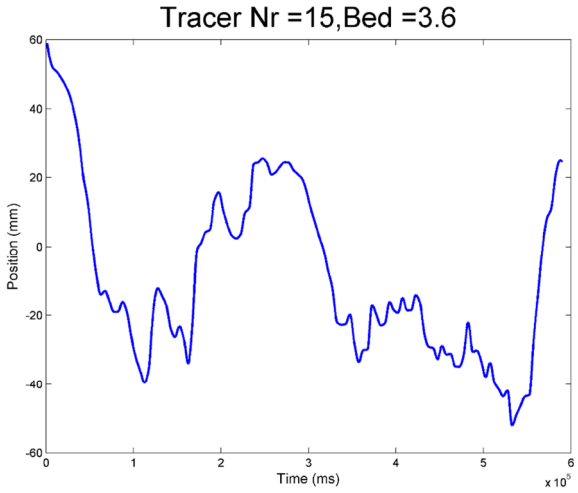

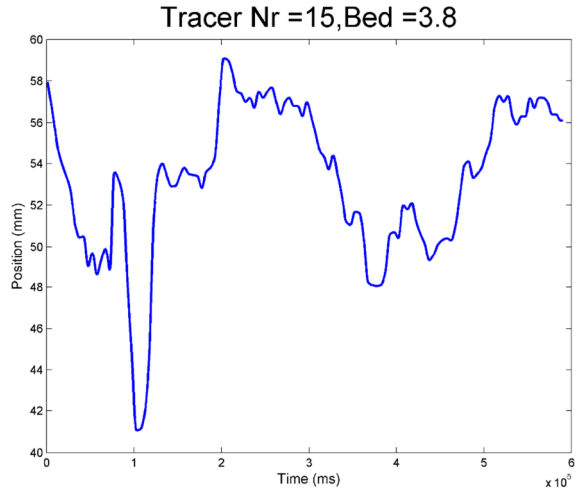

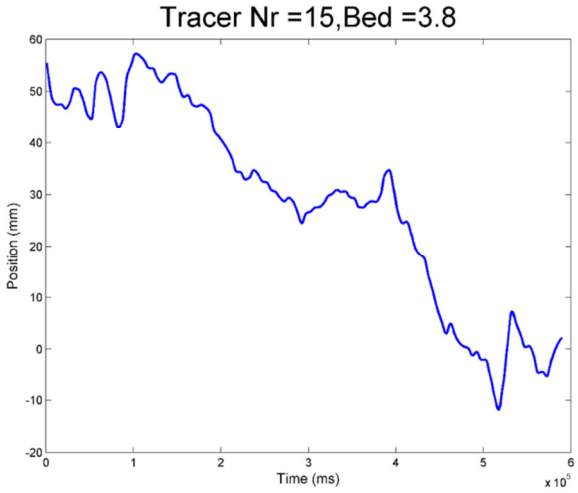

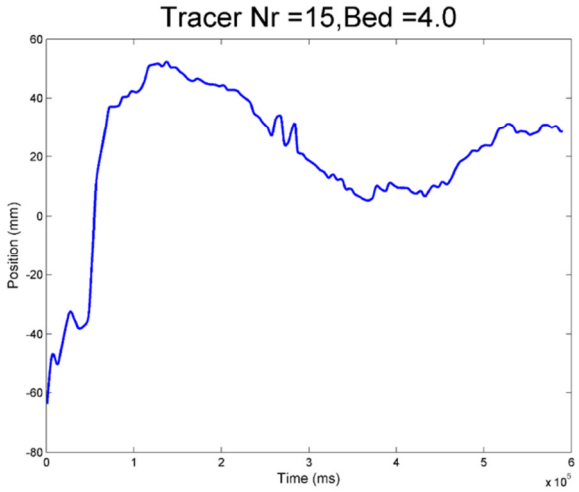

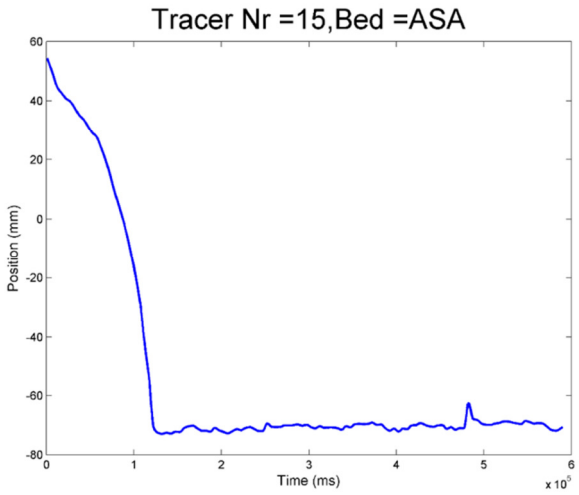

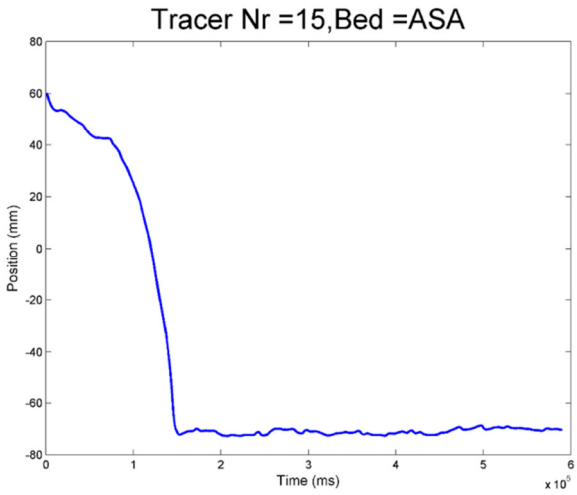

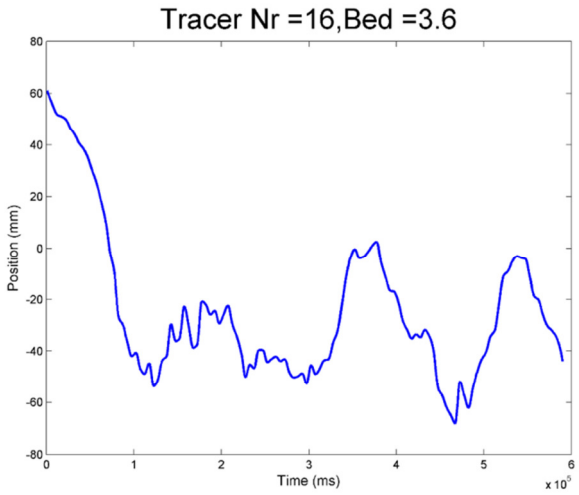

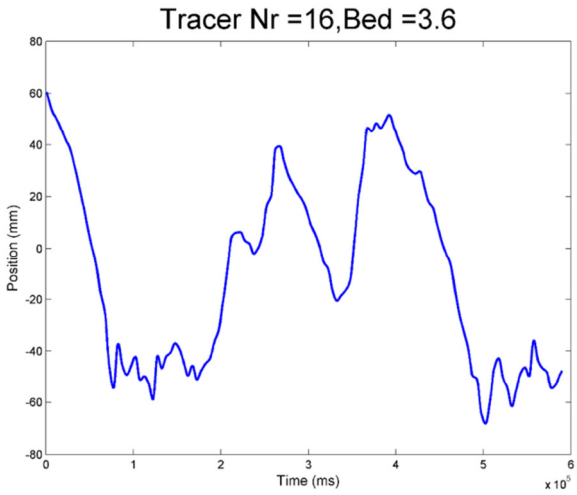

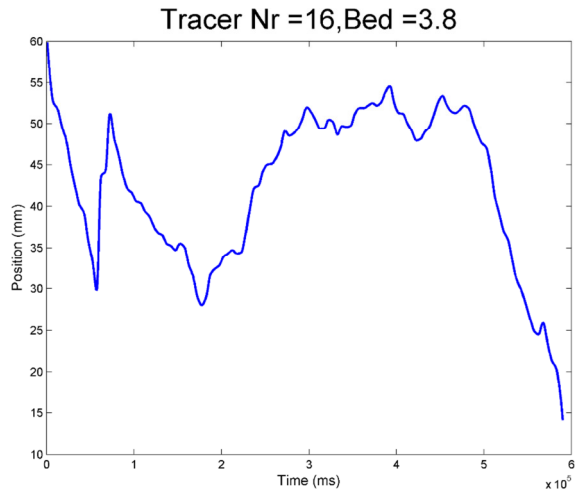

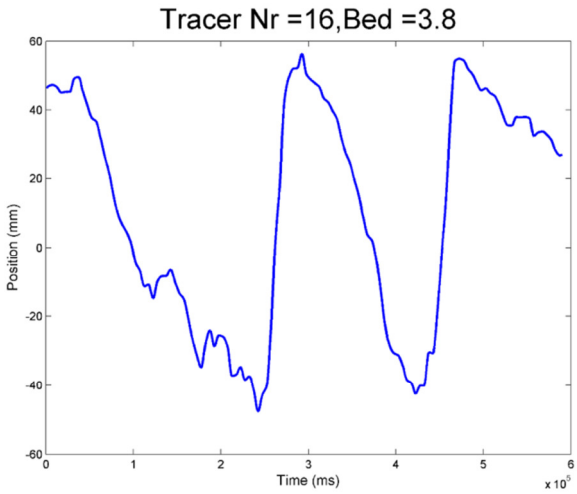

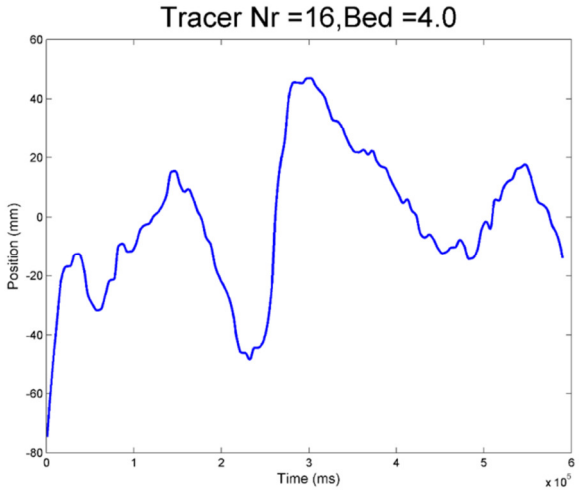

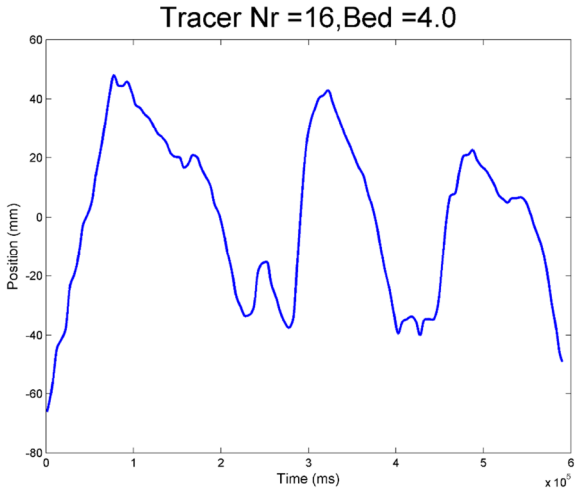

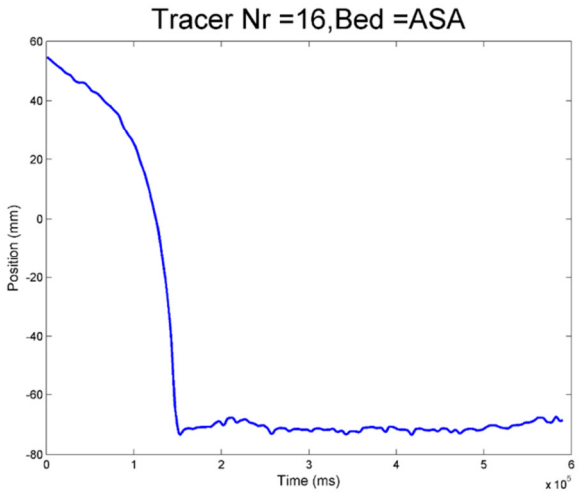

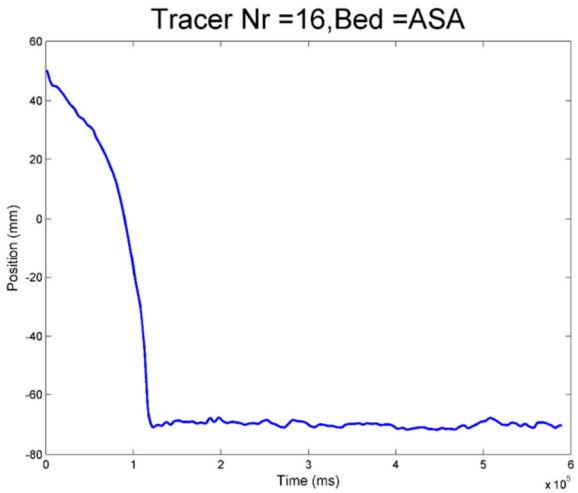

10.4 The code for the function that creates the input page

```
1.  Sub KingSetupSize()
2.
3.
4.      Dim ws  As Worksheet
5.
6.
7.      Dim D As Double
8.      Dim S As Double
9.      Dim Heading(5) As String
10.     Dim rng As Range
11.     Dim InputRange As Range
12.     Dim SizeRange As Range
13.     Dim DensityRange As Range
14.     Dim SizeNumbers As Range
15.     Dim DensityNumbers As Range
16.     Dim R1 As Range
17.
18.
19.     Set ws = ActiveSheet
20.     On Error Resume Next
21.     txt = "Number of Density Fractions"
22.     D = Application.InputBox(txt, Type:=1)
23.
24.     txt = "Number of Size Fractions"
25.     S = Application.InputBox(txt, Type:=1)
26.
27.     Range("b1").Value = S
28.     Range("a2").Value = D
29.
30.     Range("c1").Value = "Size"
31.     Range("A3").Value = "Density"
32.
33.     Set InputRange = Range(Cells(3, 3), Cells(2 + D, 2 + S))
34.     Set SizeRange = Range(Cells(1, 3), Cells(1, 2 + S))
35.     Set DensityRange = Range(Cells(3, 1), Cells(2 + D, 1))
36.     Set SizeNumbers = Range(Cells(2, 3), Cells(2, 2 + S))
37.     Set DensityNumbers = Range(Cells(3, 2), Cells(2 + D, 2))
38.     Set R1 = Range(Cells(1, 1), Cells(2, 2))
39.     Set Aname = Range(Cells(2, S + 3), Cells(2, S + 4))
40.     Set AValue = Range(Cells(3, S + 3), Cells(3, S + 4))
41.     Set Tname = Range(Cells(4, S + 3), Cells(4, S + 3))
42.     Set TValue = Range(Cells(4, S + 4), Cells(4, S + 4))
43.
44.     Aname(1).Value = "A"
45.     Aname(2).Value = "b"
46.     Tname(1).Value = "Relative Time"
47.     'Formatting
48.         With R1.Interior
49.         .Pattern = xlSolid
50.         .PatternColorIndex = xlAutomatic
51.         .ThemeColor = xlThemeColorAccent2
52.         .TintAndShade = 0.599993896298105
53.         .PatternTintAndShade = 0
54.         End With
55.         With Tname
56.             With .Interior
57.             .Pattern = xlSolid
58.             .PatternColorIndex = xlAutomatic
59.             .ThemeColor = xlThemeColorAccent2
60.             .TintAndShade = 0.599993896298105
61.             .PatternTintAndShade = 0
62.             End With
```

```
63.             With .Borders(xlEdgeBottom)
64.             .LineStyle = xlContinuous
65.             .ColorIndex = 0
66.             .TintAndShade = 0
67.             .Weight = xlThin
68.             End With
69.             With .Borders(xlEdgeTop)
70.             .LineStyle = xlContinuous
71.             .ColorIndex = 0
72.             .TintAndShade = 0
73.             .Weight = xlThin
74.             End With
75.             With .Borders(xlEdgeLeft)
76.             .LineStyle = xlContinuous
77.             .ColorIndex = 0
78.             .TintAndShade = 0
79.             .Weight = xlThin
80.             End With
81.             With .Borders(xlEdgeRight)
82.             .LineStyle = xlContinuous
83.             .ColorIndex = 0
84.             .TintAndShade = 0
85.             .Weight = xlThin
86.             End With
87.         End With
88.
89.         With TValue
90.             With .Interior
91.             .Pattern = xlSolid
92.             .PatternColorIndex = xlAutomatic
93.             .ThemeColor = xlThemeColorAccent3
94.             .TintAndShade = 0.599993896298105
95.             .PatternTintAndShade = 0
96.             End With
97.             With .Borders(xlEdgeBottom)
98.             .LineStyle = xlContinuous
99.             .ColorIndex = 0
100.                    .TintAndShade = 0
101.                    .Weight = xlThin
102.                    End With
103.                    With .Borders(xlEdgeTop)
104.                    .LineStyle = xlContinuous
105.                    .ColorIndex = 0
106.                    .TintAndShade = 0
107.                    .Weight = xlThin
108.                    End With
109.                    With .Borders(xlEdgeLeft)
110.                    .LineStyle = xlContinuous
111.                    .ColorIndex = 0
112.                    .TintAndShade = 0
113.                    .Weight = xlThin
114.                    End With
115.                    With .Borders(xlEdgeRight)
116.                    .LineStyle = xlContinuous
117.                    .ColorIndex = 0
118.                    .TintAndShade = 0
119.                    .Weight = xlThin
120.                    End With
121.                End With
122.
123.
124.                With Aname
125.                    With .Interior
126.                    .Pattern = xlSolid
127.                    .PatternColorIndex = xlAutomatic
128.                    .ThemeColor = xlThemeColorAccent2
```

```
                    .TintAndShade = 0.599993896298105
                    .PatternTintAndShade = 0
                    End With
                    With .Borders(xlEdgeBottom)
                    .LineStyle = xlContinuous
                    .ColorIndex = 0
                    .TintAndShade = 0
                    .Weight = xlThin
                    End With
                    With .Borders(xlEdgeTop)
                    .LineStyle = xlContinuous
                    .ColorIndex = 0
                    .TintAndShade = 0
                    .Weight = xlThin
                    End With
                    With .Borders(xlEdgeLeft)
                    .LineStyle = xlContinuous
                    .ColorIndex = 0
                    .TintAndShade = 0
                    .Weight = xlThin
                    End With
                    With .Borders(xlEdgeRight)
                    .LineStyle = xlContinuous
                    .ColorIndex = 0
                    .TintAndShade = 0
                    .Weight = xlThin
                    End With
                End With

                With AValue
                    With .Interior
                    .Pattern = xlSolid
                    .PatternColorIndex = xlAutomatic
                    .ThemeColor = xlThemeColorAccent3
                    .TintAndShade = 0.599993896298105
                    .PatternTintAndShade = 0
                    End With
                    With .Borders(xlEdgeBottom)
                    .LineStyle = xlContinuous
                    .ColorIndex = 0
                    .TintAndShade = 0
                    .Weight = xlThin
                    End With
                    With .Borders(xlEdgeTop)
                    .LineStyle = xlContinuous
                    .ColorIndex = 0
                    .TintAndShade = 0
                    .Weight = xlThin
                    End With
                    With .Borders(xlEdgeLeft)
                    .LineStyle = xlContinuous
                    .ColorIndex = 0
                    .TintAndShade = 0
                    .Weight = xlThin
                    End With
                    With .Borders(xlEdgeRight)
                    .LineStyle = xlContinuous
                    .ColorIndex = 0
                    .TintAndShade = 0
                    .Weight = xlThin
                    End With
                End With

            With InputRange
                With .Interior
                .Pattern = xlSolid
```

```
195.                .PatternColorIndex = xlAutomatic
196.                .ThemeColor = xlThemeColorAccent3
197.                .TintAndShade = 0.599993896298105
198.                .PatternTintAndShade = 0
199.                End With
200.                With .Borders(xlEdgeBottom)
201.                .LineStyle = xlContinuous
202.                .ColorIndex = 0
203.                .TintAndShade = 0
204.                .Weight = xlThin
205.                End With
206.                With .Borders(xlEdgeTop)
207.                .LineStyle = xlContinuous
208.                .ColorIndex = 0
209.                .TintAndShade = 0
210.                .Weight = xlThin
211.                End With
212.                With .Borders(xlEdgeLeft)
213.                .LineStyle = xlContinuous
214.                .ColorIndex = 0
215.                .TintAndShade = 0
216.                .Weight = xlThin
217.                End With
218.                With .Borders(xlEdgeRight)
219.                .LineStyle = xlContinuous
220.                .ColorIndex = 0
221.                .TintAndShade = 0
222.                .Weight = xlThin
223.                End With
224.                With .Borders(xlInsideHorizontal)
225.                .LineStyle = xlContinuous
226.                .ColorIndex = 0
227.                .TintAndShade = 0
228.                .Weight = xlThin
229.                End With
230.                With .Borders(xlInsideVertical)
231.                .LineStyle = xlContinuous
232.                .ColorIndex = 0
233.                .TintAndShade = 0
234.                .Weight = xlThin
235.                End With
236.            End With
237.
238.            With SizeRange
239.                With .Interior
240.                .Pattern = xlSolid
241.                .PatternColorIndex = xlAutomatic
242.                .ThemeColor = xlThemeColorAccent2
243.                .TintAndShade = 0.599993896298105
244.                .PatternTintAndShade = 0
245.                End With
246.                With .Borders(xlEdgeBottom)
247.                .LineStyle = xlContinuous
248.                .ColorIndex = 0
249.                .TintAndShade = 0
250.                .Weight = xlThin
251.                End With
252.                With .Borders(xlEdgeTop)
253.                .LineStyle = xlContinuous
254.                .ColorIndex = 0
255.                .TintAndShade = 0
256.                .Weight = xlThin
257.                End With
258.                With .Borders(xlEdgeLeft)
259.                .LineStyle = xlContinuous
260.                .ColorIndex = 0
```

```
                .TintAndShade = 0
                .Weight = xlThin
                End With
                With .Borders(xlEdgeRight)
                .LineStyle = xlContinuous
                .ColorIndex = 0
                .TintAndShade = 0
                .Weight = xlThin
                End With
            End With


            With SizeNumbers
                With .Interior
                .Pattern = xlSolid
                .PatternColorIndex = xlAutomatic
                .ThemeColor = xlThemeColorDark1
                .TintAndShade = -0.249977111117893
                .PatternTintAndShade = 0
                End With
                With .Borders(xlEdgeBottom)
                .LineStyle = xlContinuous
                .ColorIndex = 0
                .TintAndShade = 0
                .Weight = xlThin
                End With
                With .Borders(xlEdgeTop)
                .LineStyle = xlContinuous
                .ColorIndex = 0
                .TintAndShade = 0
                .Weight = xlThin
                End With
                With .Borders(xlEdgeLeft)
                .LineStyle = xlContinuous
                .ColorIndex = 0
                .TintAndShade = 0
                .Weight = xlThin
                End With
                With .Borders(xlEdgeRight)
                .LineStyle = xlContinuous
                .ColorIndex = 0
                .TintAndShade = 0
                .Weight = xlThin
                End With
            End With

            With DensityRange
                With .Interior
                .Pattern = xlSolid
                .PatternColorIndex = xlAutomatic
                .ThemeColor = xlThemeColorAccent2
                .TintAndShade = 0.599993896298105
                .PatternTintAndShade = 0
                End With
                With .Borders(xlEdgeBottom)
                .LineStyle = xlContinuous
                .ColorIndex = 0
                .TintAndShade = 0
                .Weight = xlThin
                End With
                With .Borders(xlEdgeTop)
                .LineStyle = xlContinuous
                .ColorIndex = 0
                .TintAndShade = 0
                .Weight = xlThin
                End With
```

```
327.                With .Borders(xlEdgeLeft)
328.                .LineStyle = xlContinuous
329.                .ColorIndex = 0
330.                .TintAndShade = 0
331.                .Weight = xlThin
332.                End With
333.                With .Borders(xlEdgeRight)
334.                .LineStyle = xlContinuous
335.                .ColorIndex = 0
336.                .TintAndShade = 0
337.                .Weight = xlThin
338.                End With
339.            End With
340.
341.            With DensityNumbers
342.                With .Interior
343.                .Pattern = xlSolid
344.                .PatternColorIndex = xlAutomatic
345.                .ThemeColor = xlThemeColorDark1
346.                .TintAndShade = -0.249977111117893
347.                .PatternTintAndShade = 0
348.                End With
349.                With .Borders(xlEdgeBottom)
350.                .LineStyle = xlContinuous
351.                .ColorIndex = 0
352.                .TintAndShade = 0
353.                .Weight = xlThin
354.                End With
355.                With .Borders(xlEdgeTop)
356.                .LineStyle = xlContinuous
357.                .ColorIndex = 0
358.                .TintAndShade = 0
359.                .Weight = xlThin
360.                End With
361.                With .Borders(xlEdgeLeft)
362.                .LineStyle = xlContinuous
363.                .ColorIndex = 0
364.                .TintAndShade = 0
365.                .Weight = xlThin
366.                End With
367.                With .Borders(xlEdgeRight)
368.                .LineStyle = xlContinuous
369.                .ColorIndex = 0
370.                .TintAndShade = 0
371.                .Weight = xlThin
372.                End With
373.            End With
374.
375.
376.            With DensityRange
377.                .HorizontalAlignment = xlCenter
378.                .VerticalAlignment = xlCenter
379.                .WrapText = False
380.                .Orientation = 90
381.                .AddIndent = False
382.                .IndentLevel = 0
383.                .ShrinkToFit = False
384.                .ReadingOrder = xlContext
385.                .MergeCells = True
386.            End With
387.
388.
389.            With SizeRange
390.                .HorizontalAlignment = xlCenter
391.                .VerticalAlignment = xlCenter
392.                .WrapText = False
```

```
393.                .Orientation = 0
394.                .AddIndent = False
395.                .IndentLevel = 0
396.                .ShrinkToFit = False
397.                .ReadingOrder = xlContext
398.                .MergeCells = True
399.            End With
400.        End Sub
```

10.5 Code for the main function

```
1.  Public Sub KingModeSize()
2.
3.      Dim ws  As Worksheet
4.
5.
6.
7.      Dim Height() As Double
8.      Dim Density() As Double
9.      Dim DensityH() As Double
10.     Dim IntA() As Double
11.     Dim Distr() As Variant
12.     Dim Err1() As Double
13.     Dim rng2() As Double
14.     Dim Error As Double
15.     Dim Inp As Range
16.
17.     Dim i   As Long
18.     Dim n   As Long
19.     Dim S   As Long
20.     Dim D   As Long
21.     Dim m   As Long
22.     Dim cf()   As Double
23.     Dim co()   As Double
24.     Dim A   As Double
25.     Dim B   As Double
26.
27.
28.     Dim rho() As Double
29.     Dim C()   As Double
30.     Dim Csum()   As Double
31.     Dim Cnew()   As Double
32.     Dim NewD()   As Double
33.
34.     Dim alpha()  As Double
35.     Dim Size()  As Double
36.     Dim densityAve As Double
37.     Dim densityParticle As Double 'Change
38.     Dim massParticle As Double 'Change
39.     Dim sizeParticle As Double 'Change
40.     Dim densityFactor As Double 'Change
41.     Dim dF As Double 'Change
42.     Dim heightCompare As Double 'Change
43.     Dim SizeCalc As Double 'Change
44.     Dim Mass As Double 'Change
45.     Dim Step As Double
46.     Dim RT As Double
47.
48.
49.     'setup
50.     Step = 0.001
51.
52.     D = Range("A2") 'number of density clases
53.     S = Range("B1") 'number of size clases
54.     A = Range(Cells(3, S + 3), Cells(3, S + 3)) 'Value of A
55.     B = Range(Cells(3, S + 4), Cells(3, S + 4)) 'value of B
56.     RT = Range(Cells(4, S + 4), Cells(4, S + 4)) 'Value of Relative time
57.
58.
59.     m = D * S
60.
61.     'get input values
62.
```

```
    Set Inp = Range(Cells(2, 2), Cells(D + 1, S + 1))


    ReDim cf(1 To m)
    ReDim co(1 To m)
    ReDim rho(1 To m)
    ReDim alpha(1 To m)
    ReDim Size(1 To m)

    'Create Size and Density Array cf=concentration array

    count1 = 0
    For i = 1 To D
        For Z = 1 To S
        count1 = count1 + 1
        cf(count1) = Inp(i + 1, Z + 1)
        rho(count1) = Inp(i + 1, 1)
        Size(count1) = Inp(1, Z + 1)
        alpha(count1) = A * Size(count1) ^ B 'calculate alpha

        Next Z
    Next i
    'alpha = Range("e2")
    densityAve = 0

   'Density Average
    For i = 1 To m

        densityAve = densityAve + cf(i) * rho(i)

    Next i


    n = 1 / Step

        ReDim Height(1 To n + 1, 1 To 2)
        ReDim Density(1 To n + 1, 1 To 2)
               ReDim IntA(1 To n + 1, 1 To 2)
               ReDim DensityH(1 To n + 1, 1)

               ReDim Err1(1 To n + 1, 1)
               ReDim rng2(1 To n + 1, 1 To m)
               ReDim C(1 To n + 1, 1 To m)
               ReDim Cnew(1 To n + 1, 1 To m)


          For i = 0 To n
              Height(i + 1, 1) = i * Step
              Density(i + 1, 1) = densityAve 'initial density array
          Next i

          'p(0-h)
        For y = 1 To 50
          Error = 5


          'Do While Error > 1


          Erase NewD()
          Erase Csum()
          Erase IntA()
          ReDim Csum(1 To n + 1, 1)
          ReDim NewD(1 To n + 1, 1)
          ReDim IntA(1 To n + 1, 1 To 2)
```

```
129.            S1 = 0
130.
131.            For i = 1 To n + 1
132.                S1 = S1 + Density(i, 1)
133.                DensityH(i, 1) = S1 / i
134.            Next i
135.
136.
137.            'clear variables Csum,Cnew,C
138.
139.            For Z = 1 To m
140.
141.                IntB = 0
142.                Int1 = 0
143.                Erase Distr()
144.                ReDim Distr(1 To n + 1, 1)
145.
146.
147.            'Integral
148.
149.                For i = 1 To n
150.
151.                    Int1 = Int1 + (Height(i + 1, 1) -
    Height(i, 1)) * (Density(i + 1, 1) + Density(i, 1)) / 2
152.                    IntA(i + 1, 1) = Int1
153.                Next i
154.
155.            'Distribution Function
156.            'New Stuff
157.                    densityParticle = rho(Z)
158.                    sizeParticle = Size(Z)
159.                    massParticle = 0.5236 * sizeParticle ^ 3 * densityParticle
160.
161.                    AverageDensity = 0.00017
162.
163.                    densityFactor = 1 - Exp((-1 * (massParticle -
    AverageDensity) ^ 2) / (2 * 0.000017 ^ 2))
164.
165.
166.                For i = 1 To n + 1
167.
168.                    Distr(i, 1) = Exp(1 * alpha(Z) * (IntA(i, 1) -
    rho(Z) * Height(i, 1)))
169.
170.                Next i
171.            'Bottom integral
172.                For i = 1 To n
173.                    IntB = IntB + (Height(i + 1, 1) -
    Height(i, 1)) * (Distr(i + 1, 1) + Distr(i, 1)) / 2
174.                Next i
175.
176.
177.                For i = 1 To n + 1
178.
179.                C(i, Z) = Distr(i, 1) * cf(Z) / IntB
180.
181.                Next i
182.
183.            Next Z
184.
185.            For Z = 1 To m
186.               For i = 1 To n + 1
187.                Csum(i, 1) = Csum(i, 1) + C(i, Z)
188.
189.               Next i
190.            Next Z
```

```
191.
192.
193.            For Z = 1 To m
194.               For i = 1 To n + 1
195.
196.                   Cnew(i, Z) = C(i, Z) / Csum(i, 1)
197.
198.               Next i
199.            Next Z
200.
201.            For Z = 1 To m
202.               For i = 1 To n + 1
203.            'new Density
204.                   NewD(i, 1) = NewD(i, 1) + Cnew(i, Z) * rho(Z)
205.
206.               Next i
207.            Next Z
208.            E = 0
209.            For i = 1 To n + 1
210.                Err1(i, 1) = (NewD(i, 1) - Density(i, 1)) ^ 2
211.                E = E + Err1(i, 1)
212.                Density(i, 1) = NewD(i, 1)
213.
214.            Next i
215.            Error = Error - 1
216.         Next y
217.
218.
219.        With Range(Cells(3, S + 6), Cells(n + 1, S + 6))
220.        .ClearContents
221.        .Resize(n + 1, 1).Name = "MyNamedRange"
222.        End With
223.        Range("MyNamedRange").Value2 = Height
224.
225.        With Range(Cells(3, S + 7), Cells(n + 1, m + S + 7))
226.        .ClearContents
227.        .Resize(n + 1, m).Name = "MyNamedRange"
228.        End With
229.        Range("MyNamedRange").Value2 = Cnew
230.
231.        With Range(Cells(1, S + 7), Cells(1, m + S + 7))
232.        .ClearContents
233.        .Resize(1, m).Name = "MyNamedRange"
234.        End With
235.        Range("MyNamedRange").Value2 = rho
236.
237.        With Range(Cells(2, S + 7), Cells(2, m + S + 7))
238.        .ClearContents
239.        .Resize(1, m).Name = "MyNamedRange"
240.        .Borders(xlEdgeBottom).LineStyle = xlContinuous
241.        End With
242.        Range("MyNamedRange").Value2 = Size
243.
244.
245.
246.
247.        Exit_Handler:
248.             Set rng = Nothing
249.            Set shp = Nothing
250.            Set ws = Nothing
251.            Exit Sub
252.
253.        Err_Handler:
254.            MsgBox Err.Number & vbNewLine & Err.Description
255.            Resume Exit_Handler
256.
```

```
257.        End Sub
```